AD 728751

THE DISTRIBUTION AND HISTORY OF TEMPERATURE IN CIRCULAR CYLINDERS EXPOSED TO THE THERMAL RADIATION PULSE OF A NUCLEAR DETONATION

By
Donald M. Wilson

14 JUNE 1971
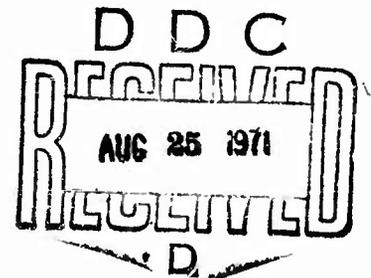
D D C
RECEIVED
AUG 25 1971
D

NOL

NAVAL ORDNANCE LABORATORY, WHITE OAK, SILVER SPRING, MARYLAND

APPROVED FOR PUBLIC RELEASE;
DISTRIBUTION UNLIMITED

142

DOCUMENT CONTROL DATA - R & D

(Security classification of title, body of abstract and indexing annotation must be entered when the overall report is classified)

1. ORIGINATING ACTIVITY *(Corporate author)*	2a. REPORT SECURITY CLASSIFICATION
Naval Ordnance Laboratory White Oak; Silver Spring Maryland 20910	UNCLASSIFIED
	2b. GROUP

3. REPORT TITLE

THE DISTRIBUTION AND HISTORY OF TEMPERATURE IN CIRCULAR CYLINDERS EXPOSED TO THE THERMAL RADIATION PULSE OF A NUCLEAR DETONATION

4. DESCRIPTIVE NOTES *(Type of report and inclusive dates)*

5. AUTHOR(S) *(First name, middle initial, last name)*

Donald M. Wilson

6. REPORT DATE	7a. TOTAL NO. OF PAGES	7b. NO. OF REFS
14 June 1971	144	6

8a. CONTRACT OR GRANT NO.	9a. ORIGINATOR'S REPORT NUMBER(S)
b. PROJECT NO. SF 26553001-11292	NOLTR 71-61
c.	9b. OTHER REPORT NO(S) *(Any other numbers that may be assigned this report)*
d.	

10. DISTRIBUTION STATEMENT

Approved for public release; distribution unlimited.

11. SUPPLEMENTARY NOTES	12. SPONSORING MILITARY ACTIVITY
	Naval Ships Systems Command

13. ABSTRACT Temperature distribution histories were calculated in detail for cylinders exposed to the thermal radiation pulse from a low altitude nuclear weapon detonation. Results are presented in terms of dimensionless groups and charts covering a wide range of the parameters - weapon yield, radiant exposure, cylinder wall thickness, outer radius, and material. The temperatures are for circular cylinders whose absorptance, thermal conductivity, density and specific heat are constant with temperature and time. The effect of convective cooling on maximum temperature is considered separately and shown to be small for cylinders of practical application and was not used in the dimensionless presentations. The dimensionless charts of this report can be used to determine temperatures in cylindrical structural elements exposed to the thermal radiation pulse. This report will show what effect the changes in cylinder or weapon parameters have on the manner in which temperature is distributed in cylinders.

The rear half of a cylinder exposed to a nuclear weapon thermal radiation pulse is unheated and the front half is heated in a spatially non-uniform manner. Therefore, internal heat conduction and the resultant temperature distribution histories in cylinders are more complex than for simpler elements such as flat plates. The influence of parameter changes on the internal heat transfer and the resulting temperature distributions and histories will be discussed to give insight into the selection of cylindrical elements to withstand a nuclear weapons attack.

DD FORM NOV 65 **1473** (PAGE 1)

S/N 0101-807-6801

14	LINK A		LINK B		LINK C	
KEY WORDS	ROLE	WT	ROLE	WT	ROLE	WT
Effect of Nuclear Weapon Temperature Distribution Thermal Radiation Shipboard Structures						

DD FORM 1473 (BACK)
1 NOV 65

NOLTR 71-61

THE DISTRIBUTION AND HISTORY OF TEMPERATURE IN CIRCULAR CYLINDERS EXPOSED TO THE THERMAL RADIATION PULSE OF A NUCLEAR DETONATION

Prepared by
Donald M. Wilson

ABSTRACT: Temperature distribution histories were calculated in detail for cylinders exposed to the thermal radiation pulse from a low altitude nuclear weapon detonation. Results are presented in terms of dimensionless groups and charts covering a wide range of the parameters - weapon yield, radiant exposure, cylinder wall thickness, outer radius, and material. The temperatures are for circular cylinders whose absorptance, thermal conductivity, density and specific heat are constant with temperature and time. The effect of convective cooling on maximum temperature is considered separately and shown to be small for cylinders of practical application and was not used in the dimensionless presentations. The dimensionless charts of this report can be used to determine temperatures in cylindrical structural elements exposed to the thermal radiation pulse. This report will show what effect the changes in cylinder or weapon parameters have on the manner in which temperature is distributed in cylinders.

The rear half of a cylinder exposed to a nuclear weapon thermal radiation pulse is unheated and the front half is heated in a spatially non-uniform manner. Therefore, internal heat conduction and the resultant temperature distribution histories in cylinders are more complex than for simpler elements such as flat plates. The influence of parameter changes on the internal heat transfer and the resulting temperature distributions and histories will be discussed to give insight into the selection of cylindrical elements to withstand a nuclear weapons attack.

NAVAL ORDNANCE LABORATORY
WHITE OAK, SILVER SPRING, MARYLAND

i

NOLTR 71-61

NOLTR 71-61   14 June 1971

THE DISTRIBUTION AND HISTORY OF TEMPERATURE IN CIRCULAR CYLINDERS
EXPOSED TO THE THERMAL RADIATION PULSE OF A NUCLEAR DETONATION

This work represents part of a continuing effort to determine
techniques to protect shipboard elements from the combined thermal
radiation and airblast of a nuclear weapon detonation. This report
presents the temperature response of homogeneous circular cylinders
due to the thermal radiation pulse of the weapon. The results of
calculations of cylinder temperatures are correlated and given in
dimensionless plots of temperature versus time.

This work is being sponsored by the Naval Ship Systems Command
under Task Number 11292 - subproject SF 26-553-001.

CONTENTS

TABLES

ILLUSTRATIONS

INTRODUCTION

The purpose of this report is to present the results of a study on the temperature response in circular cylinders exposed to the thermal radiation pulse of a nuclear detonation. The main objective of this study was to prepare a set of charts which will allow a quick estimate of the temperature history in these cylinders to be made. A second objective is to analyze the temperature responses in order to find how the temperature histories will be affected by weapon or cylinder conditions. The findings of these studies will be presented in the form of charts. The charts generated in this report can be readily employed in vulnerability and design studies. Their use will facilitate the efficient design of cylindrical structures or equipment to withstand the thermal radiation effects from a nuclear weapon attack. Specifically, the following data will be presented in graphical form:

1. Temperature histories for several angular and radial positions on the cylinder. From these, it will be possible to obtain a complete picture of the temperature response of a cylinder.

2. The maximum cylinder temperature in terms of basic dimensionless parameters which represent the combined effects of cylinder size, thickness, material and weapon yield on temperature.

3. The individual influence of wall thickness, outer radius size, cylinder material, weapon yield and convective cooling on the maximum temperature realized on the cylinder.

All of these, except for material influence, will be exemplified by giving the maximum temperature rise in a typical aluminum alloy cylinder (6061-T6) for different values of the mentioned variables. The influence of material on maximum temperature will be shown by comparing the maximum temperature in aluminum with that in stainless steel and with that in a mild steel.

4. Temperature histories for aluminum alloy cylinders where the basic internal heat conduction patterns differ. These are presented as an aid in predicting other than the maximum temperature in the cylinders.

This report is organized such that the above four sets of data can be easily located. That is, the general temperature history charts, item (1), with instructions and examples on their use are given in Appendices A and B. The remaining items are presented

1

and discussed in turn in the main body of this report. This discussion will present an increasingly - detailed description of the temperature behavior in circular cylinders which have been exposed to the thermal radiation pulse of a nuclear weapon.

All of the temperatures given in this report were calculated by means of a large computer program which uses an explicit finite difference scheme. The use of this program is discussed later.

Thermal radiation and airblast effects are damage mechanisms of primary concern at weapon to target separation distances appropriate to vulnerability and hardening studies of shipboard and aircraft structures and systems. The airblast pressure pulse is caused by the very high pressures and temperatures which result when a large amount of energy is released in a limited space. Nuclear explosions differ from the conventional kind in that in the nuclear reaction temperatures of several tens of millions of degrees are reached whereas in the conventional chemical reaction, the maximum temperatures are approximately 10,000°C. Hence, in the detonation of a nuclear weapon a large portion of the weapon's energy appears as electromagnetic radiation. Furthermore, the temperature of the air surrounding the nuclear detonation (the fireball) remains relatively high for a short period of time. When these temperatures decrease to less than a few thousand degrees centigrade, the earth's atmosphere is nearly transparent to much of the electromagnetic radiation produced and it can be transmitted great distances. A target exposed to the nuclear explosion will absorb a portion of the incident thermal radiation and be heated by it. Since a large amount of thermal radiation is emitted in a relatively short time, the resulting temperatures on the target may be high enough to cause structural damage or the ignition of combustibles. Even if the thermal radiation is not great enough to immediately damage the target, the resulting temperature increase will cause a reduction in the strength of the materials which compose the target, and may induce significant thermal stresses as well. The oncoming blast wave, which arrives at the target after a considerable portion of the thermal pulse has been absorbed, will then encounter a heated target of reduced structural strength and will therefore be more damaging to it.

The starting point in the determination of vulnerability or design of equipment or structural elements on a target to withstand a nuclear attack is the determination of the expected temperature levels. Since the fireball size is related to the weapon yield, the thermal radiant exposure from nuclear weapons can be scaled to the size of the weapon. Scaling the radiant heating avoids the problem of solving the heating problem for each weapon yield. However, prediction of the temperature history of a body undergoing transient radiation heating is still a difficult problem. The practical way of computing these histories is by means of numerical analysis with the aid of a high-speed computer. Also, the principles of dimensional analysis can be used to condense the data computed so that the temperature histories can be readily found for a wide choice of target material, size or geometry and weapon yield.

2

This approach was followed in a previous report (reference (1)) which presented the temperature response of plates exposed to the thermal radiation from a nuclear detonation.

The report concludes the effort to find the temperature response of homogeneous circular cylinders exposed to the thermal pulse of a nuclear weapon. Future work will be to correlate and condense this large amount of temperature data and to derive simple laws which allow quick estimates of cylinder temperatures to be made. These relationships can be included in future handbooks on nuclear weapon effects.

SYMBOLS

A	absorptance
c	specific heat at constant pressure
k	thermal conductivity
h	heat transfer coefficient for convective cooling
H	irradiance
H^*	dimensionless irradiance (H/H_m)
H_m	maximum irradiance
Q	radiant exposure
r	cylinder radius
r^*	dimensionless cylinder radius (r/R_o)
R_i	cylinder inner radius
R_i^*	dimensionless cylinder inner radius (R_i/R_o)
R_o	cylinder outer radius
t	time
t_m	time at which maximum irradiance of nuclear weapon thermal pulse occurs
T	temperature
T^*	dimensionless temperature (see equation (8))
TI	initial temperature
T_∞	temperature of surrounding air
α	thermal diffusivity $(k/\rho c)$
ϕ	included cylinder angle, measured from the most forward point on the cylinder
ϕ^*	dimensionless included cylinder angle (ϕ/π)
ρ	density

MATHEMATICAL ANALYSIS OF THE CYLINDER HEATING PROBLEM

The distribution and history of temperature will be computed for a circular cylinder exposed to the radiant heating of a nuclear weapon detonation. This will be accomplished by numerically solving the governing partial differential equation with appropriate boundary conditions. The analysis will be simplified by applying the principles of dimensional analysis to normalize the governing equations. Details of this mathematical analysis follow.

3

The partial differential equation for two-dimensional (radial and angular) heat transfer in a circular cylinder is:

$$\frac{k}{r} \frac{\partial}{\partial r} \left(r \frac{\partial T}{\partial r} \right) + \frac{k}{r^2} \frac{\partial^2 T}{\partial \phi^2} = \rho c \frac{\partial T}{\partial t} \tag{1}$$

Equation (1) applies to isotropic, homogeneous cylinders whose thermophysical properties are assumed constant. It represents a heat energy rate balance where the first term represents the radial heat conduction, the second term the angular (circumferential) heat conduction, and the third term accounts for the heat energy stored. The appropriate boundary conditions for the thermal radiation heating received from a nuclear explosion are:

$$r = Ro \qquad -k\left(\frac{\partial T}{\partial r}\right) = \begin{cases} A\ H\ \cos \phi - h\ (T - T_\infty), \phi \le \pm \frac{\pi}{2} \\ \\ \quad\quad - h\ (T - T_\infty), \phi > \pm \frac{\pi}{2} \end{cases} \tag{2}$$

$$r = Ri \qquad -k\left(\frac{\partial T}{\partial r}\right) = 0 \tag{3}$$

The first boundary condition, equation (2), states that the cylindrical surface receives and absorbs thermal radiation energy from the nuclear fireball while simultaneously losing energy by convection to the ambient air. The second boundary condition, equation (3), simply states that no energy is lost or gained at the inner surface of the cylinder.

Equations (1) to (3) will be normalized by introducing the following dimensionless variables.

$$r* = r/Ro \tag{4}$$
$$Ri* = Ri/Ro \tag{5}$$
$$H* = H/H_m \tag{6}$$
$$t* = t/t_m \tag{7}$$
$$T* = (T - T_\infty)/(AH_m\ Ro/k) \tag{8}$$
$$\phi* = \phi/\pi \tag{9}$$

The above choices are dictated by applying the principles of dimensional analysis to equations (1) to (3). They allow equations (1) to (3) to be transformed such that the total number of variables describing the transient temperature in a cylinder will be minimized. That is, when the variables defined by equations (4) to (9) are substituted into equations (1) to (3), the following normalized equations are obtained,

$$\frac{1}{r*} \frac{\partial}{\partial r*} \left(r* \frac{\partial T*}{\partial r*} \right) + \frac{1}{-2_r*^2} \frac{\partial^2 T*}{\partial \phi*^2} = \frac{Ro^2}{\alpha t_m} \frac{\partial T*}{\partial t*} \tag{10}$$

$$r* = 1 \qquad -\frac{\partial T*}{\partial r*} = H* \cos(\text{-}\phi*) - \frac{hRo}{k} \; T* \qquad (11)$$

$$r* = Ri* \qquad -\frac{\partial T*}{\partial r*} = 0 \qquad\qquad\qquad (12)$$

It is seen by comparison that equations (10) to (12) are identical to equations (1) to (3) except for the change of variable notation and constant parameters. Thus, a solution of the problem expressed by equations (10) to (12) in dimensionless variables represents a solution to the original problem given by equations (1) to (3).

An inspection of equations (10) to (12) shows that the non-dimensional temperature, $T*$, is a function of seven dimensionless parameters, i.e.,

$$T* = F \left(H*, \; t*, \; r*, \; Ri*, \; \phi*, \; \frac{\alpha t_m}{Ro^2}, \; \frac{hRo}{k} \right) \qquad (13)$$

The shape of the nuclear weapon thermal radiation pulse (i.e., dependence of irradiance on time) has been standardized (reference (2)), and given in Figure 1.1. Since $H*$ is a unique function of $t*$, it can be eliminated from the list of parameters in equation (13) which uniquely specify the non-dimensional temperature. Eliminating $H*$, equation (13) becomes,

$$T* = F \left(t*, \; r*, \; Ri*, \; \phi*, \; \frac{\alpha t_m}{Ro^2}, \; \frac{hRo}{k} \right) \qquad (14)$$

The distribution and history of temperature in a circular cylinder exposed to the thermal radiation of a nuclear weapon will be computed by numerically solving equations (1) to (3). Equation (14) will subsequently be used as the basis for correlating and presenting the results. This equation shows that the temperature history of a point on or inside the circular cylinder depends on the location of the point $(r*, \phi*)$ and the values of three basic parameters, $Ri*$, $\alpha t_m/Ro^2$, and hRo/k. The parameter hRo/k will be set equal to zero (no convective cooling) in computing the temperature histories for this report, but an indication of its effect on the maximum cylinder temperature will be given. Dimensionless temperature histories ($T*$ versus $t*$) will be given for selected values of the spatial variables and for selected values of the remaining basic parameters. These selected values are given in Figure 2.1. They represent a wide range of cylinder materials, sizes and nuclear weapon yields. Table 1 also shows that the ten chosen values of $\alpha t_m/Ro^2$ correspond to values of outer radius between 2.5 and 79.8 centimeters for aluminum alloy (6061-T6) cylinders exposed to the thermal radiation pulse of a one megaton weapon ($t_m = 1.0$ second). These particular cylinders will later be used to illustrate the behavior of temperature in a cylinder.

5

ACCURACY OF THE NUMERICAL SOLUTION

The computations of this report were made by numerically solving the problem given by equations (1) to (3). To accomplish this, the cylinder is sub-divided into many radial and circumferential elements. Equation (1) in finite difference form is then solved for each element with the boundary elements subjected to the conditions given by equations (2) and (3). (See reference (3)). A computer program (reference (4)) was written incorporating all of the finite difference equations into an explicit scheme for the step by step calculation of cylinder temperatures. Accurate solutions require careful selection of the size of the elements composing the cylinder and of the real time interval between successive calculations. Since only the average temperature of each element is computed, the elements should be chosen such that they are thermally-thin for the amount of heat transferred to them. The choice of element size to insure accurate results in the present work was found by studying the effect of element size on accuracy of the solution. This was done by varying the element size for the case of constant thermal radiation input to a solid cylinder, a problem for which the exact solution is known (reference (5)). Element sizes giving accurate results for this problem were subsequently used as guides in the initial calculations of temperature for the nuclear thermal radiation pulse. The actual element sizes used were then easily found from a few trial runs. It was found that if element sizes are made too large, the elements will not be uniformly heated and the resulting average temperatures computed will be low. Hence, the element sizes for an accurate solution were chosen by making the elements smaller until the calculated temperatures did not increase.

RESULTS OF THE COMPUTATIONS

Dimensionless temperature histories and distributions for cylinders exposed to the thermal radiation pulse from a nuclear detonation were calculated for values of the spatial variables (r^*, ϕ^*) and the basic dimensionless parameters $(Ri^*, \alpha t_m/Ro^2)$ given in Figure 2.1. From the data of these calculations, plots of the dimensionless temperature versus dimensionless time for dimensionless time up to 20.0 were prepared with the factor $\alpha t_m/Ro^2$ as a parameter. These are presented in Appendix A for the five inner radius ratios of this study. For each inner radius ratio, there are separate figures for the six angular and the three radial locations shown in Figure 2.1. Thus Appendix A presents 18 figures for each inner radius ratio and on each of these the dimensionless temperature history is given for the ten values of $\alpha t_m/Ro^2$.

The maximum temperatures of the cylinders can be readily found from the large amount of data generated in this study. These always occur at the point on the cylinder closest to the source of radiation ($\phi* = 0$, $r* = 1.0$) since this point receives the maximum heating. Figure 3.1 correlates the maximum dimensionless temperatures with the basic parameter $\alpha t_m/Ro^2$ for the five inner radius ratios of this report. This figure shows that the maximum dimensionless cylinder temperatures increase with increasing values of the parameter, $\alpha t_m/Ro^2$. Thus, increasing the weapon yield (increasing the time at which the peak heating rate occurs) or the thermal diffusivity of the cylinder material will result in larger dimensionless temperatures, while increasing the cylinder's outer radius results in smaller dimensionless temperatures. But increases in the maximum dimensionless temperature may not result in an increase in the actual maximum temperature. This is true because the actual temperatures are proportional to the dimensionless temperature ($T*$) and the cylinder outer radius (Ro), and are inversely proportional to the material thermal conductivity (k). Thus, increases in the dimensionless temperature due to increasing the factor, α/Ro^2, may be offset in the determination of the actual temperature by the resulting decrease in the factor, Ro/k. An important influence of cylinder thickness (variable Ri*) on actual maximum temperature can be deduced from Figure 3.1. This is that a cylinder is thermally-thick for sufficiently small values of the basic parameters $\alpha t_m/Ro^2$. However, as $\alpha t_m/Ro^2$ is increased, values termed "branch points" will be reached where the cylinder ceases being thermally-thick. It will be shown that if a cylinder is thermally-thick, the actual maximum temperature of it is minimized. Hence, the branch points on Figure 3.1 can be used to choose the cylinder thickness that will minimize the maximum cylinder temperature for a given value of $\alpha t_m/Ro^2$.

The behavior of the actual maximum temperatures will be shown by considering the influence of cylinder thickness, weapon yield, material and convective cooling coefficient in turn. That is, figures showing the actual maximum temperatures plotted against the outer radius will be presented for selected values of the wall thickness (inner radius ratio), weapon yield, material properties and convective cooling coefficient. The actual maximum temperatures also depend on the material absorptance (A) and the maximum irradiance (H_m). These are chosen arbitrarily and for convenience to be 1.0 and 48.6 cal/cm^2-sec, respectively, for all of the calculations presented in this report. Since these quantities appear only in the definition of dimensionless temperature, actual cylinder temperatures for other combinations of absorptance and maximum irradiance can be scaled from the given values, i.e., new cylinder temperatures would be equal to the given temperatures multiplied by the new values of A and/or H_m and divided by 48.6 cal/cm^2-sec.

The influence of wall thickness on maximum temperature is presented in Figure 4.1 for an aluminum alloy (6061-T6) cylinder exposed to a weapon of 1 megaton yield (t = 1.0 second). Wall

thickness in this figure is indicated by the inner radius ratio (Ri^*). Increasing the outer radius for a constant inner radius ratio results in increasingly thicker cylinders. Thus, the cylinders shown in Figure 4.1 become thermally-thick once an outer radius corresponding to the branch point values of $\alpha t_m/Rc^2$ are reached. The maximum cylinder temperature can then be expected to rise rapidly, as shown in this figure, once the cylinder leaves the thermally-thick region.

The influence of weapon yield (characterized by the time to maximum irradiance, t_m) on maximum temperature is given in Figure 4.2 for aluminum alloy cylinders having an inner radius ratio of 0.9. Increasing the peak heating time increases the total time over which thermal radiation is received from a nuclear weapon (see Figure 1.1). Since the peak heating rate is constant, the total radiant exposure is increased accordingly. (See equation (B-1). Hence, the maximum cylinder temperature, including the temperature for a thermally-thick cylinder, will also be increased. Furthermore, the peak heating time is a factor in the basic parameter, $\alpha t_m/Ro^2$. Therefore, the values of the outer radius at the branch points where cylinders leave the thermally-thick regions are also increased for increases in the peak heating time. These phenomena are clearly indicated in Figure 4.2. For a cylinder of given outer radius the relative increase in maximum cylinder temperature due to increasing the peak heating time can be found by inspecting Figure 3.1. That is, the relative increase in maximum dimensionless temperature due to increasing the basic parameter, $\alpha t_m/Ro^2$ by increasing t_m, only, is also the relative increase in actual maximum temperature. This is true because the definition of the dimensionless temperature does not contain the peak heating time.

The influence of material choice on maximum cylinder temperature is indicated in Figure 4.3 for cylinders having a radius ratio of 0.9 and subjected to a one megaton weapon ($t_m = 1.0$ second). In this figure, the maximum temperatures in terms of the outer radius are compared for cylinders of an aluminum alloy, a mild steel, and a stainless steel (see reference (5) for the thermophysical properties of these steels). Both the thermal conductivity and the thermal diffusivity are decreased in comparing aluminum with mild steel and in comparing mild steel with stainless steel. Decreasing the diffusivity will cause the branch point to occur at a smaller outer radius. Decreasing the conductivity will cause the actual maximum temperatures to rise since these are inversely proportional to the conductivity. Figure 4.3 shows both of these phenomena when the thermal conductivity and diffusivity are decreased. However, decreasing the conductivity usually causes the diffusivity to decrease which results in the lower maximum dimensionless temperature for a given outer radius and peak heating time. But the resulting decrease in actual maximum temperature is more than accounted for in Figure 4.3 by the increase due to the lower conductivity except for some small values of outer radius. In summary, decreasing the thermal conductivity will always cause an increase in the maximum temperatures of the thermally-thick cylinders. However, the maximum temperatures may not be increased for all values of the outer radius if sufficiently large decreases in the thermal diffusivity result from decreasing the conductivity.

Figures 4.1 - 4.3 have shown the behavior of maximum cylinder temperature for selected values of wall thickness, peak heating time or materials. If maximum temperatures for other than the selected values are needed, they could be derived from Figure 3.1. An alternate method of obtaining new maximum cylinder temperatures would be to modify Figures 4.1 - 4.3 by applying suitable correction factors to their scales. That is, that ratio of new to existing outer radius is found by multiplying the abscissa scale by the square root of the product of new diffusivity and peak heating time and dividing by the product of existing diffusivity and peak heating time. The ratio of new to existing maximum cylinder temperatures is found by multiplying the ordinate scale by the ratio of new to existing outer radius and the ratio of existing to new thermal conductivity. A further modification of the ordinate scale is needed if the material absorptance or maximum irradiance rate vary from the values previously given. Note that Figures 4.1 - 4.3 contain a common curve for aluminum alloy cylinders of 0.9 radius ratio subjected to a weapon having a time to maximum irradiance of 1.0 second (existing values of α, k, and t_m are 0.637 cm^2/sec, 0.397 cal/sec-cm-$^{\circ}$C and 1.0 second, respectively). These curves can be used as a standard and the axis modified on Figure 4.1 - 4.3 to find the influence of wall thickness, peak heating time or material choice for new conditions.

The influence of convective cooling on maximum cylinder temperature is shown in Figure 4.4 for aluminum alloy cylinders of 0.9 inner radius ratio and subjected to a one megaton weapon (t_m = 1.0 second). Convective cooling coefficients were chosen to represent the maximum values which would be realized for cylinders placed on ships at sea. These were estimated by calculating the coefficients on cylinders exposed to a 50 knot air flow (reference (6)). Figure 4.4 shows that convective cooling is not very effective in reducing the maximum temperature experienced by cylinders of realistic materials and dimensions. But the results of Figure 4.4 cannot be used to determine the effect of cooling for other choices of weapon yield or cylinder material. This is true because cooling is characterized by the basic parameter, hRo/k, instead of by the cooling coefficient, h. However the effect of convective cooling is largely governed by the cylinder temperature levels. Hence, cooling would not be significant unless the cylinder temperatures were much larger than those shown in Figure 4.4, i.e., much larger than 400 degrees centigrade. Therefore, it can be concluded that convective cooling will not significantly reduce the maximum temperatures, for cylinders used in practical applications on ships.

The previous paragraphs discussed the maximum temperature experienced by circular cylinders but did not explain the heat transfer phenomena causing these temperatures. However, the maximum temperature may not be the most important temperature for cylinders subjected to the thermal radiation pulse of a nuclear weapon. For example, the temperature when the airblast pressure arrives or the temperature when maximum thermal stress occurs may not be equal to the maximum temperature. In any case, a knowledge of the manner in which

9

heat is internally transferred is necessary to understanding the behavior of the temperature history in a cylinder. For example, thermally-thick cylinders will reach their maximum temperatures shortly after the peak heating time while the temperatures of a very thin cylinder may continue to rise long after the time of maximum irradiance. Also, the temperature levels will be significantly affected by angular (circumferential) heat conduction. This effect becomes increasingly important as the cylinders are made thinner. It causes the maximum temperatures to be lower and to occur at an earlier time than they would for situations where angular conduction is negligible. Therefore, a knowledge of the manner in which heat is internally transferred is necessary for the efficient design of cylindrical elements able to withstand exposure to the thermal pulse of a nuclear weapon.

Heat transfer phenomena in circular cylinders subjected to heating from a nuclear weapon detonation will be illustrated by finding regions of thermally-thick and thermally-thin cylinders in terms of the basic parameters, Ri^* and $\alpha t_m/Ro^2$. The regions where angular heat conduction is significant will also be shown. These regions will be presented as a map showing where the cylinders are thick or thin and where angular conduction is significant. Because the heat conduction effects continuously change with time, the location of these regions is also time-dependent. Figures 5.1 and 5.2 show the maps for four values of the dimensionless time (t/t_m = 2.0, 5.0, 10.0, and 20.0). The following somewhat arbitrary definitions were used to locate the regions shown in Figures 5.1 and 5.2.

1. A cylinder is thermally-thick if the back face temperature (at $r = Ri$) is less than one percent of the surface temperature at the most forward point on the cylinder ($\phi = 0^o$).

2. It is thermally-thin if the difference in surface and back face temperatures at the point $\phi = 0^o$ is less than ten percent of the surface temperature.

3. Angular conduction is significant if the surface temperature 90 degrees from the most forward point ($\phi = 0^o$) is greater than five percent of the surface temperature at the most forward point.

Figures 5.1 and 5.2 are maps showing the values of the basic parameters, Ri^* and $\alpha t_m/Ro^2$, where various heat conduction patterns predominate. The previous discussion of maximum cylinder temperatures showed that these increased as the basic parameters increased provided that the cylinders are not thermally-thick. Thus, a first-order design criterion would be to choose cylinders near the thick cylinder line in Figures 5.1 and 5.2 for the time when blast loading is its maximum. The efficient design of cylindrical elements able to withstand combined thermal and blast effects will require a detailed knowledge of the temperature history as a function of the basic parameters, $\alpha t_m/Ro^2$ and Ri^*. It will be shown that the behavior of the temperature history depends on the predominant internal heat transfer mechanism as given by the regions shown in Figures 5.1 and 5.2. This dependence will be illustrated by giving the surface

temperature histories for four values of $\alpha t_m/Ro^2$ (.0001, .001, .01, and .1) which represent different internal heat transfer situations. These are presented in Figures 6.1 - 6.4. Each figure includes histories for inner radius ratios of 0.9, 0.8, 0.6, C.4 and 0.0 for the surface temperature at $\phi = 0^o$.

Each figure also includes histories for six points on the cylindrical surface for an inner radius ratio of 0.9. All of these figures were drawn for an aluminum alloy cylinder subjected to the thermal radiation pulse of a one megaton weapon ($t_m = 1.0$ second). However, the choice of material and weapon yield serves only to set the temperature scale. These figures would be similar, although the temperature levels would be different, for other materials or weapon yields provided that the value of the parameter, $\alpha t_m/Ro^2$, remained unchanged. The following discussion of Figures 6.1 - 6.4 will illustrate the general behavior of surface temperature history in circular cylinders subjected to the thermal radiation pulse of a nuclear weapon detonation.

Figure 6.1 presents the temperature histories for $\alpha t_m/Ro^2 = 0.0001$. Figures 5.1 and 5.2 show that these cylinders are thermally-thick for inner radius ratios up to 0.9 and dimensionless times up to 20. An exception is the dimensionless inner radius of 0.9 which leaves the thick cylinder region after a dimensionless time of 10. However, this departure does not significantly change its surface temperature histories from the thick cylinder values. A further inspection of Figures 5.1 and 5.2 shows that angular conduction is insignificant for these and for all other thermally-thick cylinders. Hence, the temperature histories of Figure 6.1 will apply for all values of the basic parameters, Ri* and $\alpha t_m/Ro^2$, which are in the thick cylinder region of Figures 5.1 and 5.2. If parameter values are chosen which are in the thick cylinder region until a certain dimensionless time, the temperature histories of Figure 6.1 apply up to that value of dimensionless time only. Furthermore, Figure 6.1 could be modified to apply to any other thermally-thick cylinder of different material or weapon yield by simply finding the maximum temperature and using this to modify the ordinate scale. Figure 6.1 also shows that the surface temperature histories are approximately proportional to the cosine of the cylinder angle, ϕ. This is true because the irradiance received on the cylindrical surface is also proportional to this cosine (see equation (2)) and because angular conduction is negligible for all thick cylinders. It is emphasized that because angular conduction is unimportant in thick cylinders, the temperature history of a thick cylinder represents the minimum values of temperature a cylinder of given material will have.

Figure 6.2 presents the temperature histories for $\alpha t_m/Ro^2 = 0.001$. Figures 5.1 and 5.2 show that these cylinders are thermally-thick for all inner radius ratios up to 0.6. However, cylinders having the ratio of 0.9 become increasingly thinner with time. Also, angular conduction is insignificant for all inner radius ratios considered and for dimensionless time values up to 20. Hence, the temperature histories of Figure 6.2 for the radius of 0.9 are representative of

the non-thick cylinders for which angular conduction is negligible. The surface temperature histories of Figure 6.2 are also proportional to the cosine of the cylinder angle since angular conduction is negligible for these non-thick cylinders. The cylinders having a radius ratio of 0.9 are near the thick cylinder region at the time where the maximum thick cylinder temperature would have occurred. Hence, the maximum temperature is only slightly increased and the cylinder is thick enough to cause the temperature to decrease as the thermal radiation pulse decreases with time (see Figure 1.1). However, at a later time the cylinder becomes sufficiently thin so that the surface temperature will rise even though the heating pulse is at its low values. This behavior is characteristic of cylinders in this region unless they become sufficiently thin before the thick cylinder maximum temperature has occurred. In this case, the maximum temperature may not occur until the end of the heating pulse. Thus, cylinders which are not thick and which have negligible angular conduction can be expected to have relatively high temperatures on their heated surface.

Figure 6.3 presents the temperature histories for $\alpha t_m/Ro^2 = 0.01$. Figure 5.1 shows that these cylinders which have an inner radius ratio up to 0.6 are thermally-thick for dimensionless time up to 2.0. However, the cylinders which have radius ratios of 0.8 and 0.9 are not thick except for very small values of dimensionless time. Also, angular conduction is insignificant for dimensionless time up to 5.0, but then becomes increasingly more important as time is increased. The increasing effect of angular conduction is evident in the surface temperature histories of Figure 6.3 for a radius ratio of 0.9. Thus, the temperature histories for a radius ratio of 0.8 or 0.9 are representative of non-thick cylinders where angular conduction becomes important after the time where the maximum thick cylinder temperature would have occurred. It is seen that the behavior of the temperature history is altered by the development of angular conduction. That is, the cylinder of radius ratio 0.9 is sufficiently thin that its temperature at $\phi = 0^o$ might be expected to increase continuously throughout the exposure. However, angular conduction ultimately becomes sufficiently important to reverse the temperature rise (and cause a peak in the temperature history). Therefore a lower maximum temperature is reached than would occur in the absence of angular conduction. In the case of the cylinder having a radius ratio of 0.8, the first maximum in temperature is due to the cylinder being nearly thick at that time. But the second and larger temperature maximum has been limited by the development of angular conduction. The temperature histories for radius ratios up to 0.6 are representative of cylinders which are thermally-thick at the time when the maximum thick-cylinder temperature occurs. The temperature history of these cylinders is not radically altered by the later development of angular conduction. In summary, angular conduction is helpful in limiting the maximum temperature in these cylinders but its effect is rather small when the angular conduction is relatively late in developing.

12

Figure 6.4 presents the temperature histories for $\alpha t_m/Ro^2 = 0.1$. Figure 5.1 indicates that these cylinders leave the thermally-thick region and develop significant angular conduction at very small values of dimensionless time. The temperature histories of Figure 6.4 are representative of those cylinders which are not thick and which have significant angular conduction at the time when the maximum thick cylinder temperature would have occurred ($t* \approx 1.8$). In this figure, the initial temperature rises are governed by the thinness of the cylinders. But the rises are reversed after a short time due to the increasing effect of angular conduction. Angular conduction serves to reduce the temperatures at approximately equal values of time for all of the radius ratios shown. This happens because the development of angular conduction is practically independent of the radius ratio (or cylinder thickness). This behavior is indicated by the location of the boundary (broken line) for angular conduction in Figures 5.1 and 5.2. This independence of angular conduction, along with the fact that these cylinders are thermally-thin for all but small values of time, causes the temperature histories in Figure 6.4 to vary almost directly with cylinder thickness. Also, these temperature histories would rise to much higher values if it were not for the rapid development of angular conduction. Thus, angular conduction is very important in limiting temperatures for this type of cylinder. The surface temperature histories of Figure 6.4 show that angular conduction limits temperature on the heated surface ($-90^\circ < \phi < +90^\circ$) and results in large temperature increases on the unheated surface.

DISCUSSION AND CONCLUSION

The primary purpose of this report was to prepare a set of charts which will allow a quick estimate to be made of the temperature distribution and history in a large class of cylinders. This was accomplished by computing detailed temperature histories in terms of the dimensionless parameters which characterize the cylinder and the thermal radiation output of the weapon. These calculations considered cylinders of constant thermophysical properties (k, ρ, and c) but did not consider radiation cooling on the outer or inner surfaces or convective cooling on the inner surface. However, these restrictions do not seriously limit the utility of this report. The error due to variable thermophysical properties is not large if the temperature rise is not large. For example, aluminum alloys which find wide shipboard applications cannot be heated to more than a few hundred degrees centigrade or they will rapidly lose much of their strength. Also, these errors can be reduced by estimating the expected temperature rises and selecting values of the thermophysical properties midway between the initial and expected maximum temperature values. The error due to omitting cooling is also small for most practical shipboard applications. This is true because the cooling mechanisms require high temperatures in order to transfer heat at rates which are comparable to those of the nuclear thermal radiation pulse.

13

The work of this report showed that the temperature behavior of cylinders can be described by a dimensionless temperature, T^*, and two basic dimensionless parameters, Ri^* and $\alpha t_m/Ro^2$. It was found that the individual effects due to varying the size or material of the cylinder, and to a lesser extent the cylinder thickness and weapon yield were difficult to isolate from each other. Also, it was shown that the effect of varying the basic parameters on cylinder temperatures depended on the way in which heat is internally transferred.

The design of a cylinder to withstand a given thermal radiation exposure will require, in general, that the temperature history of several candidate cylinders be considered. But the general principles of temperature behavior in cylinders as given in this report can be used to limit the number of candidate cylinders. For example, if an application requires a cylinder of given size, it is possible to determine from Figure 3.1 the approximate range of material properties that would limit the maximum temperature to an acceptable value. From these properties, candidate cylinders could be selected and detailed temperature histories derived from the figures of Appendix A. The internal heat transfer pattern can also be used as a guide in choosing cylinders. That is, it was shown that the thermally-thick cylinders have the minimum surface temperatures at any time. It was also shown that the surface temperatures increase as the cylinder becomes thinner but decrease as the angular conduction increases. Thus Figures 5.1 and 5.2 are schematic illustrations of how the surface temperature can be expected to change as values of the basic parameters are varied. Finally, Figures 6.1 - 6.4 indicate the relative quantitative influence of changing the basic parameters.

REFERENCES

(1)   Bergman, P., Heilferty, R., and Griff, N., "Temperature Response
      Charts for Opaque Plates.Exposed to the Thermal Radiation
      Pulse from a Nuclear Detonation," Naval Applied Science
      Laboratory, Lab Project 940-105, Progress Report 10, July 1969

(2)   Glasstone, S., "Effects of Nuclear Weapons," U.S. Atomic
      Energy Commission, p. 359, Revised Edition Reprinted
      February 1964

(3)   Cohen, M. L., Koch, J. E., and Heilferty, R. J., "A Numerical
      Technique to Determine the Thermal Histories of
      Two-Dimensional Solids Exposed to the Thermal Pulse of a
      Nuclear Weapon," Naval Applied Science Laboratory,
      Lab Project 940-105, Progress Report 5, Jan 1968

(4)   Kaufman, R. and Heilferty, R. J., "Equations and Computer
      Program to Calculate the Temperature Distribution and History
      in a Cylinder Subject to Thermal Radiation From a Nuclear
      Weapon," Naval Applied Science Laboratory, Lab Project 940-105,
      Progress Report 8, July 1968

(5)   Carslaw, H. S., and Jaegar, J. C., Conduction of Heat in Solids,
      Clarendon Press, Oxford, p. 275, p. 56, 1950

(6)   Kreith, F., Principles of Heat Transfer, International Textbook
      Company, Scranton, Penn., p. 593 and p. 411, 1966

TABLE 1

THERMAL PROPERTIES AND OUTER RADIUS VALUES
OF 6061-T6 ALUMINUM CYLINDERS

1. Thermal Properties of 6061-T6 Aluminum at 200°C

    Conductivity = 0.397 cal/sec-cm-$^\circ$C

    Density = 2.71 gm/cm^3

    Specific Heat = 0.23 cal/gm-$^\circ$C

2. Outer Radius Values of the 6061-T6 Aluminum Cylinders

$\alpha t_m/Ro^2$	Ro (cm)
0.10000	2.52
0.05000	3.57
0.02500	5.05
0.01000	7.98
0.00500	11.29
0.00200	17.35
0.00100	25.24
0.00050	35.69
0.00025	50.48
0.00010	79.81
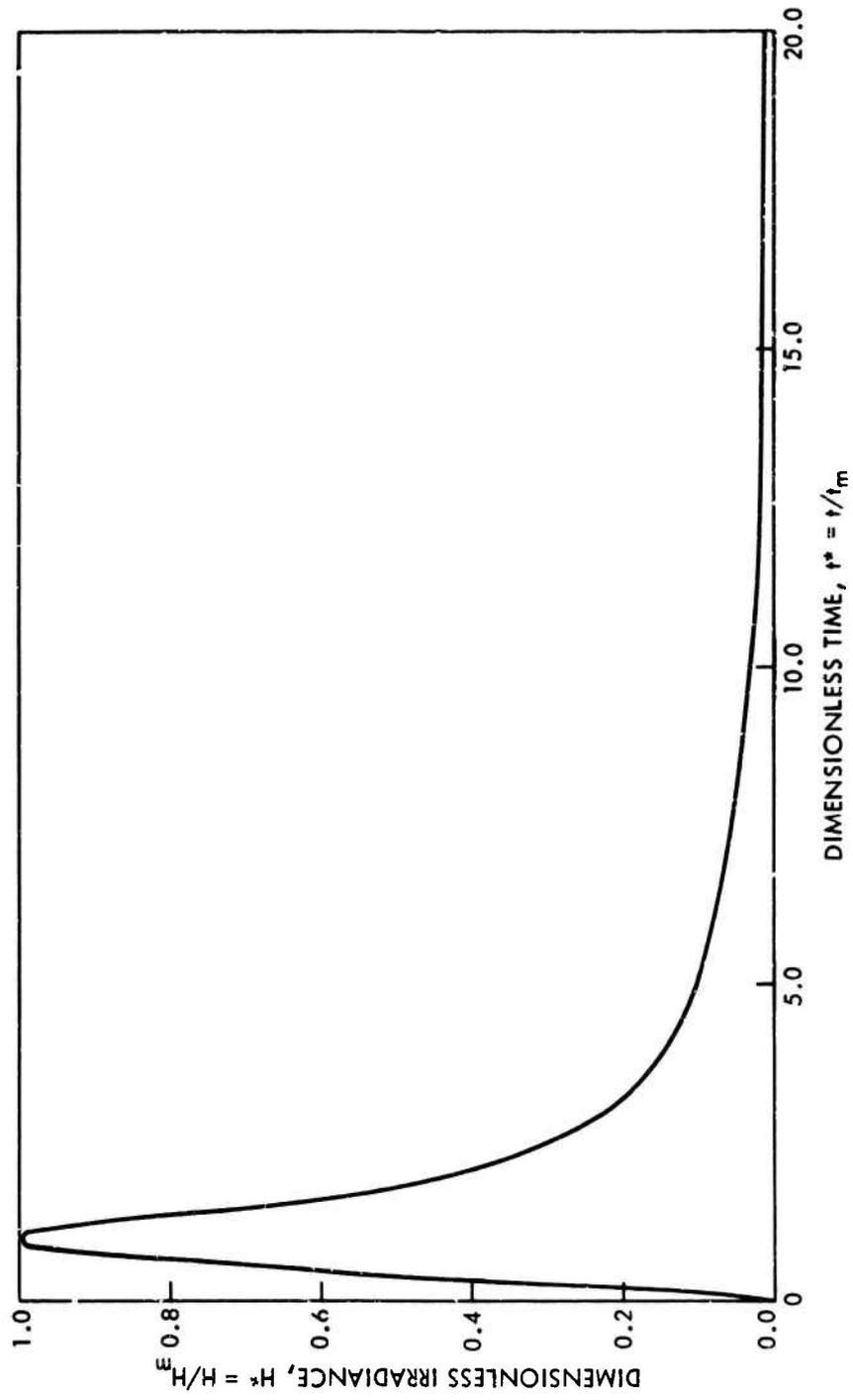
FIG. 1.1 IRRADIANCE HISTORY OF THE NUCLEAR WEAPON THERMAL RADIATION PULSE
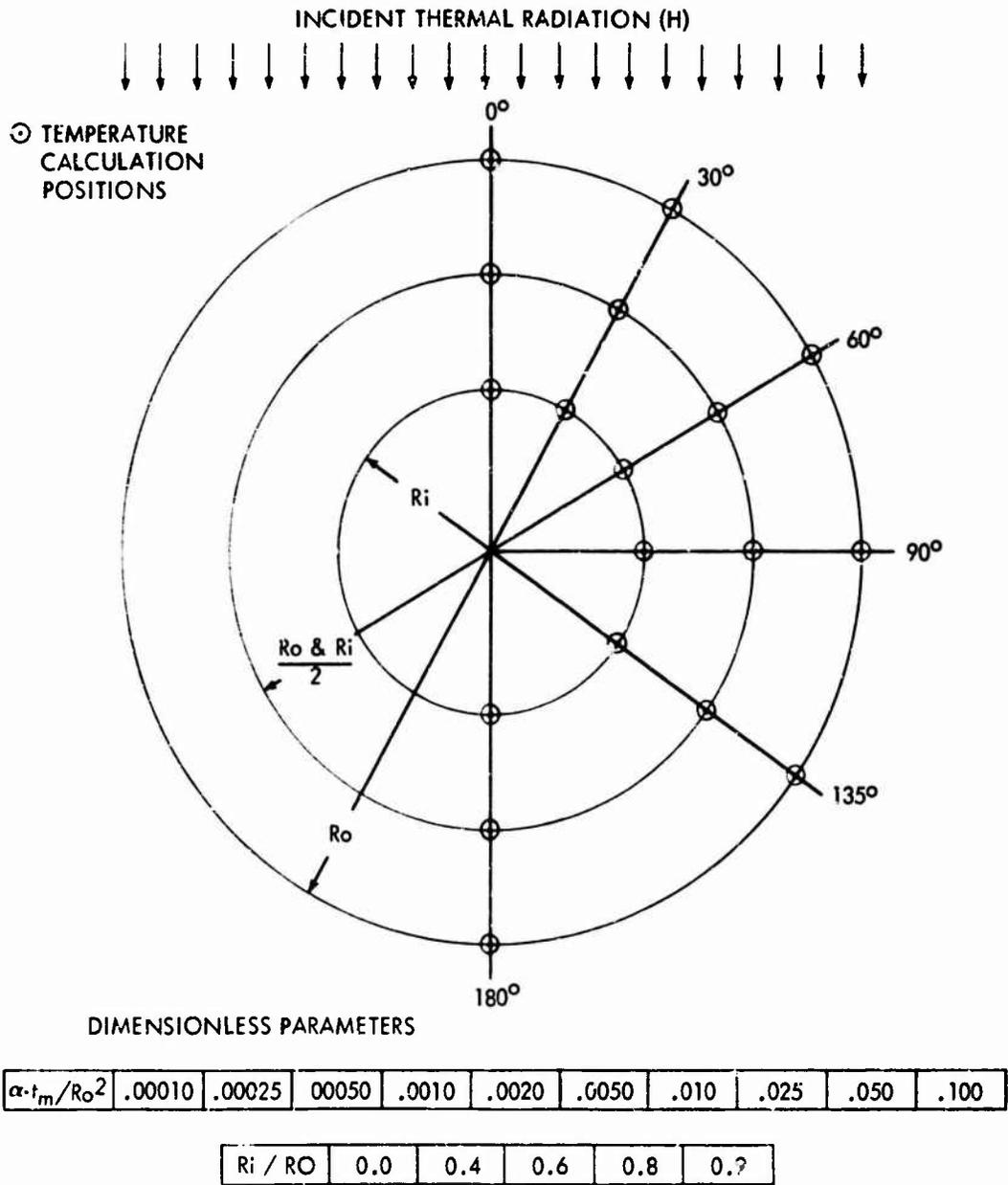
FIG. 2.1 DIMENSIONLESS PARAMETERS AND CYLINDRICAL POSITIONS FOR
WHICH TEMPERATURE CALCULATIONS ARE MADE
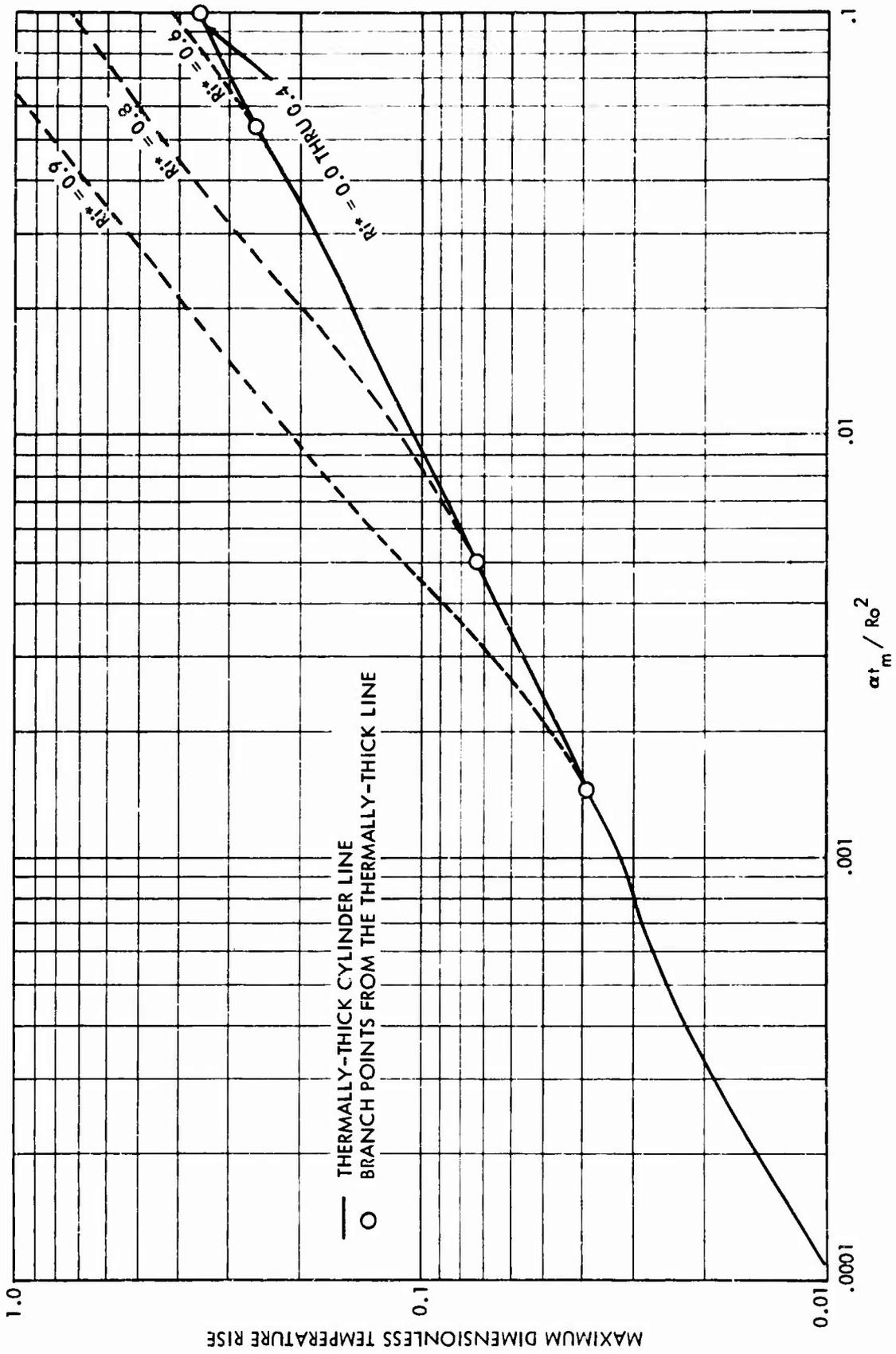
FIG. 3.1 MAXIMUM DIMENSIONLESS TEMPERATURE RISE FOR CYLINDERS EXPOSED TO THE THERMAL RADIATION PULSE OF A NUCLEAR WEAPON
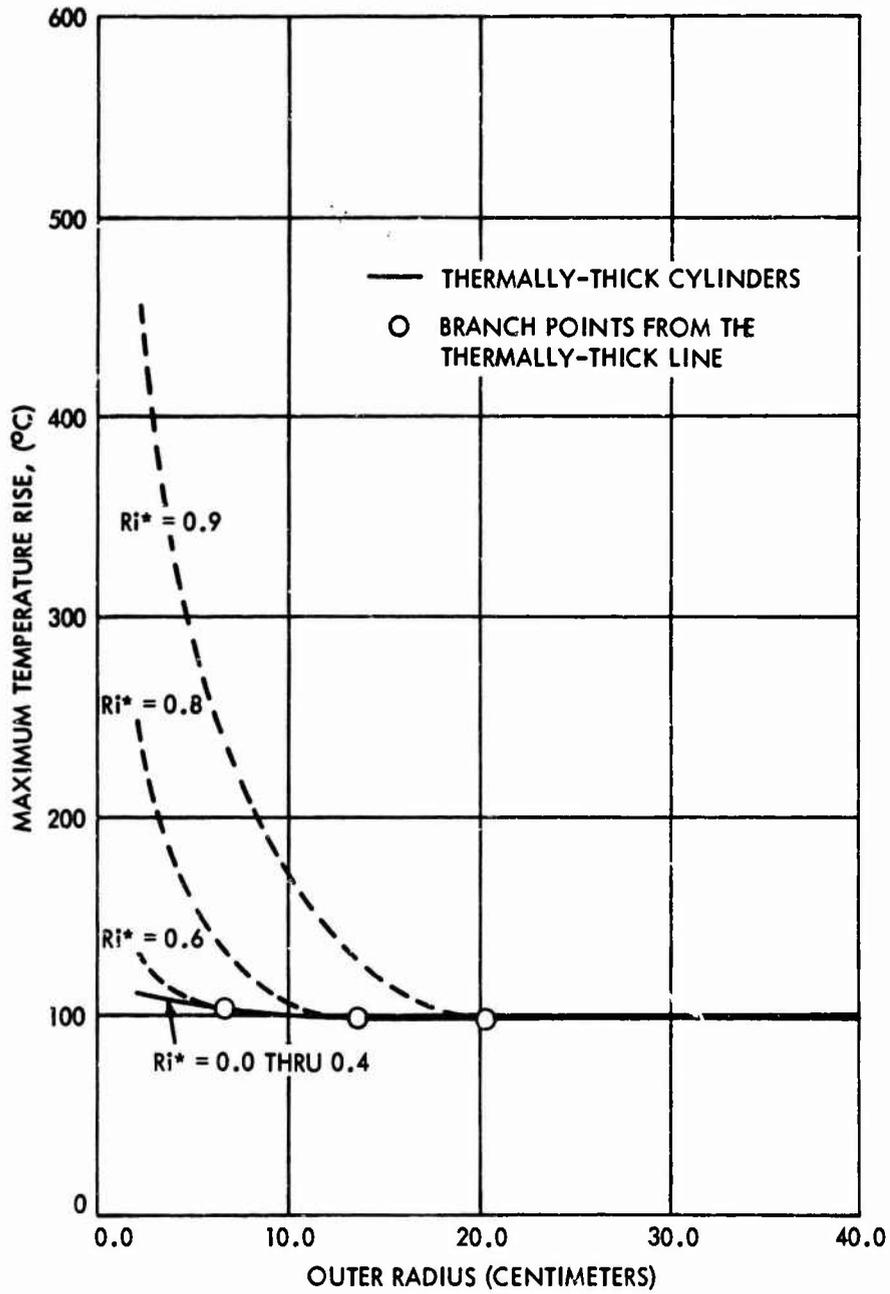
FIG. 4.1 THE EFFECT OF CYLINDER WALL THICKNESS ON THE MAXIMUM TEMPERATURE RISE IN CYLINDERS EXPOSED TO THE THERMAL RADIATION PULSE OF A NUCLEAR WEAPON
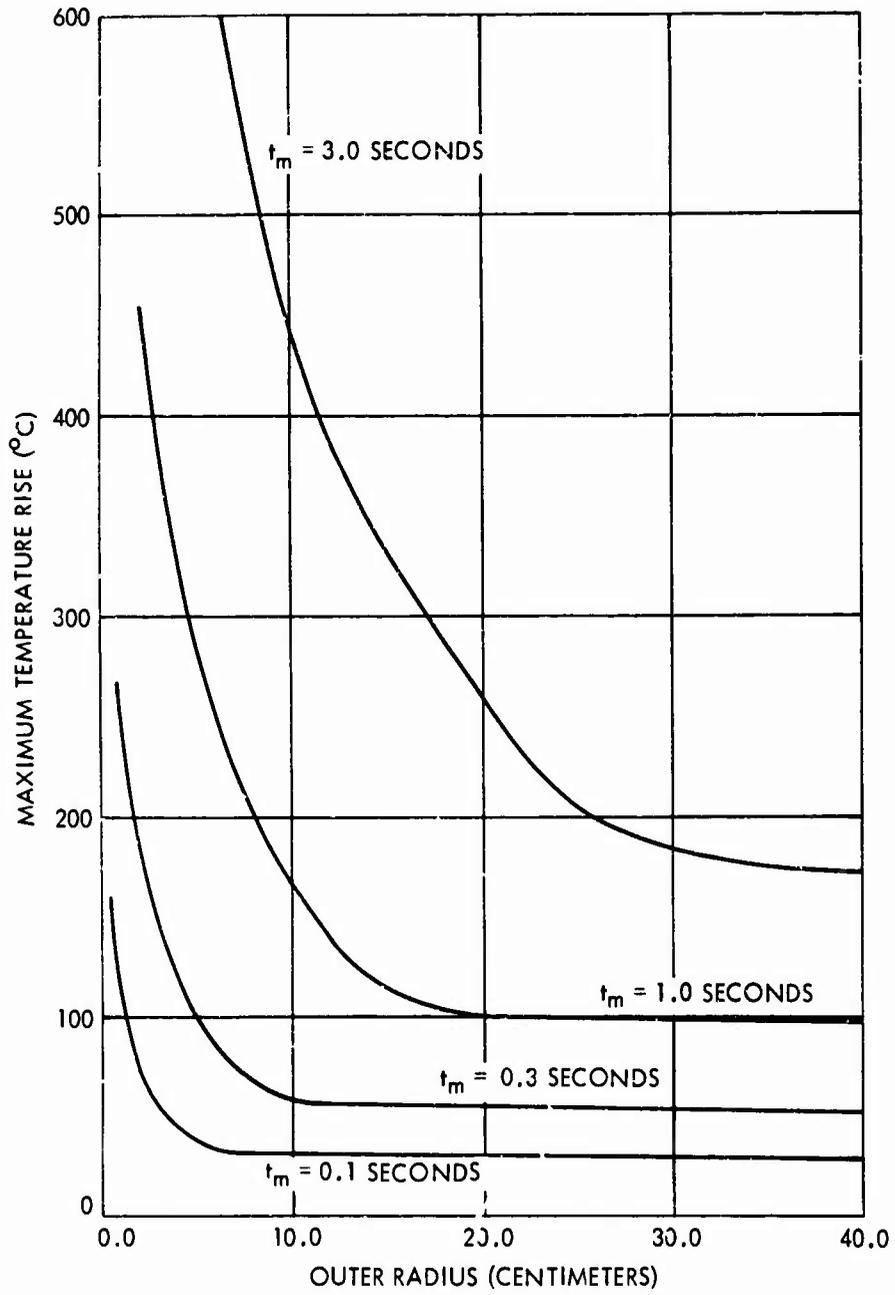
FIG. 4.2 THE EFFECT OF WEAPON YIELD ON THE MAXIMUM TEMPERATURE RISE IN
CYLINDERS EXPOSED TO THE THERMAL RADIATION PULSE OF A NUCLEAR WEAPON
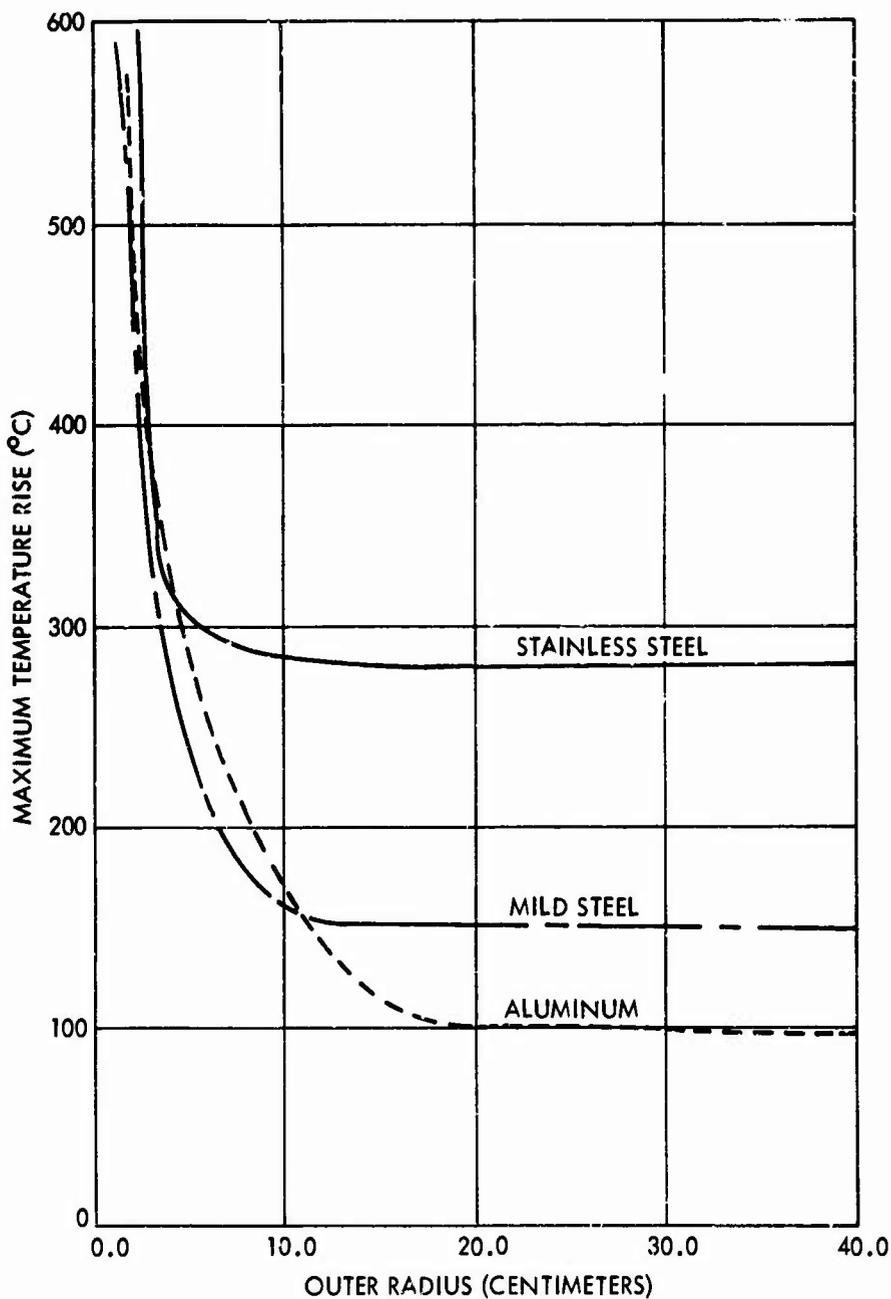
FIG. 4.3 THE EFFECT OF CYLINDER MATERIAL ON THE MAXIMUM TEMPERATURE RISE
IN CYLINDERS EXPOSED TO THE THERMAL RADIATION PULSE OF A NUCLEAR
WEAPON
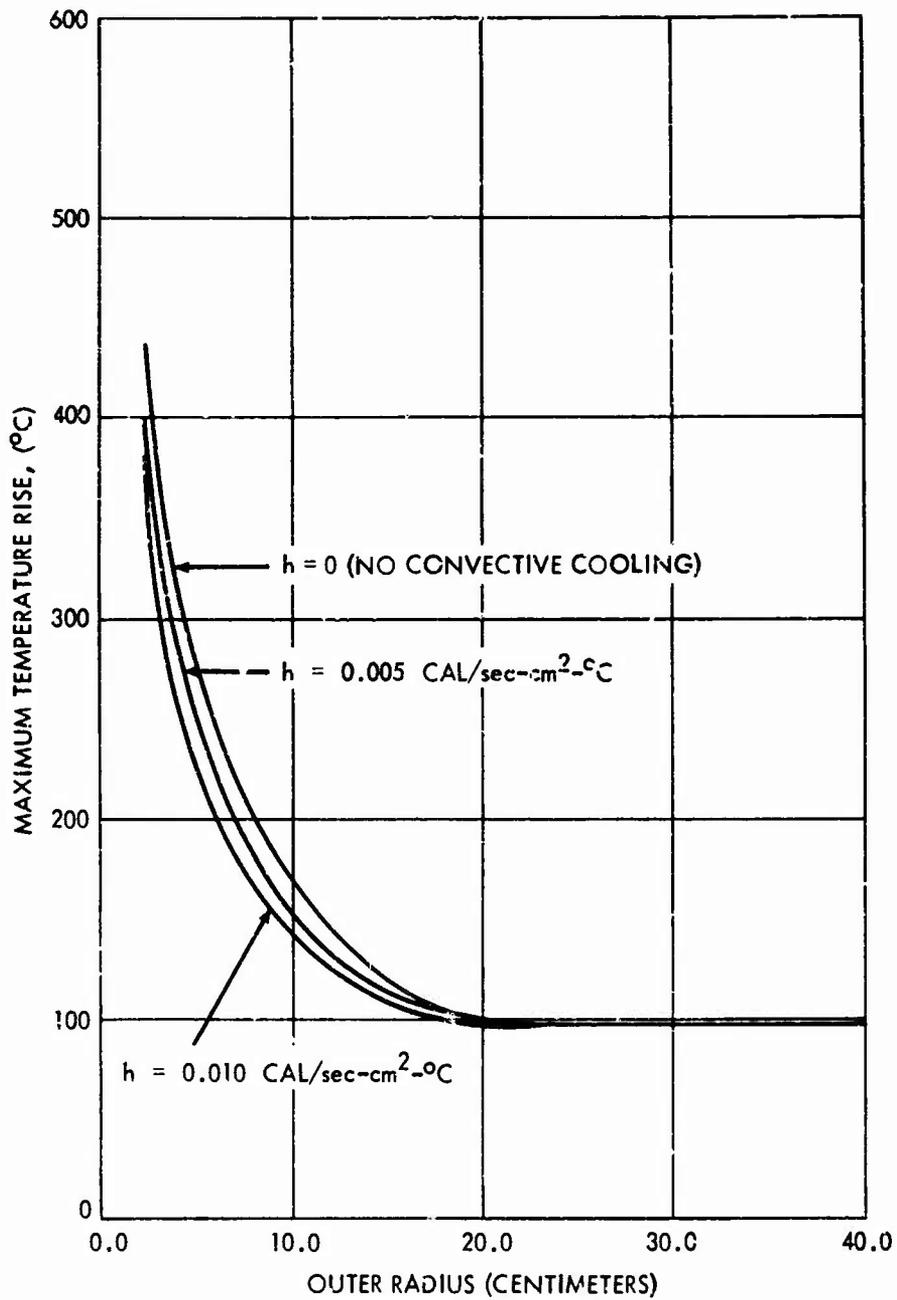
FIG. 4.4 THE EFFECT OF CONVECTIVE COOLING ON THE MAXIMUM TEMPERATURE RISE IN CYLINDERS EXPOSED TO THE THERMAL RADIATION PULSE OF A NUCLEAR WEAPON
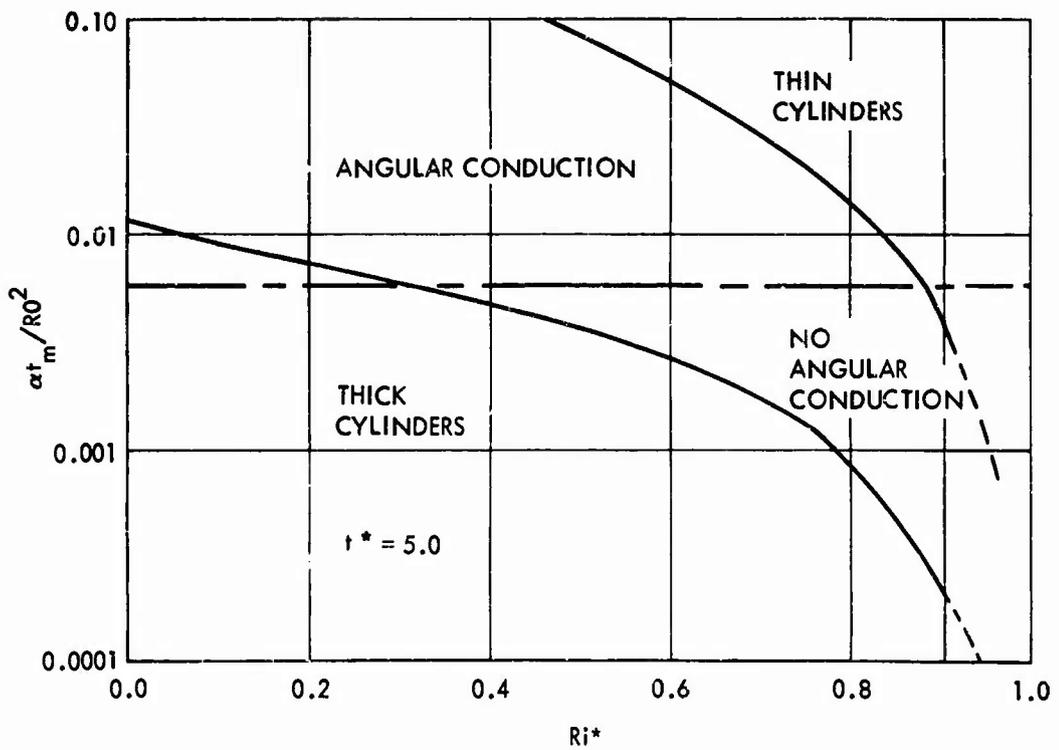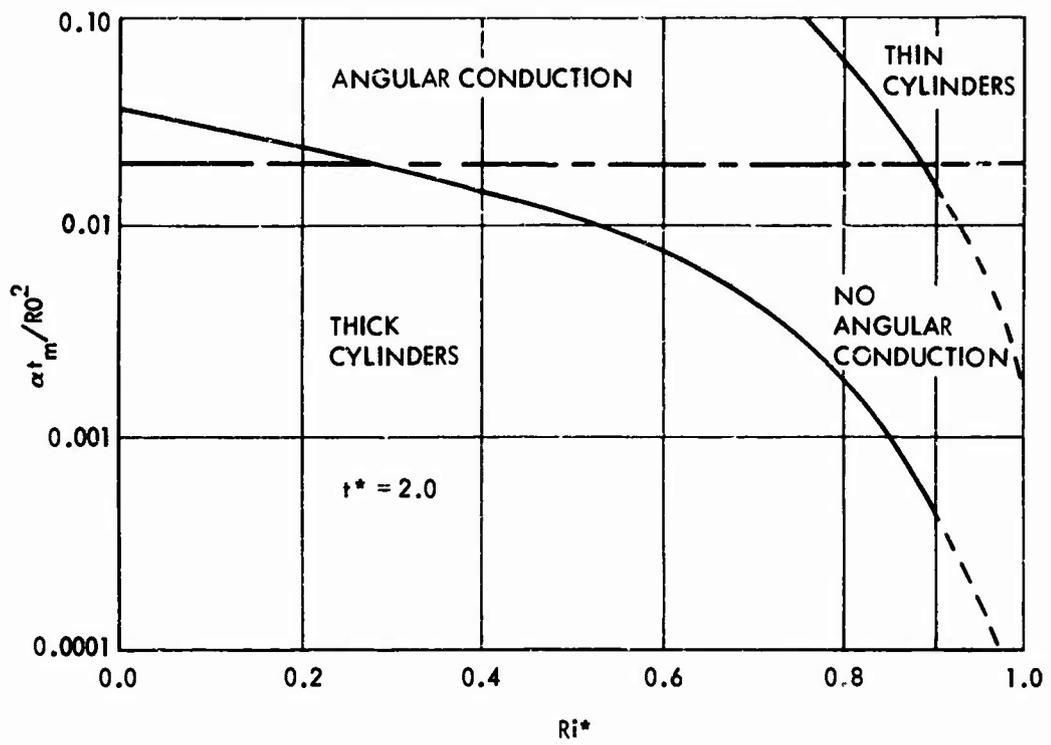
FIG. 5.1 HEAT TRANSFER REGIONS AT DIMENSIONLESS TIMES OF 2.0, AND 5.0 FOR
CYLINDERS EXPOSED TO THE THERMAL RADIATION PULSE OF A NUCLEAR WEAPON
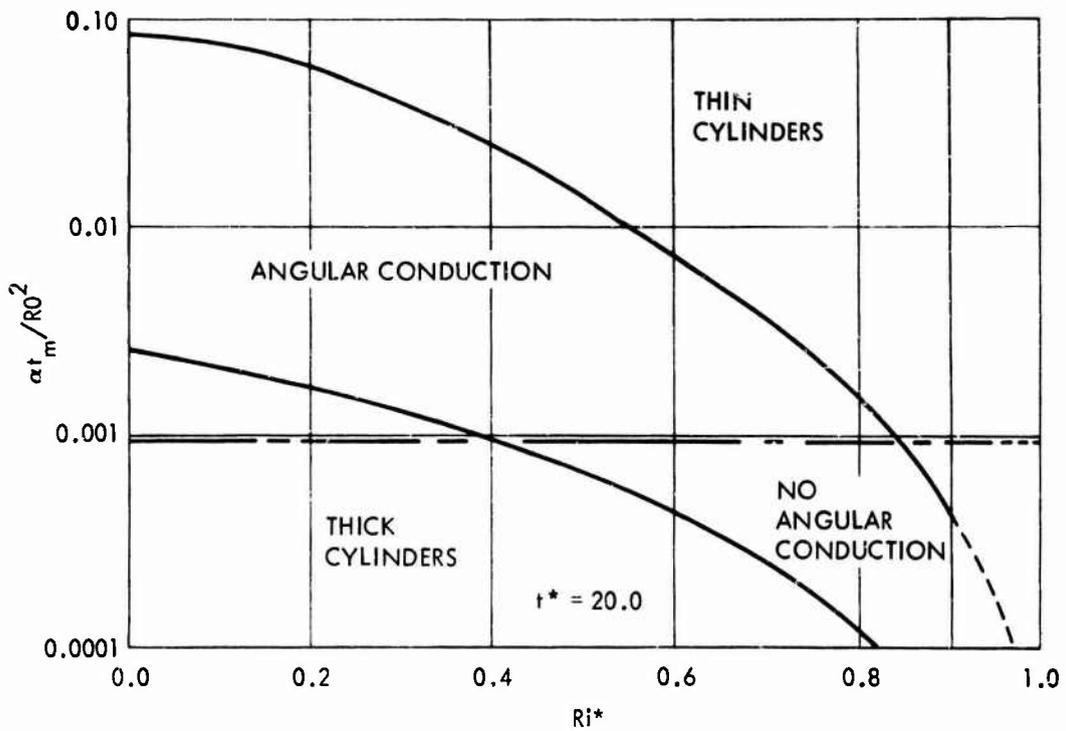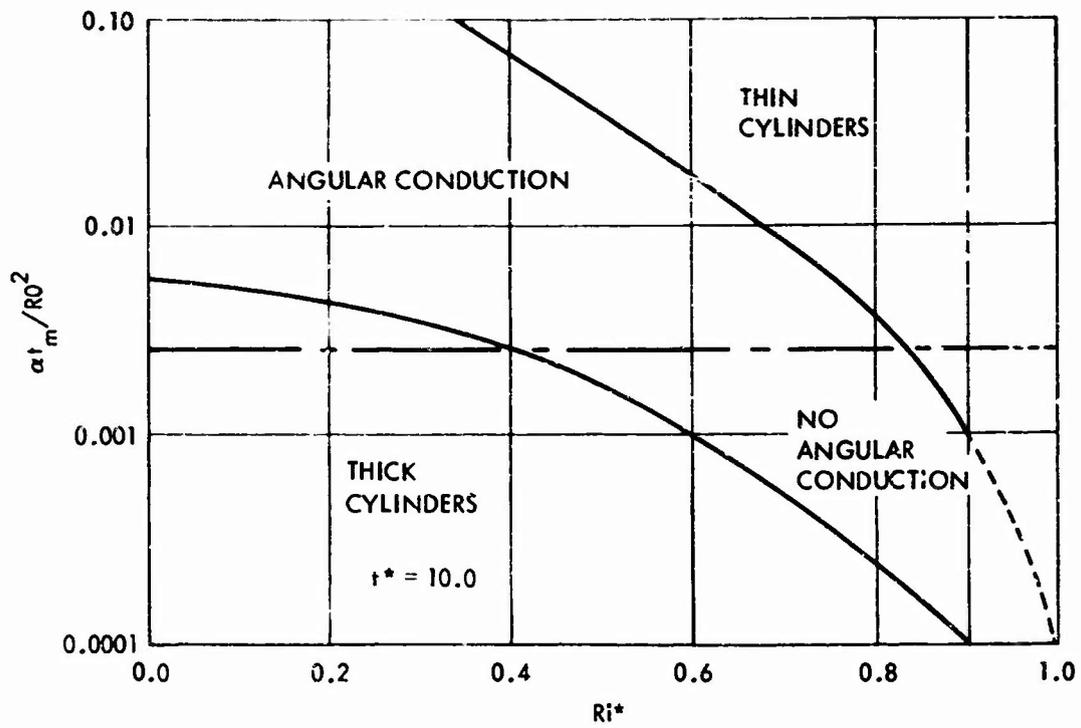
FIG. 5.2 HEAT TRANSFER REGIONS AT DIMENSIONLESS TIMES OF 10.0 AND 20.0 FOR CYLINDERS
EXPOSED TO THE THERMAL RADIATION PULSE OF A NUCLEAR WEAPON
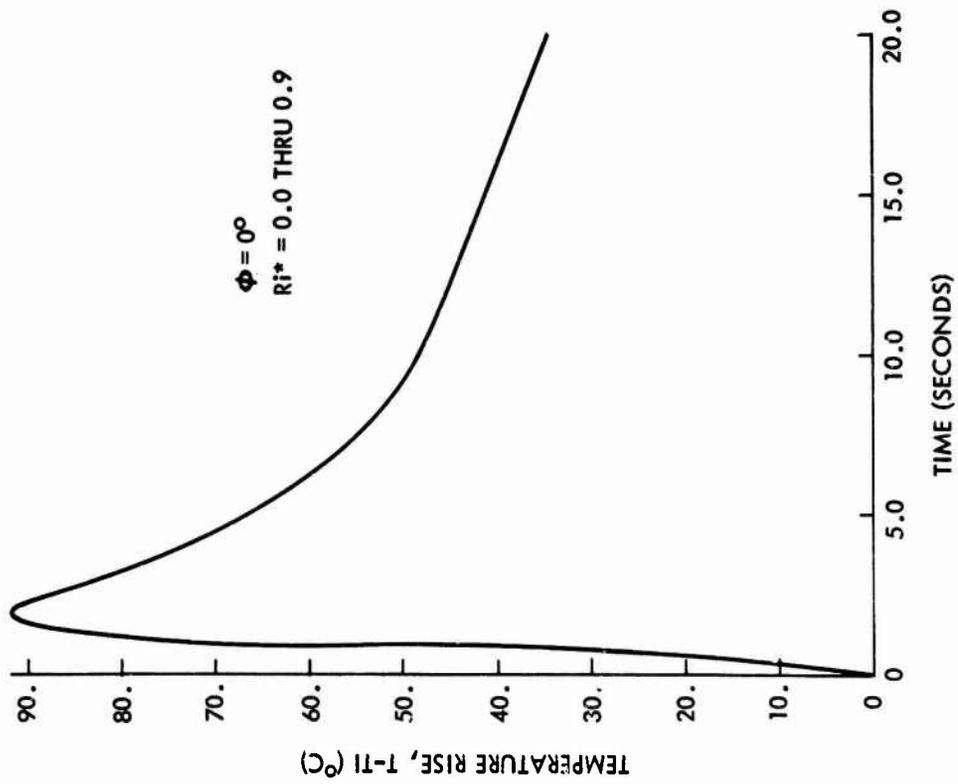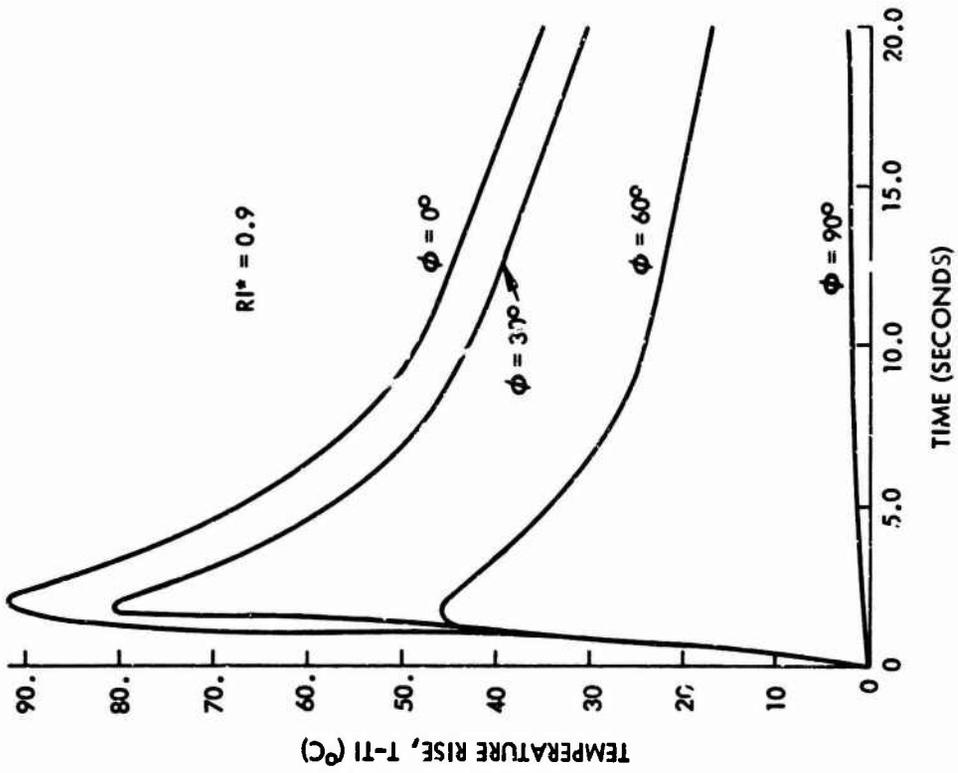
FIG. 6.1 SURFACE TEMPERATURE HISTORIES FOR CYLINDERS EXPOSED TO
THE THERMAL RADIATION PULSE OF A NUCLEAR WEAPON ($\alpha t_m / R_o^2 = 0.0001$)
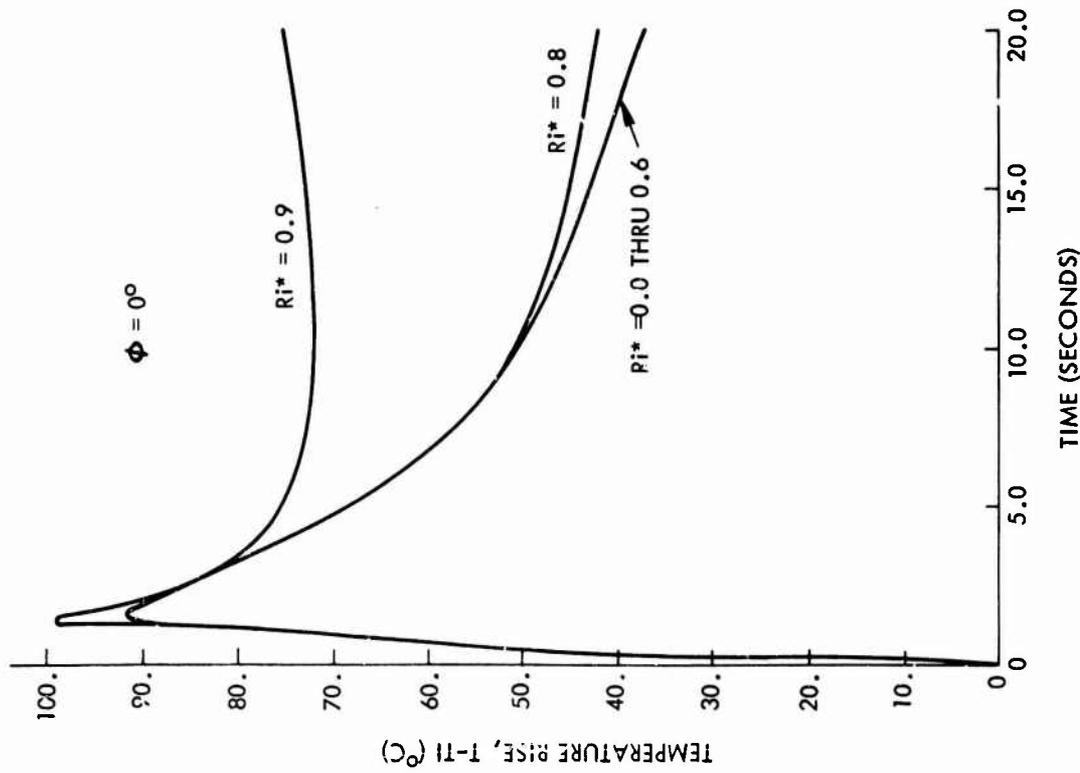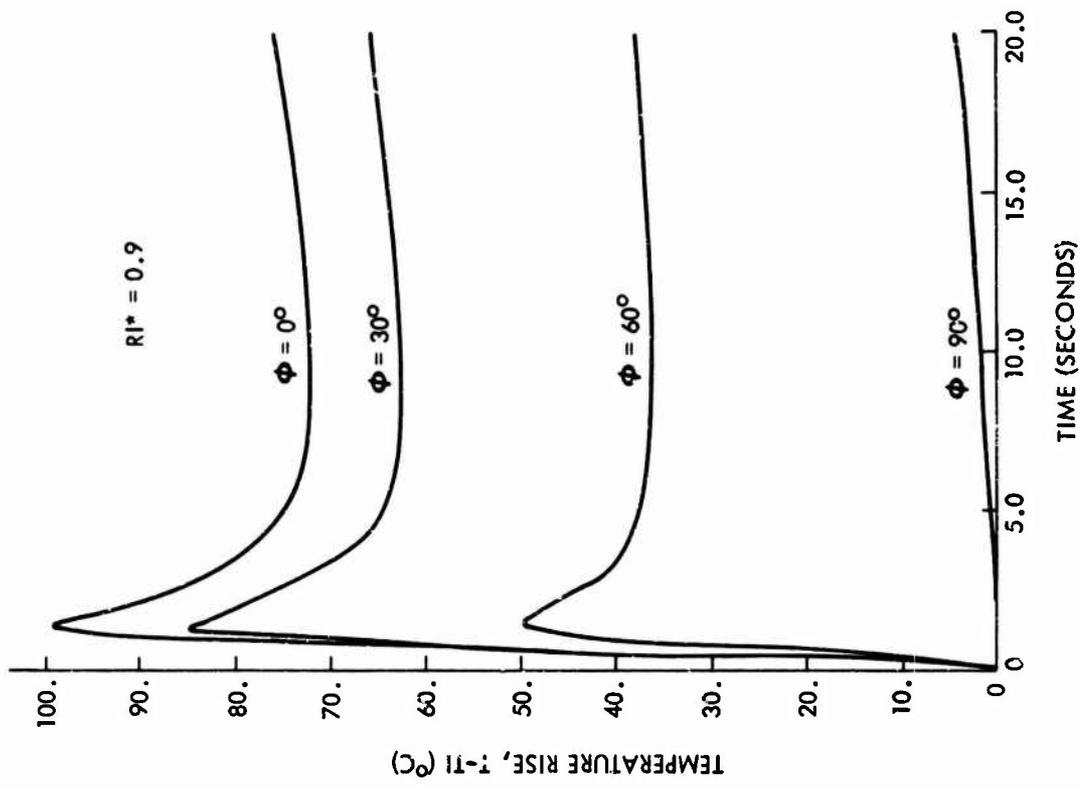
FIG. 6.2 SURFACE TEMPERATURE HISTORIES FOR CYLINDERS EXPOSED TO THE THERMAL RADIATION PULSE OF A NUCLEAR WEAPON ($\alpha\, t_m\, /\, R_o^2 = 0.001$)
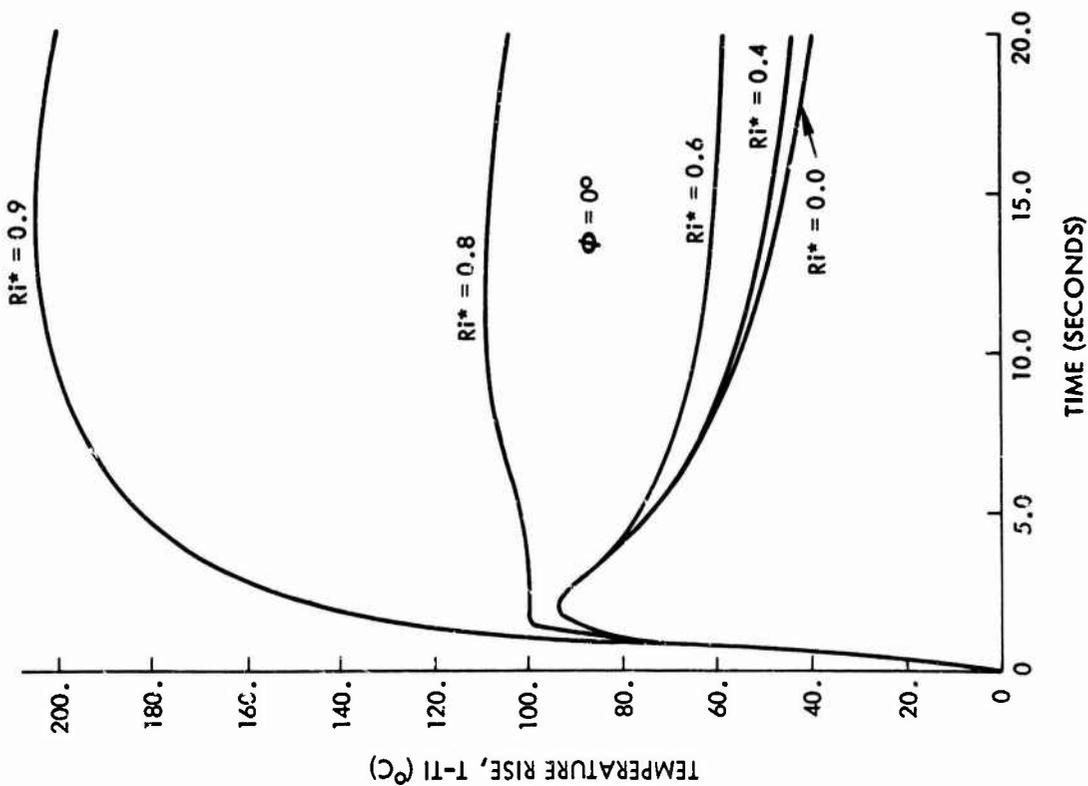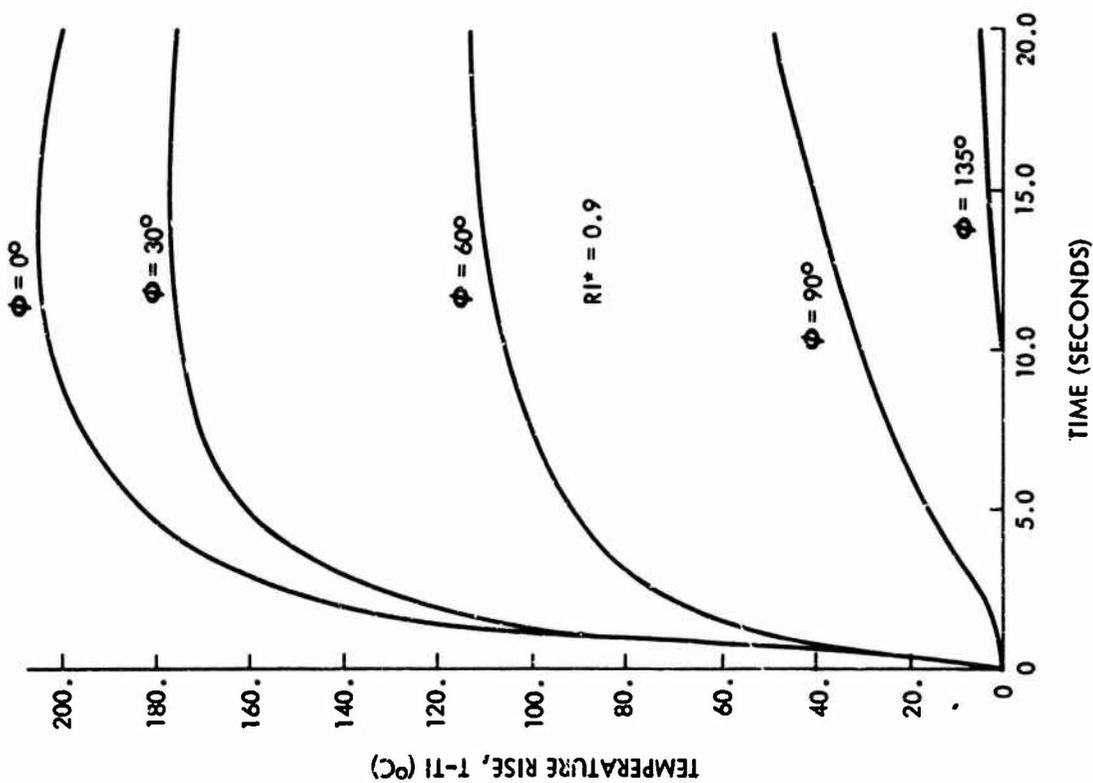
FIG. 6.3 SURFACE TEMPERATURE HISTORIES FOR CYLINDERS EXPOSED TO
THE THERMAL RADIATION PULSE OF A NUCLEAR WEAPON ($\alpha t_m / R_o^2 = 0.01$)
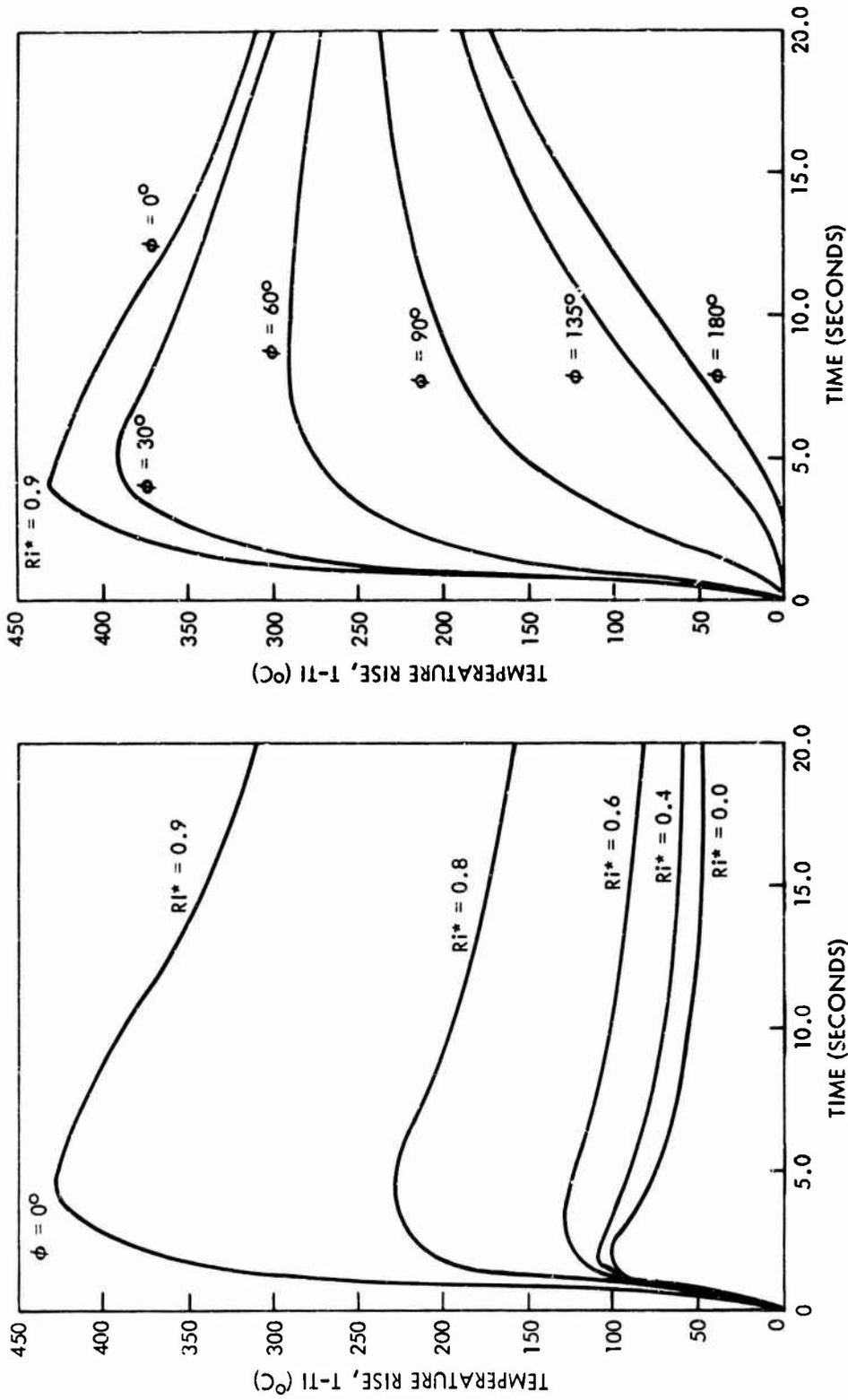
FIG. 6.4 SURFACE TEMPERATURE HISTORIES FOR CYLINDERS EXPOSED TO THE THERMAL RADIATION PULSE OF A NUCLEAR WEAPON ($\alpha t_m / R_0^2 = 0.1$)

APPENDIX A

DIMENSIONLESS TEMPERATURE HISTORIES

Dimensionless temperature plotted against dimensionless time is presented in this section for selected values of the basic dimensionless parameters, $\alpha t_m/Ro^2$ and Ri^*, and for cylinder positions which were given in Figure 2.1. The purpose of these plots is to allow a rather complete temperature history to be obtained for a wide range of cylinders subjected to thermal radiation from a wide range of nuclear weapon burst conditions. Each plot consists of dimensionless temperature versus dimensionless time for the ten chosen values of the basic parameter, $\alpha t_m/Ro^2$. The plots are logrithmic for both the temperature and time axes. The minimum value of dimensionless temperature plotted is 0.001, hence curves for some of the ten parameter values will be missing if they consist of only lower dimensionless temperatures. Missing curves usually correspond to cases where the cylinders are not significantly heated by the nuclear weapon thermal radiation pulse.

The figures of this appendix will be organized in the following manner. Figures A.1 refer to an inner radius ratio (Ri^*) of 0.9. They contain sub-figures for the surface, midplane and backface dimensionless temperatures. Thus Figures A.1.1, A.1.2, and A.1.3 refer to the surface, midplane and backface temperatures, respectively, for the inner radius ratio of 0.9. Each of the above sub-figures will also contain sub-figures referring to the position angles. Third indices of 1 thru 6 will represent angles of 0°, 30°, 60°, 90°, 135° and 180°, respectively (see Appendix B and Figure B.1.1 for a further explanation of the index notation). Figures A.2, A.3, A.4 and A.5 are organized in an identical manner for inner radius ratios of 0.8, 0.6, 0.4 and 0.0. Appendix B will give examples on the use of the figures in Appendix A along with rules for the interpolation or extrapolation of results if the basic parameters differ from those given in the plots of Appendix A. All of the figures in Appendix A were generated by a Calcomp Plotter.
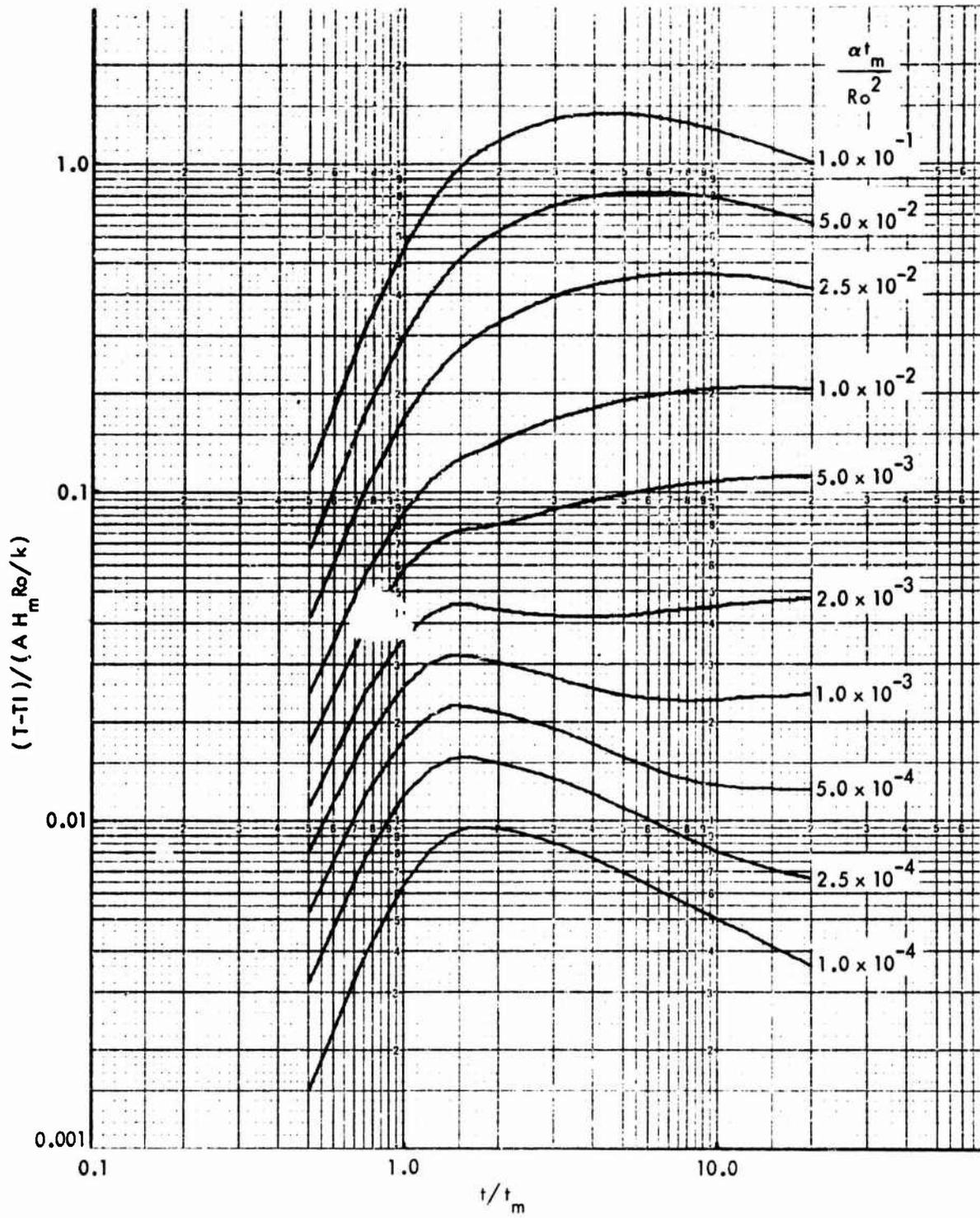
FIG. A-1.1.1   DIMENSIONLESS SURFACE TEMPERATURE HISTORIES ($Ri^* = 0.9, \phi = 0°$)
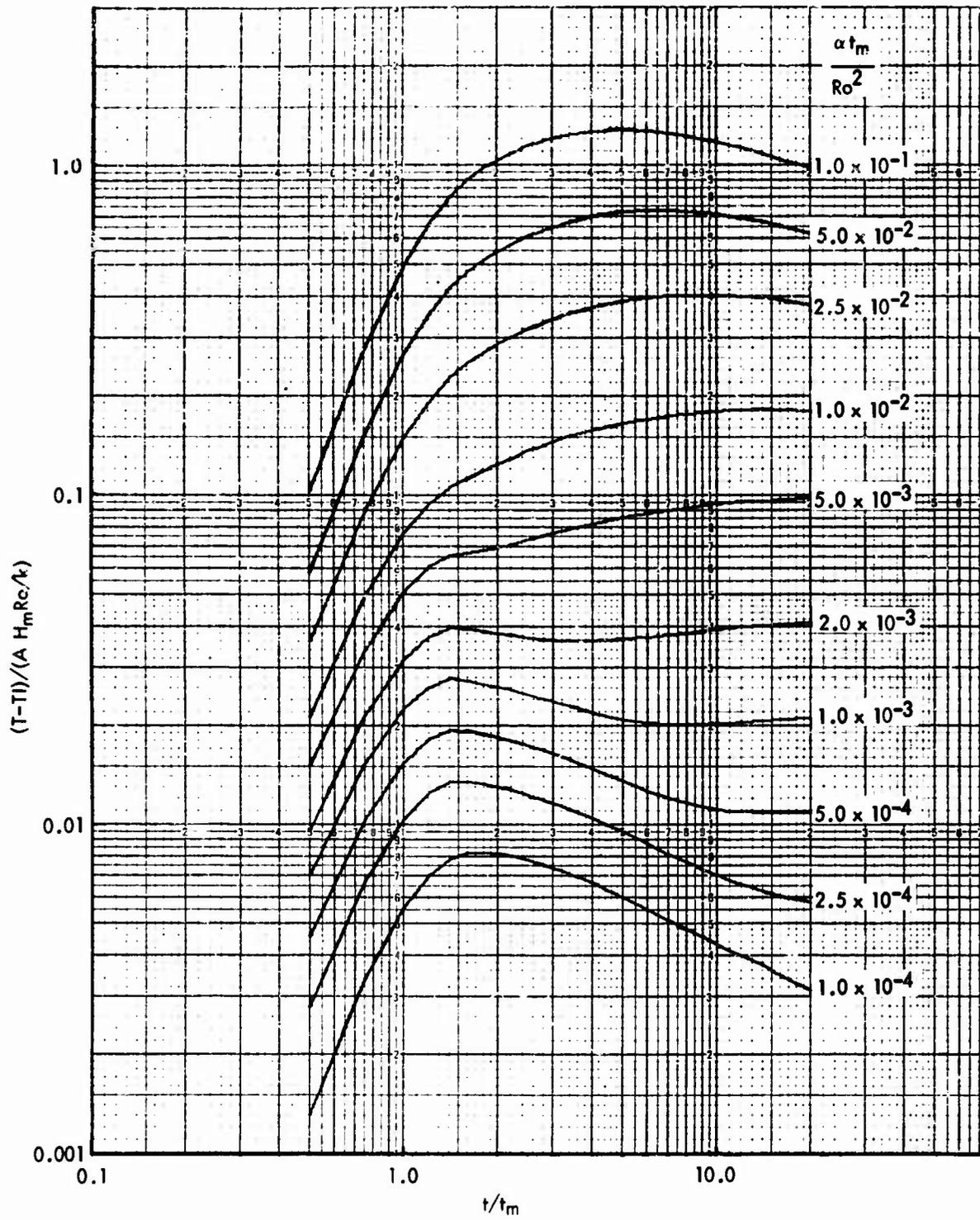
FIG. A – 1.1.2   DIMENSIONLESS SURFACE TEMPERATURE HISTORIES (Ri* = 0.9, ϕ = 30°)
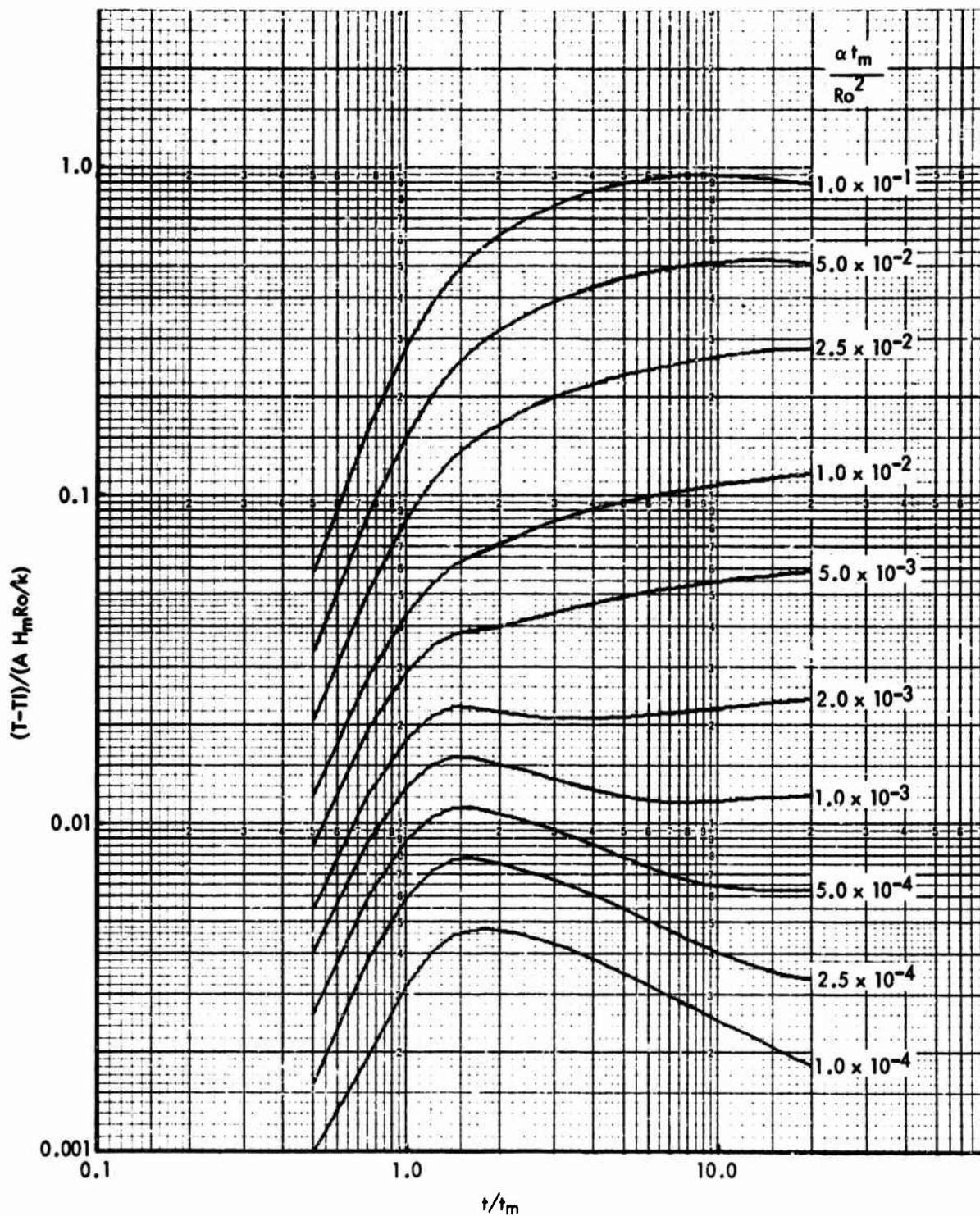
FIG. A - 1.1.3   DIMENSIONLESS SURFACE TEMPERATURE HISTORIES (Ri* = 0.9, $\phi = 60°$)
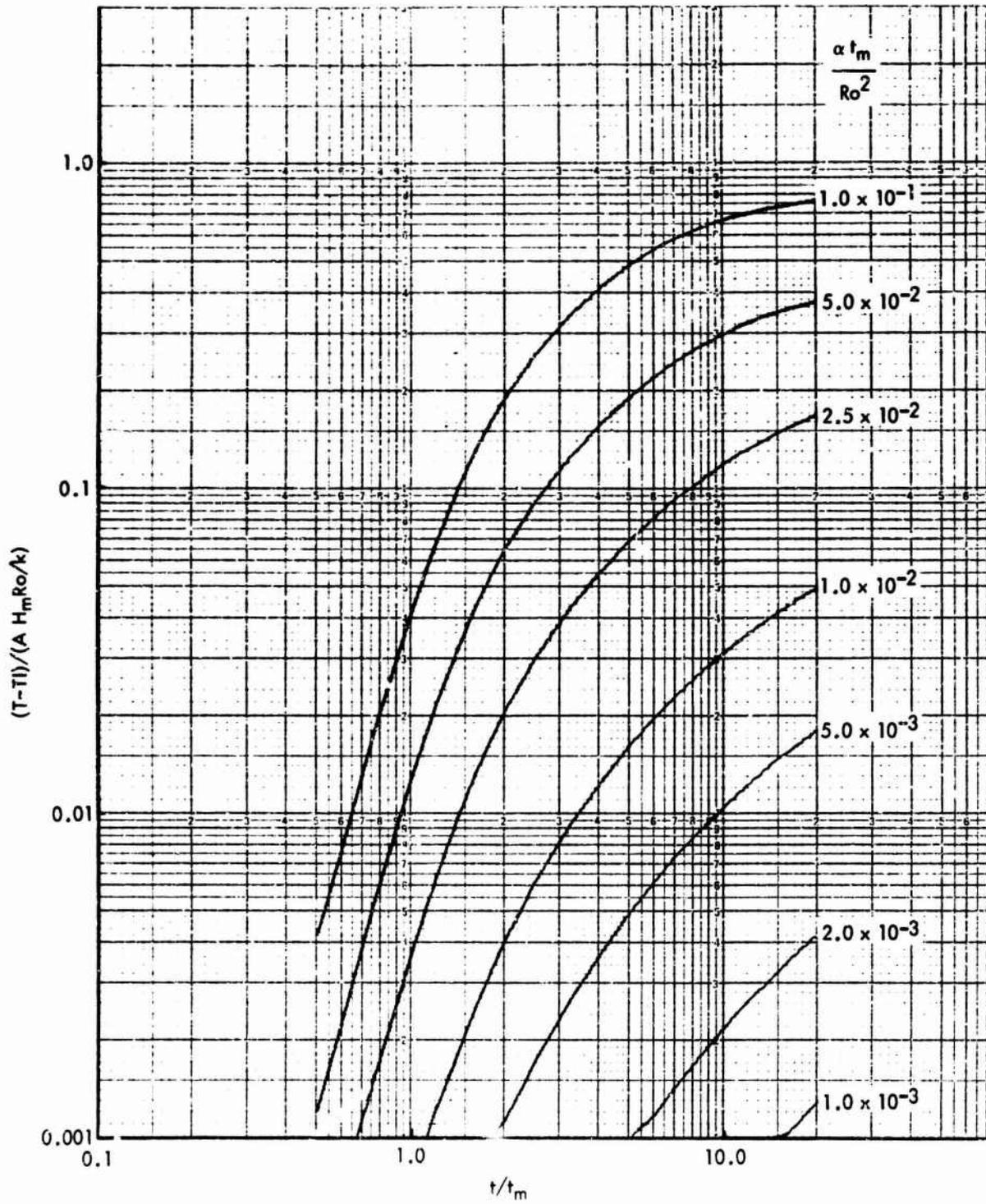
FIG. A – 1.1.4   DIMENSIONLESS SURFACE TEMPERATURE HISTORIES (Ri* = 0.9, ϕ = 90°)
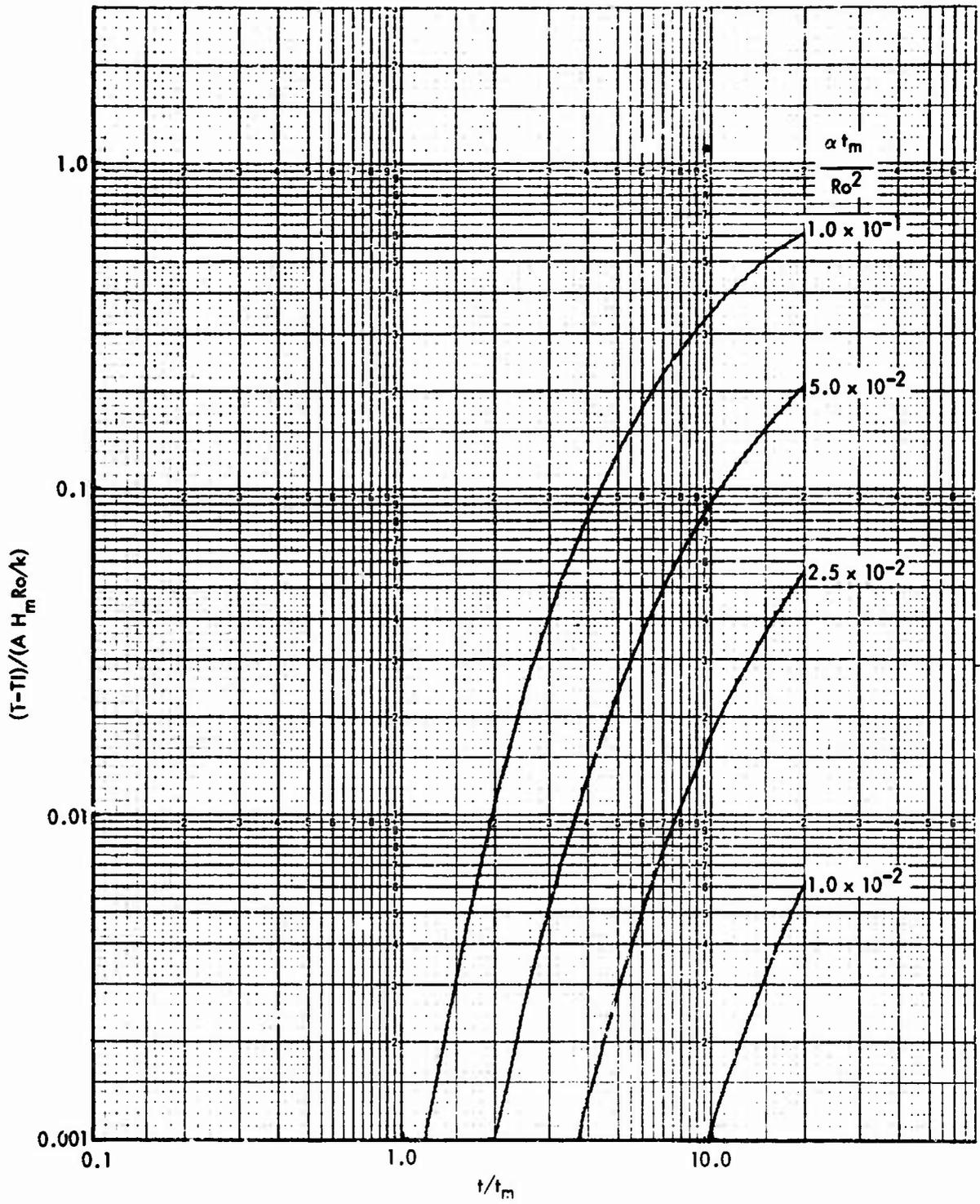
FIG. A - 1.1.5   DIMENSIONLESS SURFACE TEMPERATURE HISTORIES (Ri* = 0.9, ϕ = 135°)
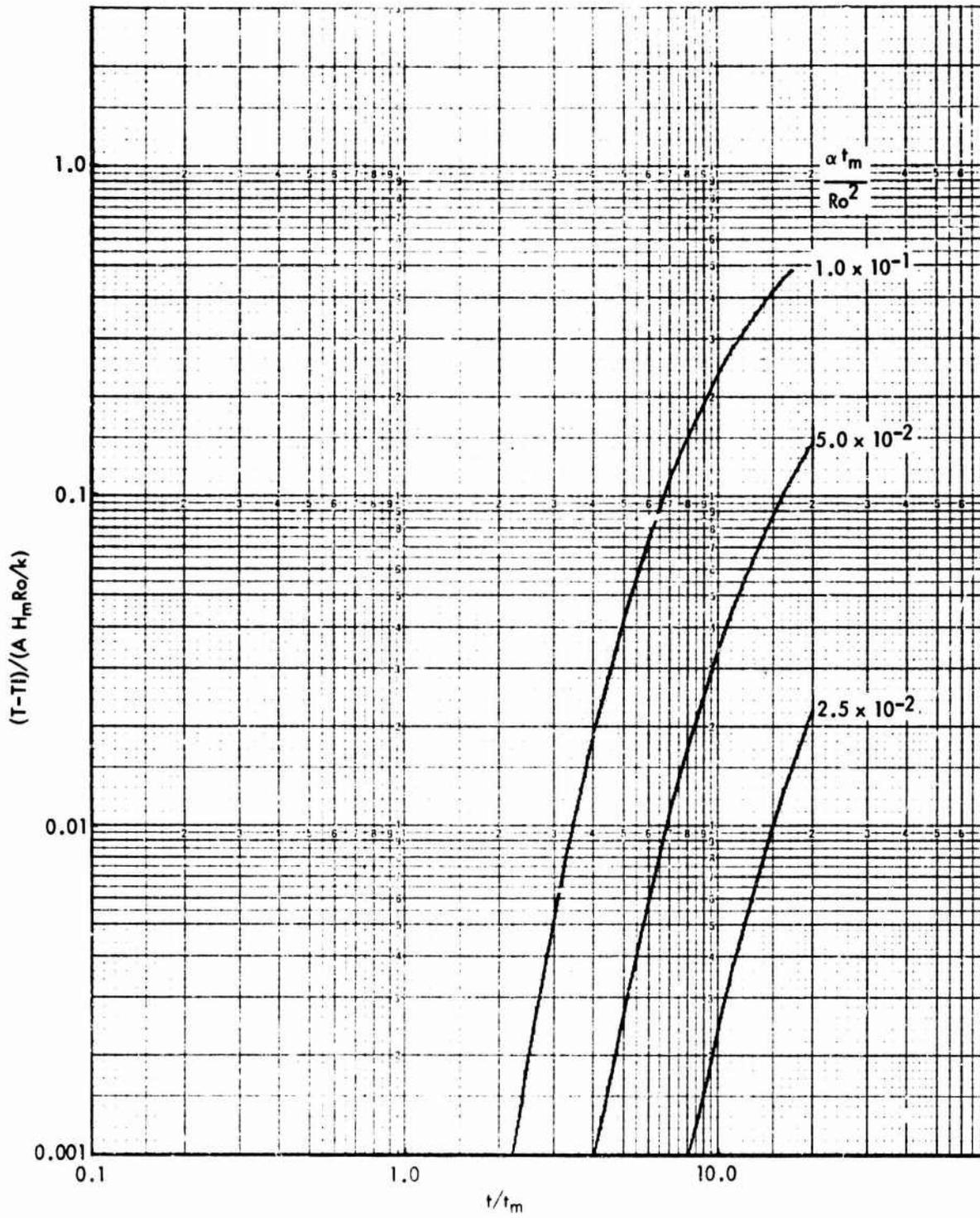
FIG. A – 1.1.6   DIMENSIONLESS SURFACE TEMPERATURE HISTORIES (Ri* = 0.9, ϕ = 180°)
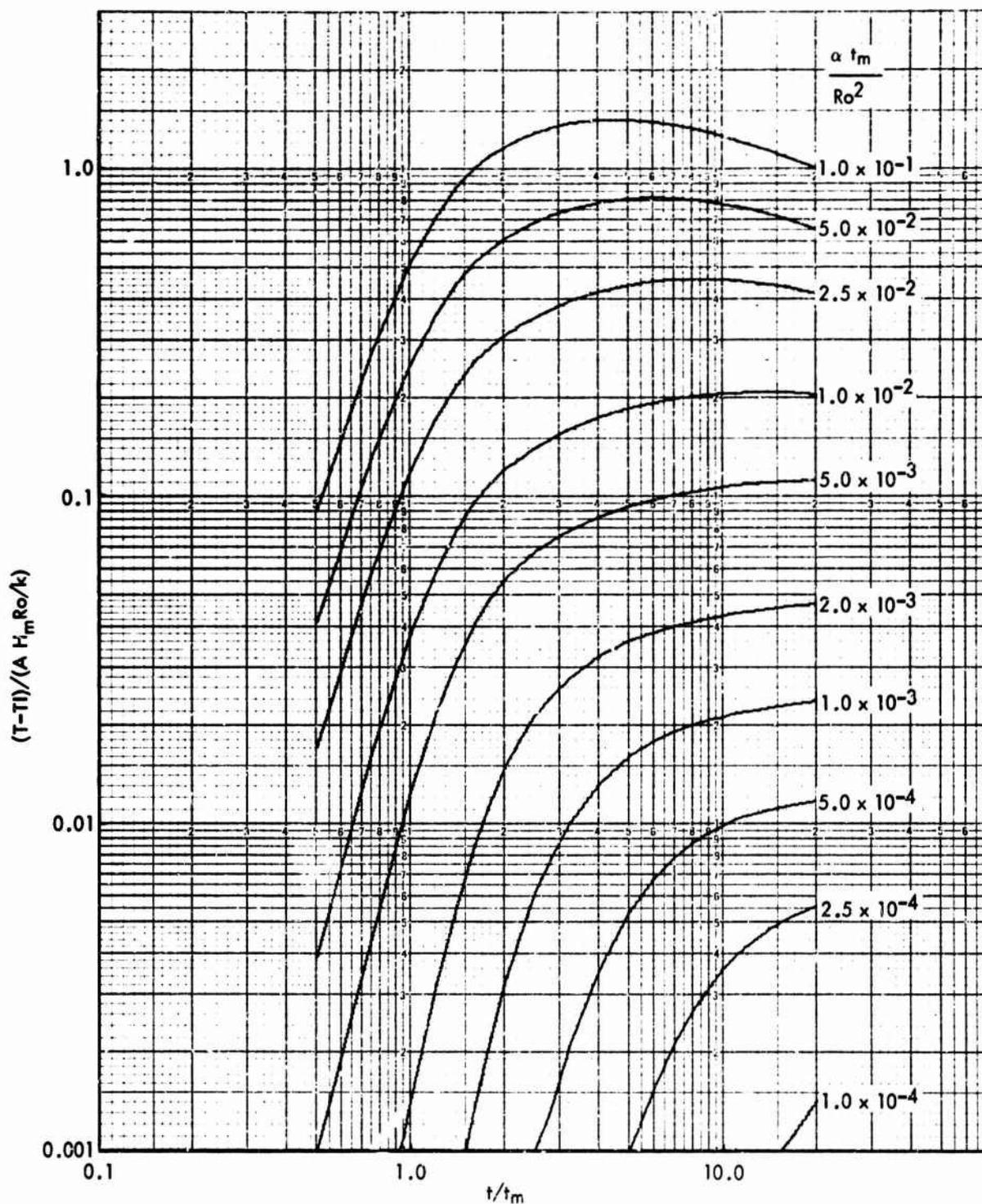
FIG. A - 1.2.1   DIMENSIONLESS MIDPLANE TEMPERATURE HISTORIES (Ri* = 0.9, ϕ = 0°)
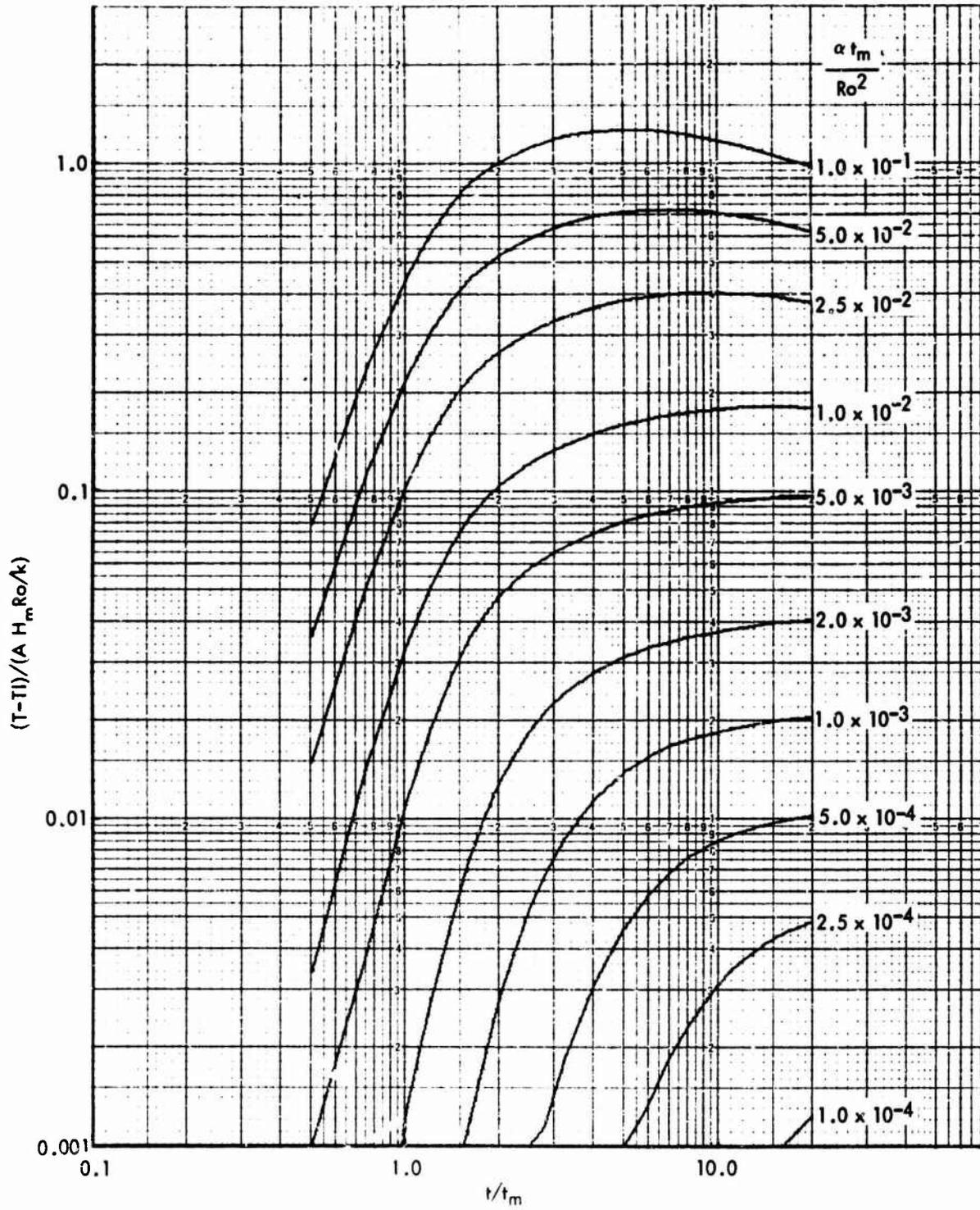
FIG. A - 1.2.2   DIMENSIONLESS MIDPLANE TEMPERATURE HISTORIES (Ri* = 0.9, $\phi = 30°$)
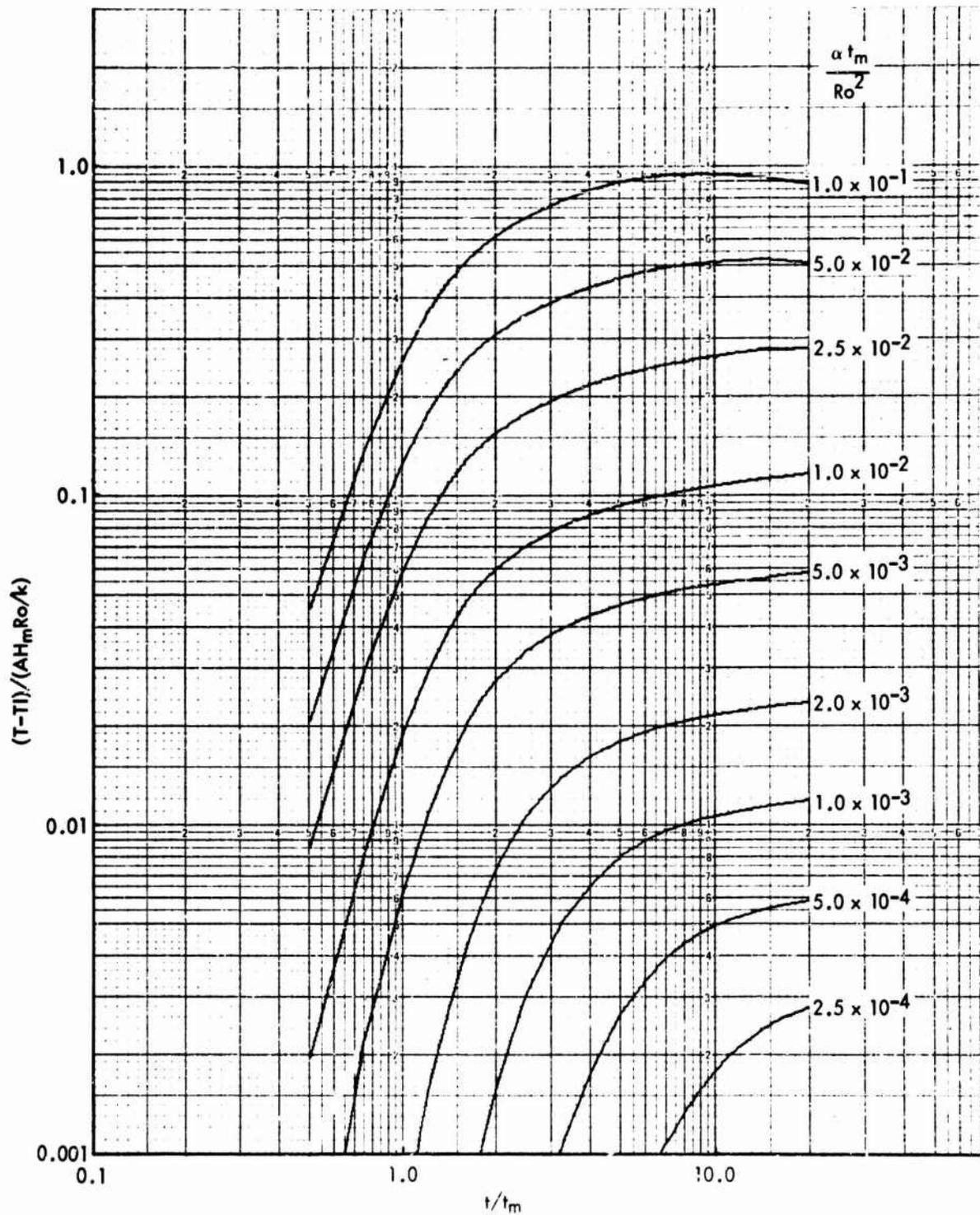
FIG. A - 1.2.3   DIMENSIONLESS MIDPLANE TEMPERATURE HISTORIES ($R_i^* = 0.9$, $\phi = 60°$)
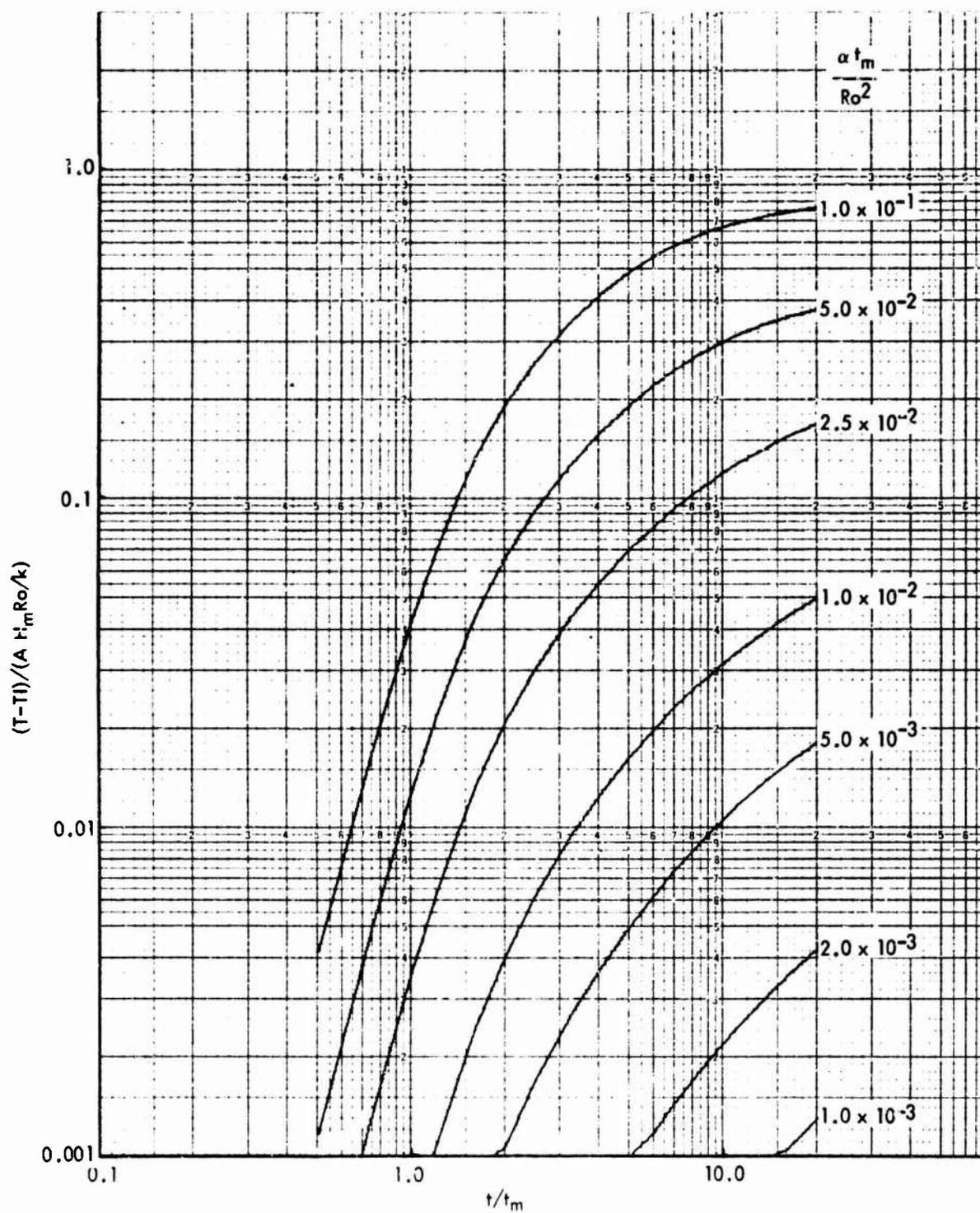
FIG. A - 1.2.4   DIMENSIONLESS MIDPLANE TEMPERATURE HISTORIES (Ri* = 0.9, ϕ = 90°)
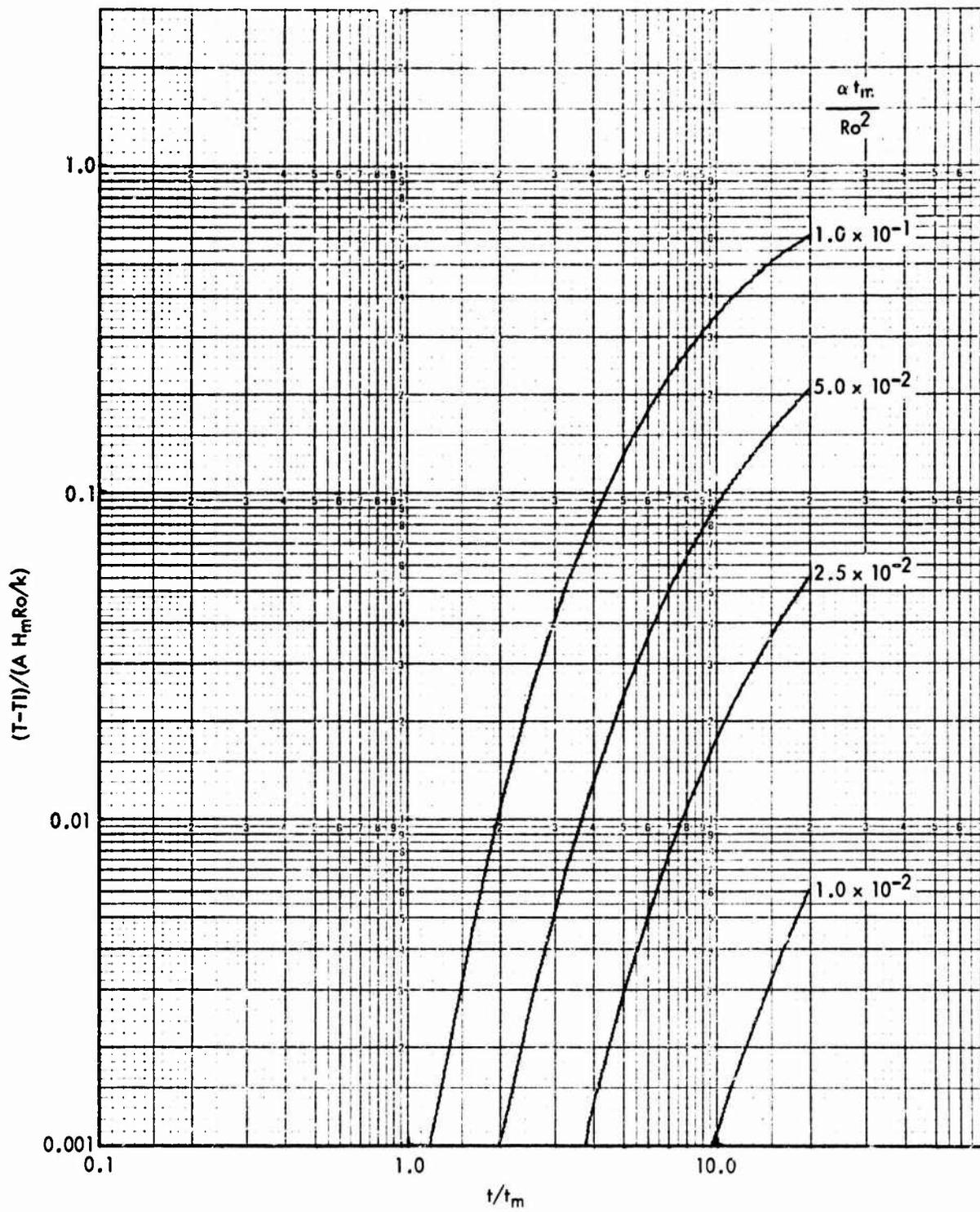
FIG. A - 1.2.5   DIMENSIONLESS MIDPLANE TEMPERATURE HISTORIES (Ri* = 0.9, $\phi = 135°$)
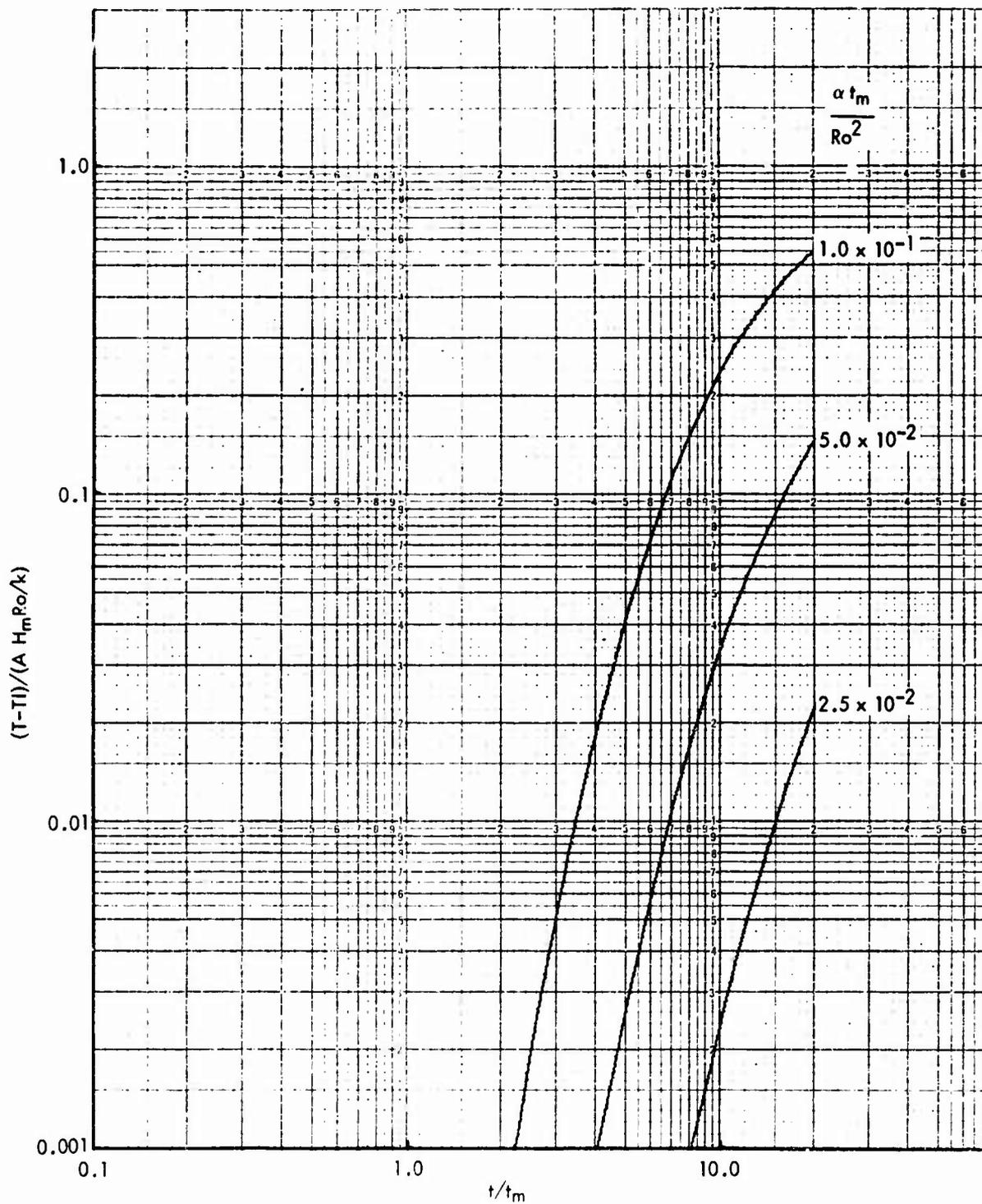
FIG. A - 1.2.6   DIMENSIONLESS MIDPLANE TEMPERATURE HISTORIES (Ri* = 0.9, ϕ = 180°)
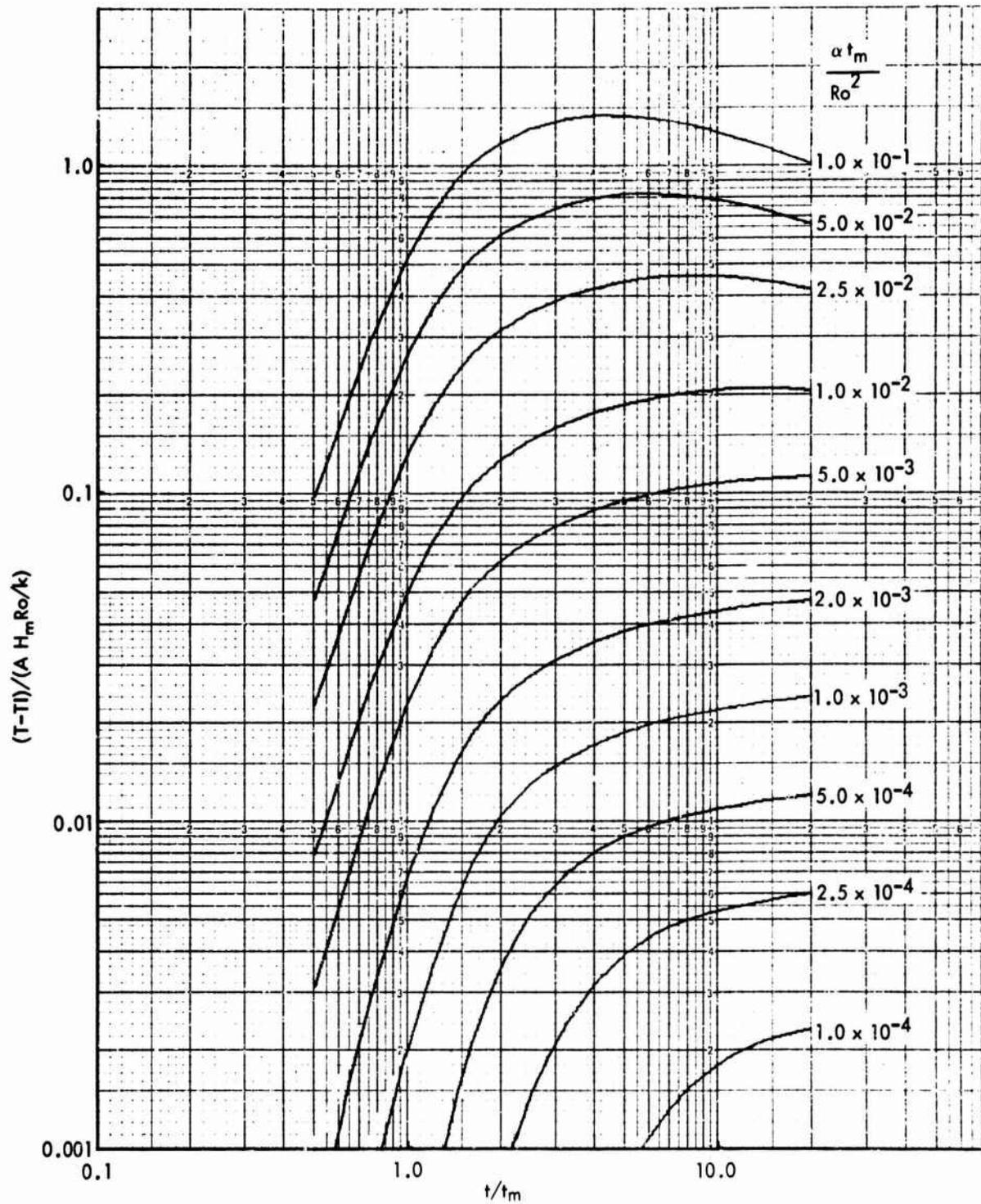
FIG. A – 1.3.1   DIMENSIONLESS BACKFACE TEMPERATURE HISTORIES (Ri* = 0.9, ϕ = 0°)
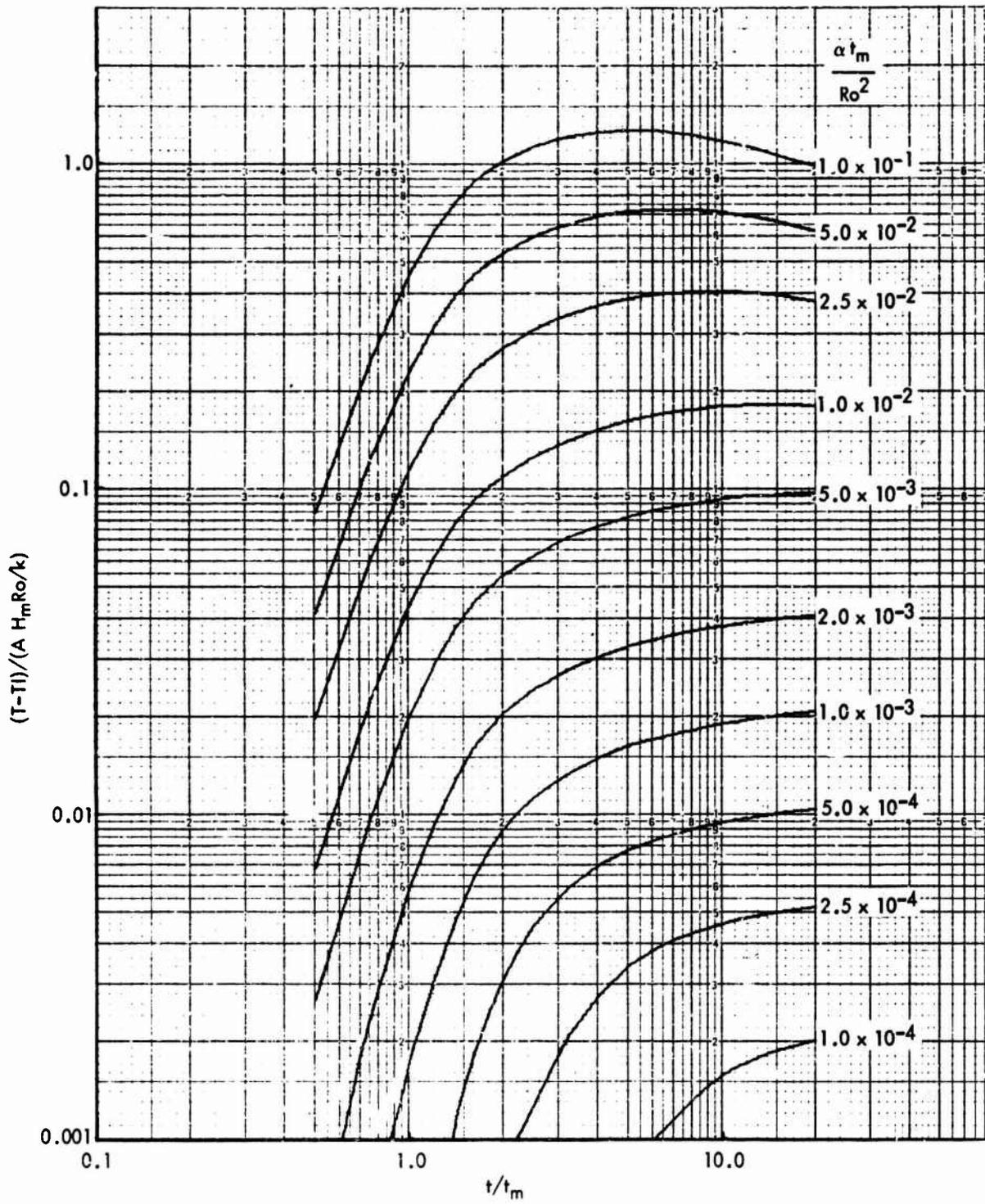
FIG. A - 1.3.2   DIMENSIONLESS BACKFACE TEMPERATURE HISTORIES ($Ri^* = 0.9$, $\phi = 30°$)
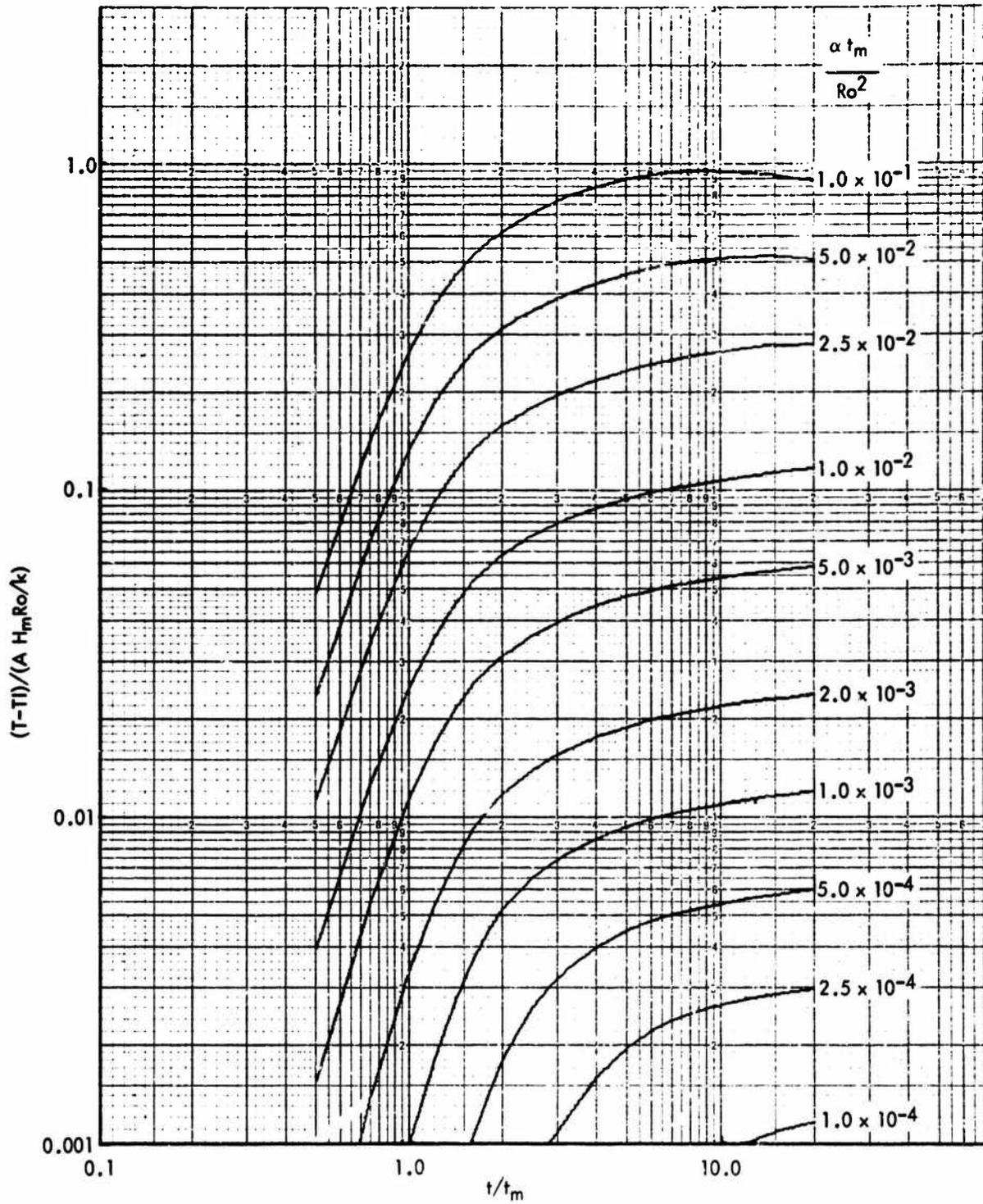
FIG. A – 1.3.3   DIMENSIONLESS BACKFACE TEMPERATURE HISTORIES ($Ri^* = 0.9$, $\phi = 60°$)
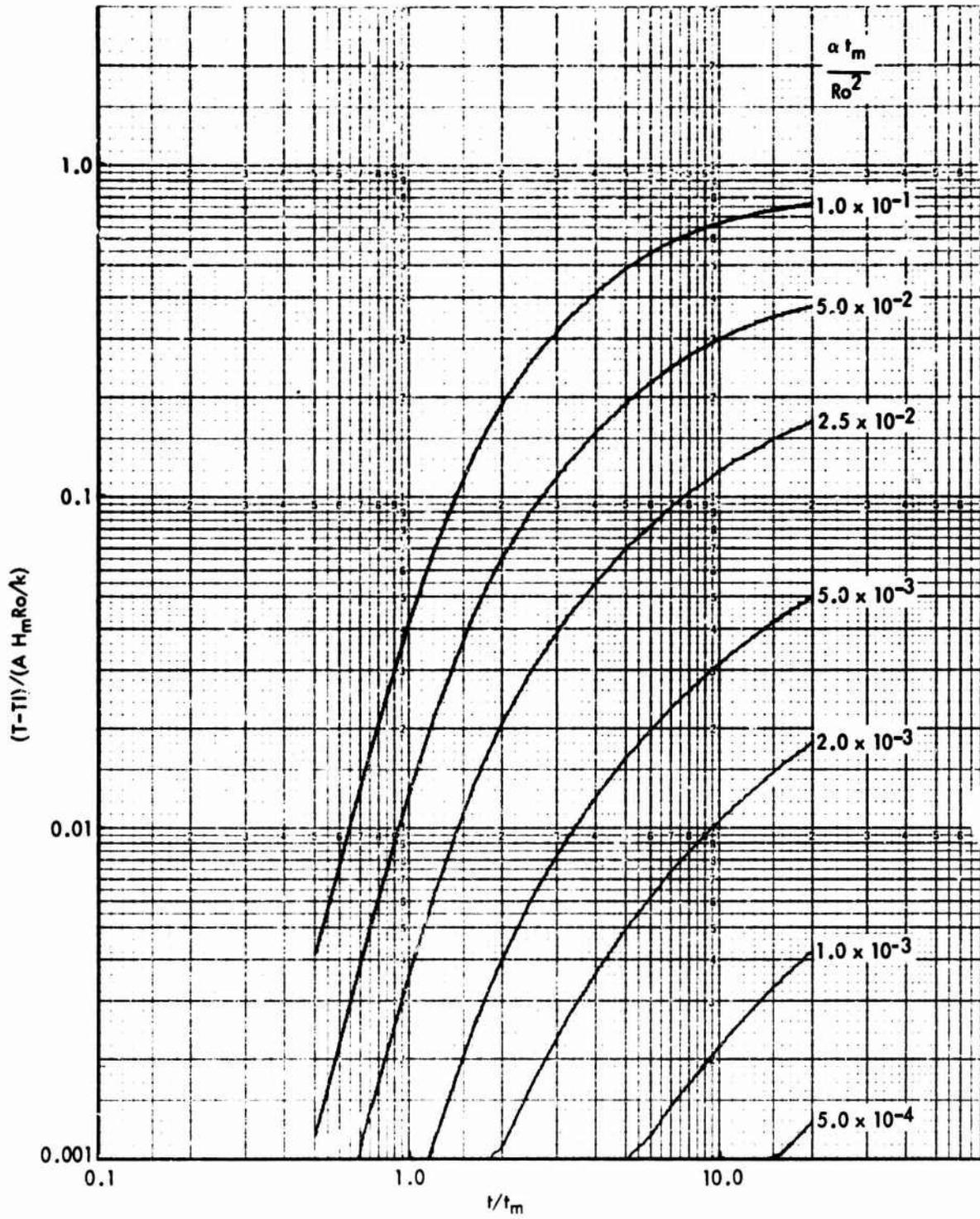
FIG. A - 1.3.4   DIMENSIONLESS BACKFACE TEMPERATURE HISTORIES (Ri* = 0.9, ϕ = 90°)
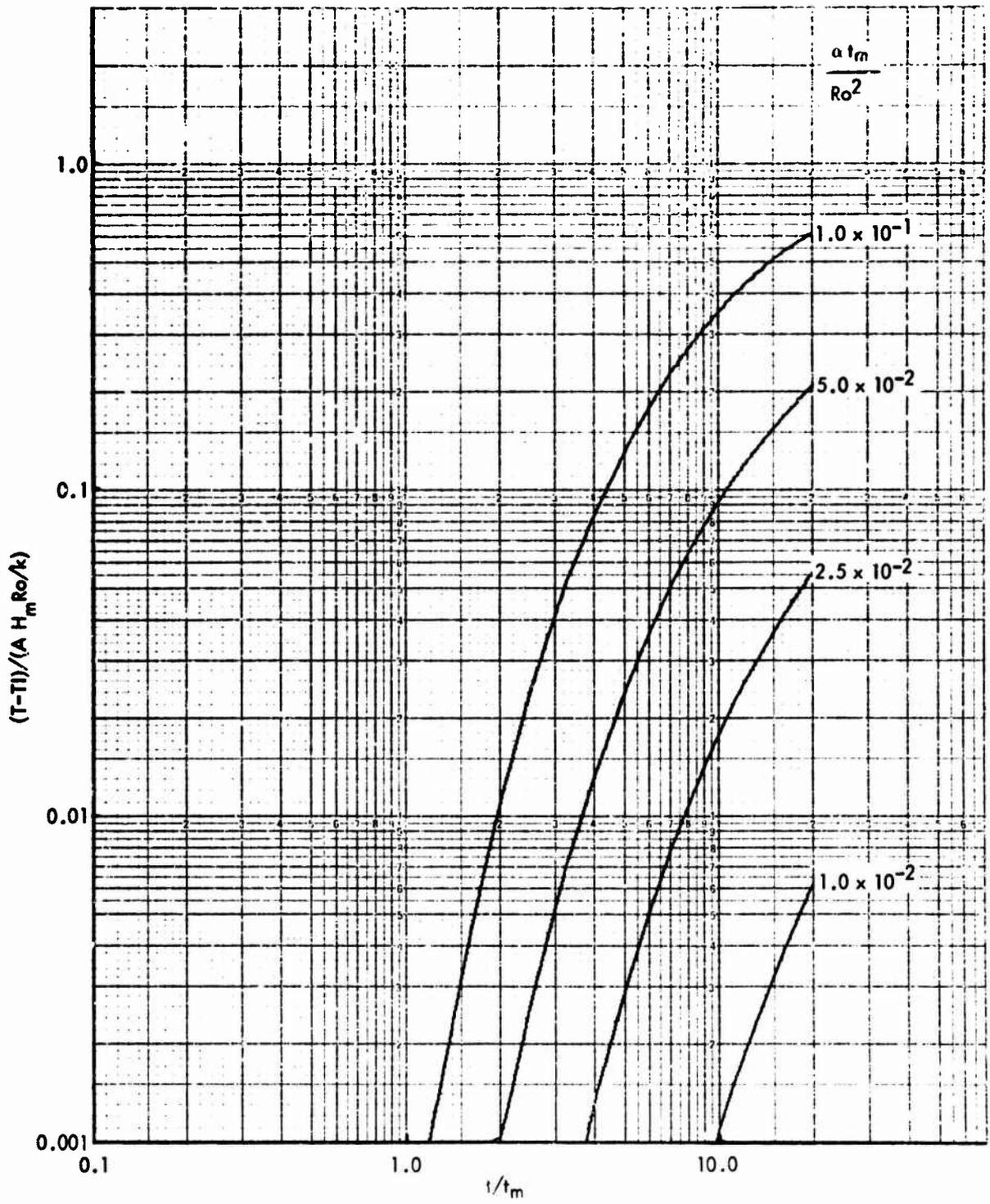
FIG. A - 1.3.5   DIMENSIONLESS BACKFACE TEMPERATURE HISTORIES (Ri* = 0.9, ϕ = 135°)
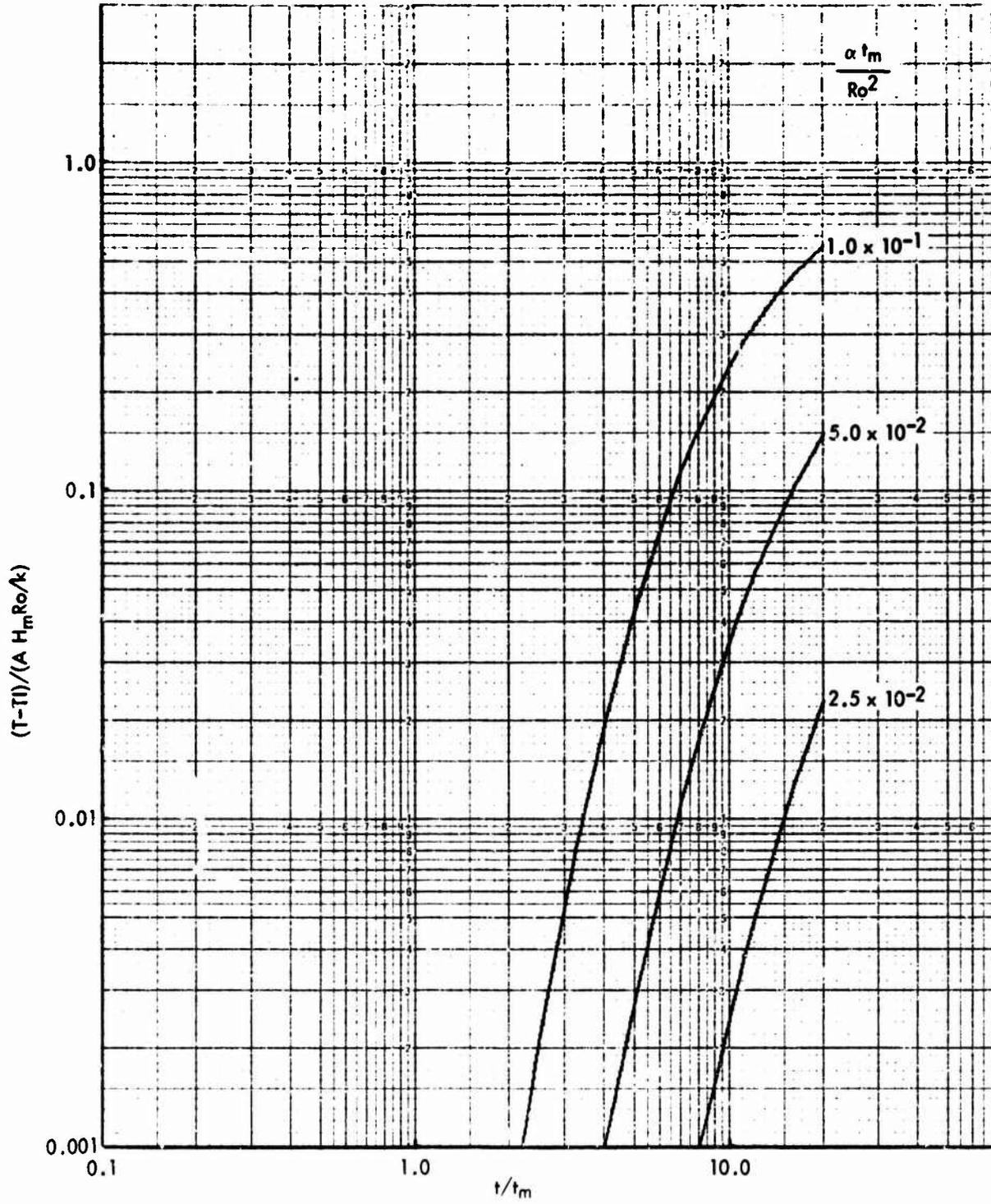
FIG. A - 1.3.6   DIMENSIONLESS BACKFACE TEMPERATURE HISTORIES (Ri* = 0.9, ϕ = 180°)
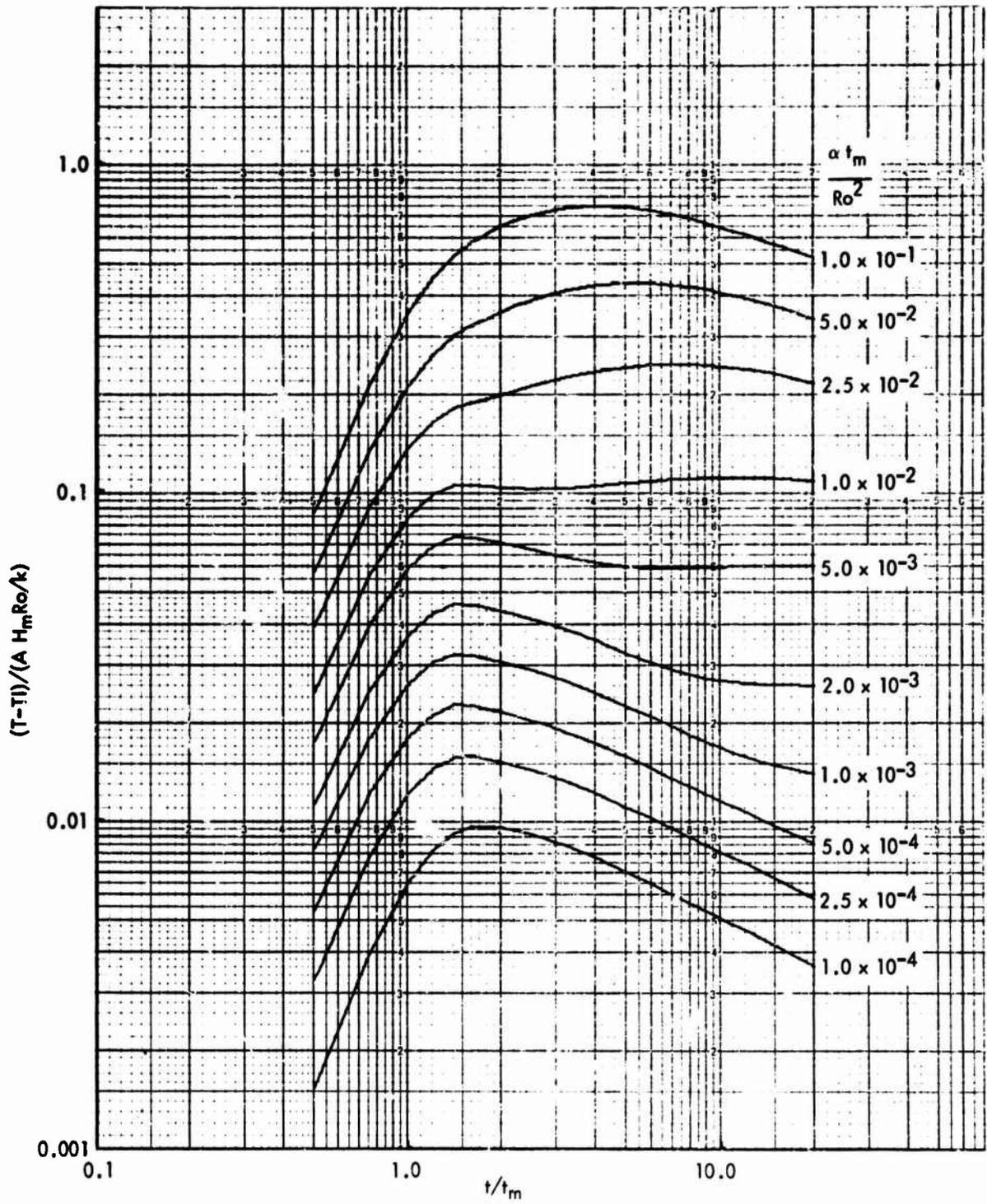
FIG. A - 2.1.1   DIMENSIONLESS SURFACE TEMPERATURE HISTORIES (Ri* = 0.8, $\phi = 0°$)
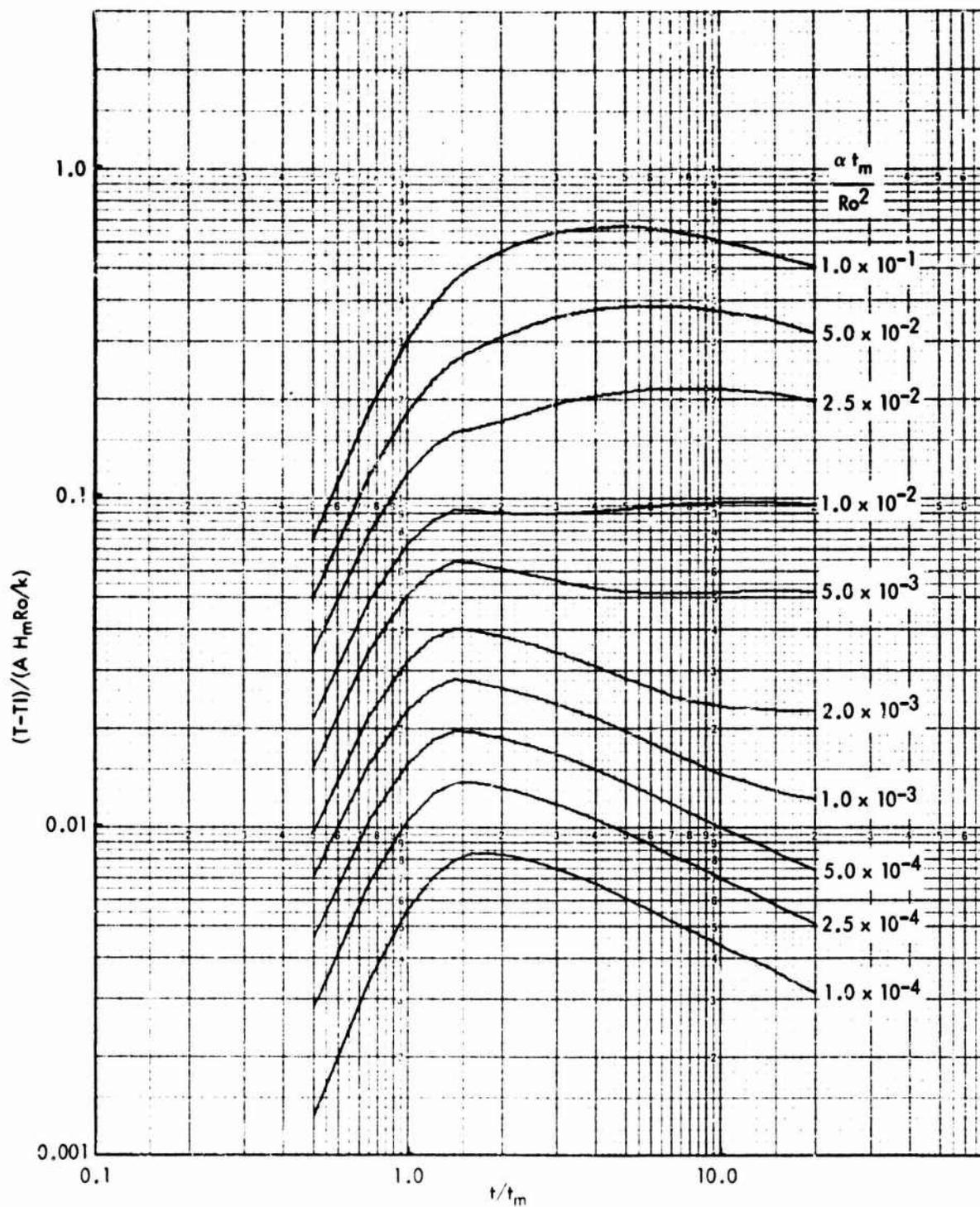
FIG. A - 2.1.2   DIMENSIONLESS SURFACE TEMPERATURE HISTORIES (Ri* = 0.8, ϕ = 30°)
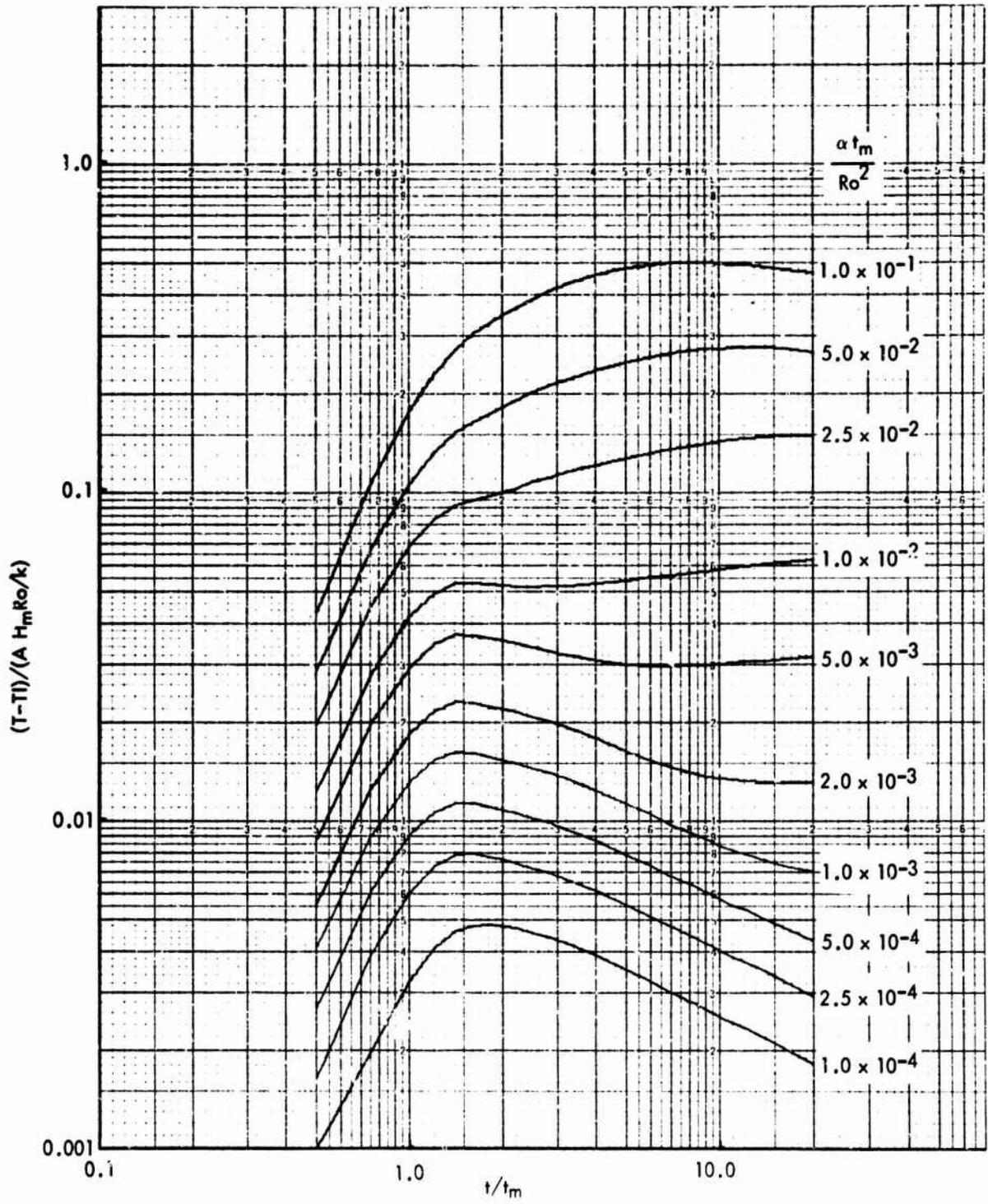
FIG. A - 2.1.3   DIMENSIONLESS SURFACE TEMPERATURE HISTORIES (Ri* = 0.8, ϕ = 60°)
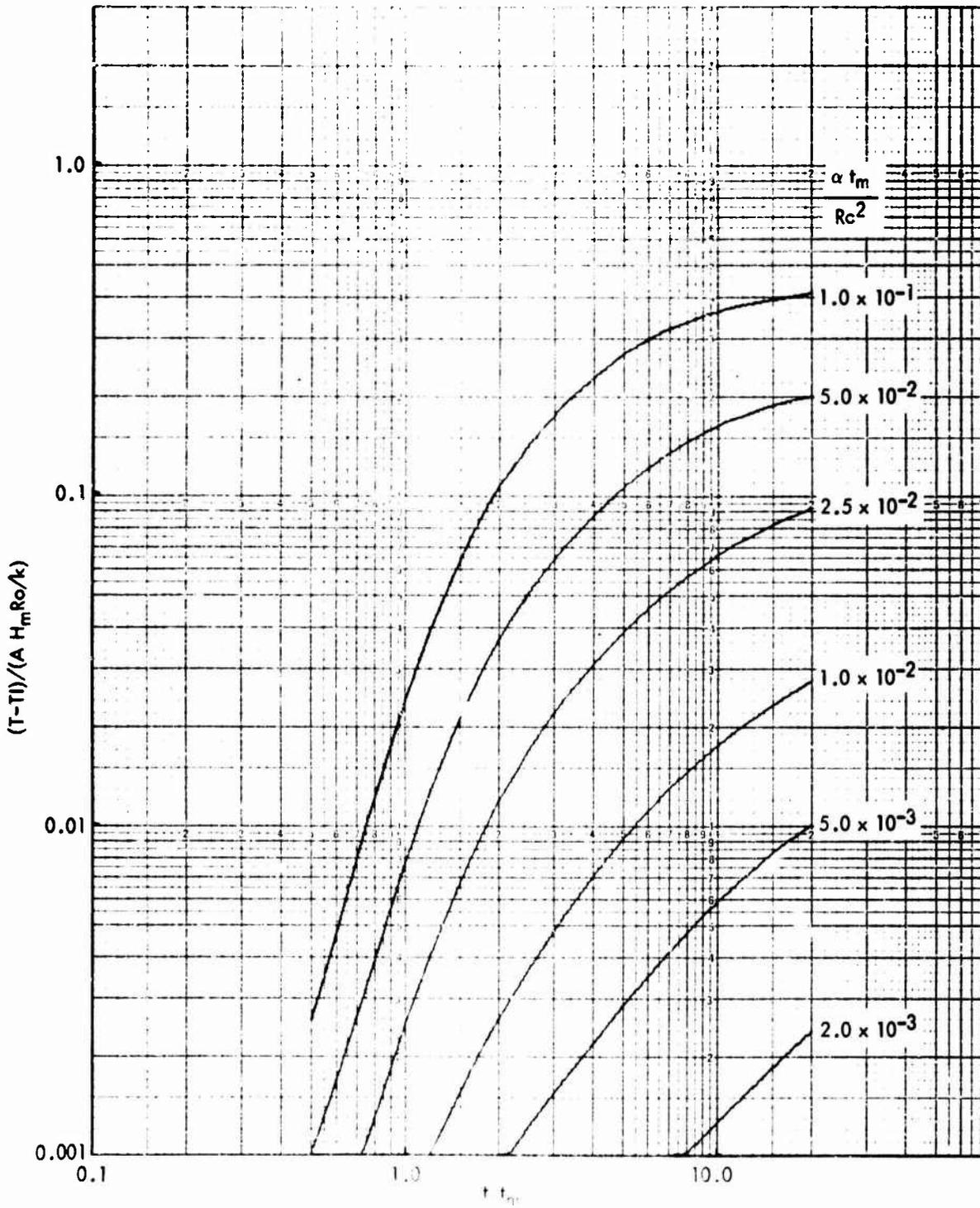
FIG. A - 2.1.4   DIMENSIONLESS SURFACE TEMPERATURE HISTORIES (Ri* = 0.8, φ = 90°)

FIG. A - 2.1.5   DIMENSIONLESS SURFACE TEMPERATURE HISTORIES (Ri* = 0.8, ϕ = 135°)
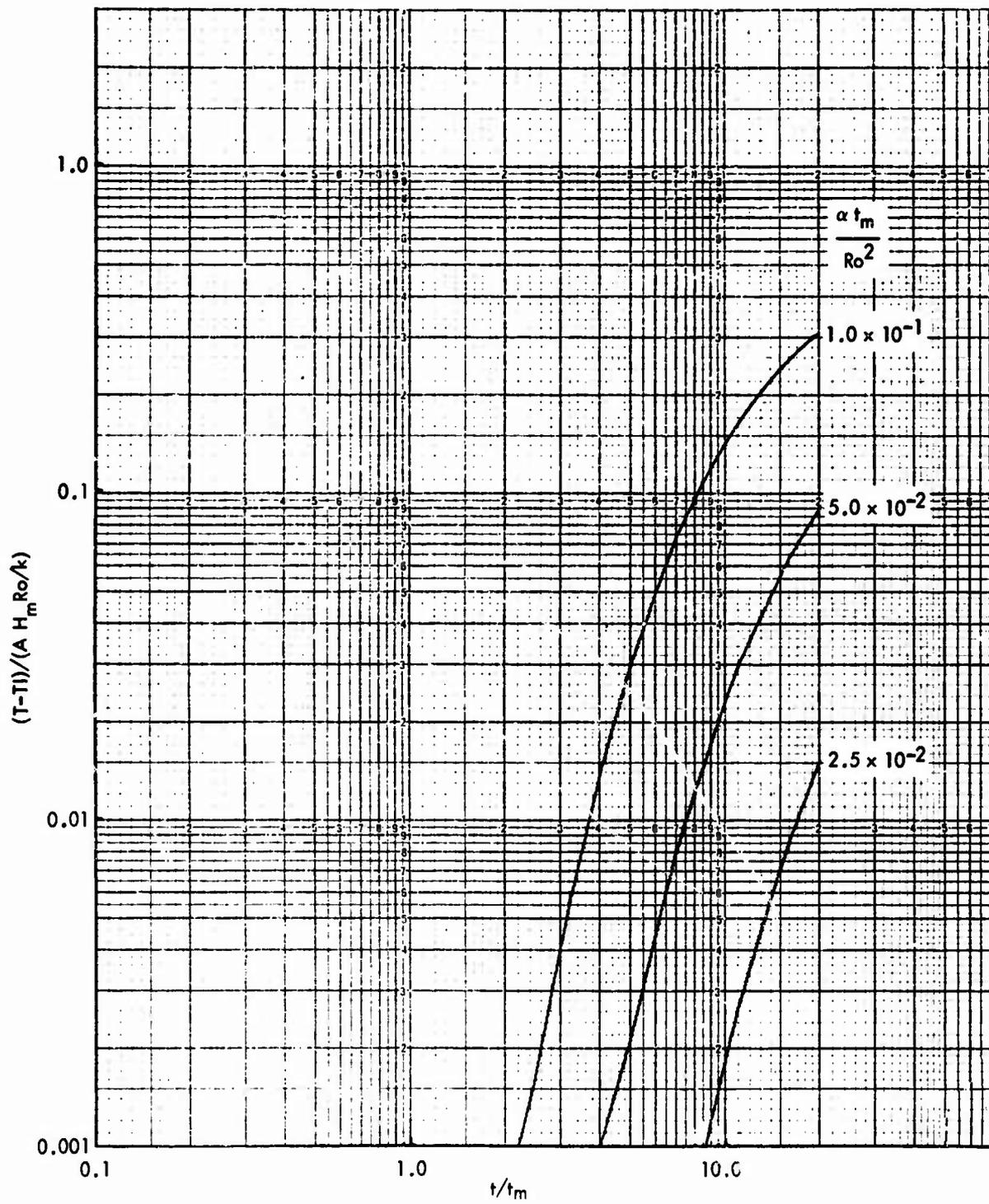
FIG. A - 2.1.6   DIMENSIONLESS SURFACE TEMPERATURE HISTORIES (Ri* = 0.8, ϕ = 180°)
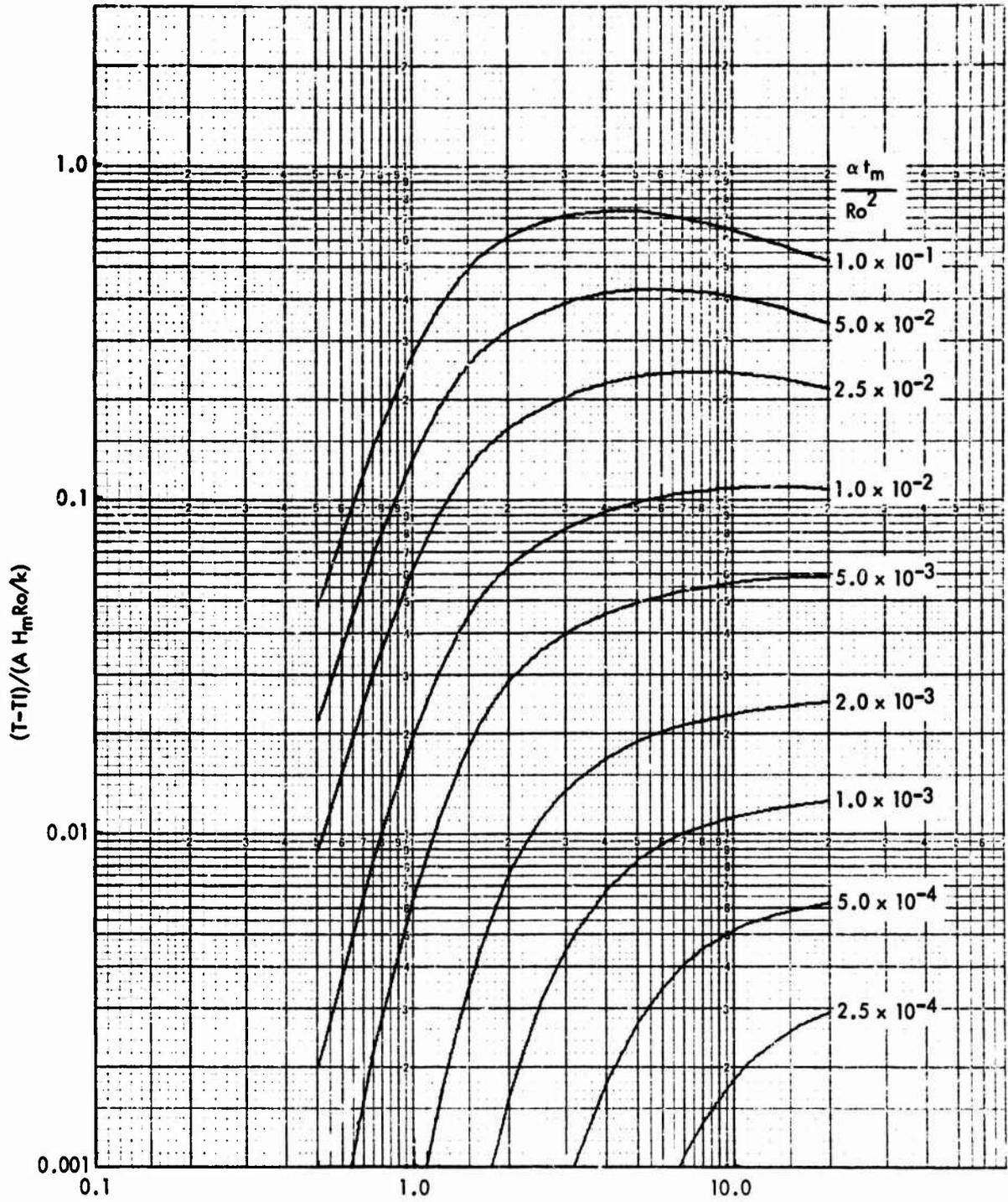
FIG. A - 2.2.1   DIMENSIONLESS MIDPLANE TEMPERATURE HISTORIES (Ri* = 0.8, $\phi = 0°$)
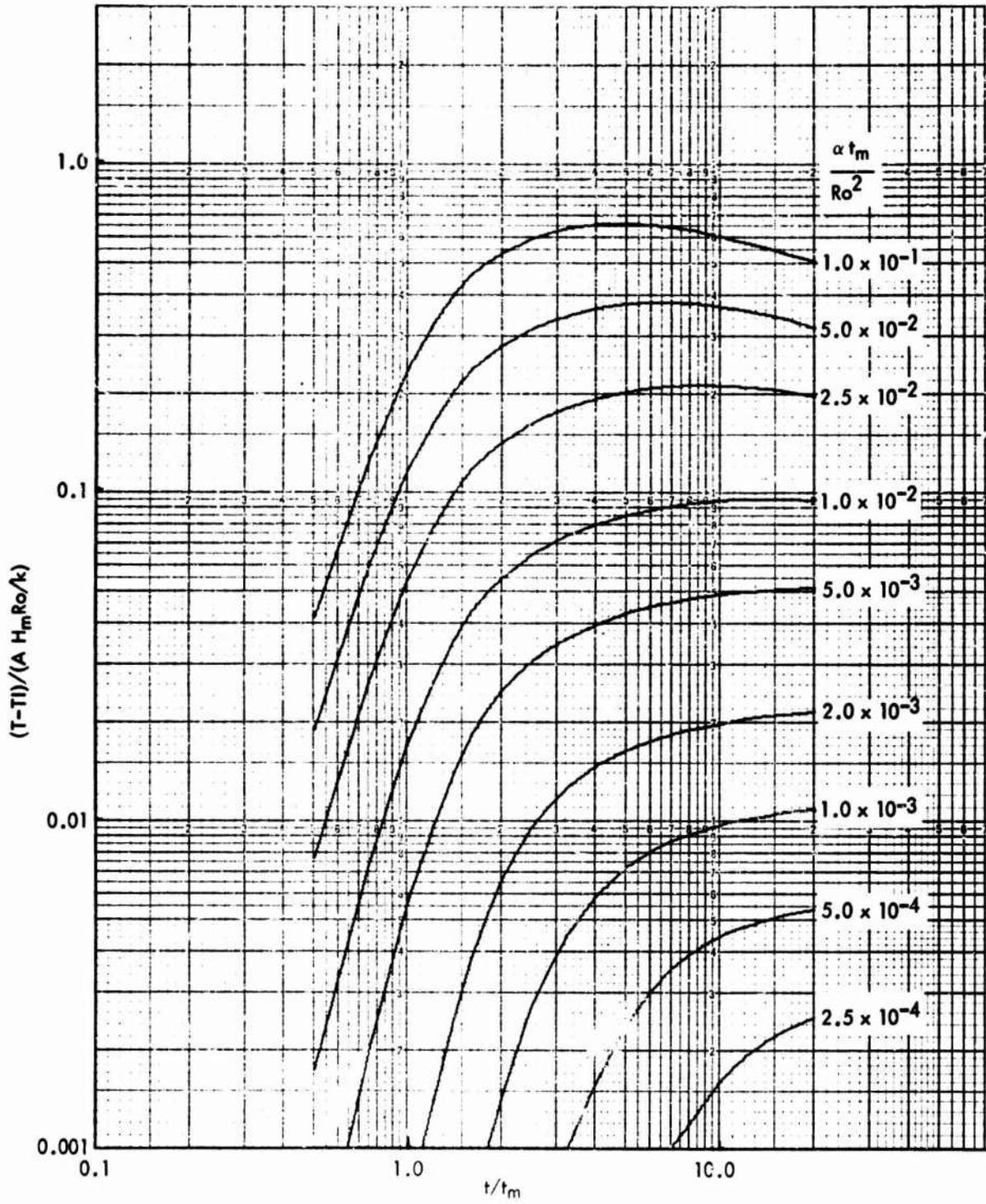
FIG. A - 2.2.2   DIMENSIONLESS MIDPLANE TEMPERATURE HISTORIES (Ri* = 0.8, $\phi = 30°$)
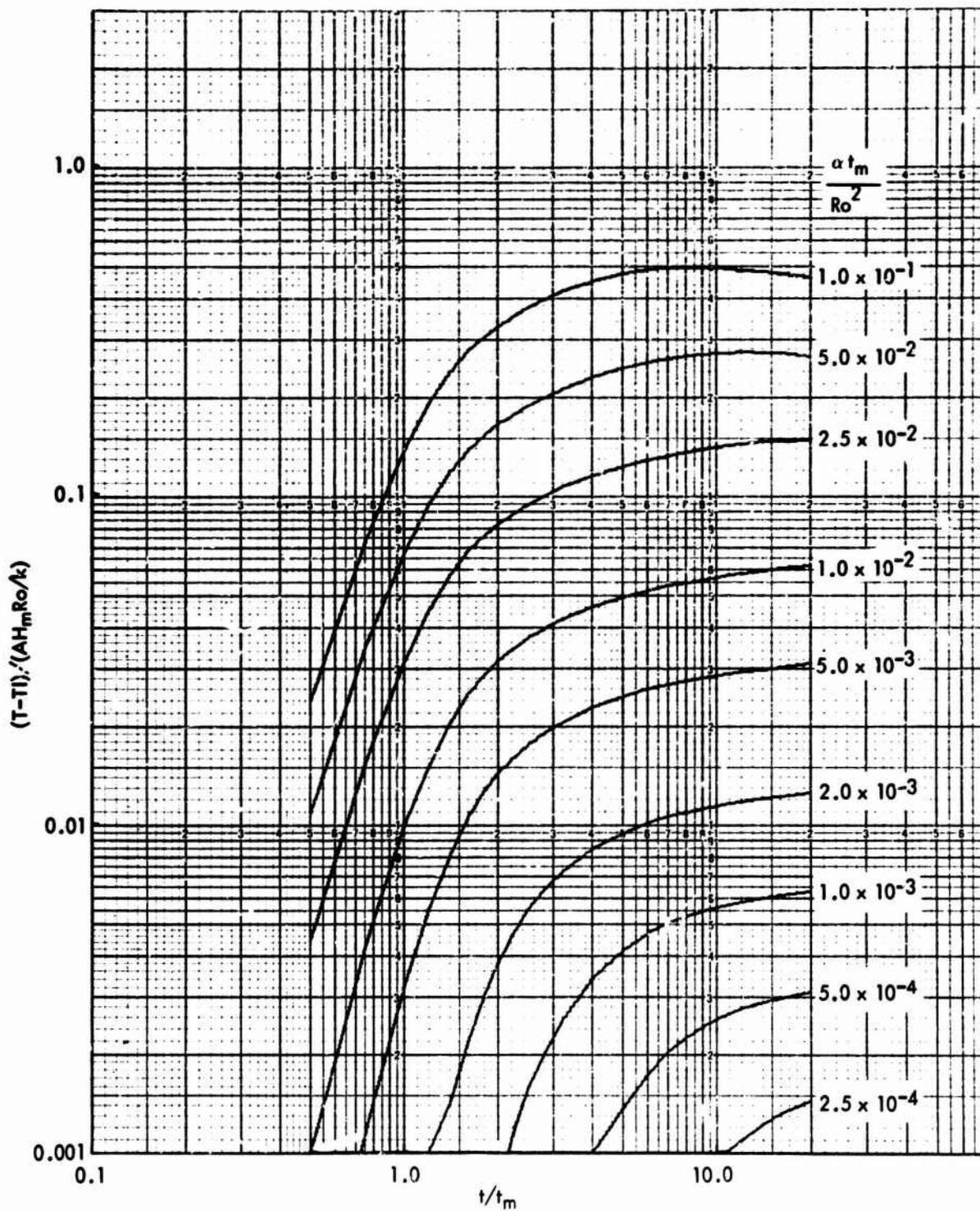
FIG. A - 2.2.3   DIMENSIONLESS MIDPLANE TEMPERATURE HISTORIES (Ri* = 0.8, ϕ = 60°)
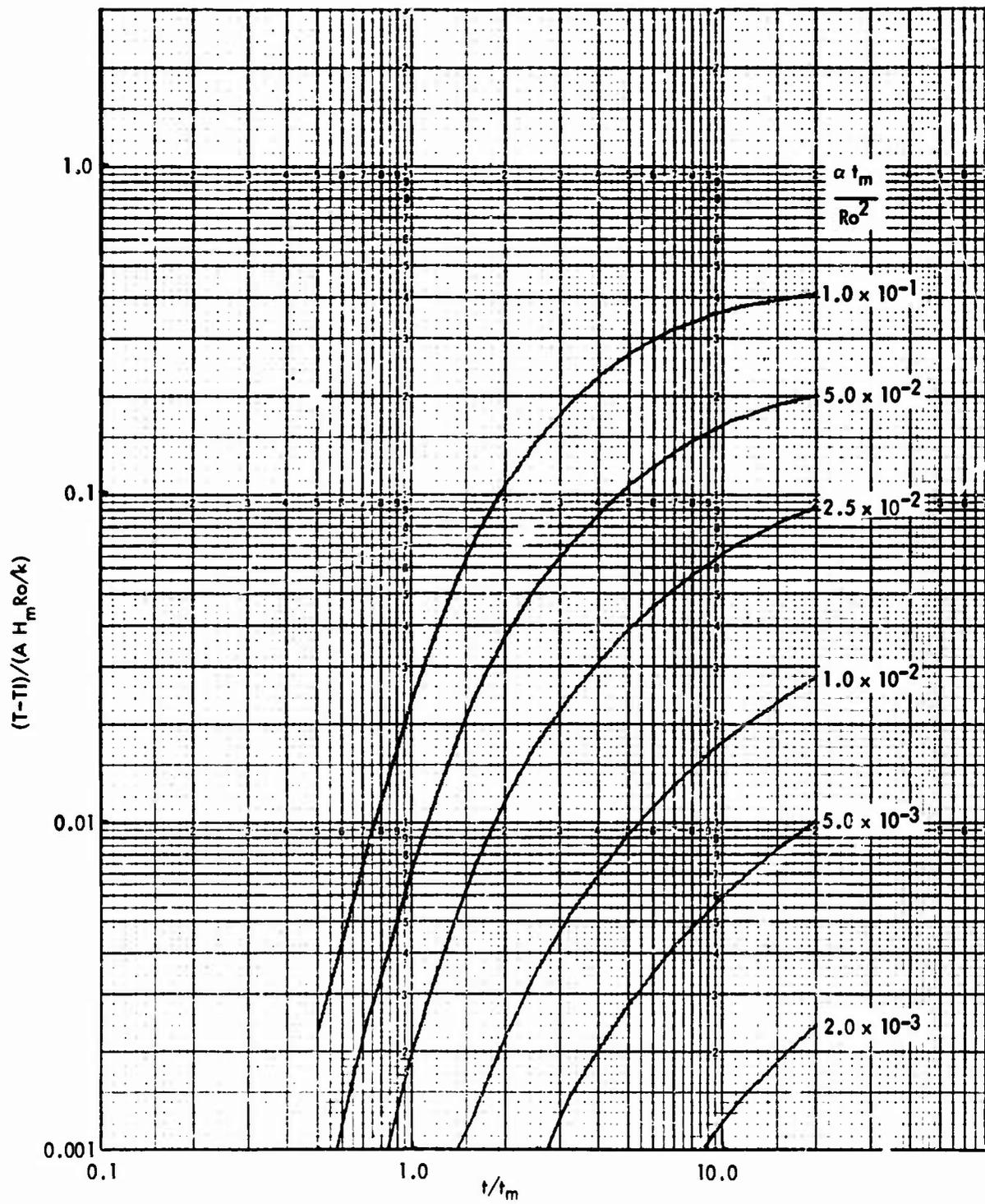
FIG. A - 2.2.4   DIMENSIONLESS MIDPLANE TEMPERATURE HISTORIES (Ri* = 0.8, ϕ = 90°)

FiG. A - 2.2.5   DIMENSIONLESS MIDPLANE TEMPERATURE HISTORIES ($Ri^* = 0.8$, $\phi = 135°$)
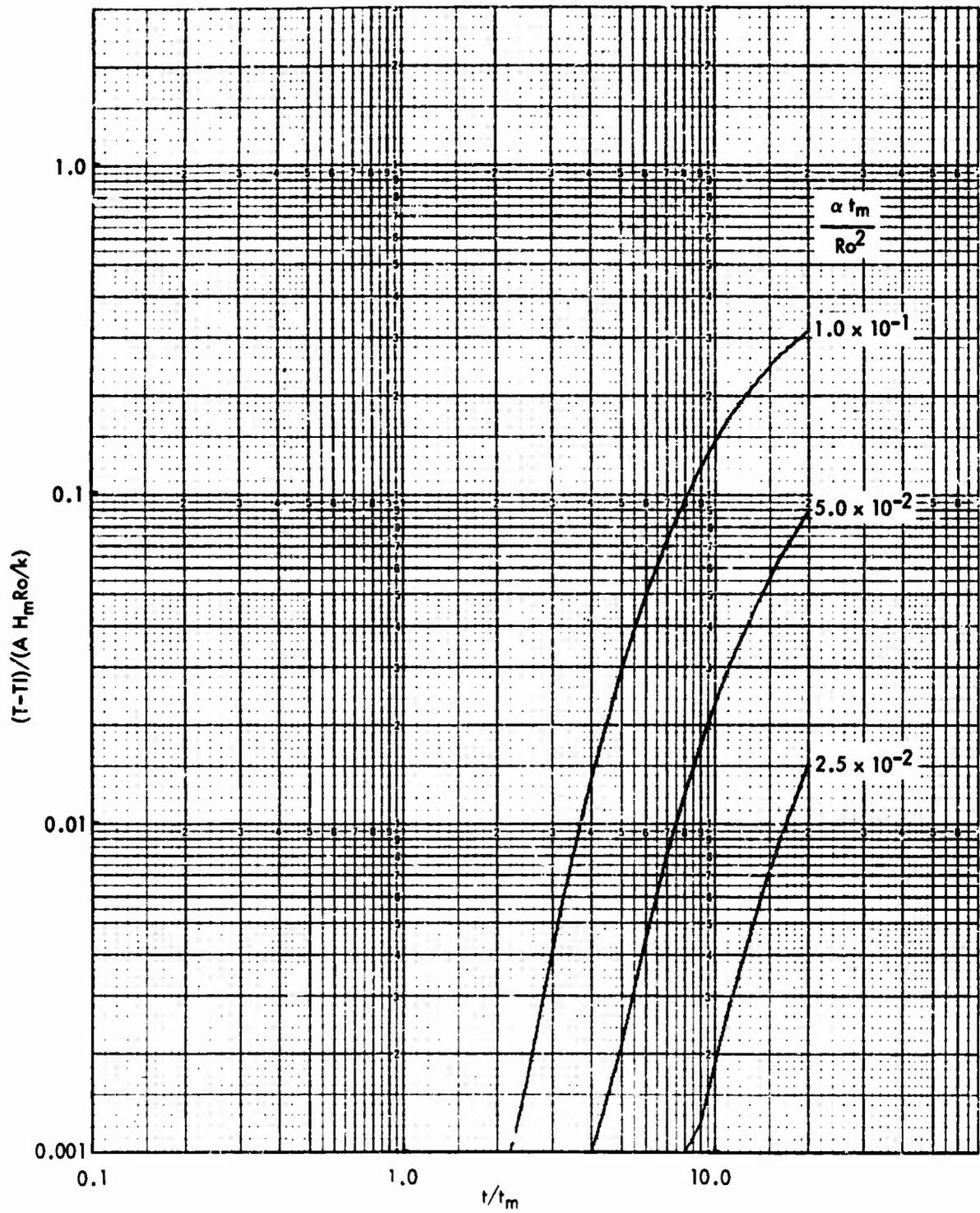
FIG. A - 2.2.6   DIMENSIONLESS MIDPLANE TEMPERATURE HISTORIES (Ri* = 0.3, $\phi = 180°$)
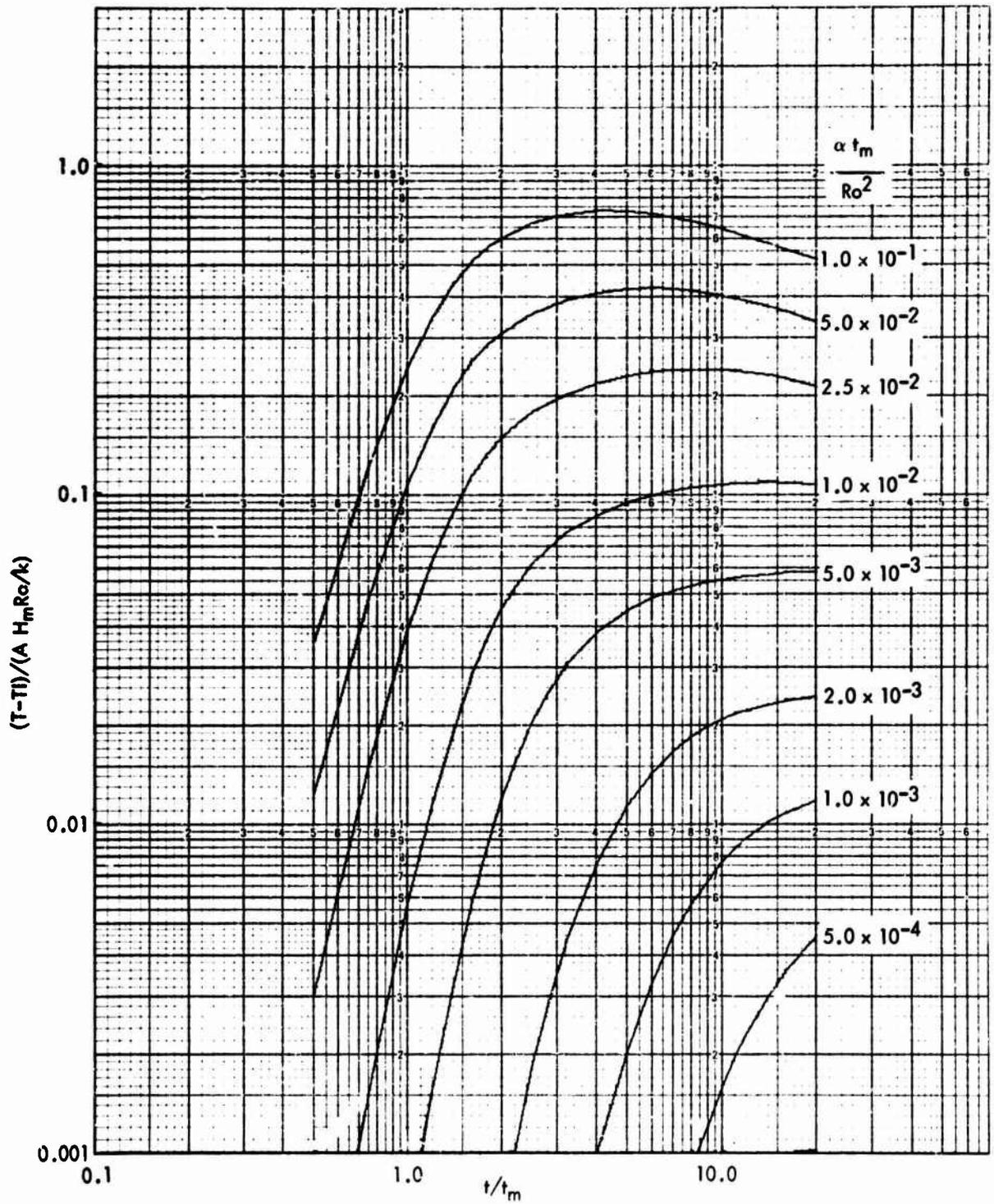
FIG. A - 2.3.1   DIMENSIONLESS BACKFACE TEMPERATURE HISTORIES (Ri* = 0.8, ϕ = 0°)
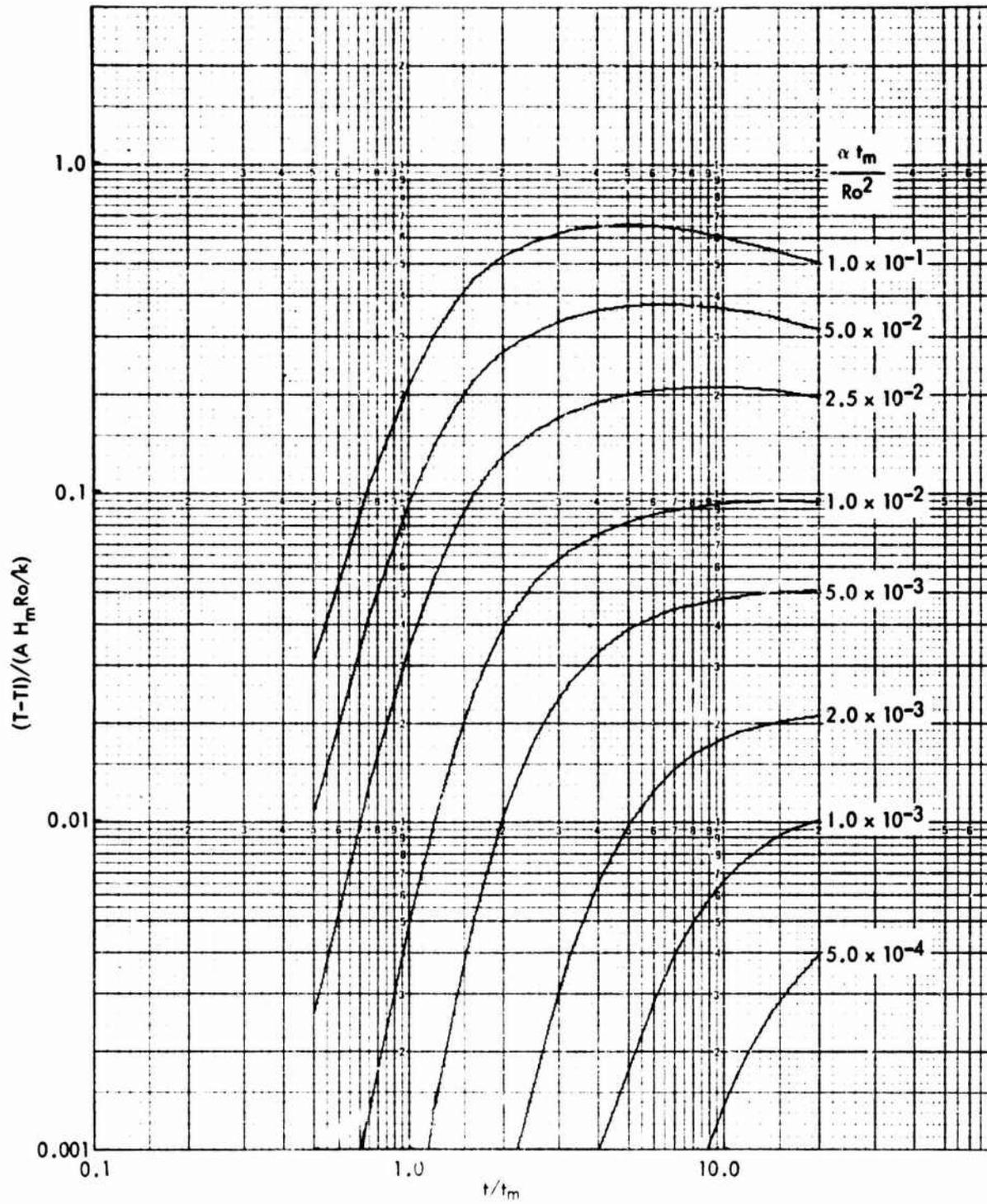
FIG. A - 2.3.2   DIMENSIONLESS BACKFACE TEMPERATURE HISTORIES (Ri* = 0.8, ϕ = 30°)
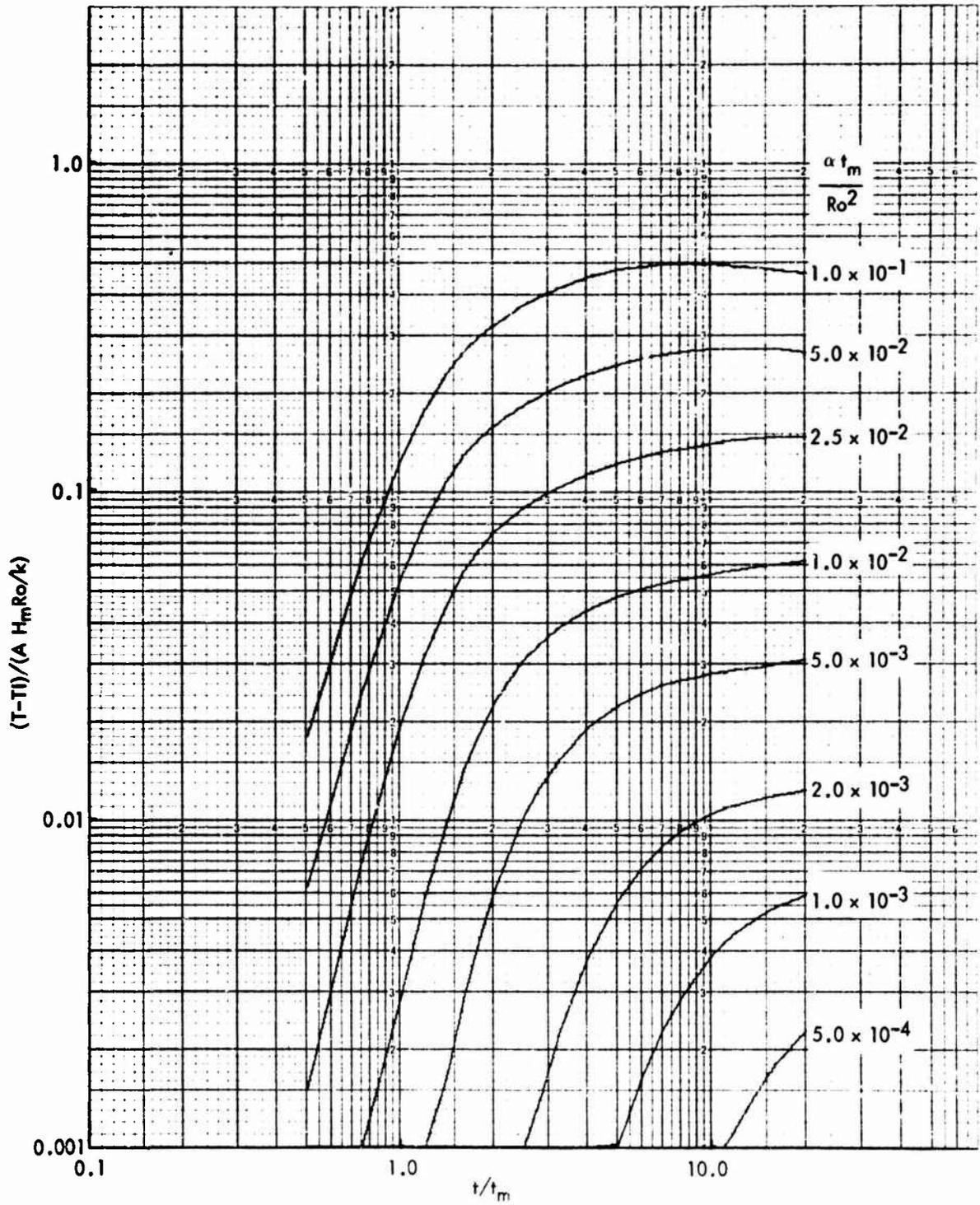
FIG. A - 2.3.3   DIMENSIONLESS BACKFACE TEMPERATURE HISTORIES (Ri* = 0.8, $\phi = 60°$)
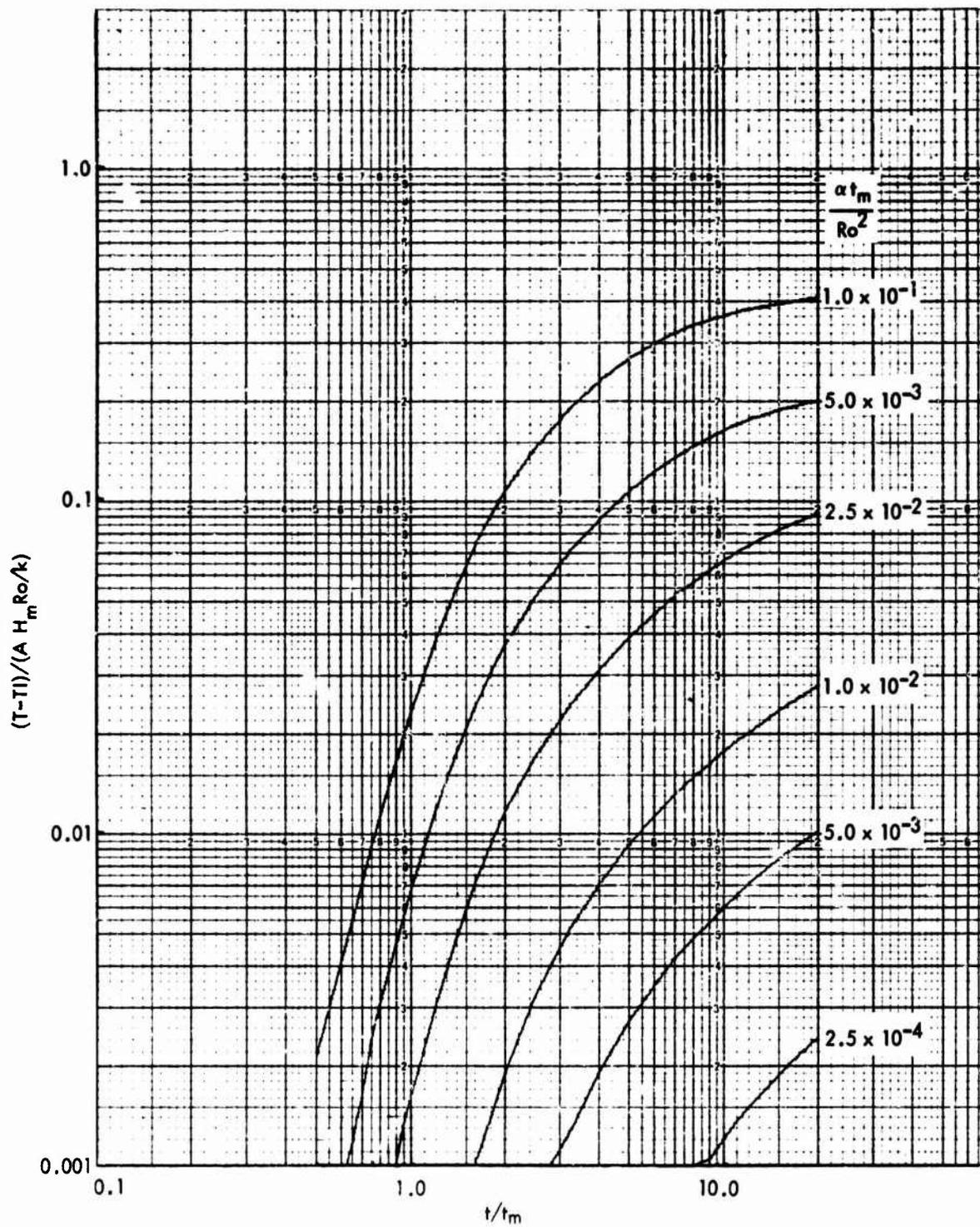
FIG. A - 2.3.4   DIMENSIONLESS BACKFACE TEMPERATURE HISTORIES (Ri* = 0.8, $\phi = 90°$)
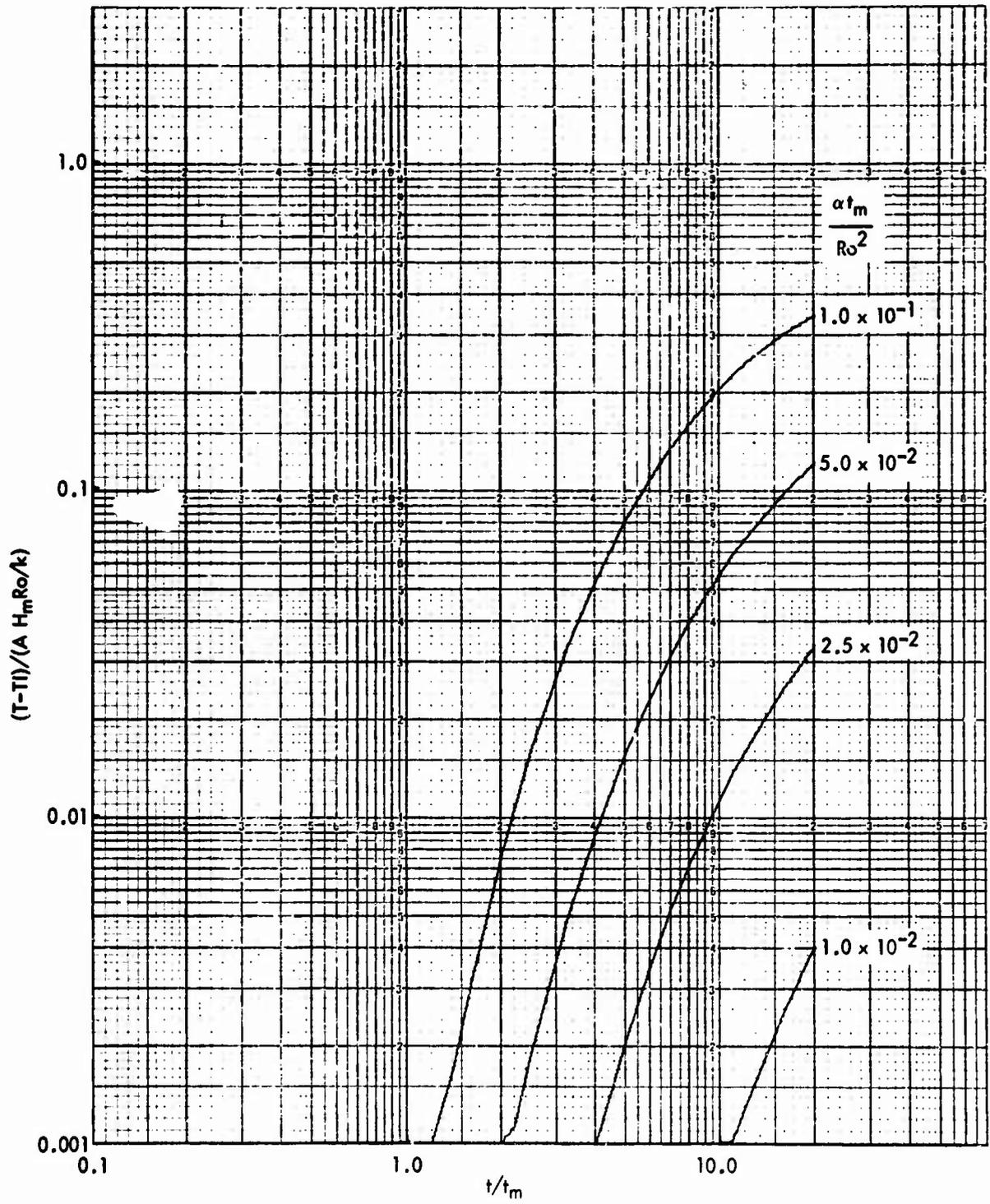
FIG. A - 2.3.5   DIMENSIONLESS BACKFACE TEMPERATURE HISTORIES (Ri* = 0.8, $\phi = 135°$)
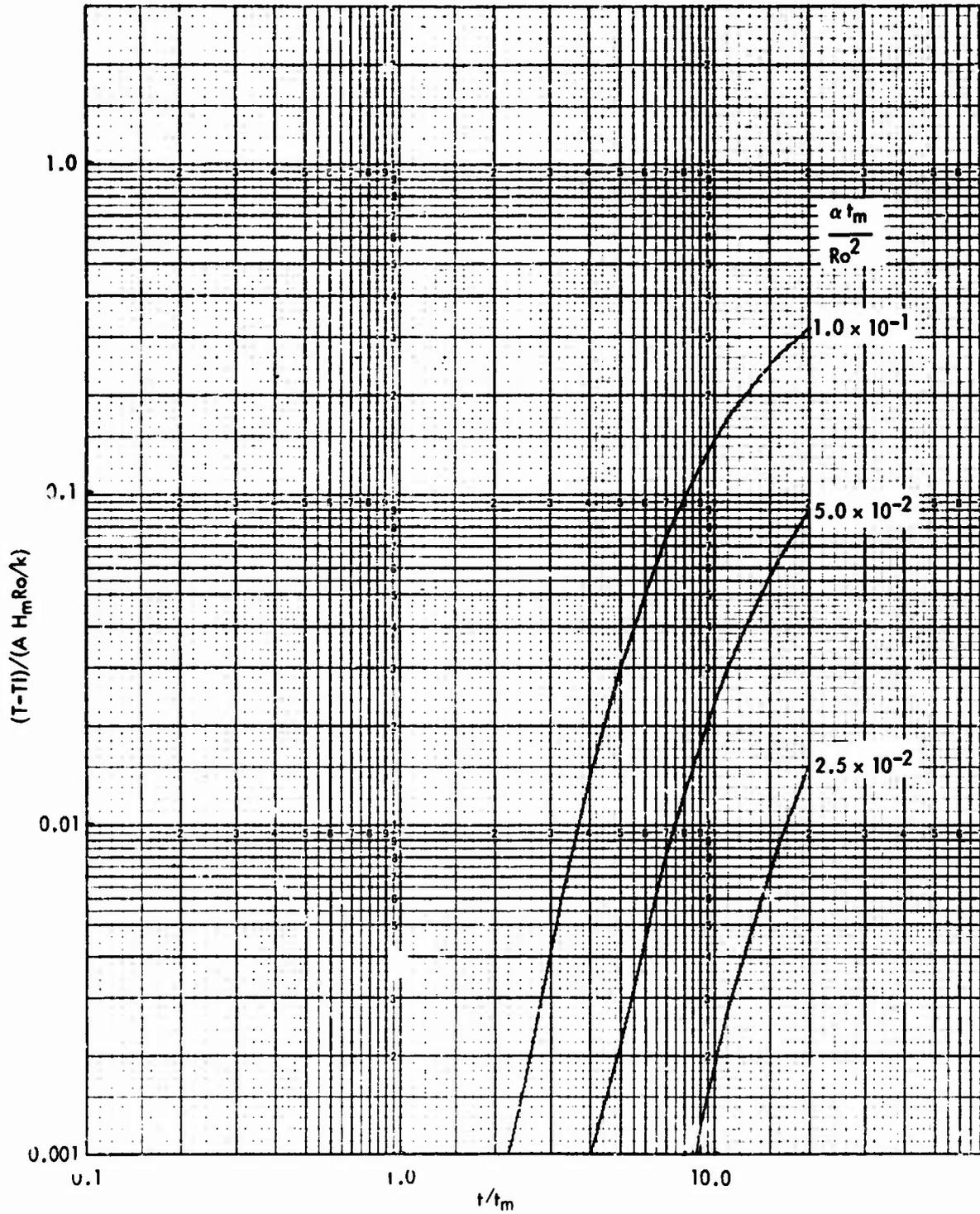
FIG. A - 2.3.6   DIMENSIONLESS BACKFACE TEMPERATURE HISTORIES (Ri* = 0.8, ϕ = 180°)
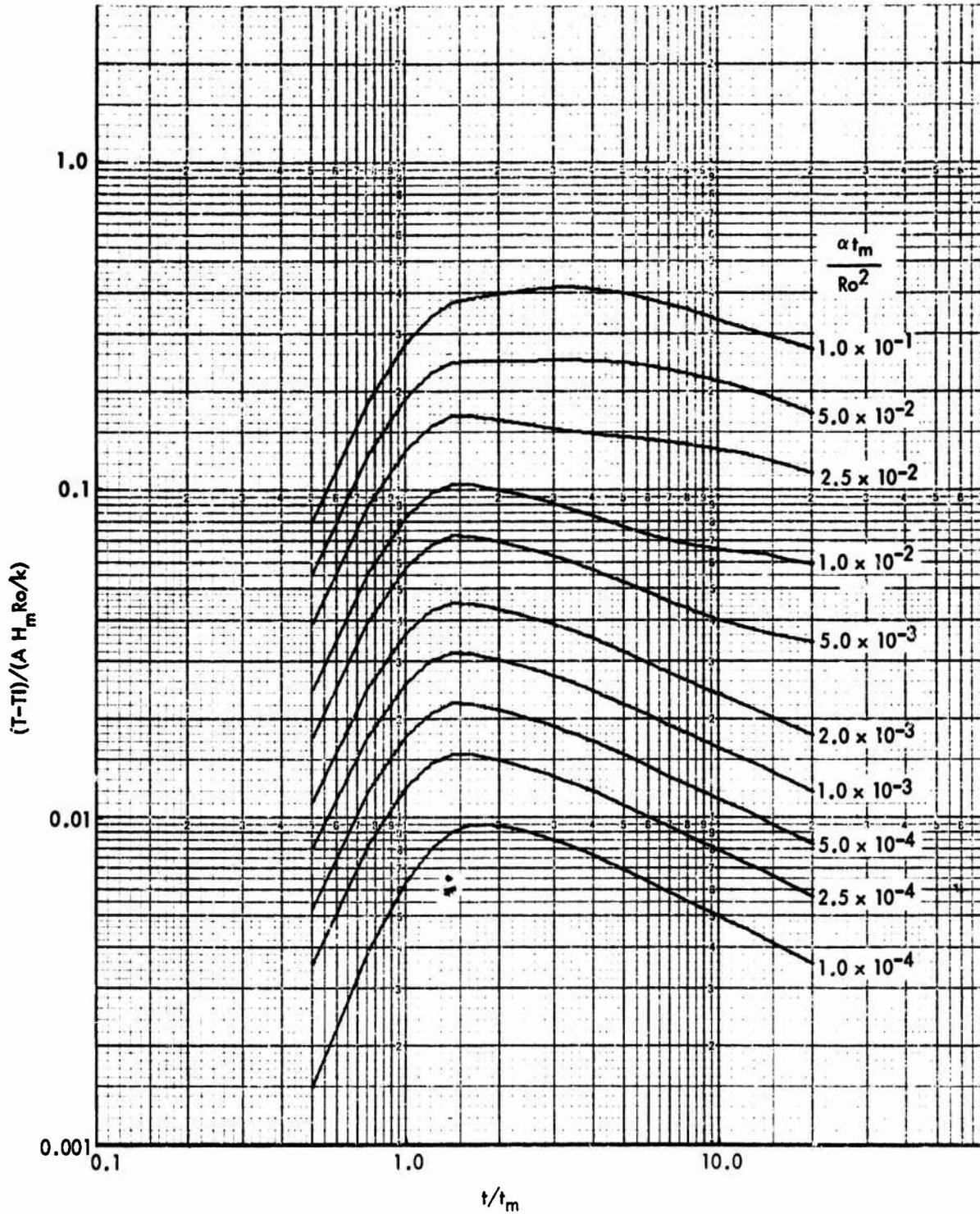
FIG. A - 3.1.1   DIMENSIONLESS SURFACE TEMPERATURE HISTORIES (Ri* = 0.6, $\phi = 0°$)
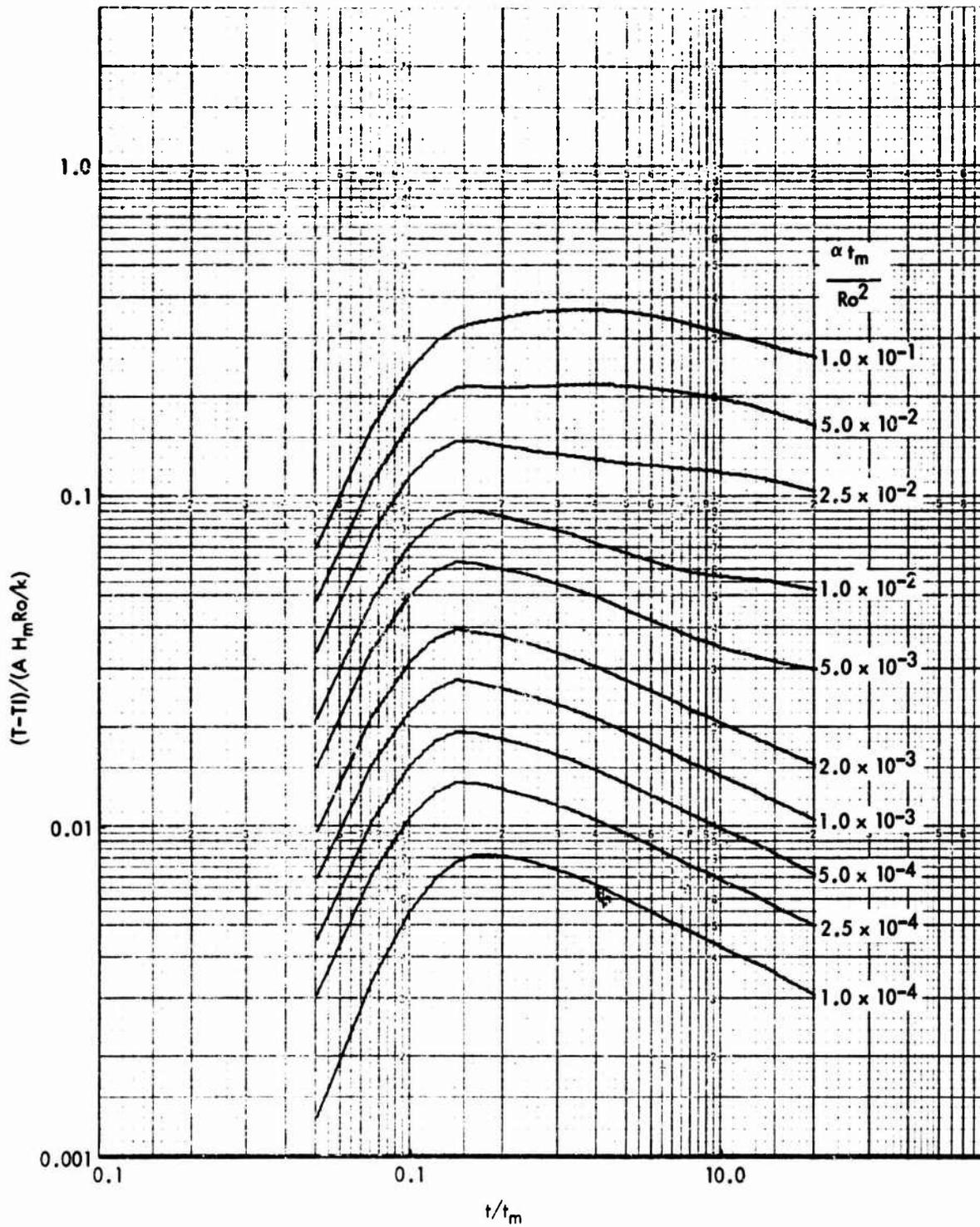
FIG. A - 3.1.2   DIMENSIONLESS SURFACE TEMPERATURE HISTORIES (Ri* = 0.6, ϕ = 30°)
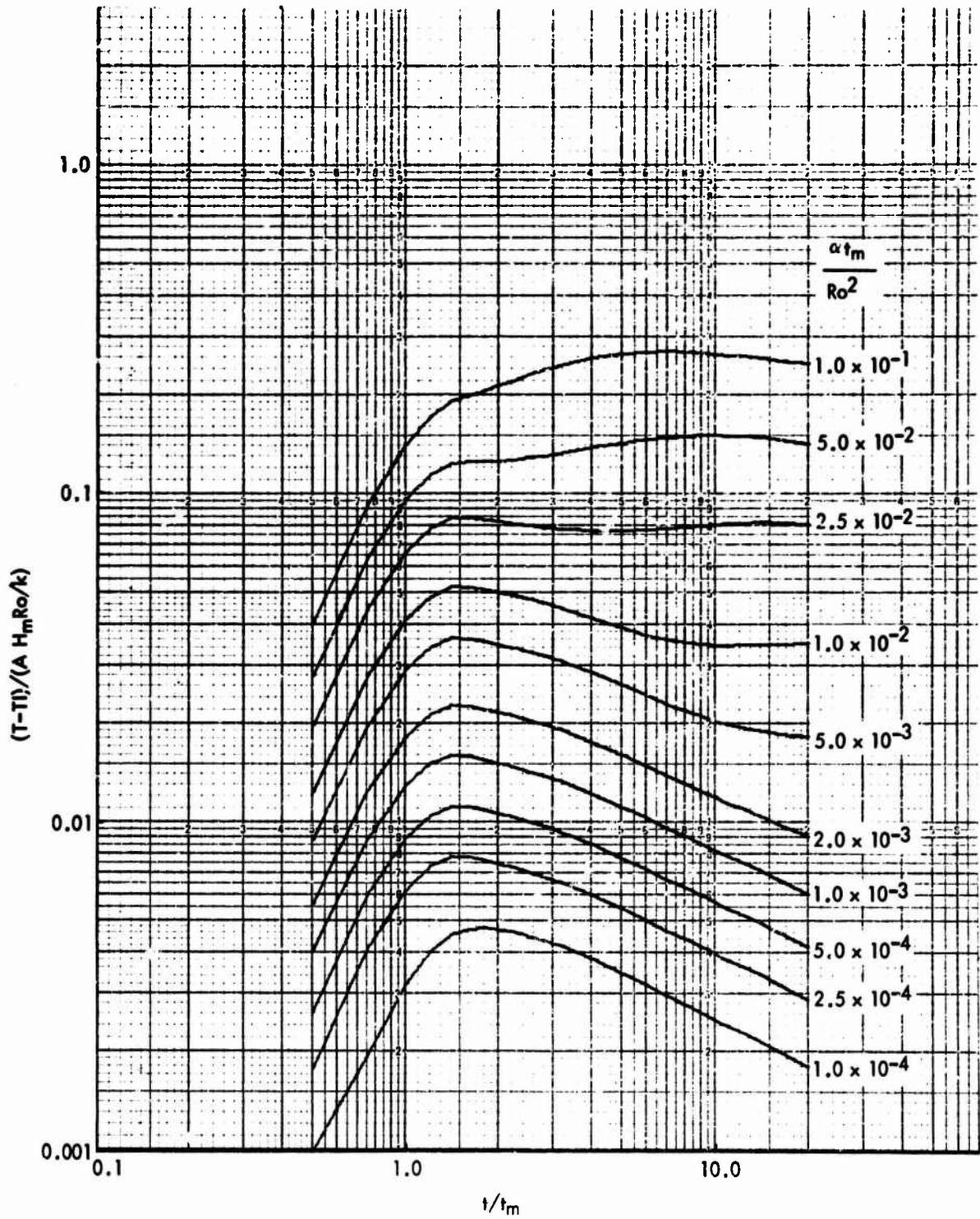
FIG. A – 3.1.3   DIMENSIONLESS SURFACE TEMPERATURE HISTORIES (Ri* = 0.6, ϕ = 60°)
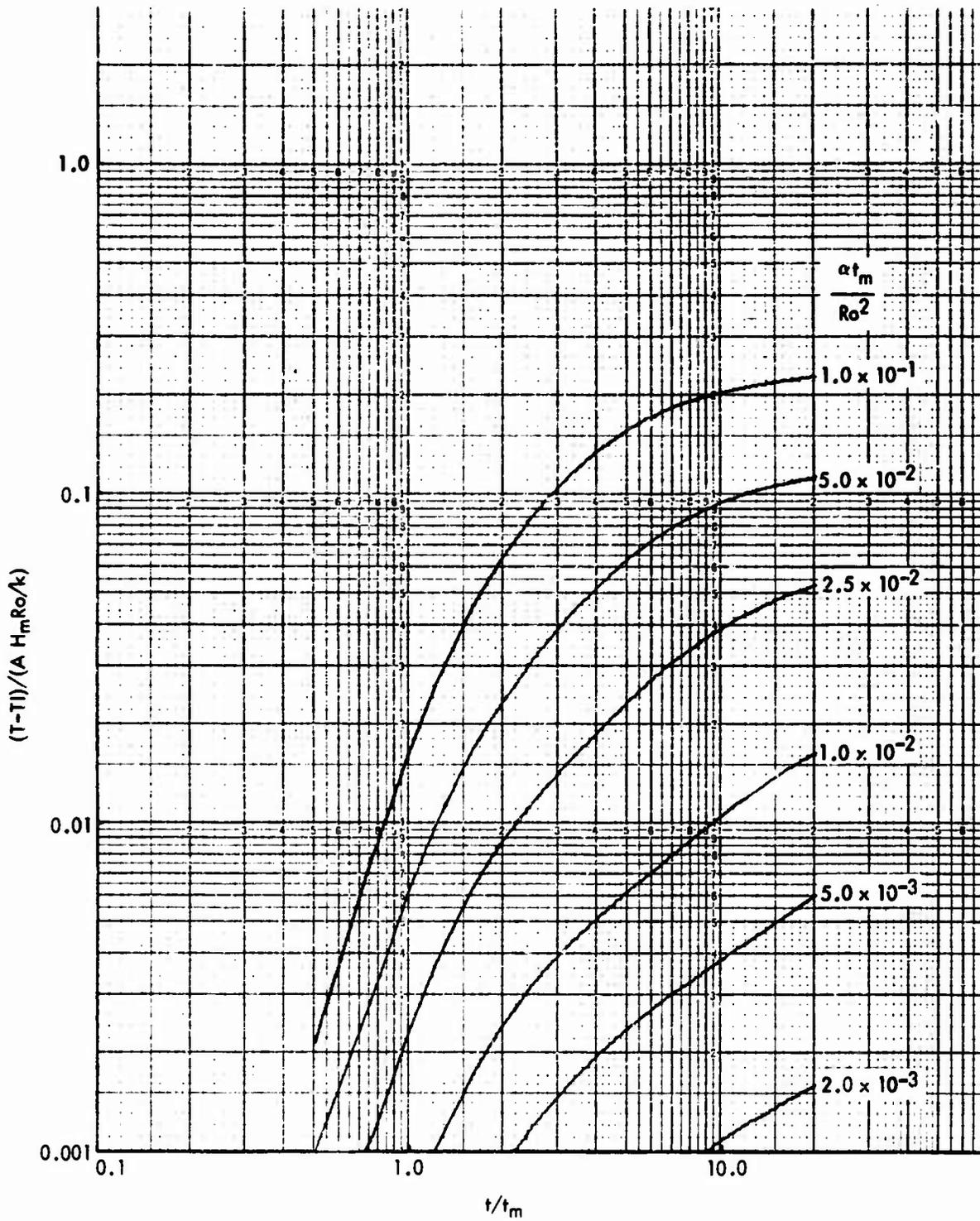
FIG. A - 3.1.4   DIMENSIONLESS SURFACE TEMPERATURE HISTORIES (Ri* = 0.6, φ = 90°)
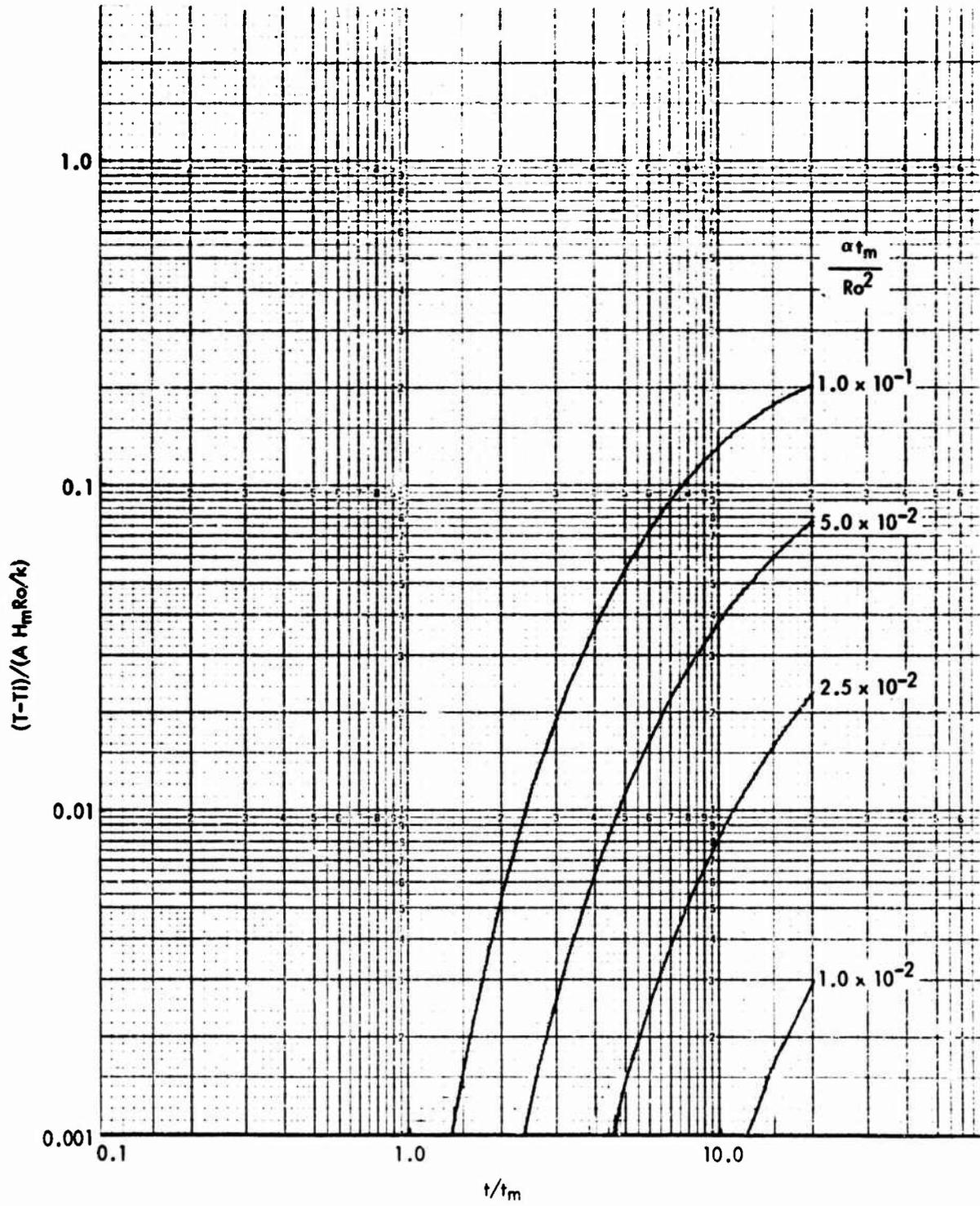
FIG. A - 3.1.5   DIMENSIONLESS SURFACE TEMPERATURE HISTORIES ($Ri^* = 0.6$, $\phi = 135°$)
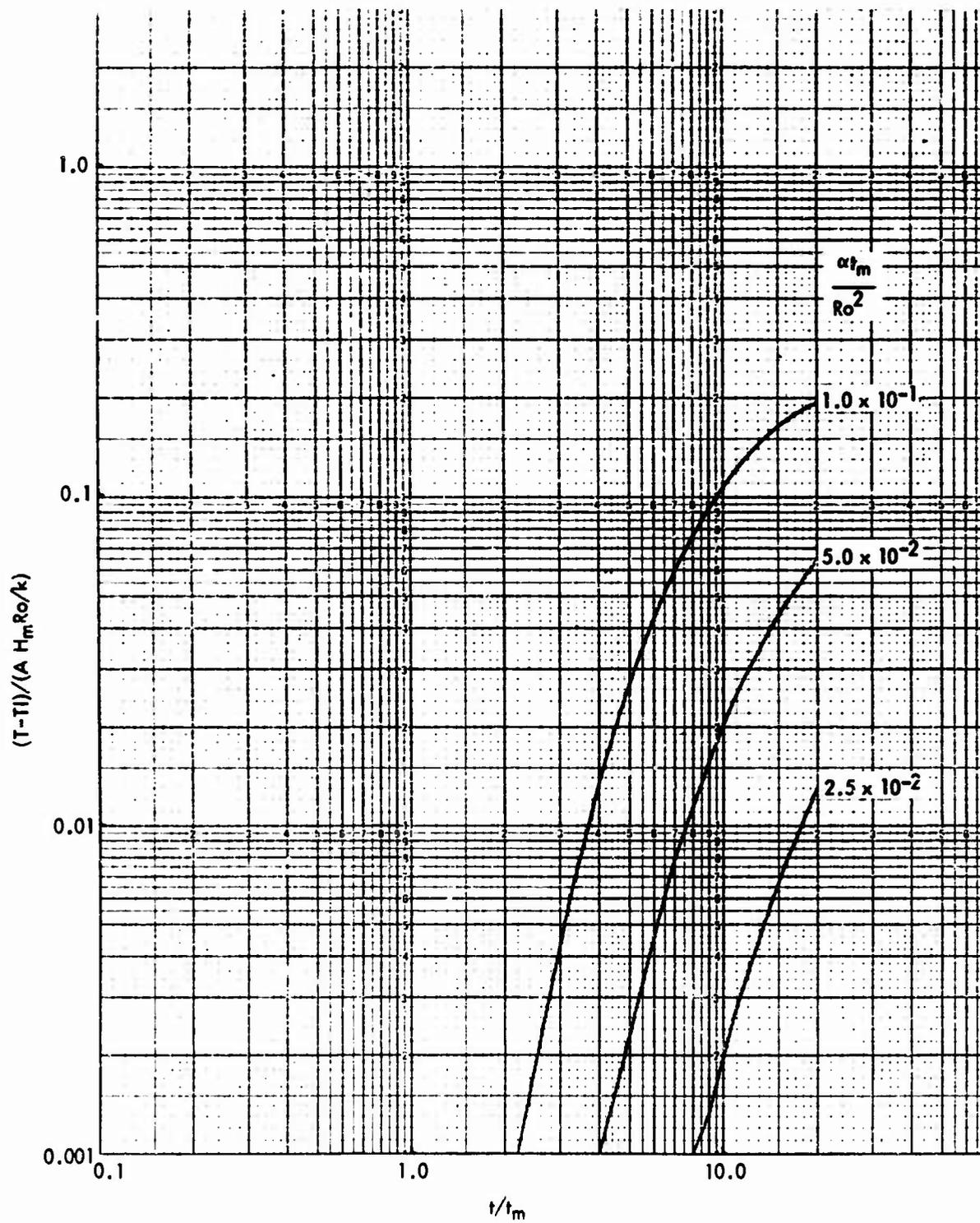
FIG. A - 3.1.6   DIMENSIONLESS SURFACE TEMPERATURE HISTORIES (Ri* = 0.6, ϕ = 180°)

FIG. A - 3.2.1   DIMENSIONLESS MIDPLANE TEMPERATURE HISTORIES (Ri* = 0.6, $\phi = 0°$)
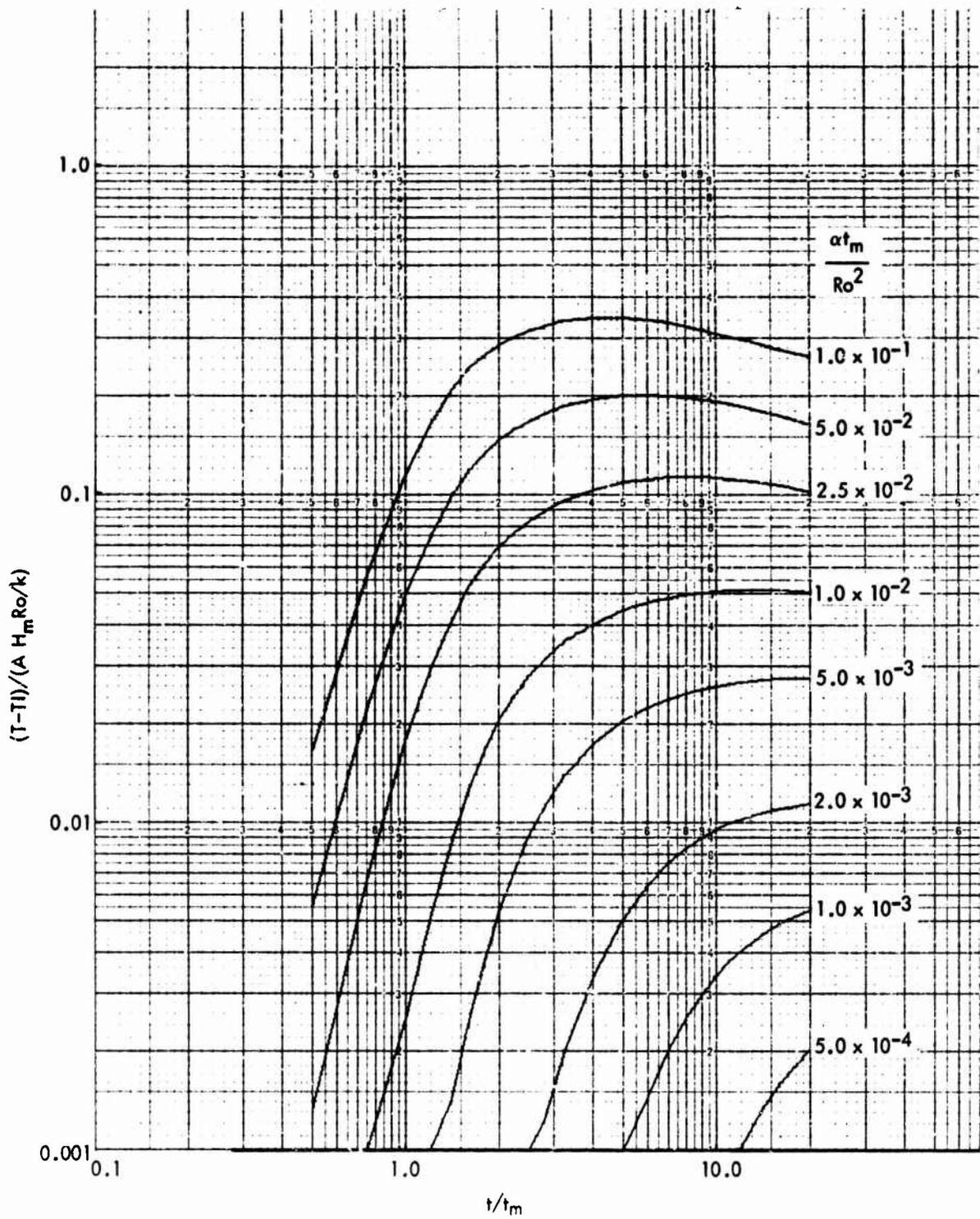
FIG. A - 3.2.2   DIMENSIONLESS MIDPLANE TEMPERATURE HISTORIES (Ri* = 0.6, ϕ = 30°)
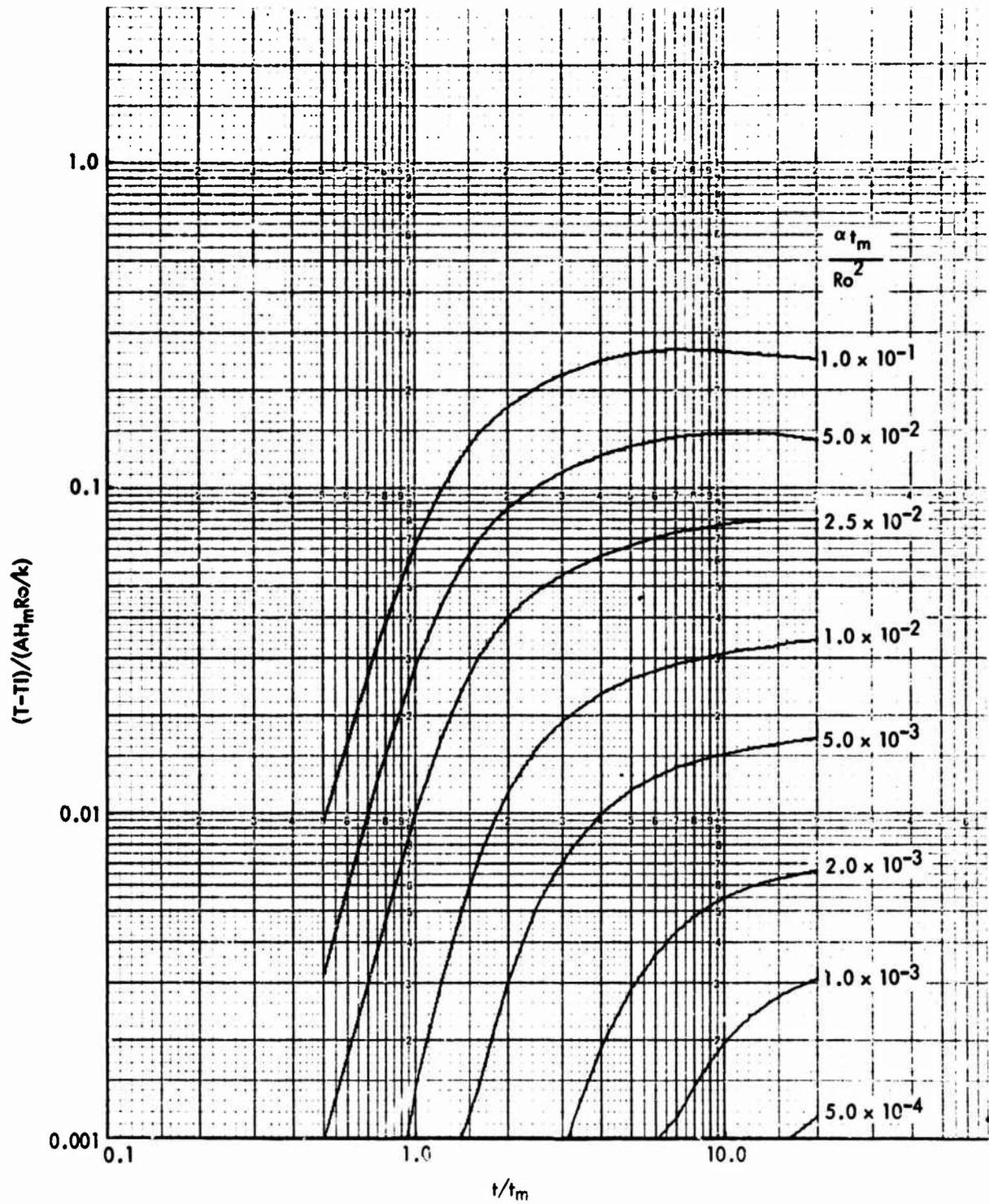
FIG. A - 3.2.3   DIMENSIONLESS MIDPLANE TEMPERATURE HISTORIES (Ri* = 0.6, $\phi = 60°$)
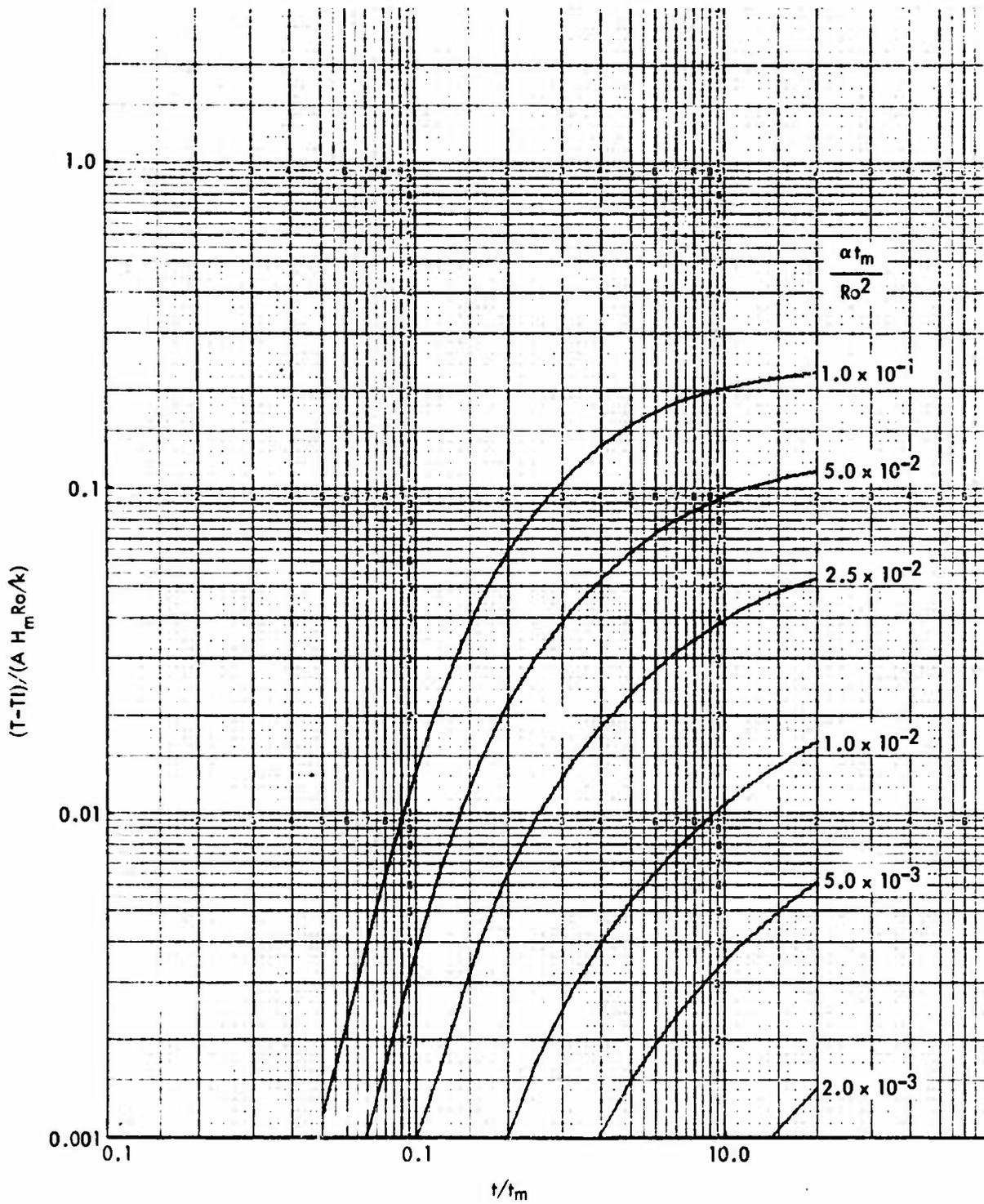
FIG. A - 3.2.4   DIMENSIONLESS MIDPLANE TEMPERATURE HISTORIES (Ri* = 0.6, $\phi = 90°$)
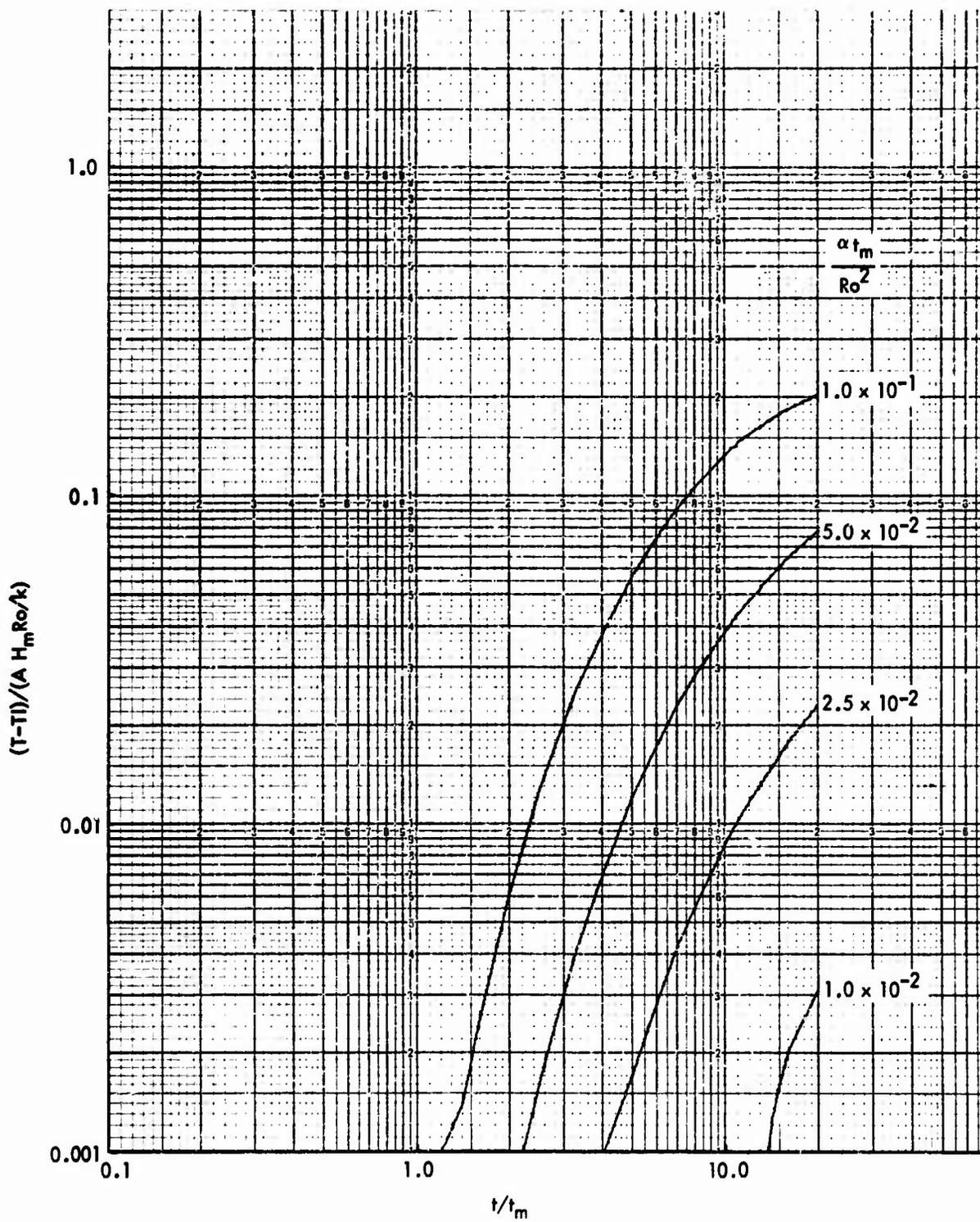
FIG. A - 3.2.5   DIMENSIONLESS MIDPLANE TEMPERATURE HISTORIES (Ri* = 0.6, ϕ = 135°)
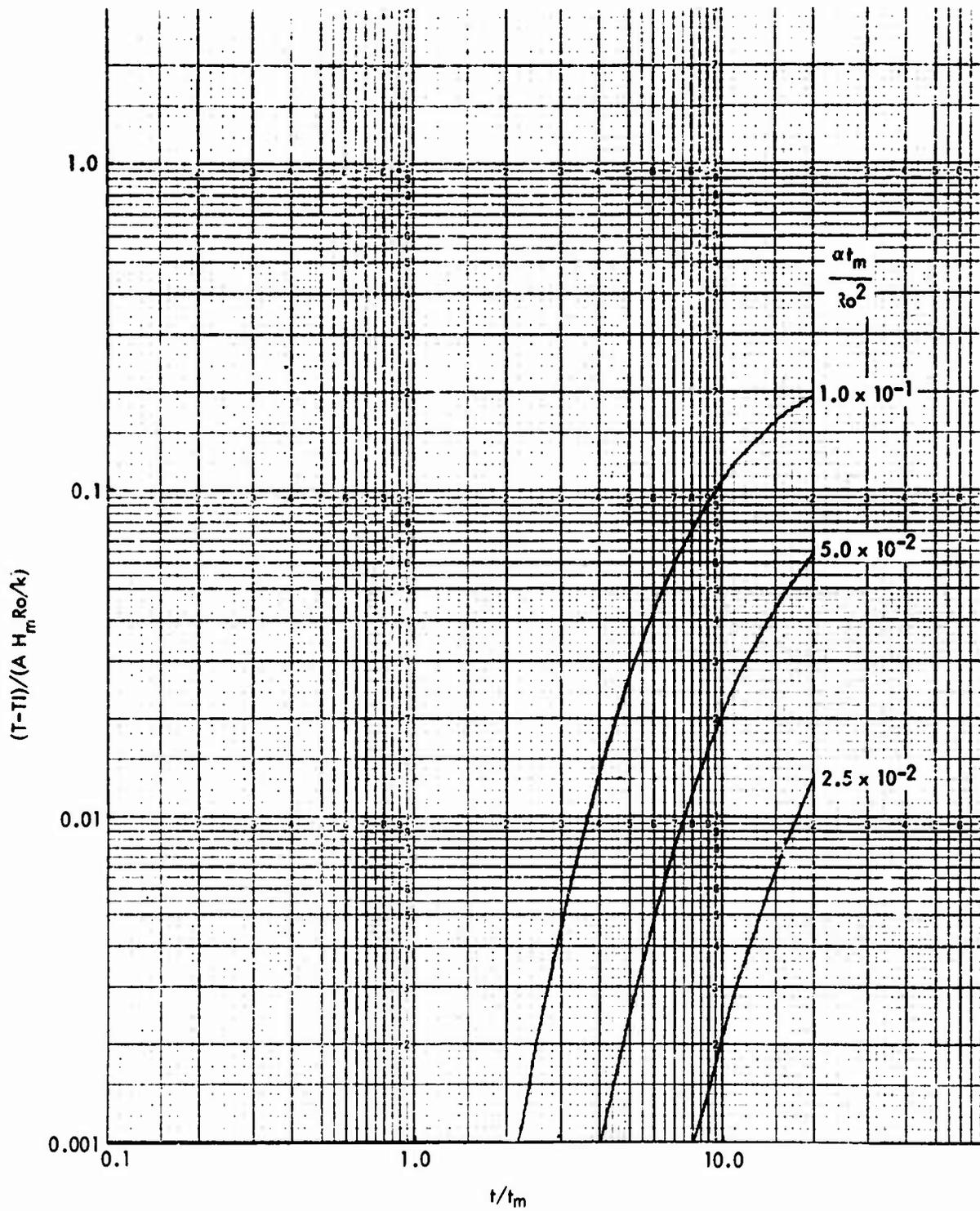
FIG. A - 3.2.6   DIMENSIONLESS MIDPLANE TEMPERATURE HISTORIES (Ri* = 0.6, ϕ = 180°)

FIG. A - 3.3.1   DIMENSIONLESS BACKFACE TEMPERATURE HISTORIES (Ri* = 0.6, $\phi = 0°$)
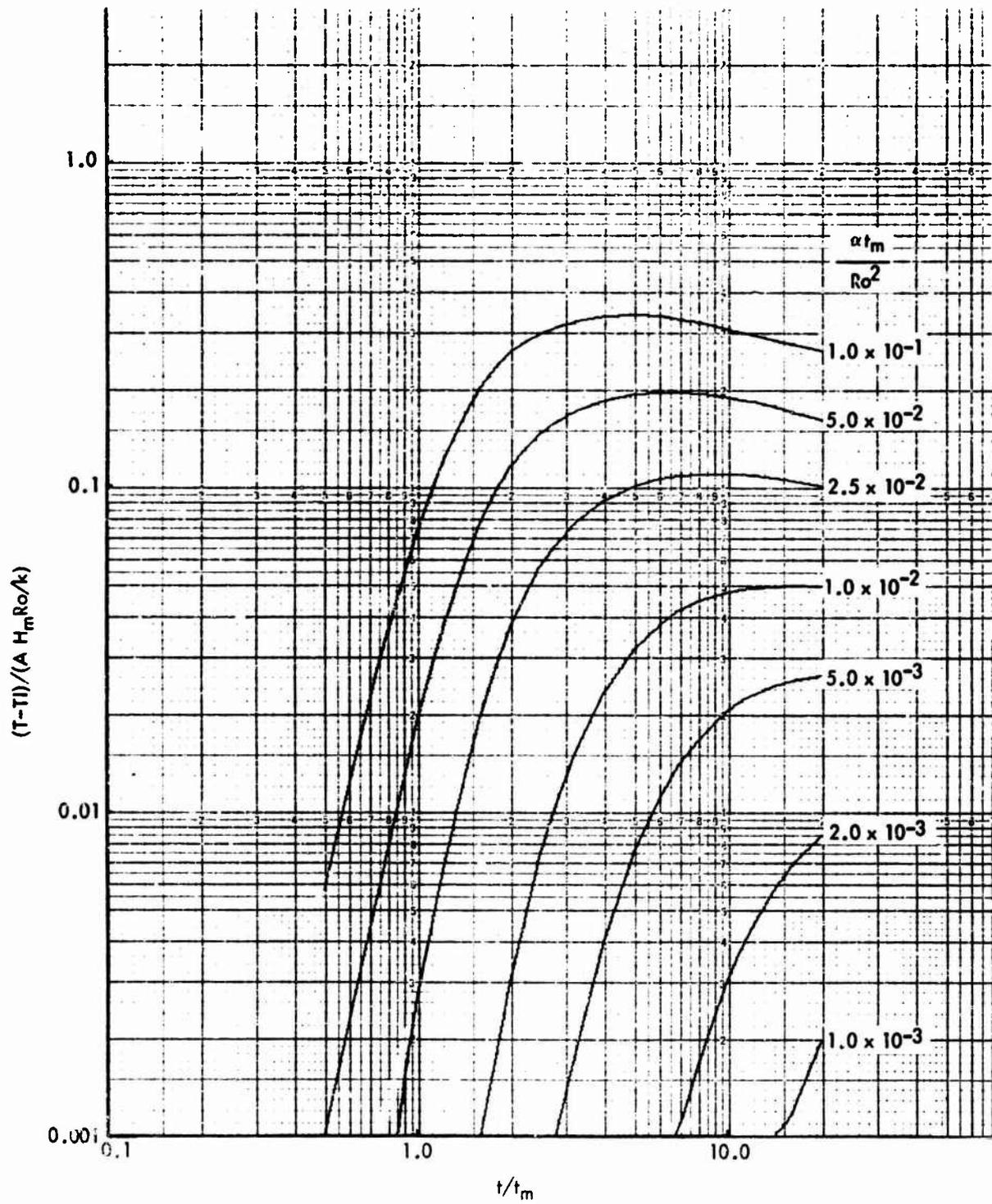
FIG. A - 3.3.2   DIMENSIONLESS BACKFACE TEMPERATURE HISTORIES (Ri* = 0.6, $\varphi = 30°$)
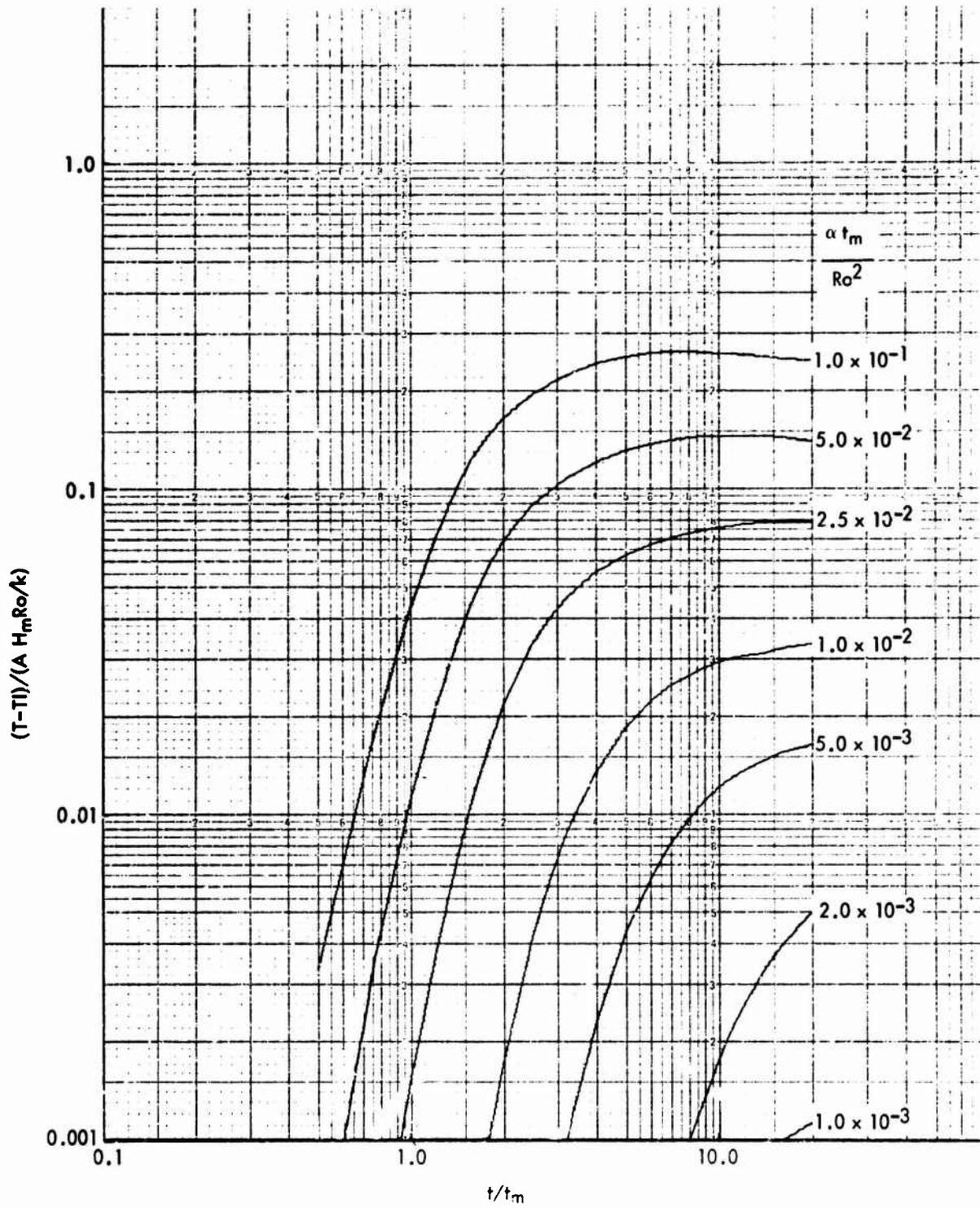
FIG. A - 3.3.3   DIMENSIONLESS BACKFACE TEMPERATURE HISTORIES ($Ri^* = 0.6$, $\phi = 60°$)
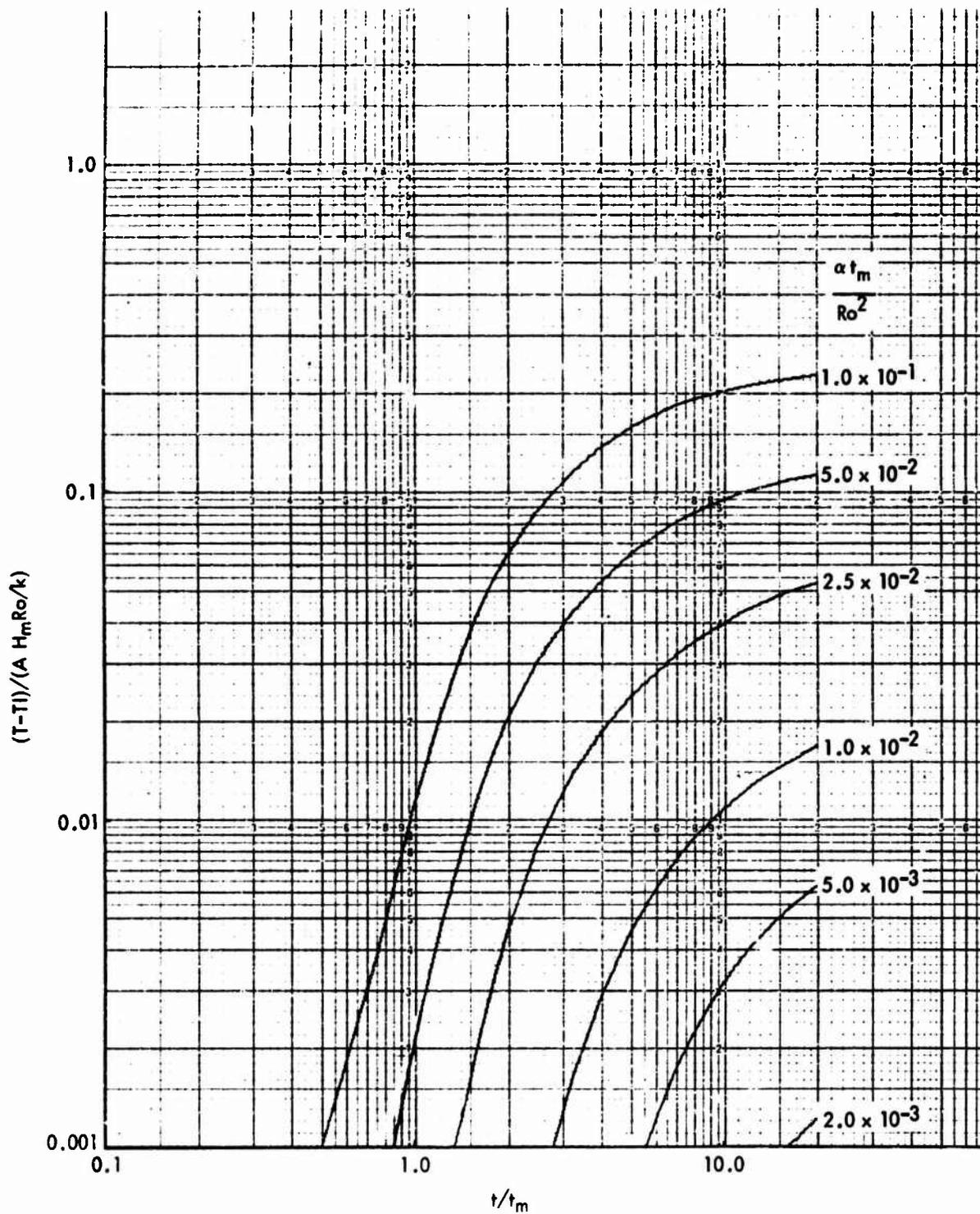
FIG. A - 3.3.4   DIMENSIONLESS BACKFACE TEMPERATURE HISTORIES (Ri* = 0.6, $\phi = 90°$)
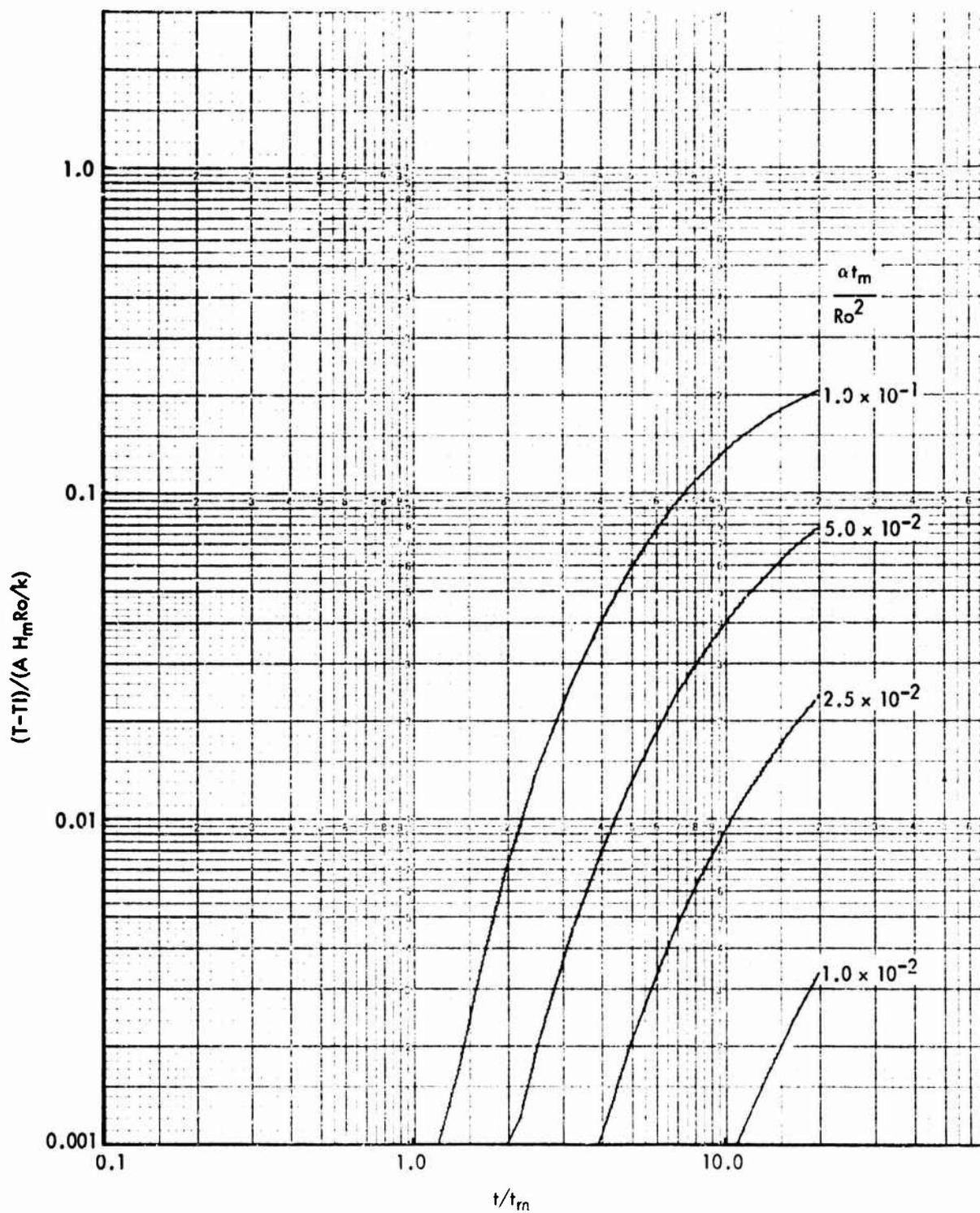
FIG. A - 3.3.5   DIMENSIONLESS BACKFACE TEMPERATURE HISTORIES (Ri* = 0.6, $\phi = 135°$)
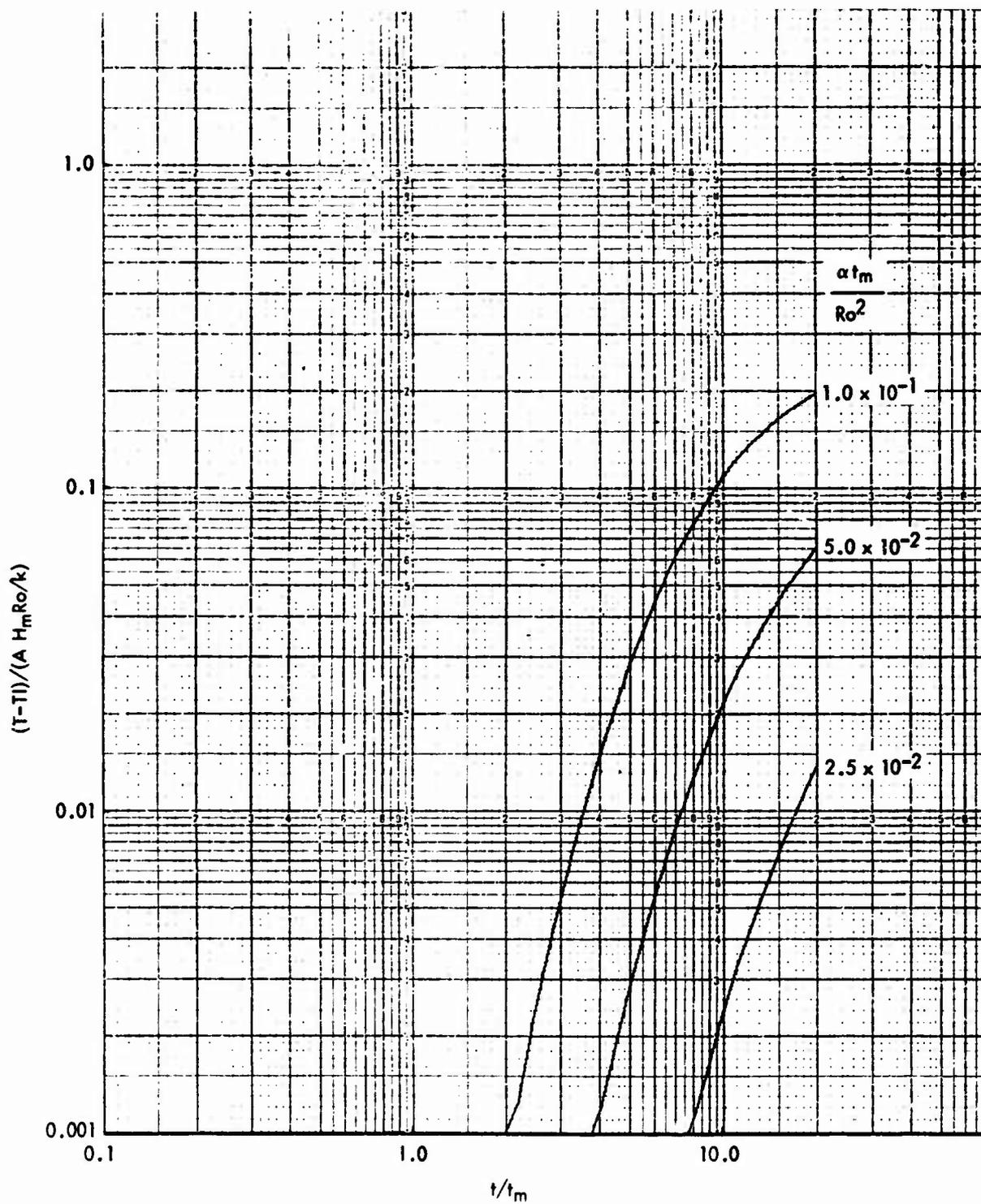
FIG. A - 3.3.6   DIMENSIONLESS BACKFACE TEMPERATURE HISTORIES ($Ri^* = 0.6$, $\phi = 180°$)
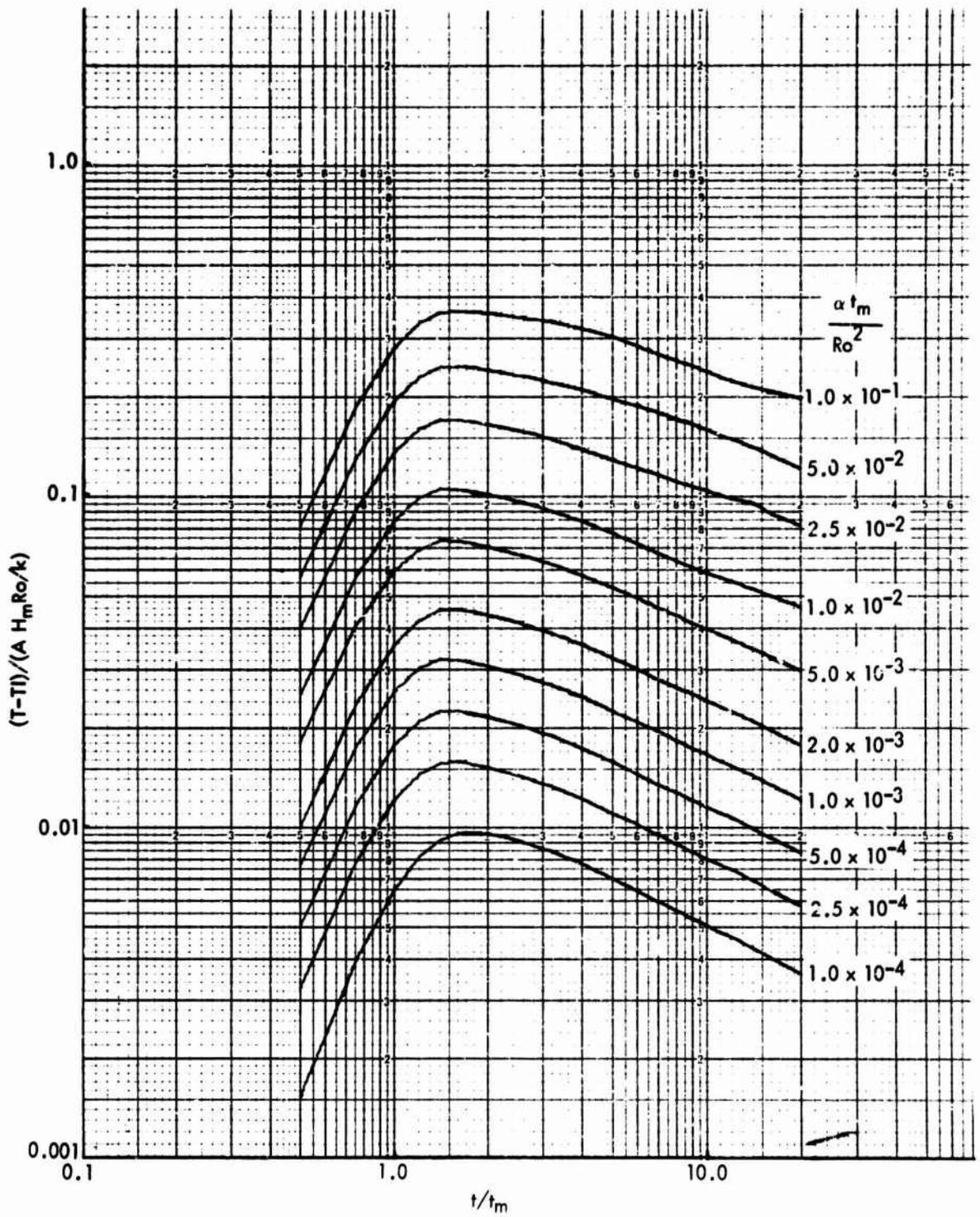
FIG. A - 4.1.1   DIMENSIONLESS SURFACE TEMPERATURE HISTORIES (Ri* = 0.4, ϕ = 0°)
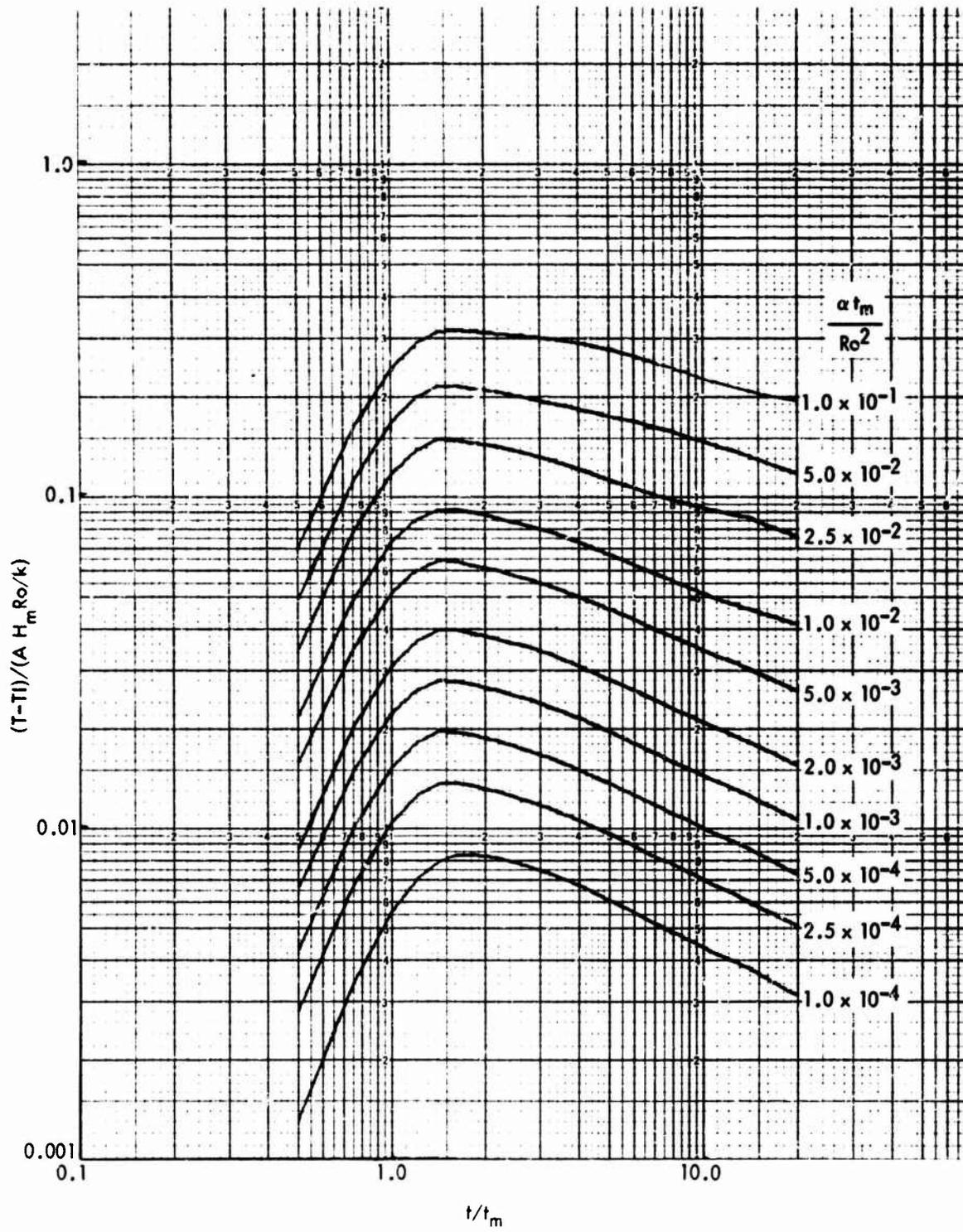
FIG. A - 4.1.2   DIMENSIONLESS SURFACE TEMPERATURE HISTORIES (Ri* = 0.4, ϕ = 30°)
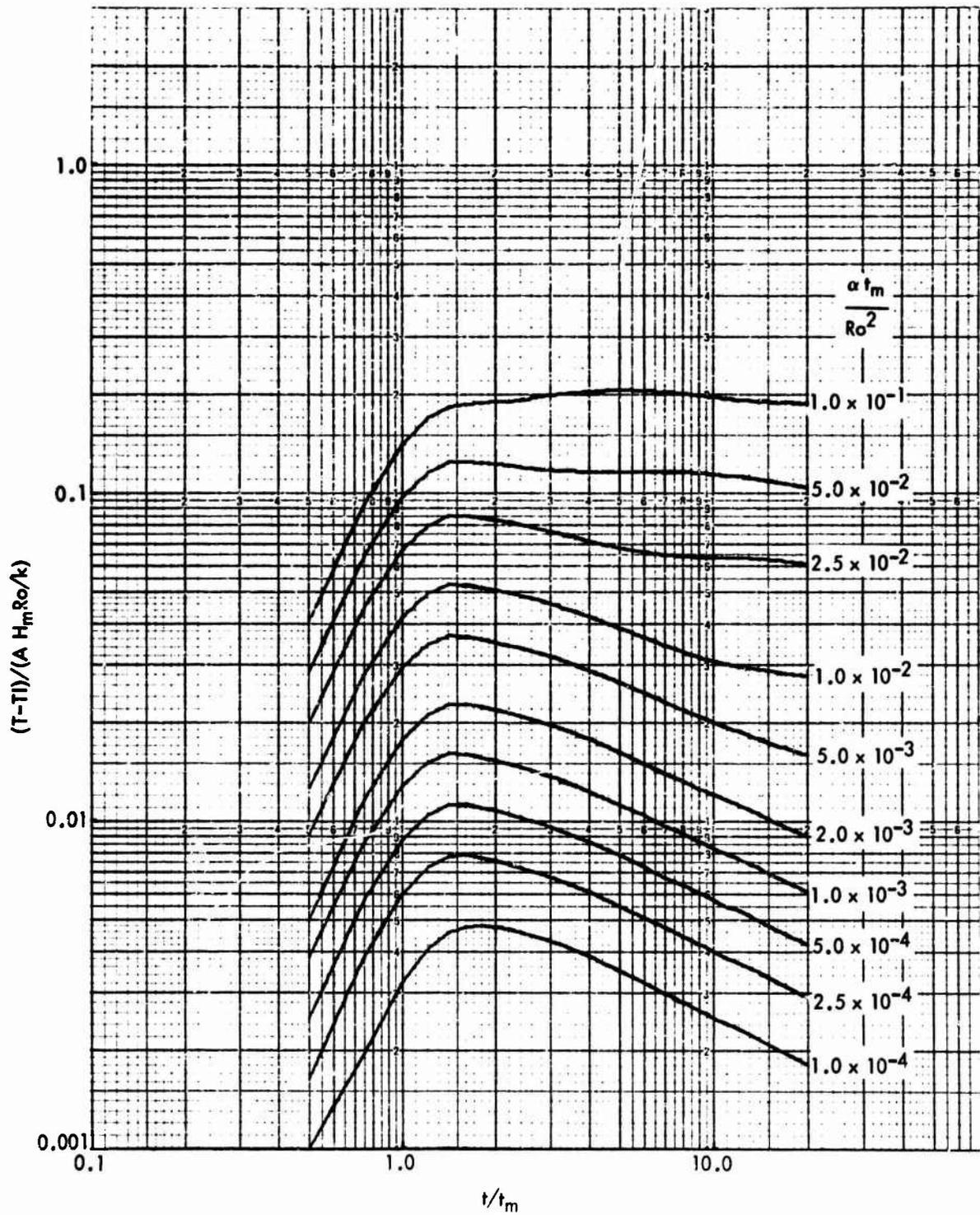
FIG. A - 4.1.3   DIMENSIONLESS SURFACE TEMPERATURE HISTORIES (Pi* = 0.4, ∉ – 60°)
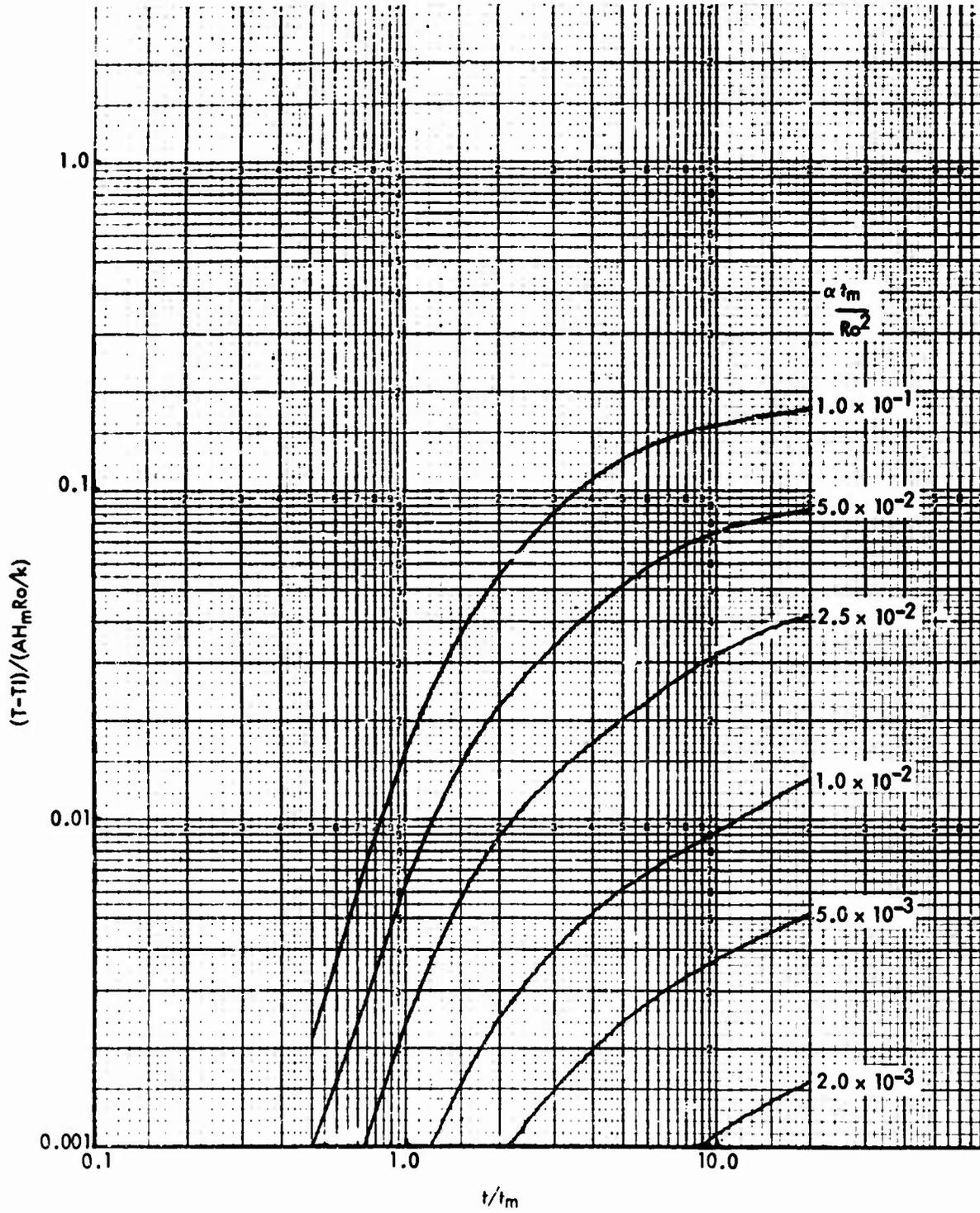
FIG. A - 4.1.4   DIMENSIONLESS SURFACE TEMPERATURE HISTORIES (Ri* = 0.4, $\phi = 90°$)
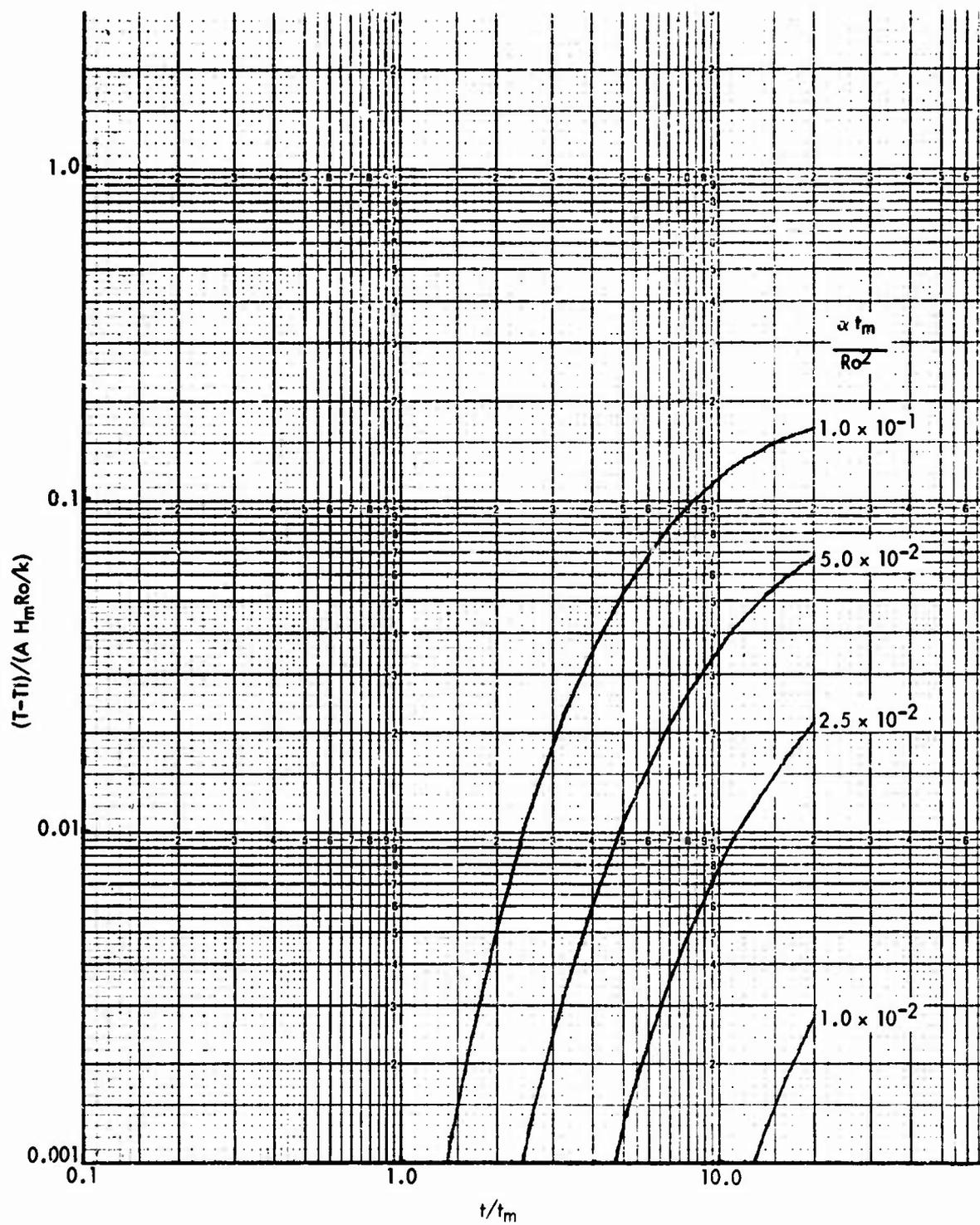
FIG. A - 4.1.5   DIMENSIONLESS SURFACE TEMPERATURE HISTORIES (Ri* = 0.4, φ = 135º)
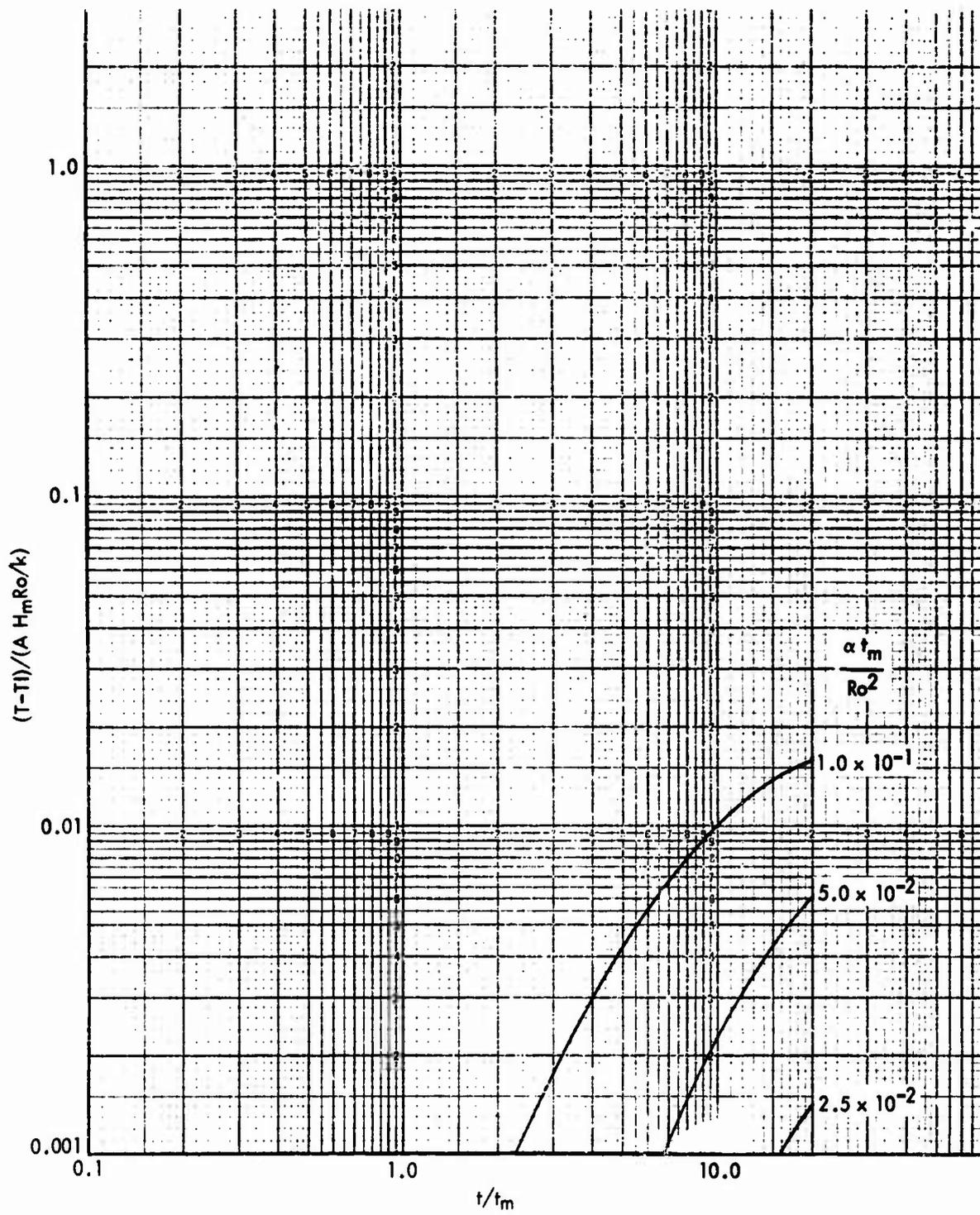
FIG. A - 4.1.6   DIMENSIONLESS SURFACE TEMPERATURE HISTORIES (Ri* = 0.4, ϕ = 180°)
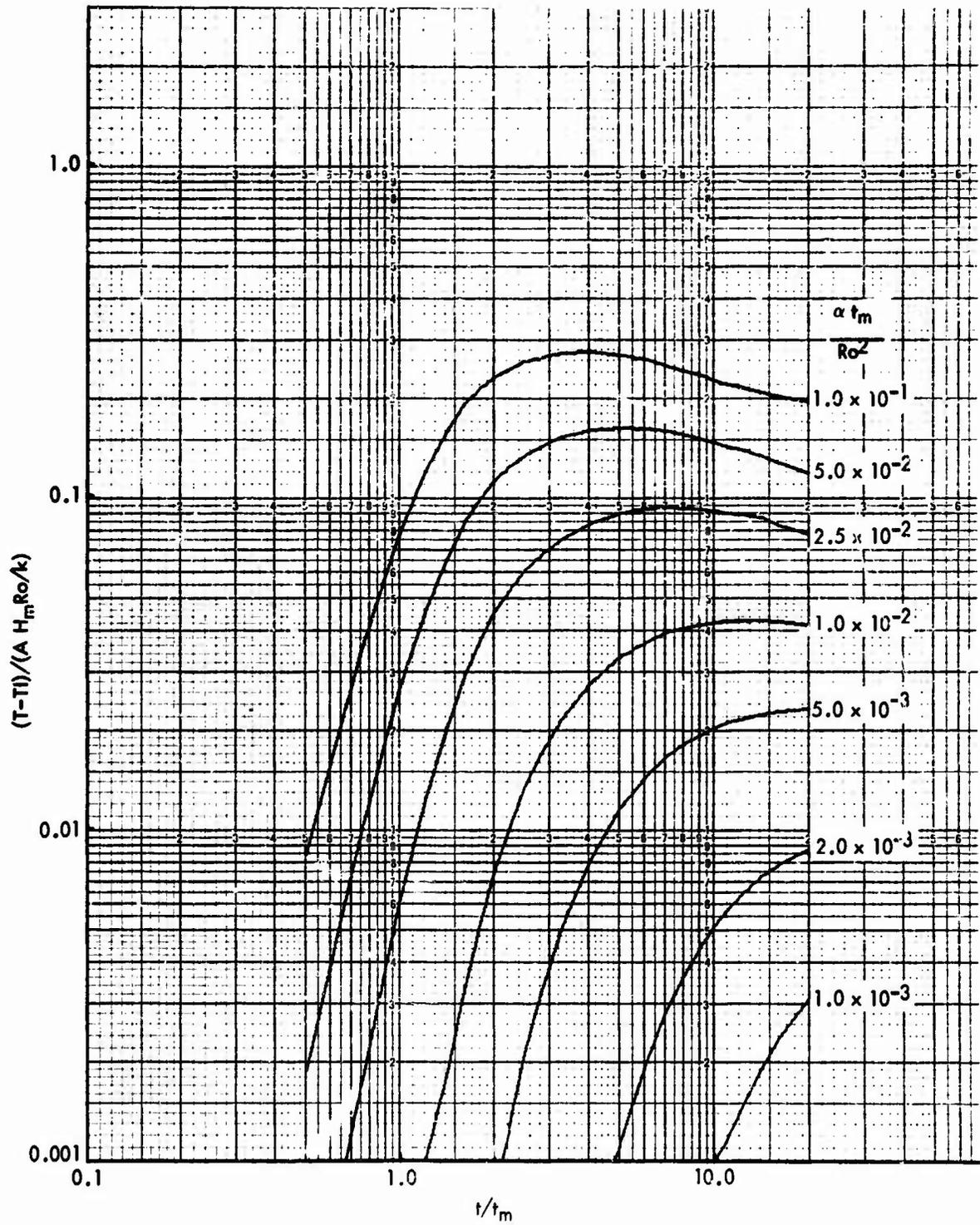
FIG. A - 4.2.1   DIMENSIONLESS MIDPLANE TEMPERATURE HISTORIES (Ri* = 0.4, $\varphi = 0°$)
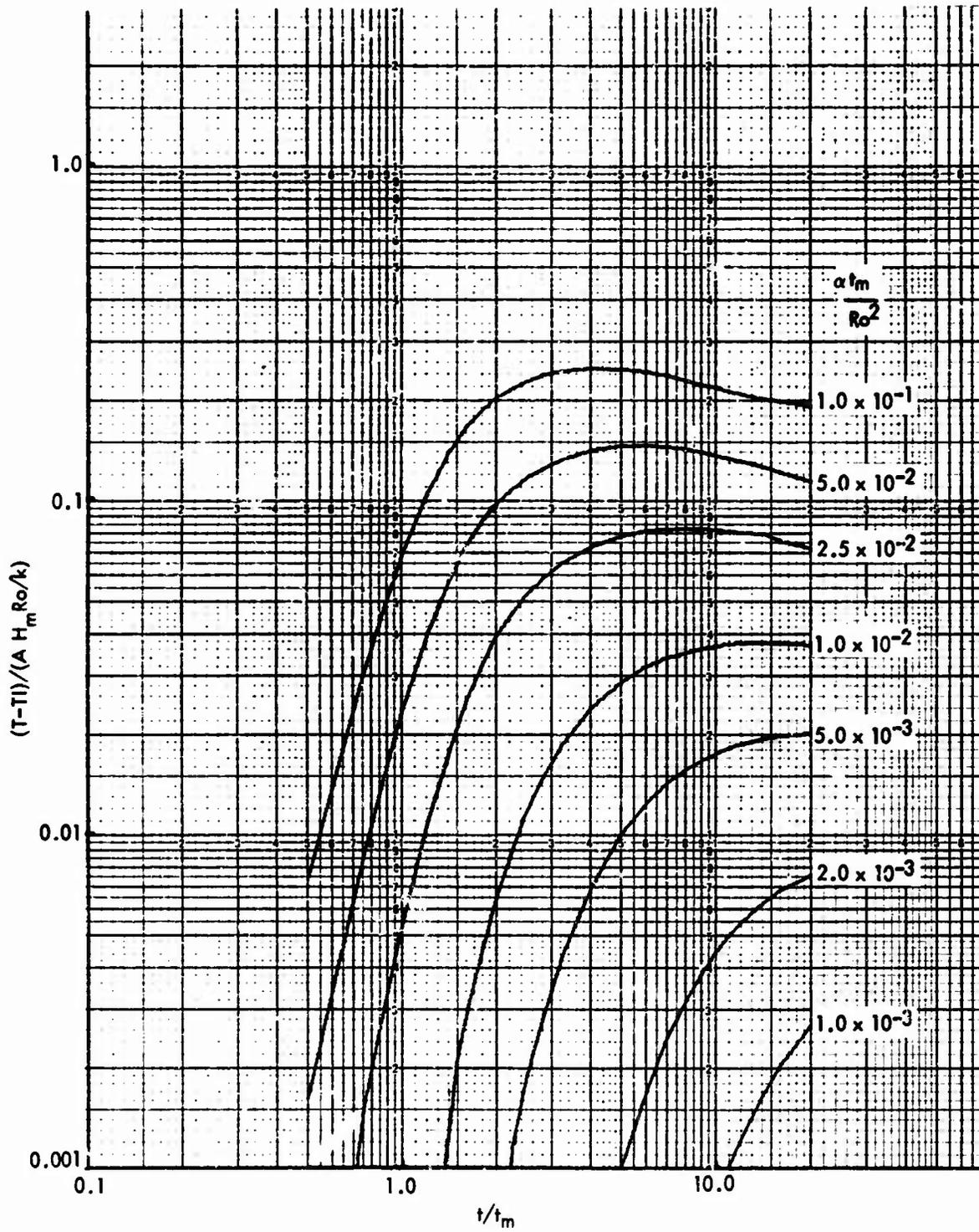
FIG. A - 4.2.2   DIMENSIONLESS MIDPLANE TEMPERATURE HISTORIES (Ri* = 0.4, ϕ = 30°)
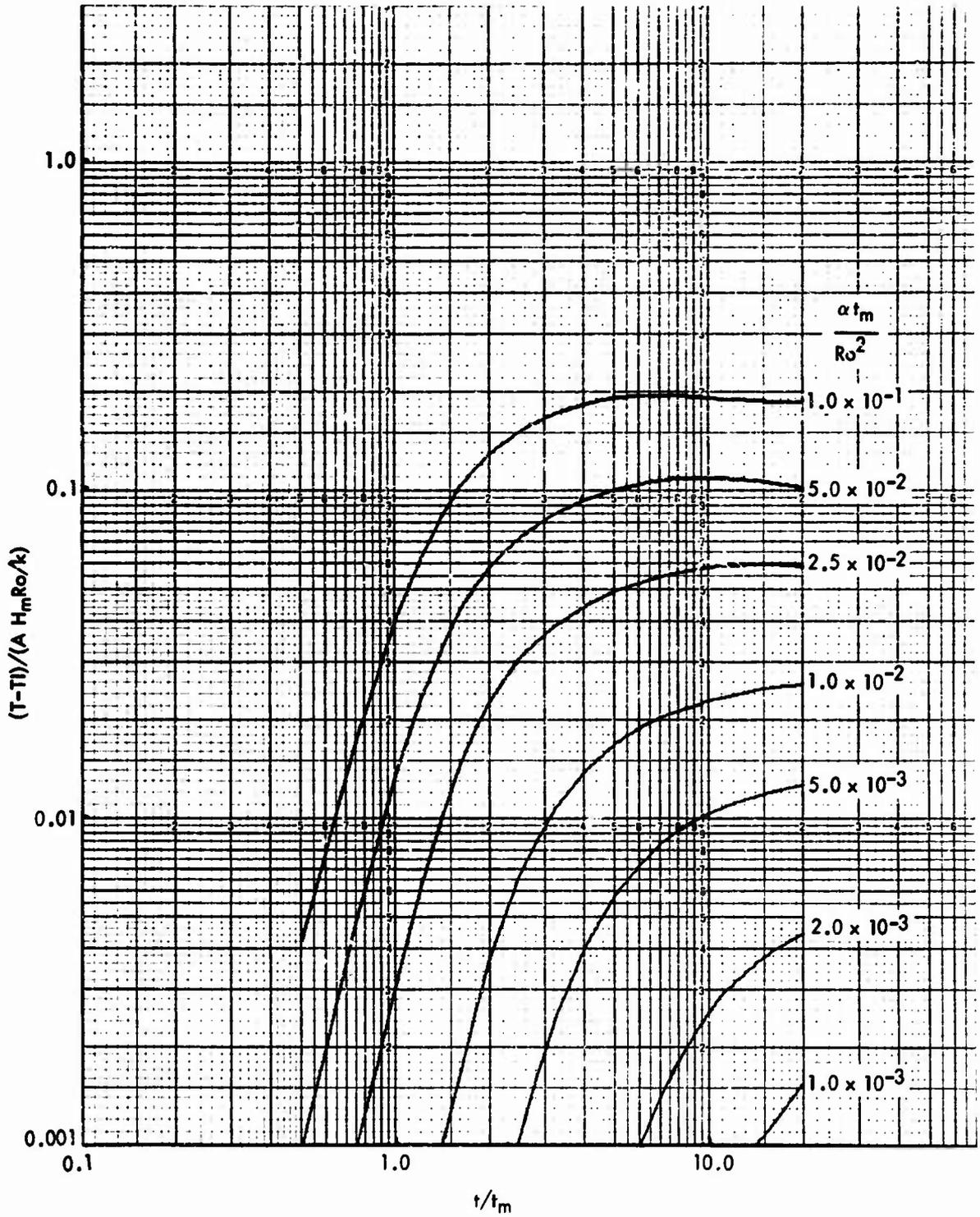
FIG. A - 4.2.3   DIMENSIONLESS MIDPLANE TEMPERATURE HISTORIES (Ri* = 0.4, ϕ = 60°)
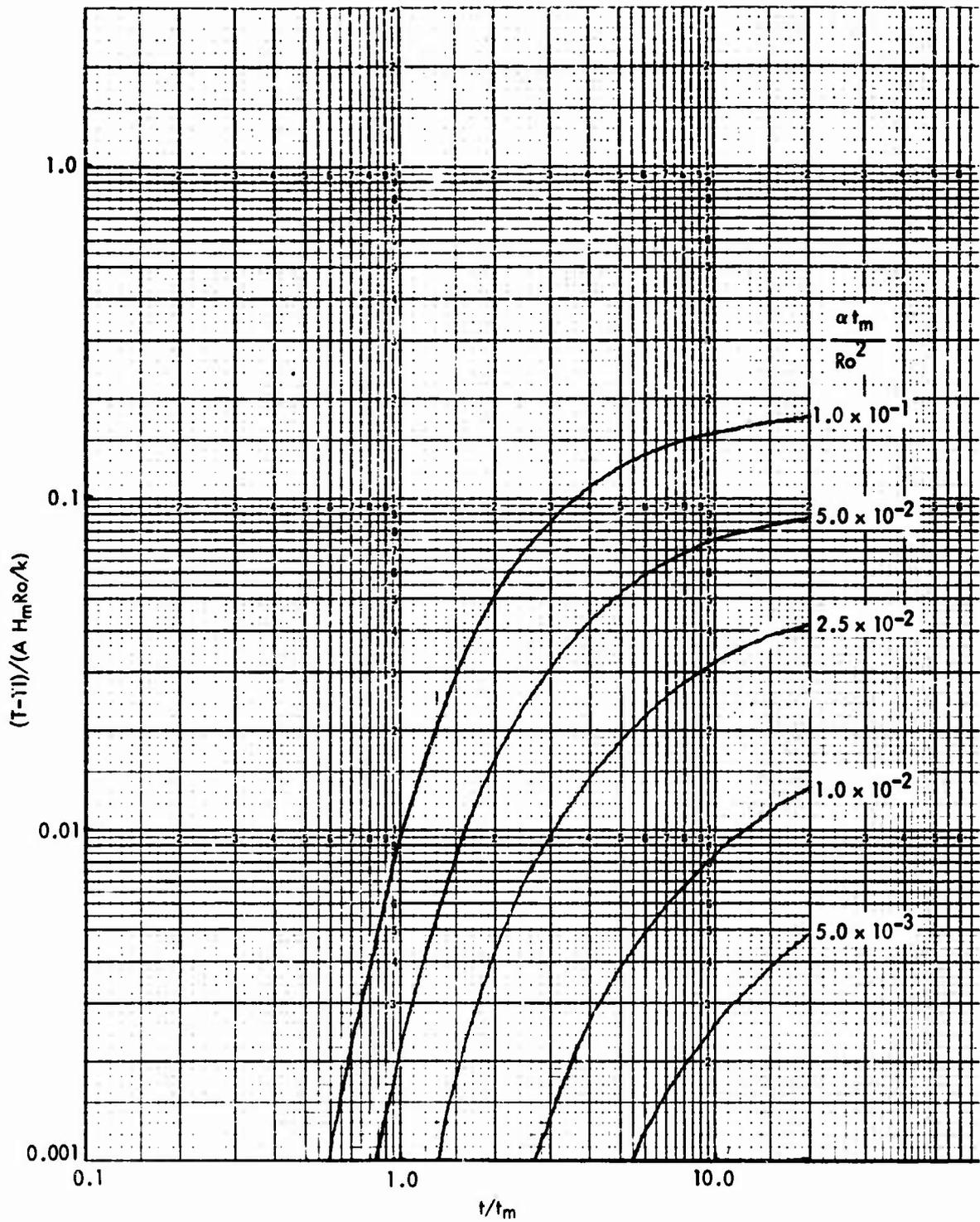
FIG. A - 4.2.4   DIMENSIONLESS MIDPLANE TEMPERATURE HISTORIES (Ri* = 0.4, ϕ = 90°)
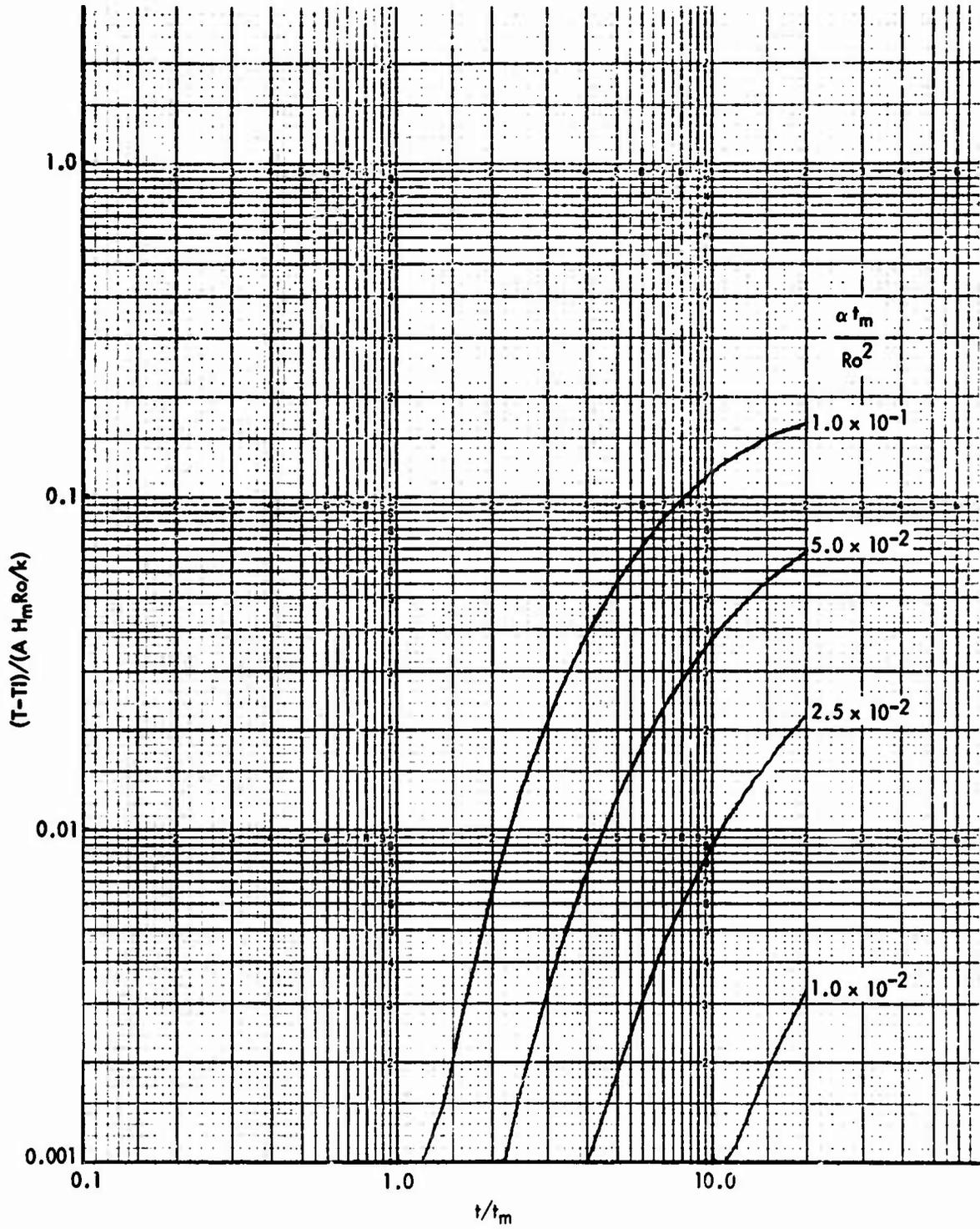
FIG. A - 4.2.5   DIMENSIONLESS MIDPLANE TEMPERATURE HISTORIES (Ri* = 0.4, ϕ = 135°)
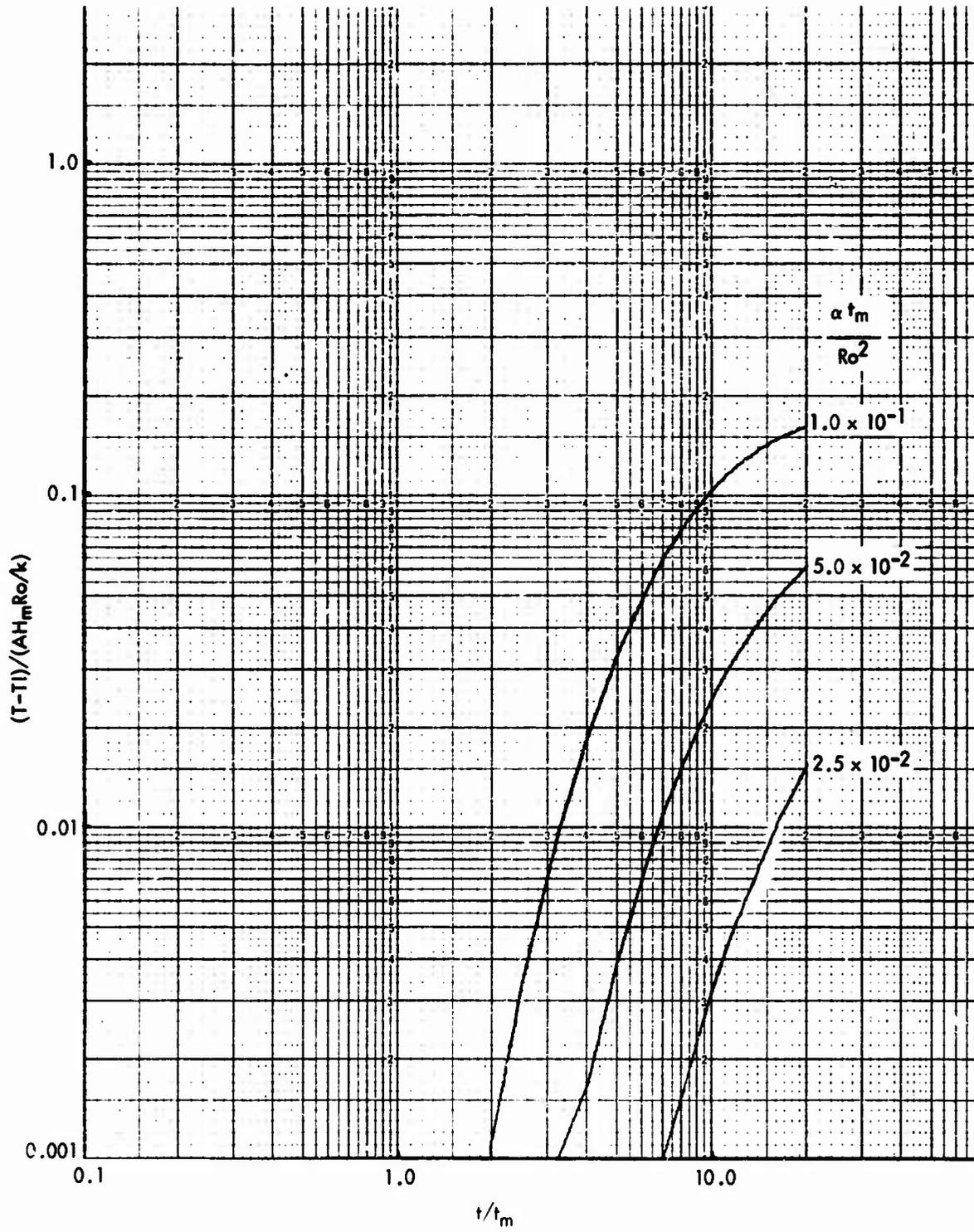
FIG. A - 4.2.6   DIMENSIONLESS MIDPLANE TEMPERATURE HISTORIES (Ri* = 0.4, ϕ = 180°)
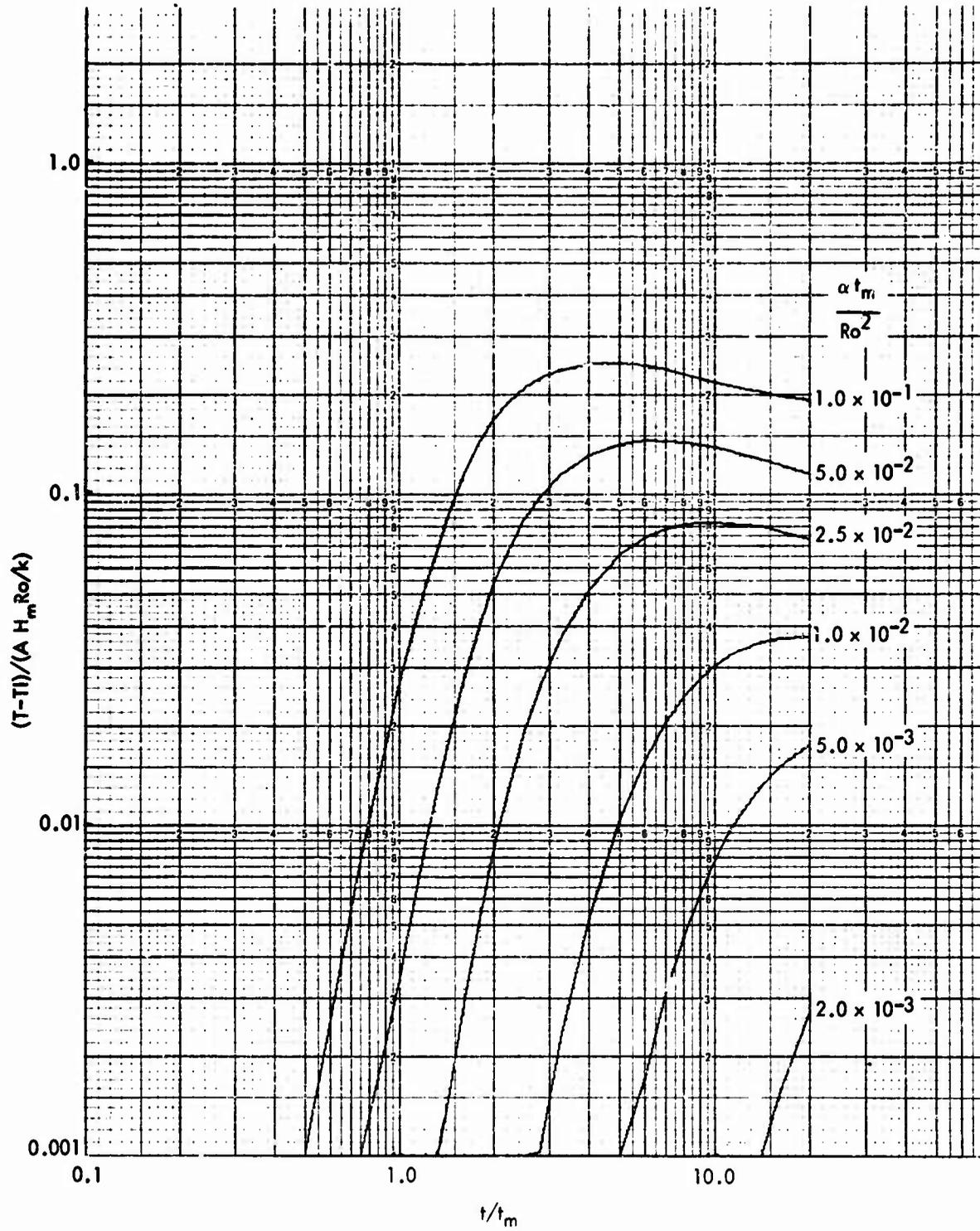
FIG. A - 4.3.1   DIMENSIONLESS BACKFACE TEMPERATURE HISTORIES (Ri* = 0.4, ϕ = 0°)
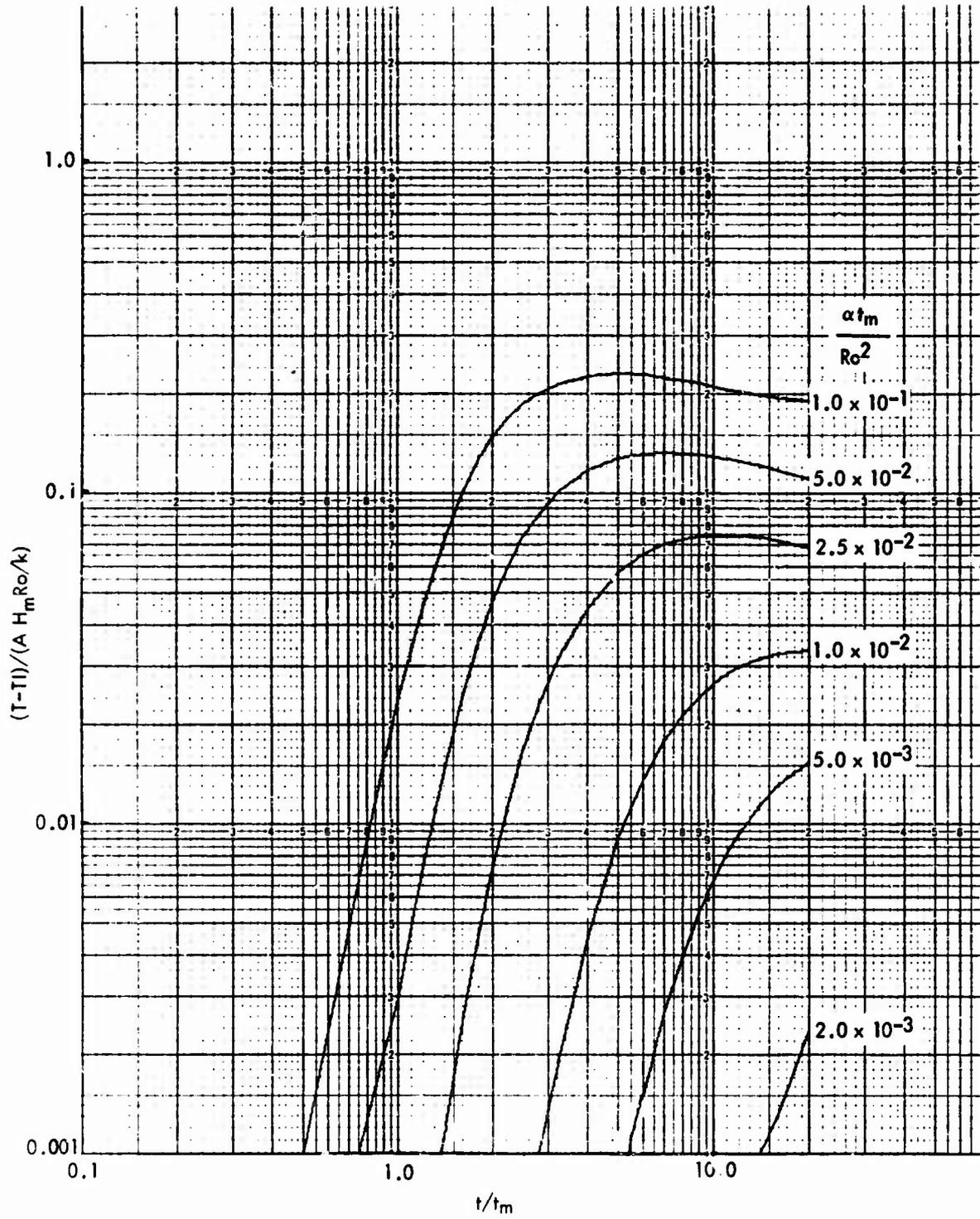
FIG. A - 4.3.2   DIMENSIONLESS BACKFACE TEMPERATURE HISTORIES $(Ri^* = 0.4, \phi = 30^o)$
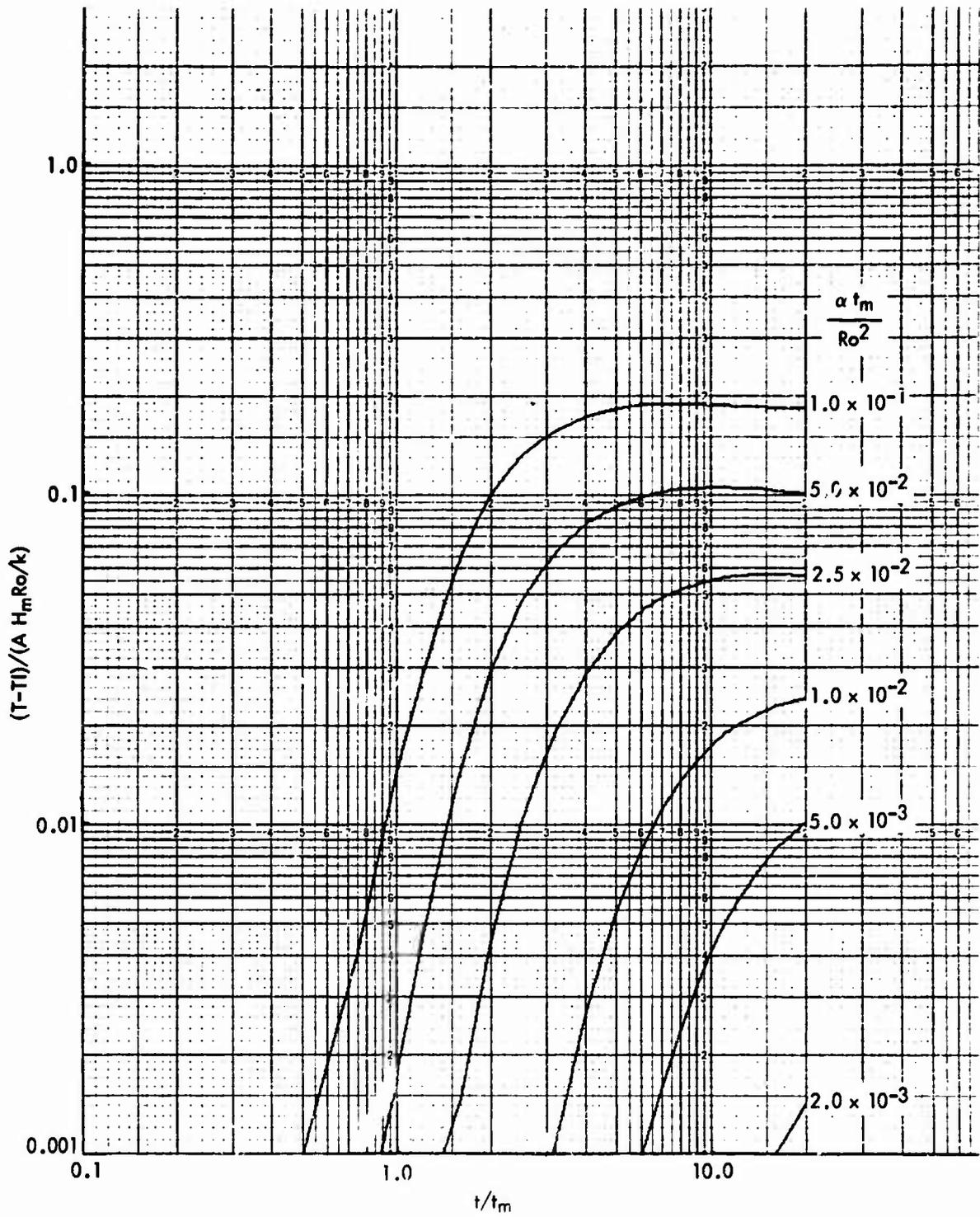
FIG. A - 4.3.3   DIMENSIONLESS BACKFACE TEMPERATURE HISTORIES (Ri* = 0.4, ϕ = 60°)
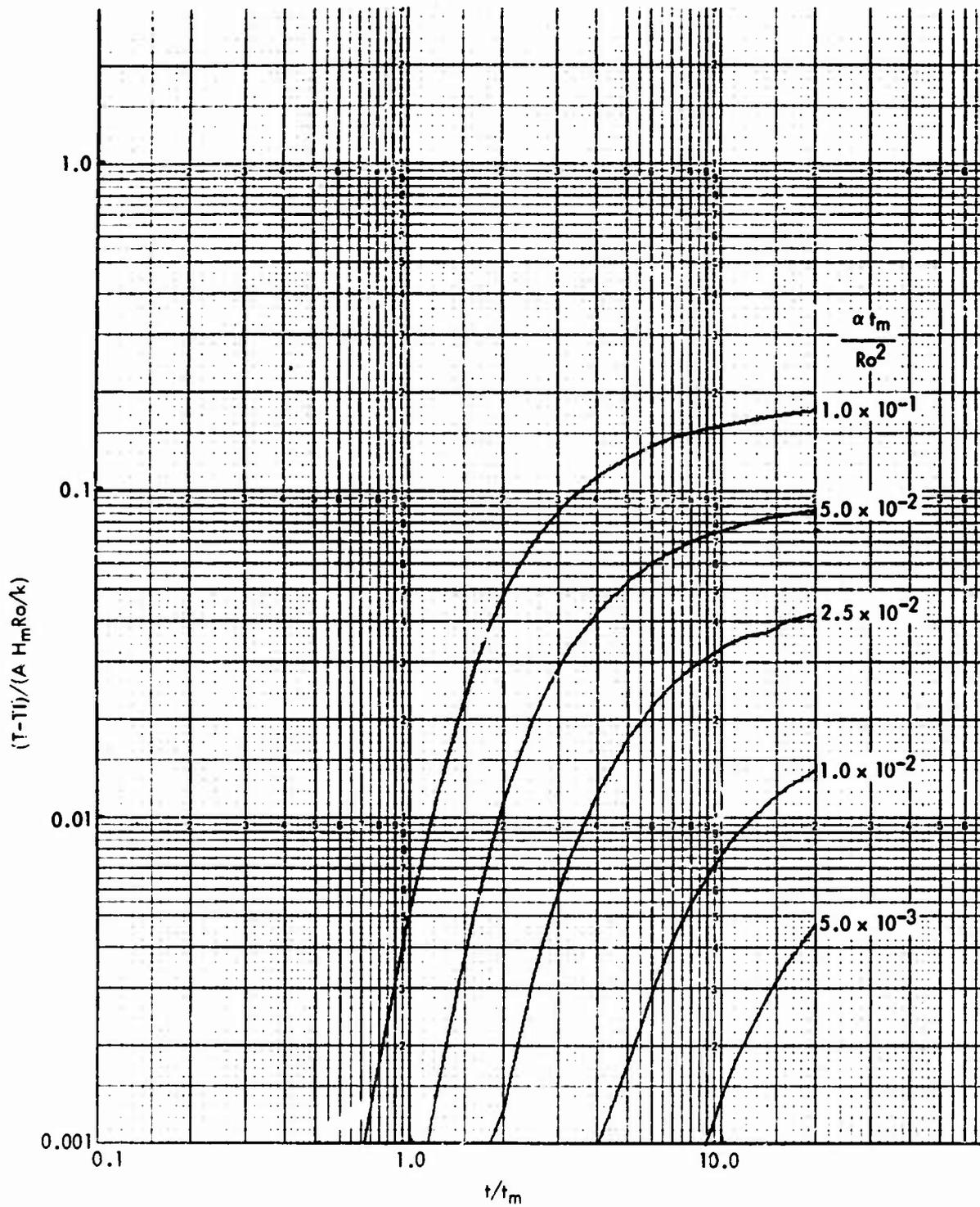
FIG. A - 4.3.4   DIMENSIONLESS BACKFACE TEMPERATURE HISTORIES (Ri* = 0.4, $\phi = 90°$)
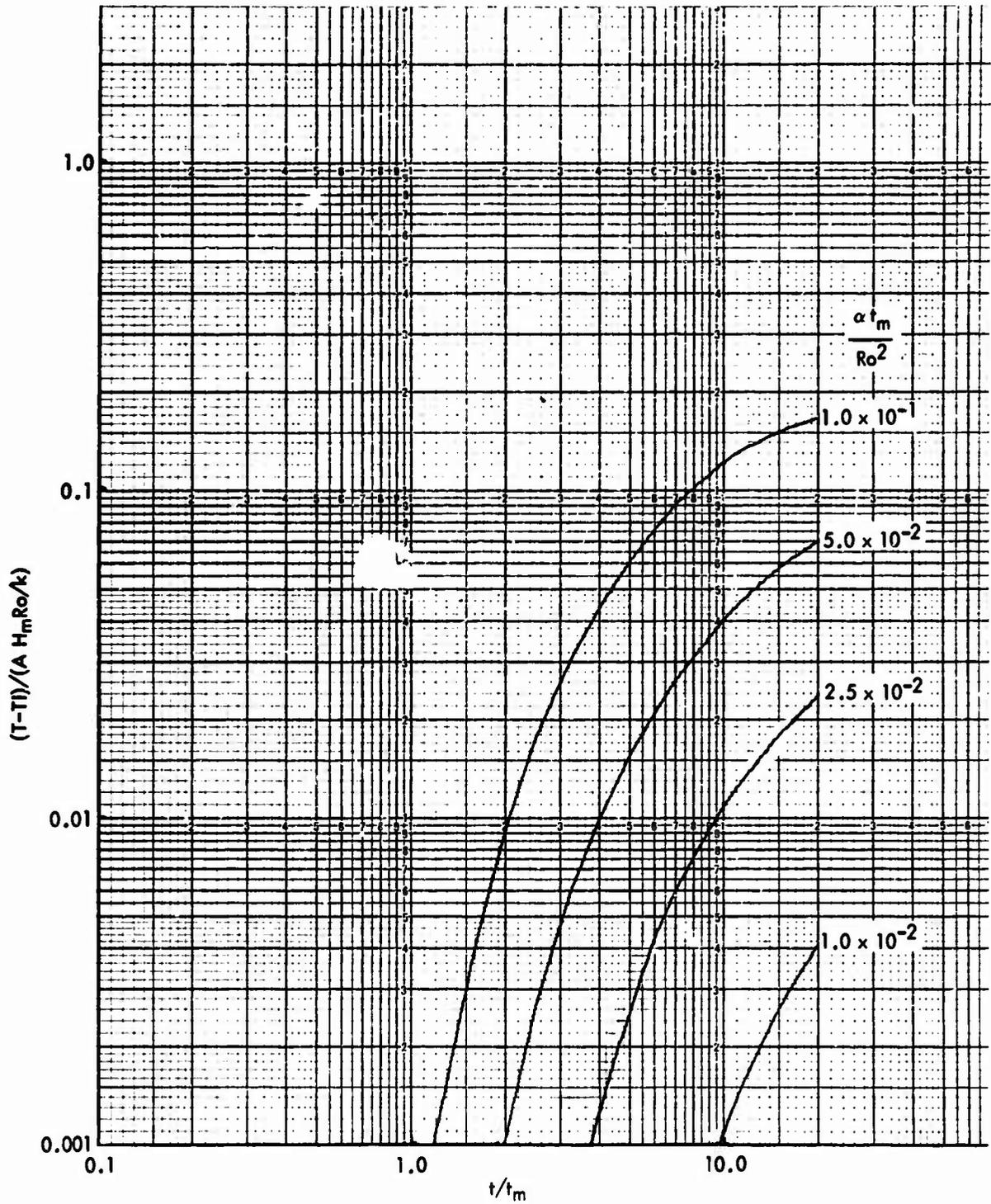
FIG. A - 4.3.5   DIMENSIONLESS BACKFACE TEMPERATURE HISTORIES (Ri* = 0.4, ϕ = 135°)
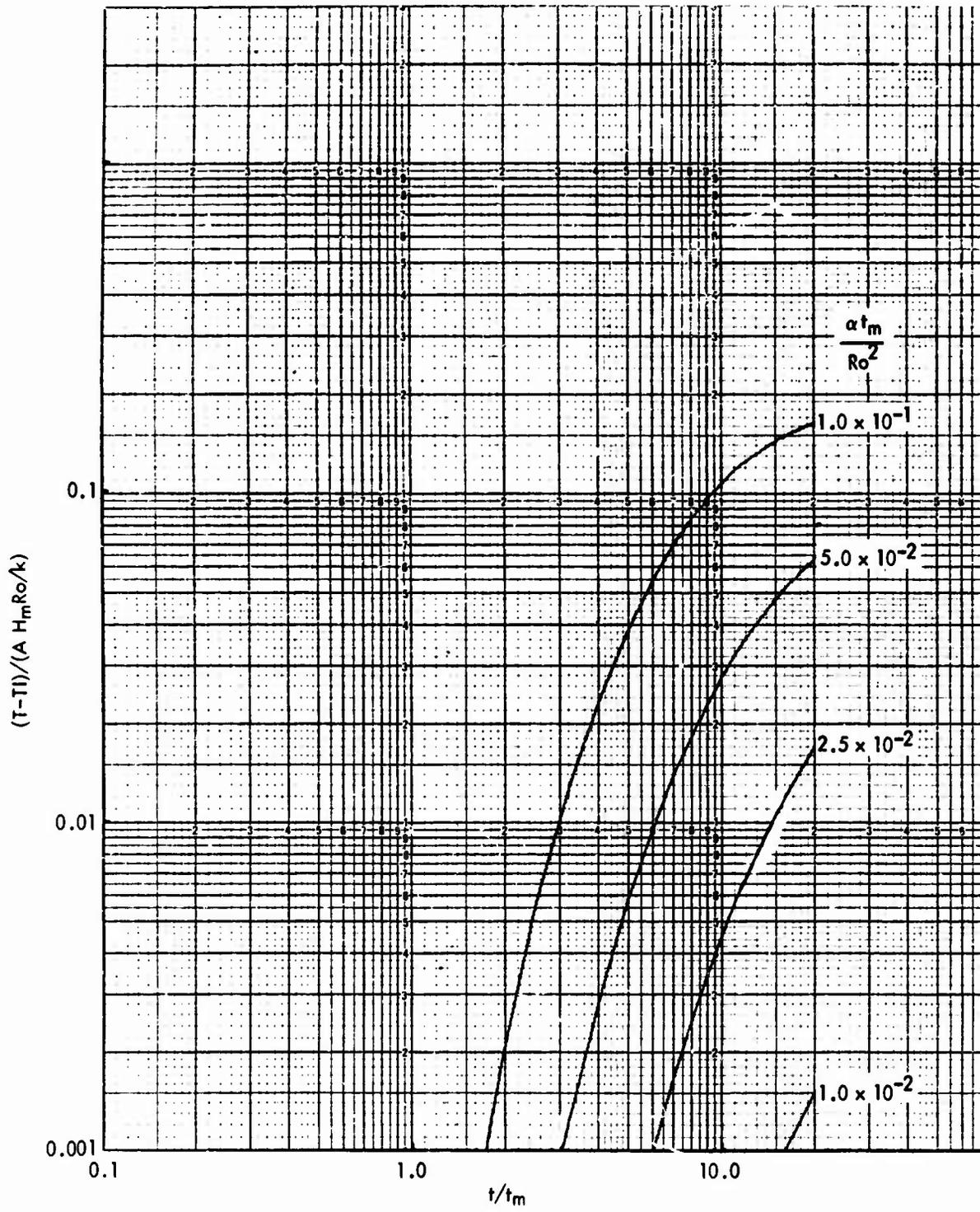
FIG. A - 4.3.6   DIMENSIONLESS BACKFACE TEMPERATURE HISTORIES (Ri* = 0.4, ϕ = 180°)
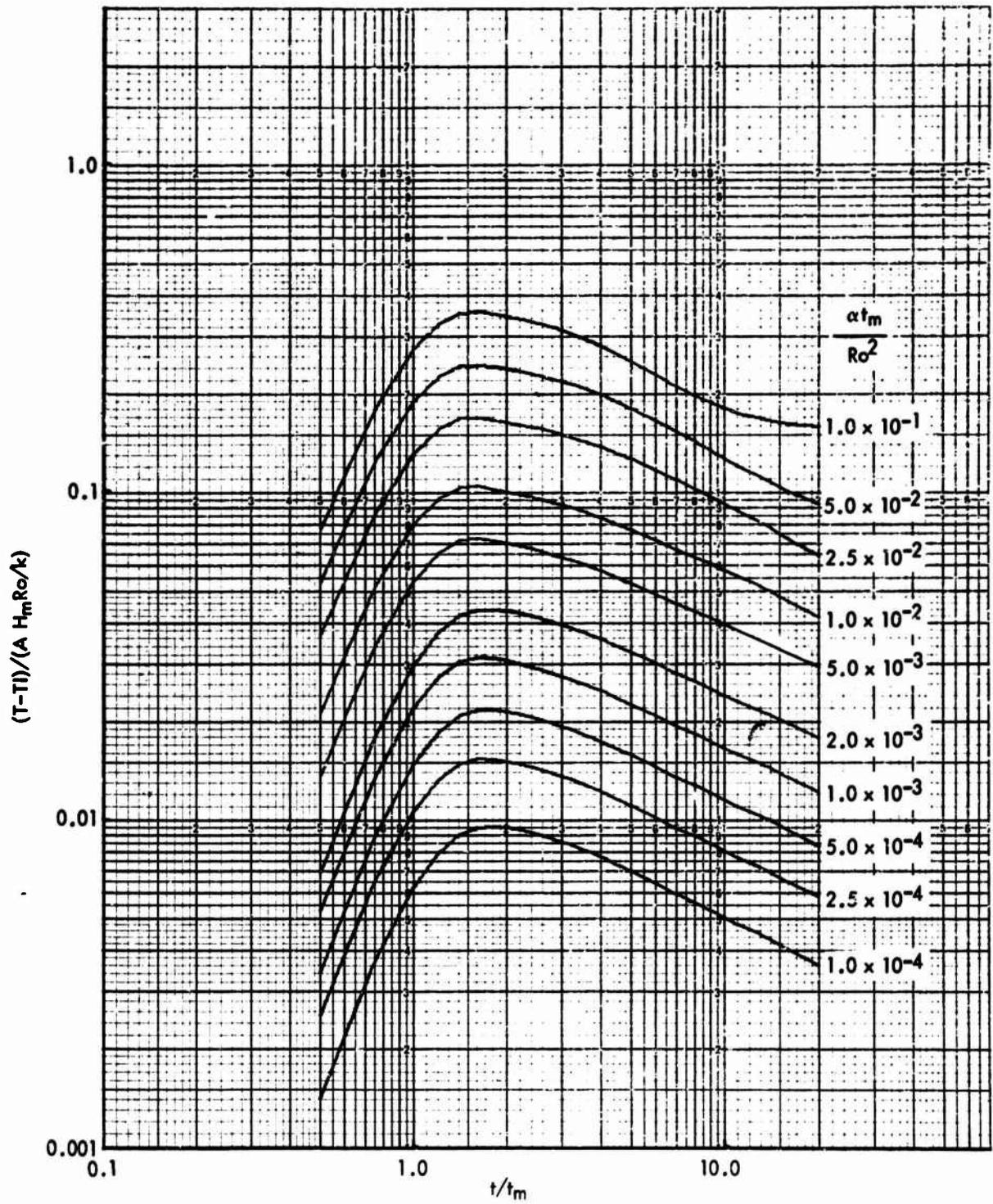
FIG. A - 5.1.1   DIMENSIONLESS SURFACE TEMPERATURE HISTORIES (Ri* = 0. , ϕ = 0°)
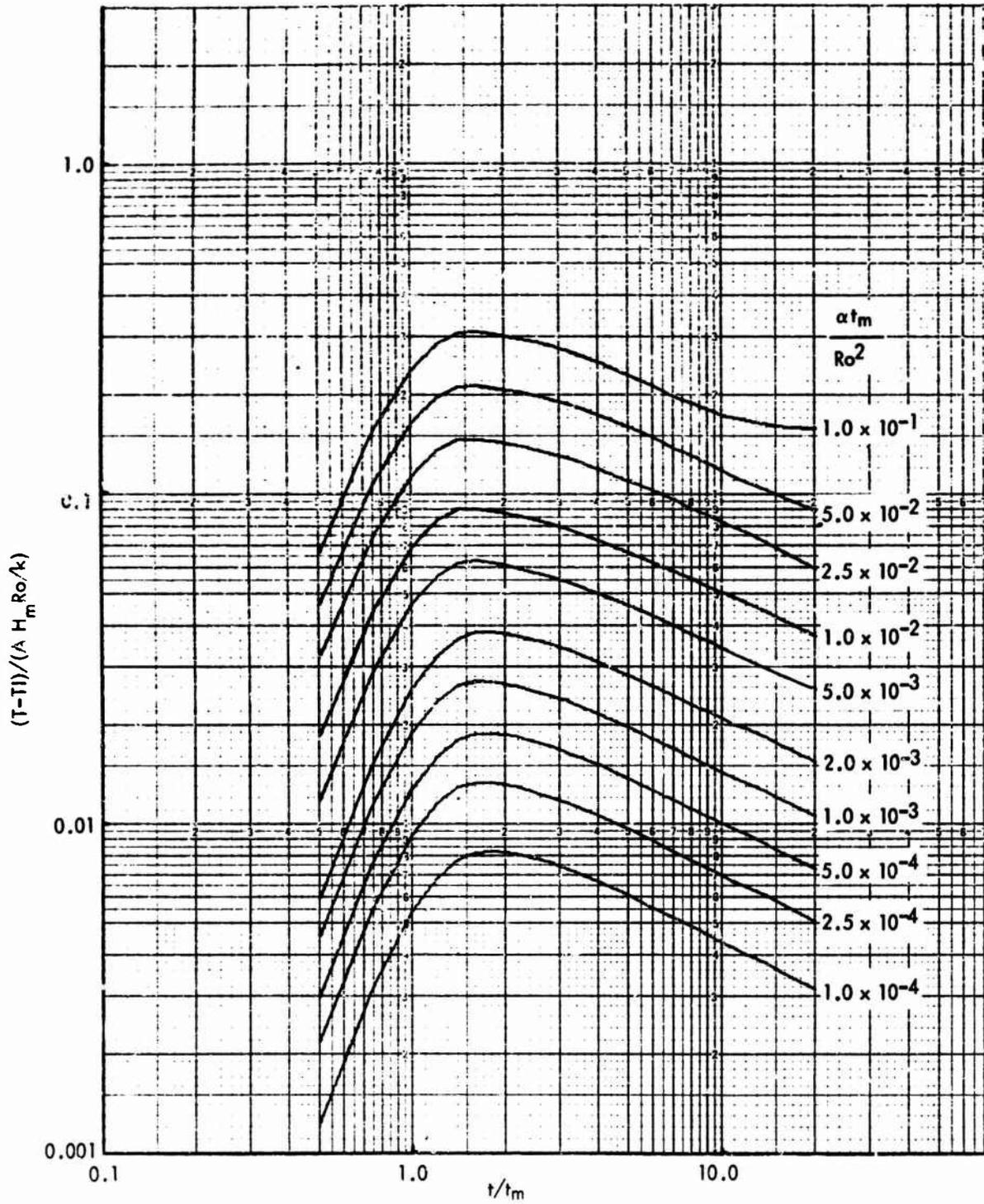
FIG. A - 5.1.2   DIMENSIONLESS SURFACE TEMPERATURE HISTORIES (Ri* = 0. , ϕ = 30°)
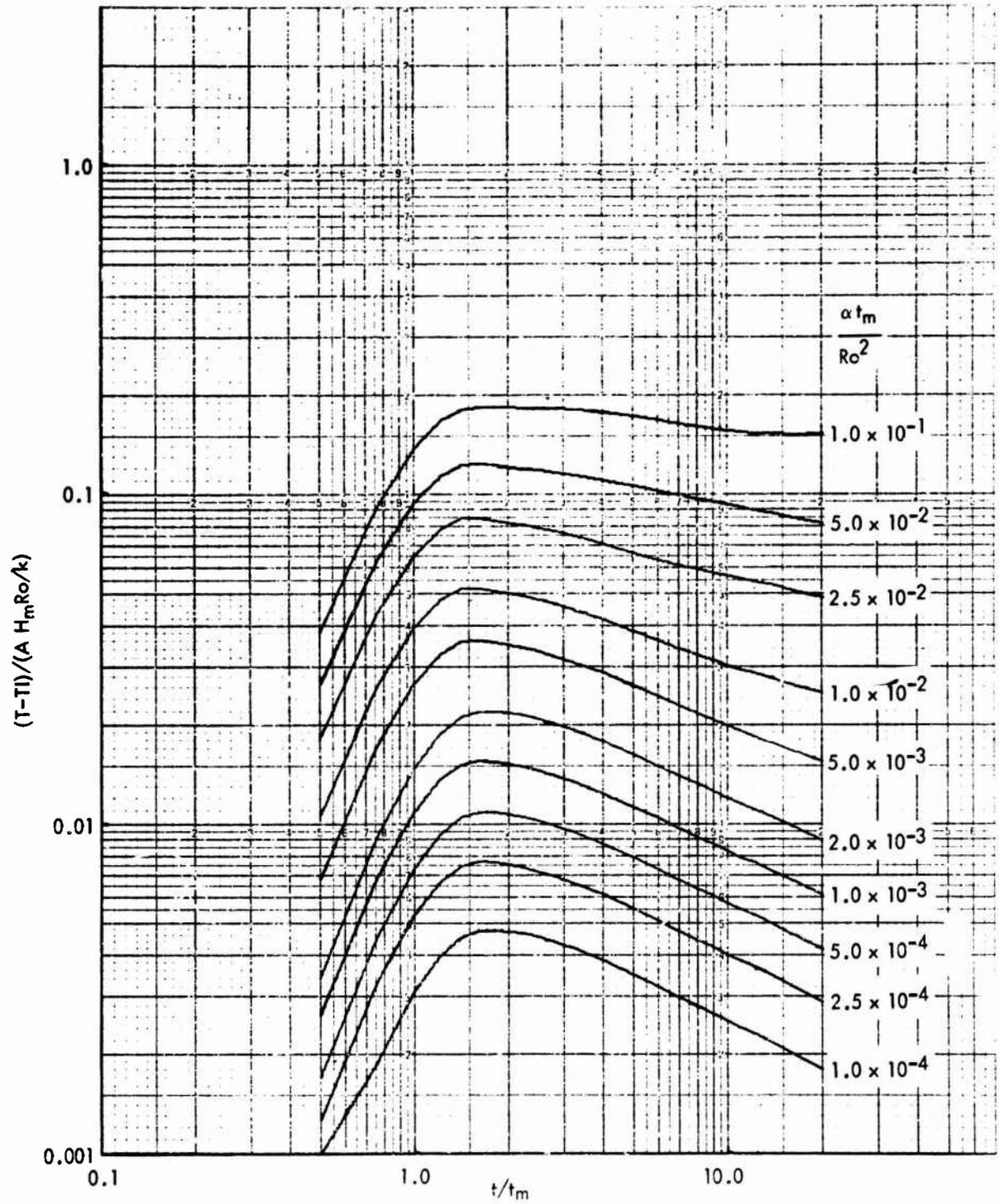
FIG. A - 5.1.3   DIMENSIONLESS SURFACE TEMPERATURE HISTORIES (Ri* = 0. , $\phi = 60°$)
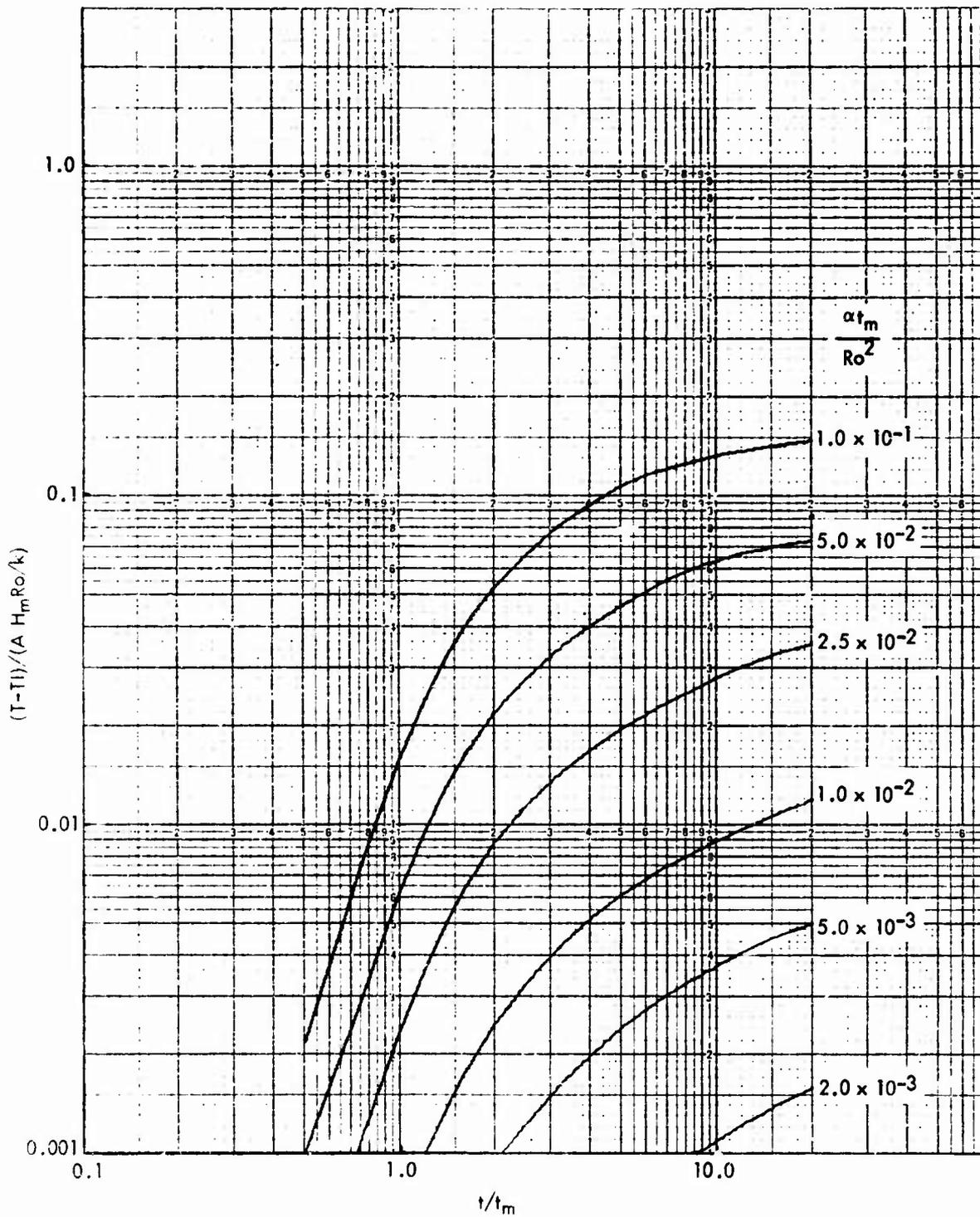
FIG. A - 5.1.4   DIMENSIONLESS SURFACE TEMPERATURE HISTORIES (Ri* = 0. , ϕ = 90°)
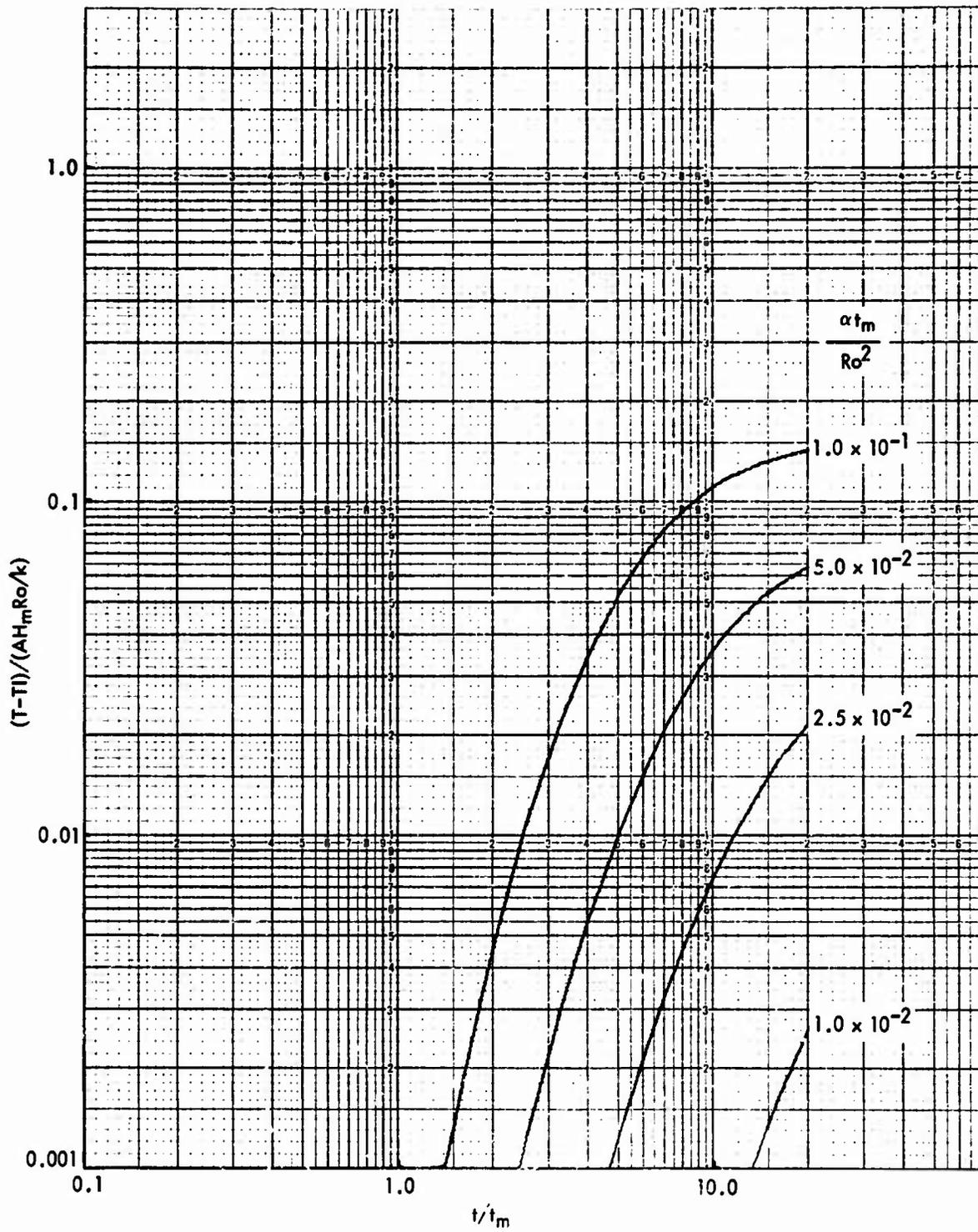
FIG. A - 5.1.5   DIMENSIONLESS SURFACE TEMPERATURE HISTORIES (Ri* = 0. , ϕ = 135°)
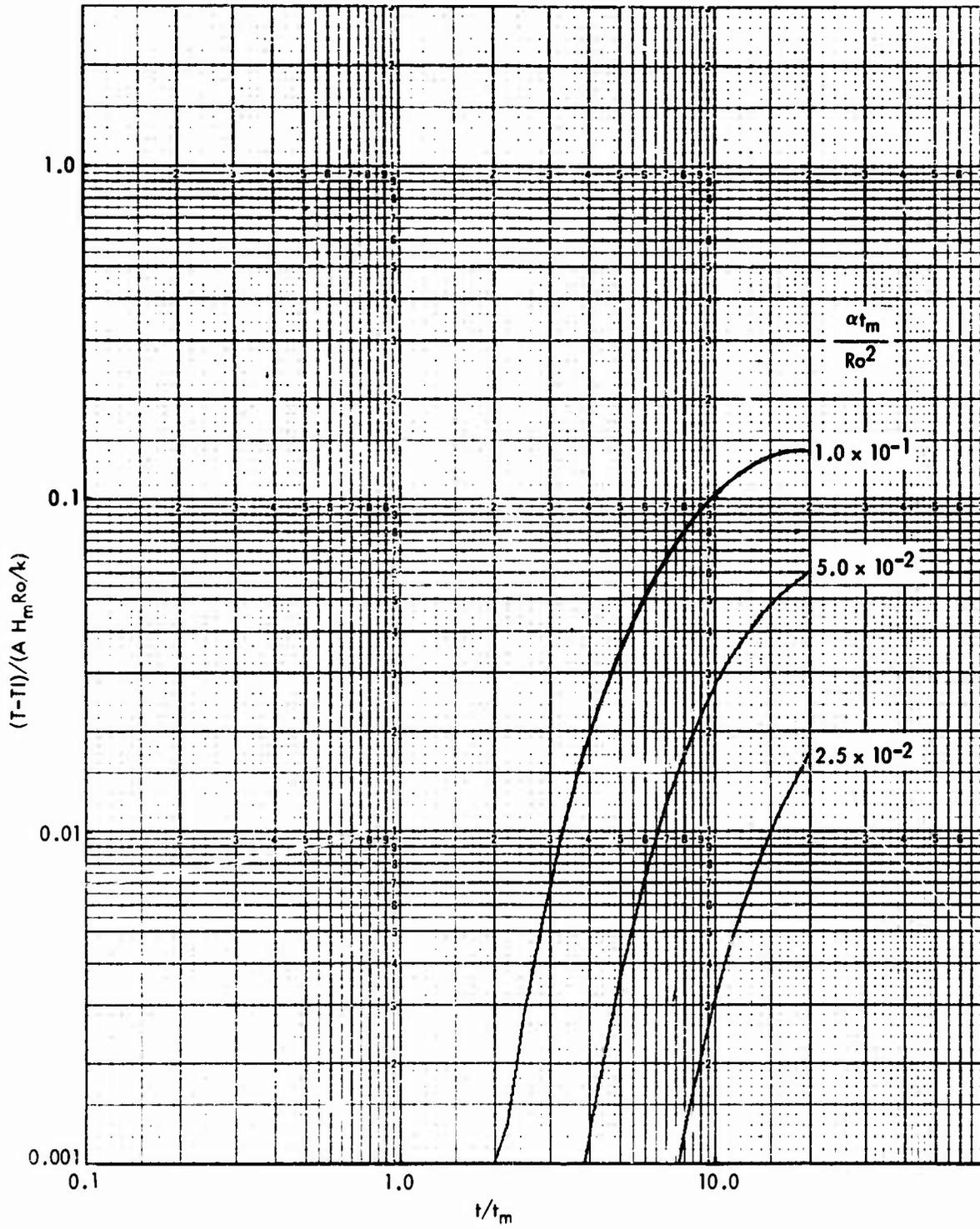
FIG. A - 5.1.6   DIMENSIONLESS SURFACE TEMPERATURE HISTORIES (Ri* = 0. , ϕ = 180°)
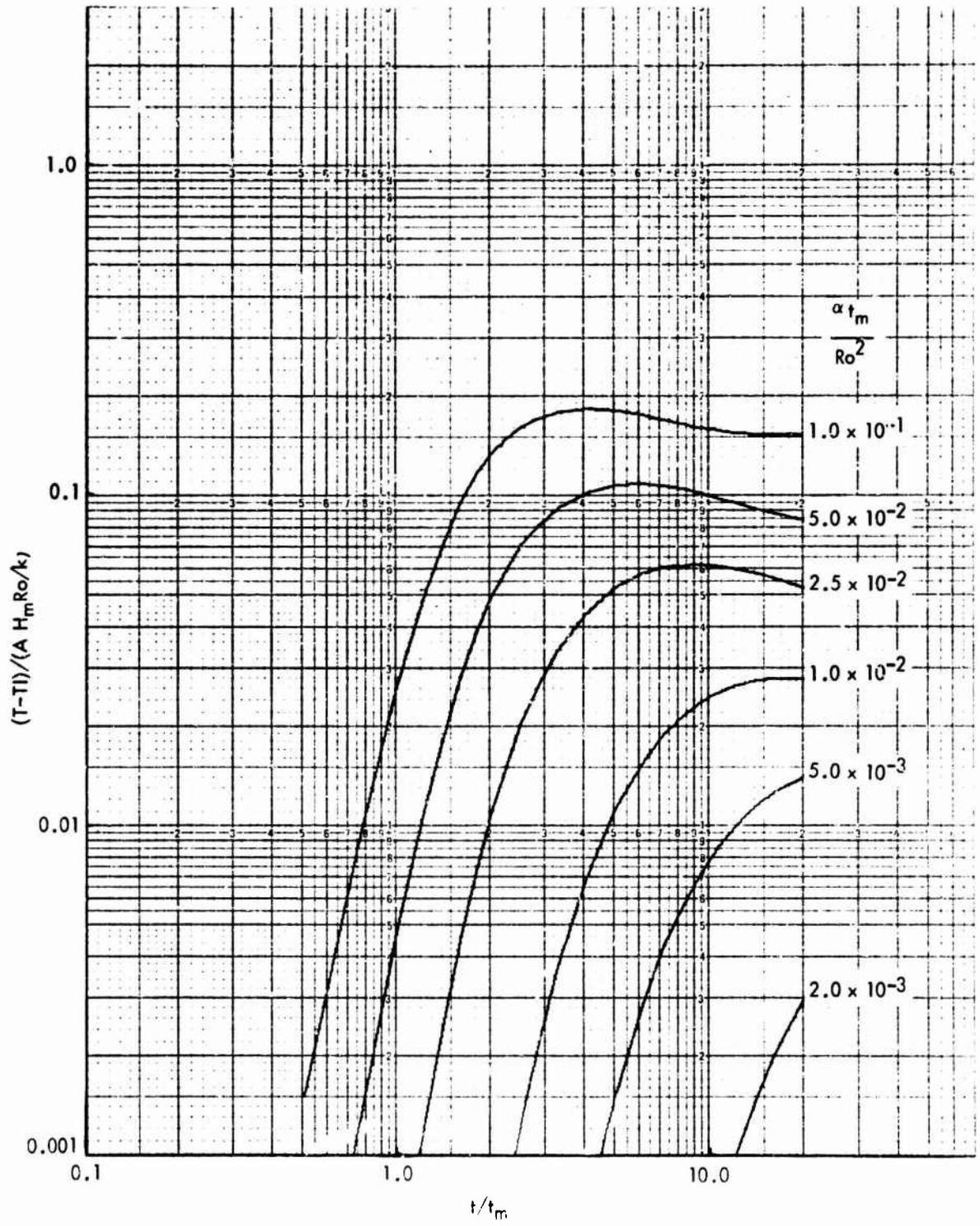
FIG. A - 5.2.1 DIMENSIONLESS MIDPLANE TEMPERATURE HISTORIES ($Ri^* = 0.$, $\phi = 0^o$)
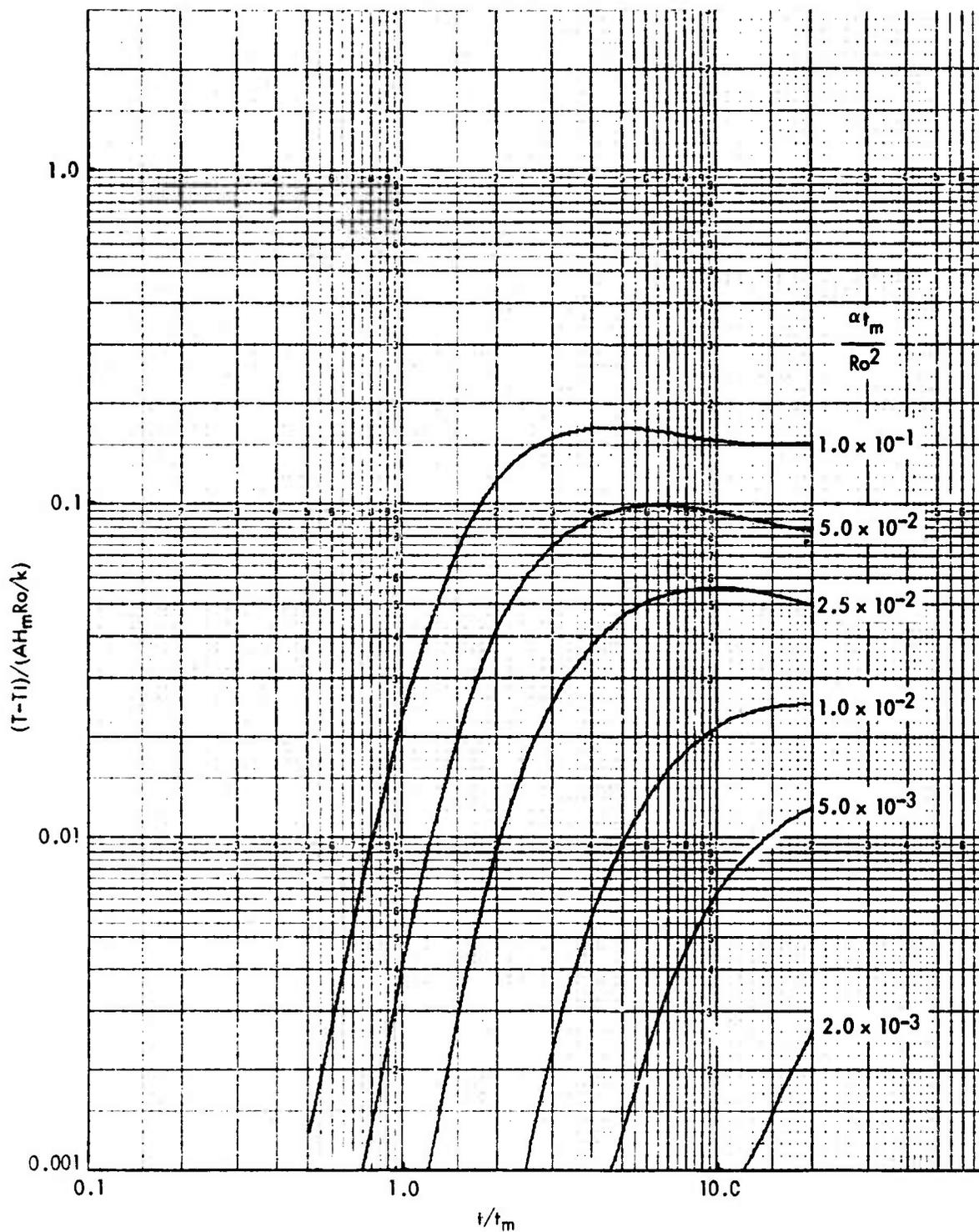
FIG. A - 5.2.2   DIMENSIONLESS MIDPLANE TEMPERATURE HISTORIES (Ri* = 0. , $\phi = 30°$)
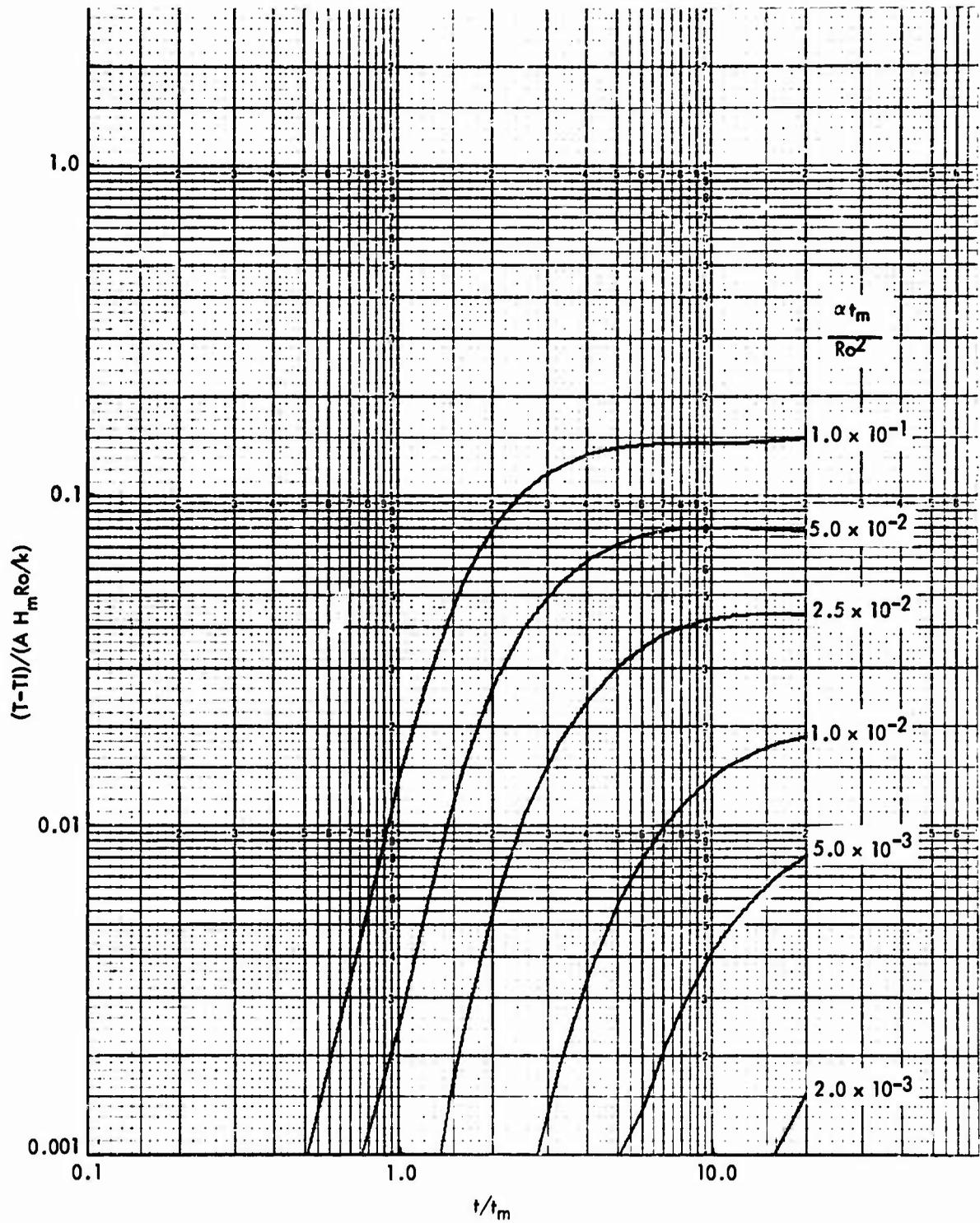
FIG. A - 5.2.3   DIMENSIONLESS MIDPLANE TEMPERATURE HISTORIES (Ri* = 0. , ϕ = 60°)
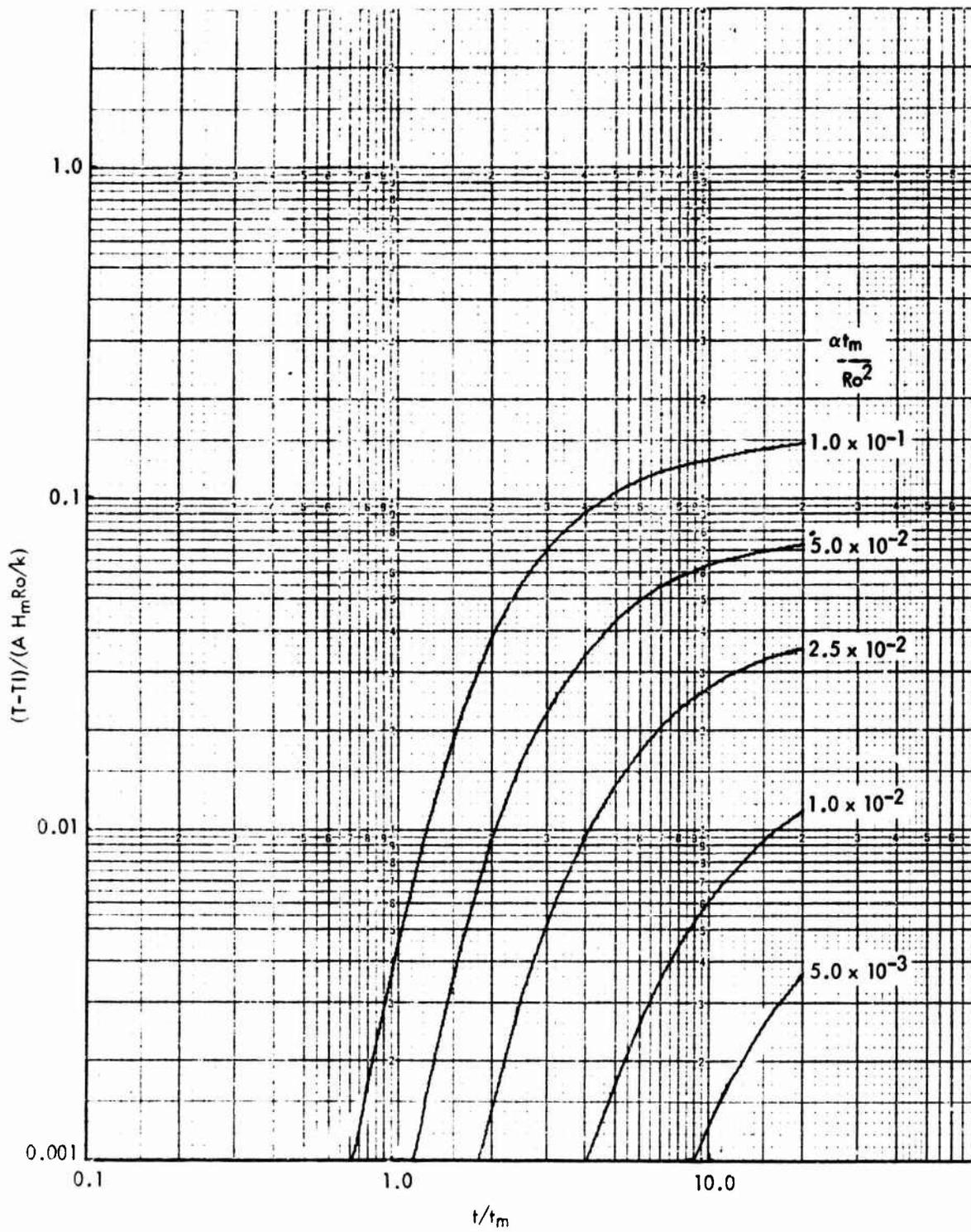
FIG. A - 5.2.4   DIMENSIONLESS MIDPLANE TEMPERATURE HISTORIES (Ri* = 0. , $\phi = 90°$)
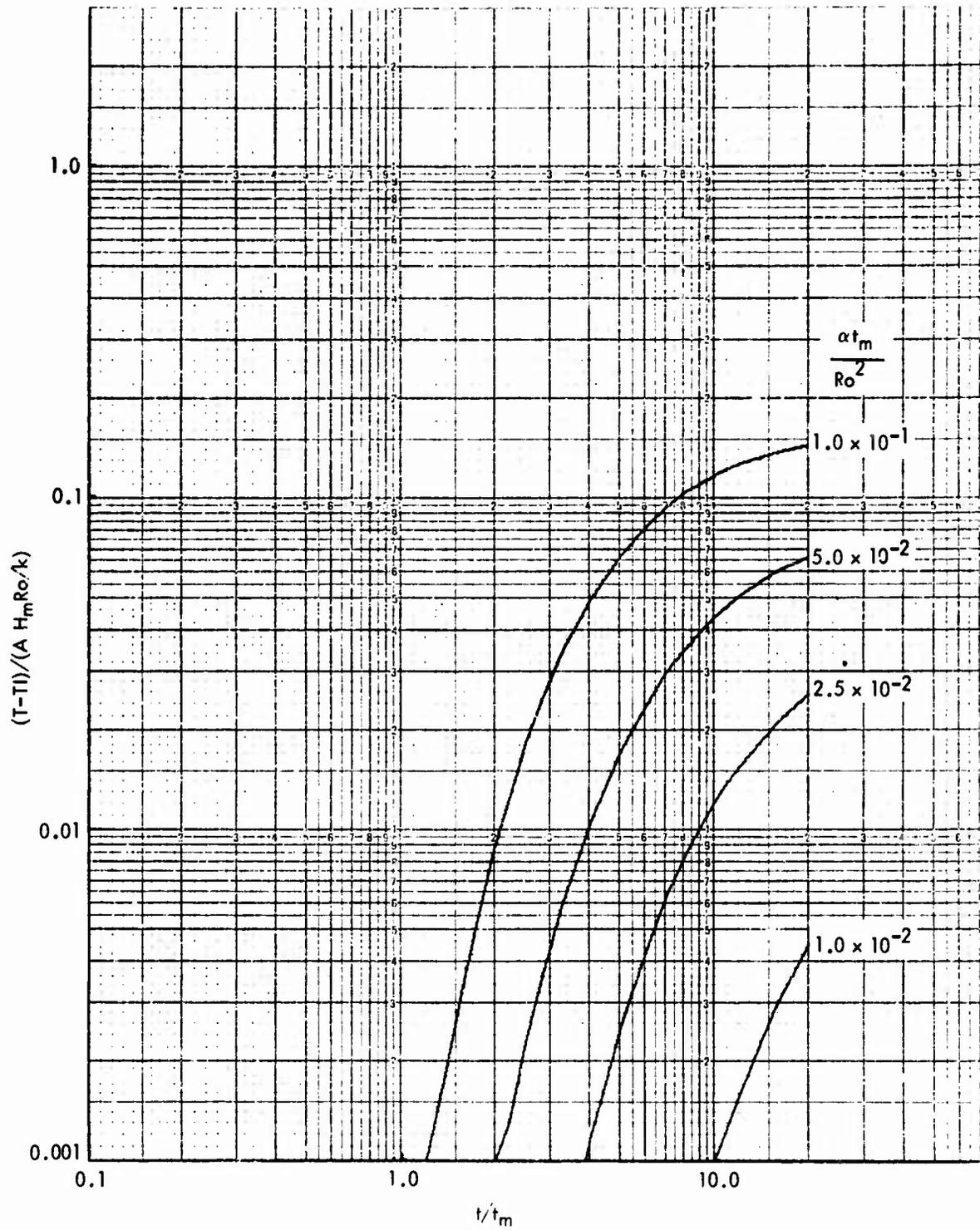
FIG. A - 5.2.5   DIMENSIONLESS MIDPLANE TEMPERATURE HISTORIES (Ri* = 0. , φ = 135°)
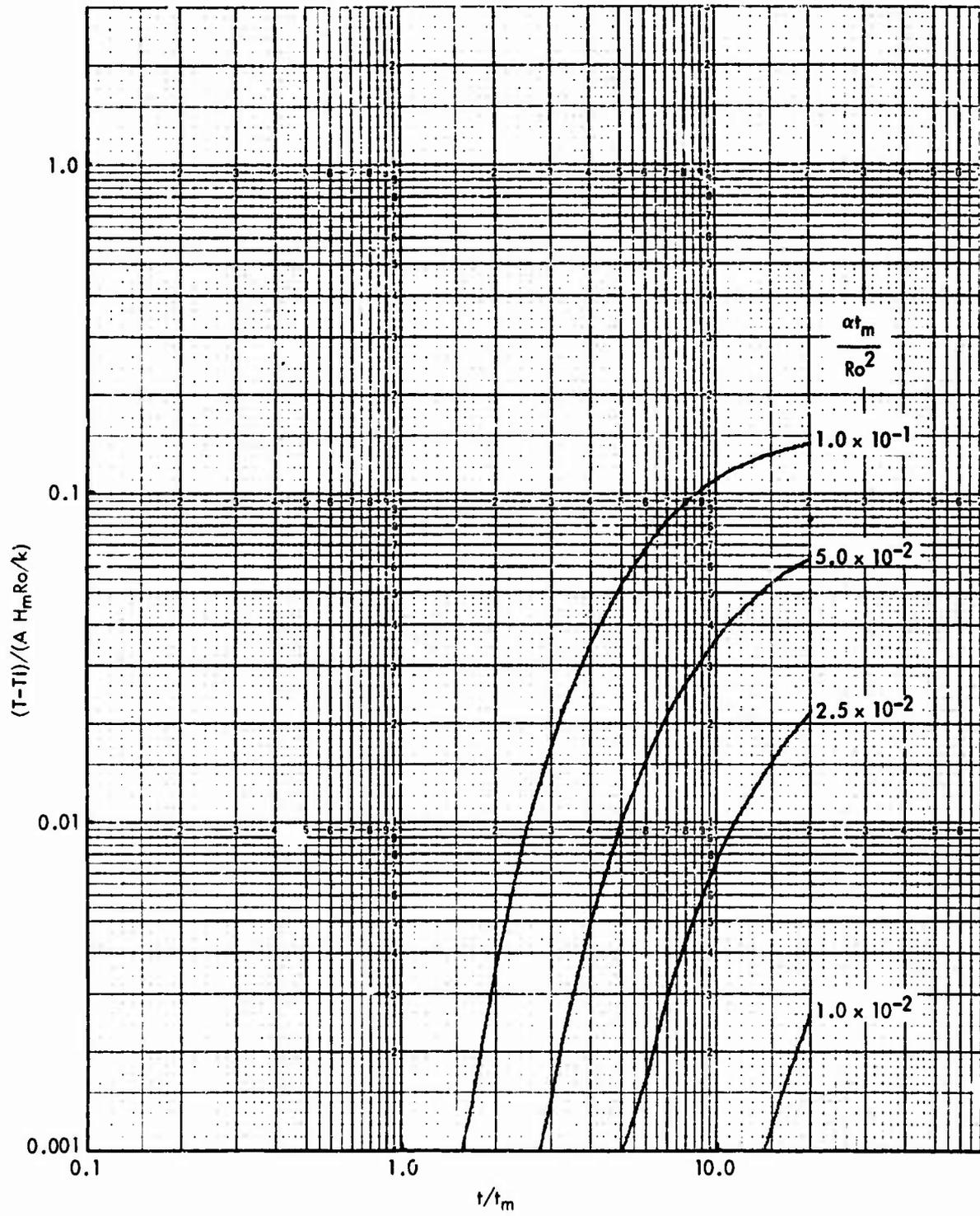
FIG. A - 5.2.6   DIMENSIONLESS MIDPLANE TEMPERATURE HISTORIES (Ri* = 0. , ϕ=180°)
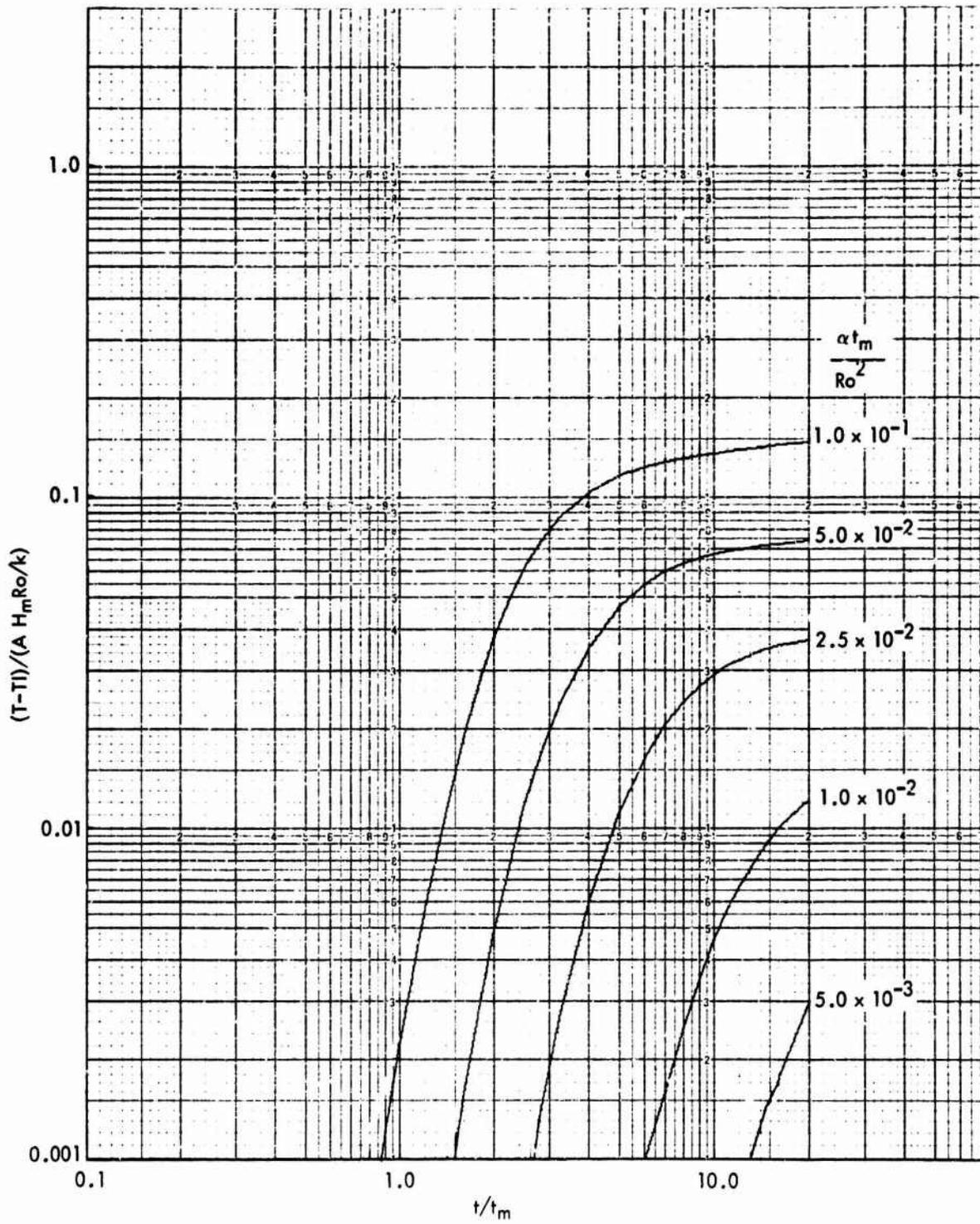
FIG. A – 5.3.1   DIMENSIONLESS BACKFACE TEMPERATURE HISTORIES ($R_i^* = 0$. , $\varphi = 0°$)
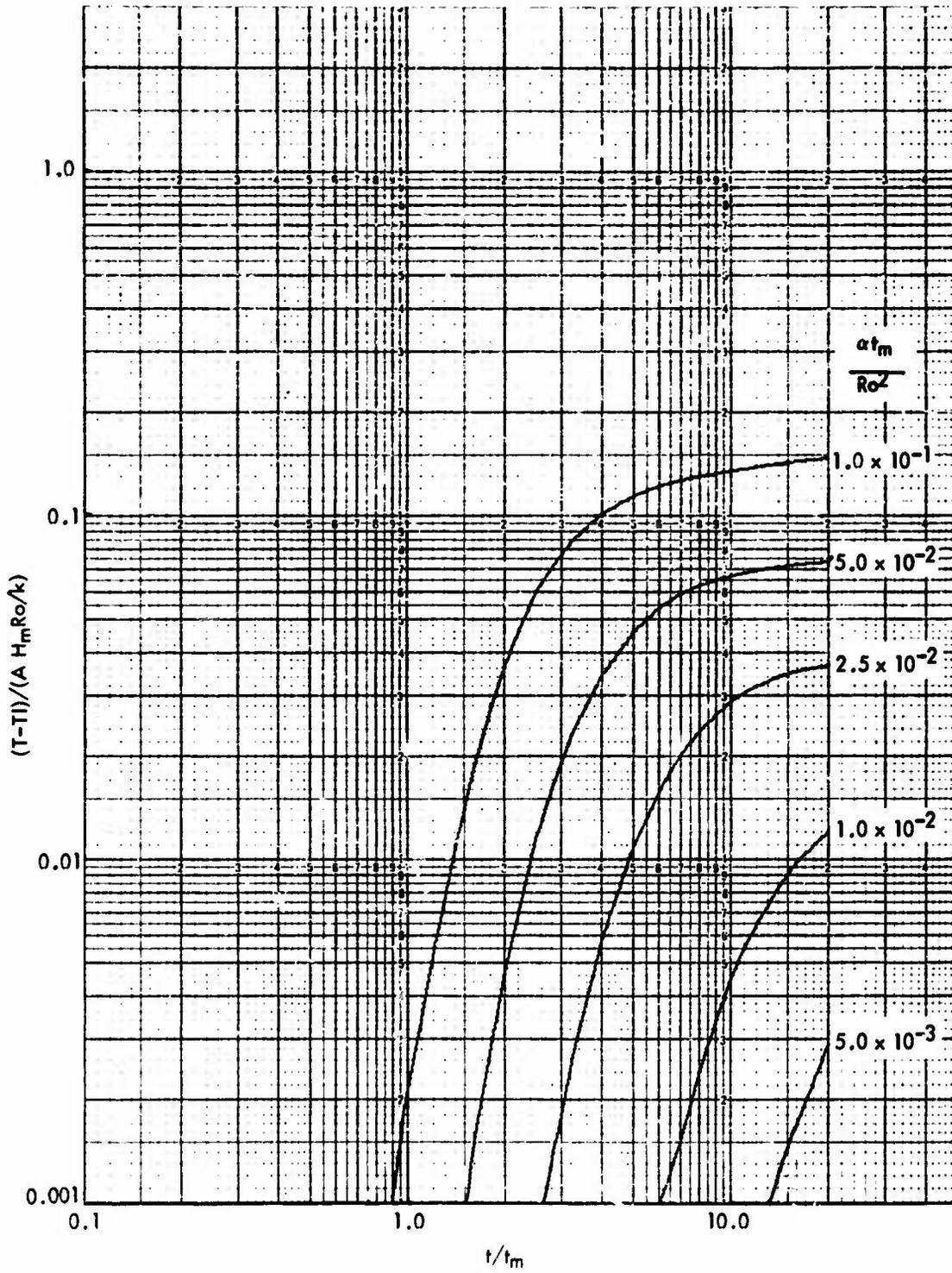
FIG. A - 5.3.2   DIMENSIONLESS BACKFACE TEMPFRATURE HISTORIES (Ri* = 0. , ϕ = 30°)
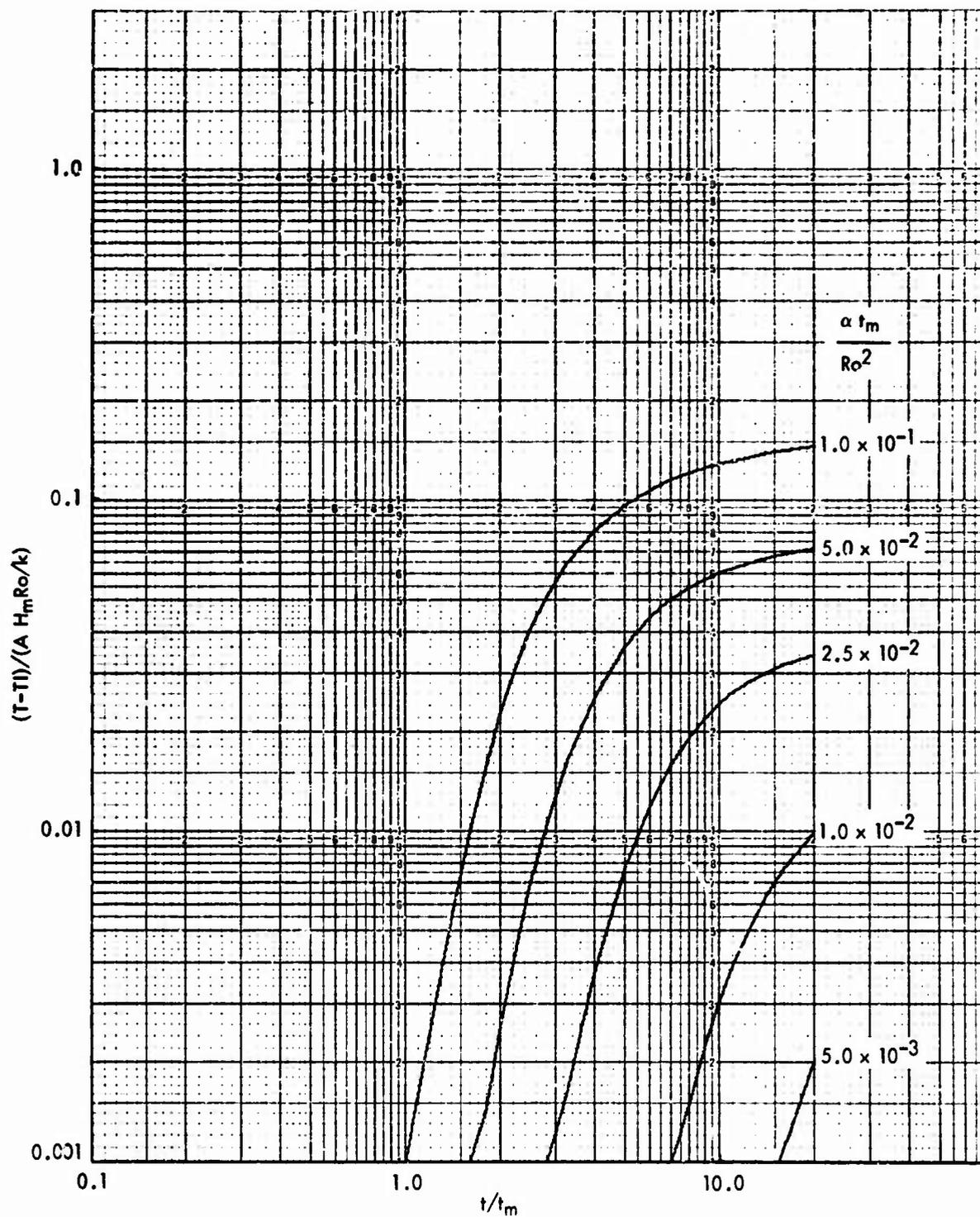
FIG. A - 5.3.5   DIMENSIONLESS BACKFACE TEMPERATURE HISTORIES (Ri* = 0. , ϕ = 135°)
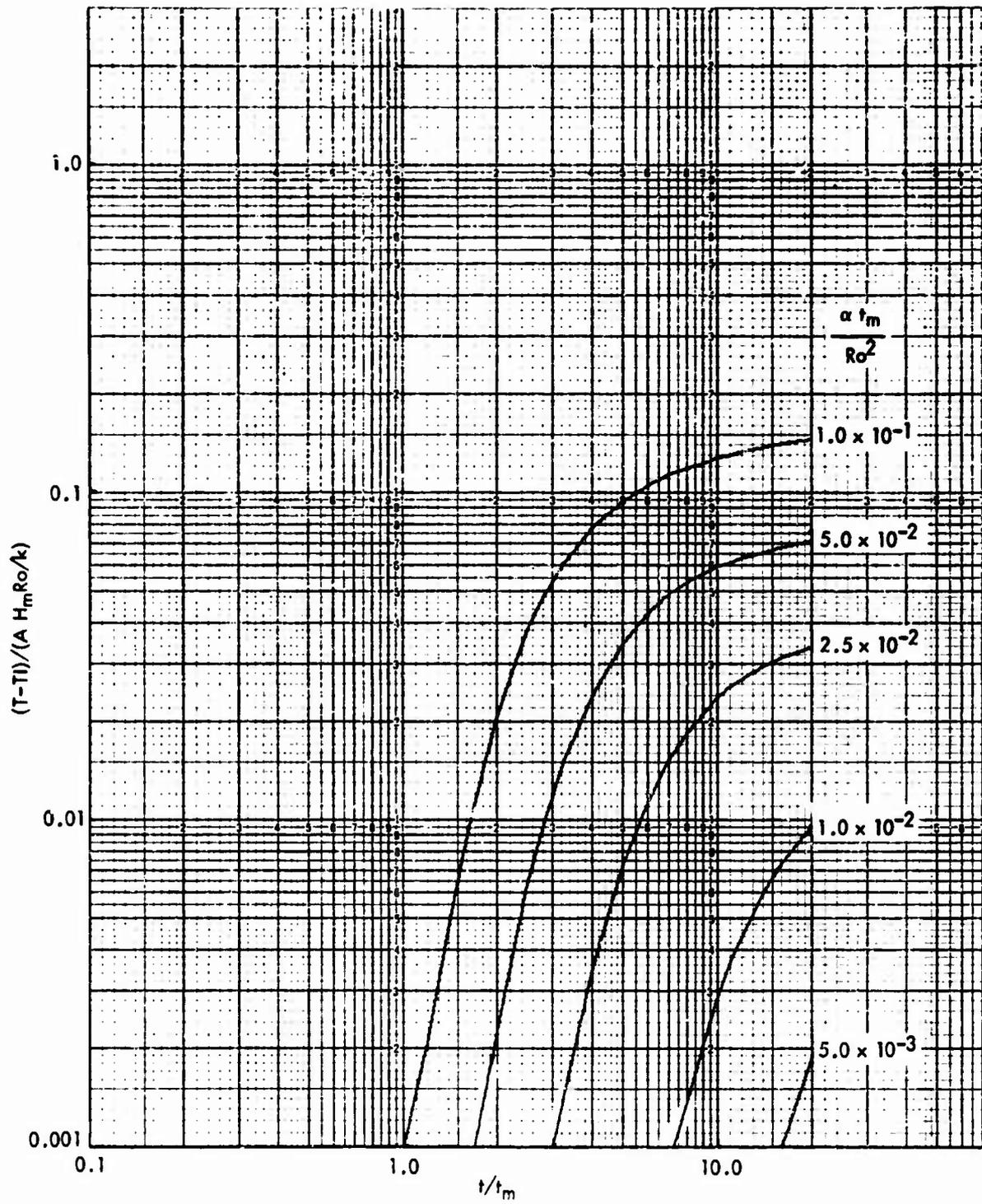
FIG. A – 5.3.6   DIMENSIONLESS BACKFACE TEMPERATURE HISTORIES (Ri* = 0. , ϕ = 180°)
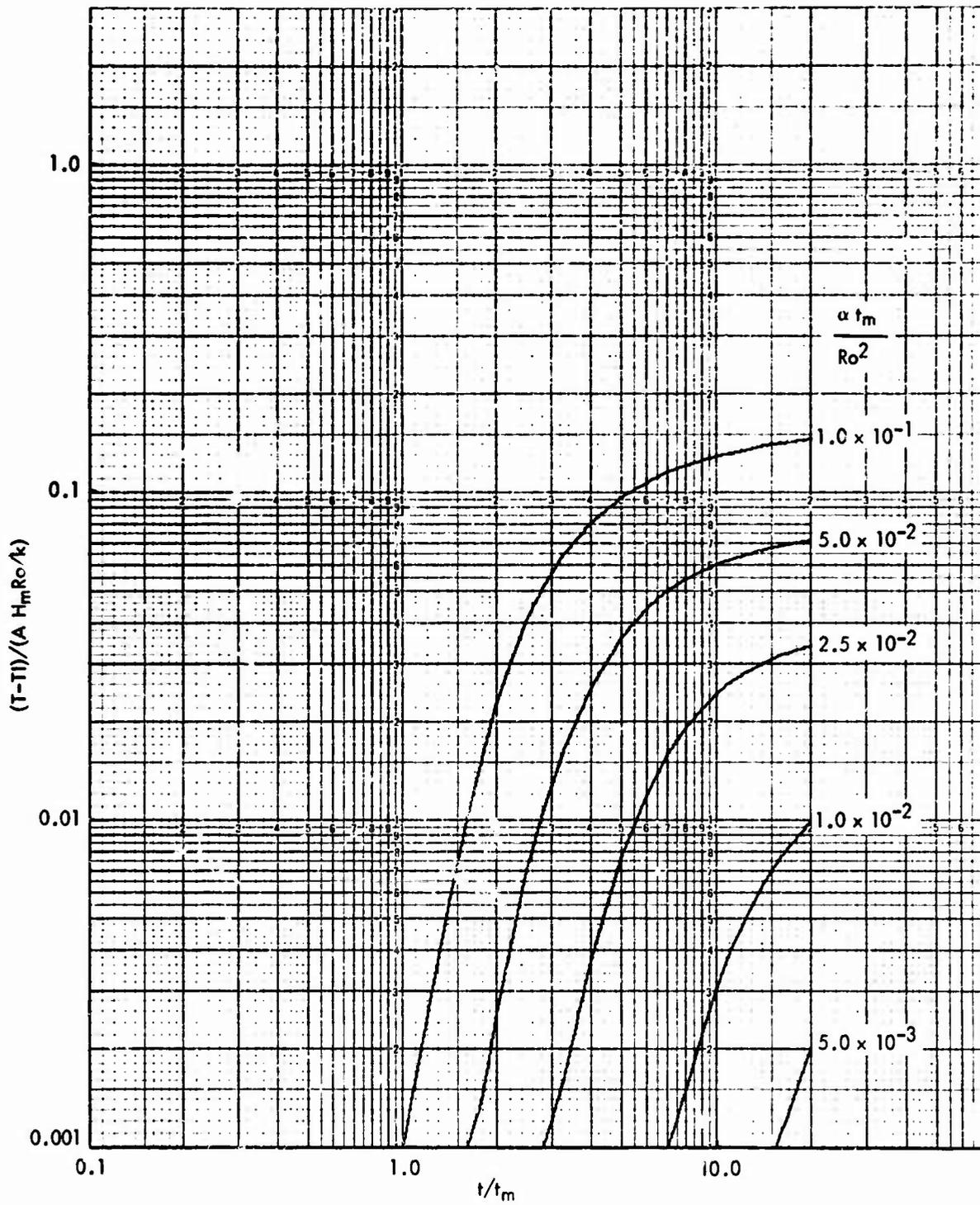
FIG. A - 5.3.5   DIMENSIONLESS BACKFACE TEMPERATURE HISTORIES (Ri* = 0. , ϕ = 135°)
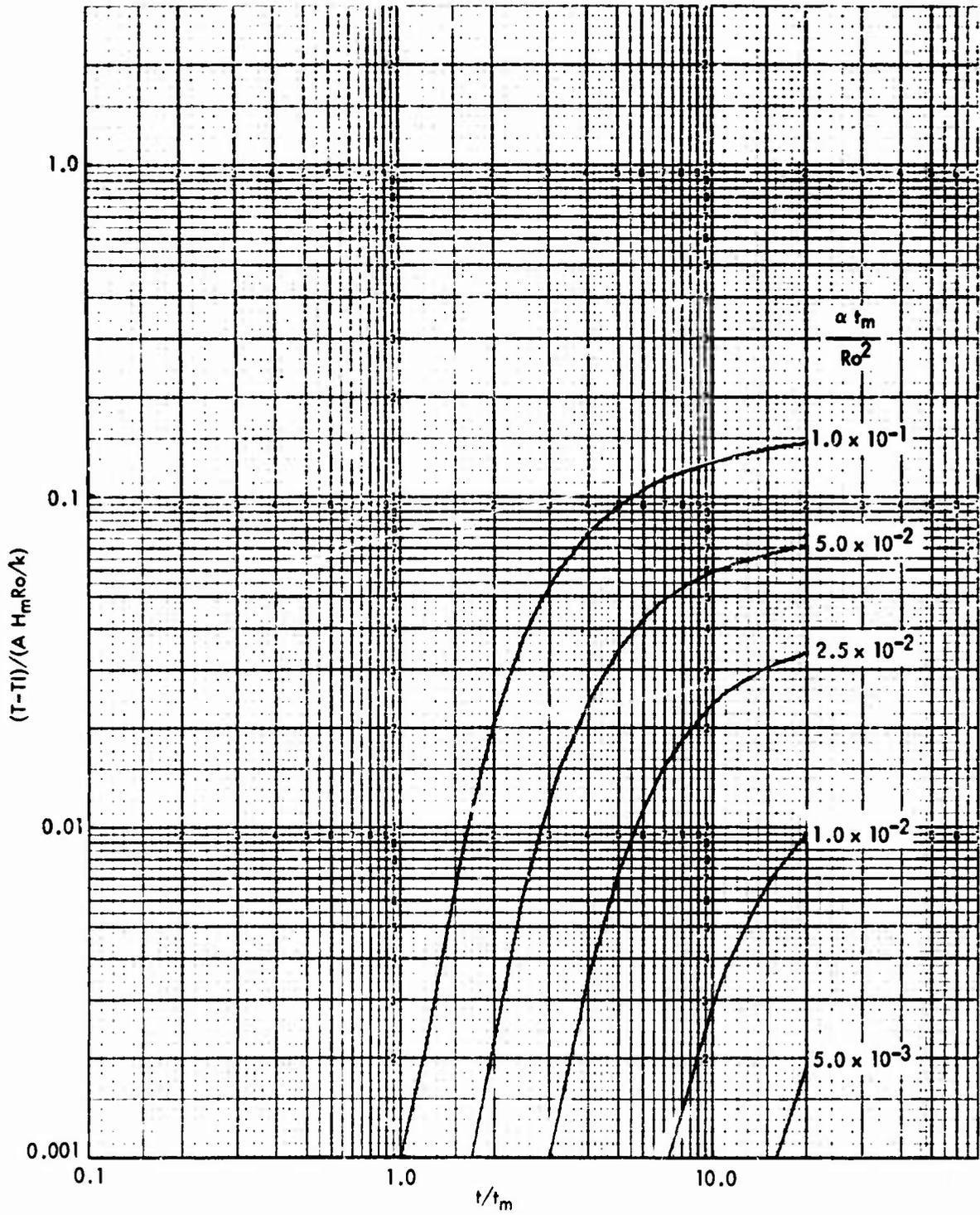
FIG. A - 5.3.6   DIMENSIONLESS BACKFACE TEMPERATURE HISTORIES (Ri* = 0. , φ = 180°)

APPENDIX B

EXAMPLES FOR THE USE OF THE DIMENSIONLESS TEMPERATURE HISTORIES

The derivation of cylinder temperatures from the dimensionless temperature histories presented in Appendix A will be illustrated by presenting suitable examples. In these examples, the basic parameters, Ri/Ro and $\alpha t_m/Ro^2$ will first be chosen to represent the case where no interpolation of the figures in Appendix A is required. For this case, Figure B-1 is a schematic showing the steps required to locate the appropriate figure from Appendix A and subsequently calculate the required cylinder temperatures. The use of this figure will also be illustrated by the example. Other examples will be given to show how temperatures are derived when it is necessary to interpolate or extrapolate results because the values of the basic parameters are not given in the figures of Appendix A.

Example 1: No Interpolation or Extrapolation of Results Required

An aluminum alloy cylinder (6061-T6) of outer radius 2.0 inches and inner radius 0.8 inches experiences a total free field radiant exposure of 128 cal/cm^2 from the detonation of a 1.0 megaton nuclear weapon in the lower atmosphere. The blast arrival time is 12.0 seconds, and the initial temperature of the cylinder is 20°C (68°F). The total radiant exposure delivered by a nuclear weapon pulse is given by

$$Q = \int_0^\infty H(t)\,dt = 2.6 H_m t_m \qquad (B-1)$$

The value of $2.6 H_m t_m$ for this integral was determined from scaling relations given in sections 7.92 and 7.93 of reference (2). Also, the time-to-thermal maximum for a nuclear weapon airblast is given by reference (2) as

$$t_m = .032 W^{\frac{1}{2}} \qquad (B-2)$$

where W is the weapon yield in kilotons
Hence for the 1 megaton (1000 kiloton) weapon of this example,

$$t_m = .032(1000)^{0.5} = 1.0 \text{ seconds}$$

and

$$H_m = \frac{Q}{2.6 t_m} = \frac{128}{2.6(1.0)} = 48.7 \text{ cal/cm}^2\text{-sec}$$

The material absorptance is taken to be 1.0. Find the following temperatures, where the cylinder angle (or the angle of incident radiation) is 0 degrees, for one-half the peak heating time, the peak heating time, the time where the maximum temperature occurs, and the blast arrival time:

    (a) Surface temperature
    (b) Midplane temperature
    (c) Backface temperature

NOTE: From Table 1, the thermal properties of 6061-T6 aluminum are $k = 0.397$ cal/sec-cm-$^{\circ}$C, $\rho = 2.71$ gm/cm^3, $c = 0.23$ cal/gm-$^{\circ}$C

Hence, $\alpha = k/\rho c = 0.637$ cm^2/sec.

Solution - (a) Surface temperature

The solution will follow the flow chart given in Figure B-1.1.

Step 1: Compute Ri/Ro, $Ri/Ro = \dfrac{0.8 \text{ in}}{2.0 \text{ in}} = 0.4$

Step 2: Enter Appendix A and find that Figures A-4 apply to the inner radius ratio of 0.4.

Step 3: Find r/Ro and ϕ, r/Ro = 1.0 (surface) $\phi = 0^{\circ}$ (given)

Step 4: Enter Figure A-4 and note that Figure A-4.1.1 applies to Ri* = 0.4, r* = 1.0 and ϕ = 0 degrees.

Step 5: Compute $\alpha t_m/Ro^2$,

$$\frac{\alpha t_m}{Ro^2} = \frac{0.637 \frac{cm^2}{sec} 1.0 \text{ sec}}{\left(2.0 \text{ in } 2.54 \frac{cm}{in}\right)^2} = .025$$

Step 6: From the computed value of $\alpha t_m/Ro^2$ and Figure A-4.1.1 note that the third curve from the top gives the dimensionless temperature history for case (a).

Step 7: Find the dimensionless temperatures for the desired times. One-half the peak heating time, the peak heating time and the blast arrival time have dimensionless time values of 0.5, 1.0 and 12.0 respectively. From Figure A-4.1.1, the corresponding dimensionless temperatures are .040 , .134, and .099 respectively. Also, the maximum dimensionless temperature is 0.170 at a dimensionless time of 1.4.

Step 8: Find t_m and $AH_m Ro/k$, $t_m = 1.0$ (given)

$$\frac{AH_m Ro}{k} = \frac{(1.0)\ (48.7 \text{ cal/cm}^2\text{-sec})\ (2.0 \text{ in})\ (2.54 \text{ cm/in})}{0.397 \text{ cal/sec-cm-}^{\circ}C} = 623^{\circ}C$$

Step 9: Compute the desired temperatures:

$$T = T^* \left(\frac{AH_m Ro}{k} \right) + TI$$

Time = 0.5 seconds T = (.040)(623) + 20 = 45°C (113°F)
Time = 1.0 seconds T = (.134)(623) + 20 = 103°C (217°F)
Time = 1.4 seconds T = (.169)(623) + 20 = 125°C (257°F)
Time = 12.0 seconds T = (.099)(623) + 20 = 82°C (180°F)

Solution: (b) Midplane temperatures

The solution for midplane temperatures follows the flow diagram and the 9 steps outlined above. Only those steps giving a different result will be repeated.

Step 3: Find r/Ro and ϕ : r/Ro = 0.7 (Midplane)

Step 4: Enter Figure A-4 and note that Figure 4.2.1 applies to Ri* = 0.4, r* = 0.7 and ϕ = 0 degrees.

Step 7: From Figure A-4.2.1 the dimensionless temperatures at one-half the peak heating time, the peak heating time and the blast arrival time are <.001, .062, and .090 respectively. The maximum dimensionless temperature is .095 and this occurs at a dimensionless time of 7.5.

Step 9: Computation of the desired temperatures

$$T = T^* \left(\frac{AH_m Ro}{k} \right) + TI$$

Time = 0.5 seconds T = (<.001)(623) + 20 = 20°C (68°F)
Time = 1.0 seconds T = (.062)(623) + 20 = 59°C (138°F)
Time = 7.5 seconds T = (.095)(623) + 20 = 79°C (174°F)
Time = 12.0 seconds T = (.090)(623) + 20 = 76°C (169°F)

Solution: (c) Backface temperatures

Since the steps in computing temperatures have been illustrated above, only the calculation of the desired temperatures will be given,

$$T = T^* \left(\frac{AH_m Ro}{k} \right) + TI$$

Time = 0.5 seconds T = (<.001)(623) + 20 = 20°C (68°F)
Time = 1.0 seconds T = (<.001)(623) + 20 = 20°C (68°F)
Time = 10.0 seconds (maximum temperature time)
                    T = (.082)(623) + 20 = 71°C (160°F)
Time = 12.0 seconds T = (.080)(623) + 20 = 70°C (158°F)

The next two examples will show how to interpolate the figures of Appendix A when the exact values of the basic parameters do not appear in the figures. The interpolation rules to be given depend on whether the cylinder is thermally-thick. The rules for a thermally-thick cylinder are developed first as follows. The definition of the dimensionless temperature which was given by equation (8) is:

$$T^* = \frac{T - T_\infty}{AH_m Ro/k} \tag{B-1}$$

now, if the cylinder is thermally-thick and no heat is conducted away angularly, the surface temperature for constant heating is given by reference (5):

$$T = \frac{2qs}{k}\sqrt{\frac{\alpha t}{\pi}} \tag{B-2}$$

where qs is the constant surface heat flux.
For the nuclear thermal pulse, the surface heat transfer rate is proportional to the product, $A\,H_m$, hence the surface temperature will be represented as,

$$T \sim \frac{A\,H_m}{k}\sqrt{\alpha t} \tag{B-3}$$

Equations (B-1) and (B-3) will be combined to get an approximate representation of the dimensionless surface temperature at the time of peak heating. The result is,

$$T^* \sim \sqrt{\frac{\alpha t_m}{Ro^2}} \tag{B-4}$$

Although this equation is only an approximation, it will be used as the basis for interpolating thick cylinder surface temperatures. The success is using equation (B-4) will be illustrated by the following example.

Example 2: Interpolation of Thick Cylinder Results

An aluminum alloy cylinder (6061-T6) of outer radius 5.31 inches and inner radius 1.86 inches is exposed to the thermal environment of the weapon in example 1 ($t_m = 1.0$ seconds, $H_m = 48.7$ cal/cm^2-sec). Find the surface temperature history where the cylinder angle is 0 degrees.

Solution

Step 1: Compute Ri/Ro. Ri/Ro = $\frac{1.86\ \text{in}}{5.31\ \text{in}}$ = 0.35. Hence a value of the inner radius ratio results for which no set of figures in Appendix A applies.

Step 2: Compute $\alpha t_m/Ro^2$.

$$\frac{\alpha t_m}{Ro^2} = \frac{0.637 \frac{cm^2}{sec} \; 1.0 \; sec}{(5.31 \; in \; 2.54 \; \frac{cm}{in})^2} = .0035$$

Figures 5.1 and 5.2 show that for these values of the basic parame $\alpha t_m/Ro^2$ and Ri*, the cylinder of this example is thermally-thick for values of dimensionless time up to nearly 20.0. The temperature history for this problem will be found from Appendix A and the interpolation rule for thick cylinders, equation (B-4), in the following manner. First, since the cylinder is thermally-thick, the surface temperature is independent of the value of radius ratio chosen, hence Ri* will be taken to be 0.0. Secondly, the nearest values of $\alpha t_m/Ro^2$ for which the temperature histories are given are $\alpha t_m/Ro^2 = 0.002$ and $\alpha t_m/Ro^2 = 0.005$. The solution for the dimensionless temperature history for the case where $\alpha t_m/Ro^2 = 0.002$ and Ri* = 0.0 follows the first seven steps of example 1. If this is done, the following dimensionless temperature history is found from Figure A-5.1.1.*

t*	0.5	1.0	1.4	1.8	2.8	4.0	8.0	12.0	20.0
T*	.0069	.0298	.0421	.0437	.0400	.0354	.0262	.0221	.0177

The dimensionless temperature history is likewise found for the case where $\alpha t_m/Ro^2 = 0.005$ and Ri* = 0. The result found from Figure A-5.1.1 is

t*	0.5	1.0	1.4	1.8	2.8	4.0	8.0	12.0	20.0
T*	.0137	.0535	.0711	.0707	.0639	.0569	.0429	.0364	.0291

The final step to find the dimensionless temperature history for the case where $\alpha t_m/Ro^2 = .0035$ is to apply the interpolation rule, equation (B-4). That is, the square root of .002, .0035, and .005 are .0447, .0592 and .0707, respectively. Hence, the dimensionless temperatures for $\alpha t_m/Ro^2 = .0035$ are equal to the dimensionless temperatures at $\alpha t_m/Ro^2 = .002$ plus (.0592 - .0447)/(.0707 - .0447) or 55.5 percent of the increment in dimensionless temperatures between those at .002 and those at .005. Calculating the dimensionless temperature history for $\alpha t_m/Ro^2 = .0035$ by this procedure leads to the following result.

t*	0.5	1.0	1.4	1.8	2.8	4.0	8.0	12.0	20.0
T*	.0106	.0429	.0582	.0587	.0533	.0473	.0355	.0300	.0240

---

* The values of dimensionless temperature given in this and the foll
ing examples were taken from the original numerical computations.
This was done so that the interpolation (and extrapolation) rules
developed herein can be verified by making similar numerical
calculations.

Once the dimensionless temperatures have been found, it remains only to do steps 8 and 9 of example 1 to find the actual temperature history.

Step 8: Find t_m and $AH_m Ro/k$. $t_m = 1.0$ second (given)

$$\frac{AH_m}{k} = \frac{1.0 \ 48.64 \ cal/cm^2 sec \ 5.31 \ in \ 2.54 \ cm/in}{0.397 \ cal/sec\text{-}cm^oC} = 1654^oC$$

Step 9: Compute the temperature history for TI = 20^oC

$$T = T^* \ \frac{AH_m Ro}{k} + TI$$

The result is:

t (second)	0.5	1.0	1.4	1.8	2.8	4.0	8.0	12.0	20.0
T (^oC)	37.5	90.9	116	117	108	98.2	78.7	69.6	59.7

A calculation using the computer program described in reference (4) was made to check the result derived by the interpolation rule. The corresponding temperature history found by the laborious numerical calculation is;

t (second)	0.5	1.0	1.4	1.8	2.8	4.0	8.0	12.0	20.0
T (^oC)	42.8	98.4	117	117	107	97.6	78.4	69.6	59.7

Thus, it can be concluded that the interpolation rule, equation (B-4), can be used to accurately find the surface temperatures for thick cylinders having basic dimensionless parameters which are not given in Appendix A.

An interior temperature can be found in a similar manner but it will not occur at the midplane. However, the choice of radius ratio has importance since the only interior temperature above the initial temperature given in Appendix A is the midplane temperature corresponding to the radius ratio chosen. Thus, if example 2 is repeated to find the interior temperature, it would occur at the midplane of a cylinder having a radius ratio of 0.0. This would be the temperature at r/Ro = 0.5 but it is not the midplane temperature of the given cylinder because its inner radius ratio was 0.35. The interior temperature found in this manner occurs at a radius of 2.65 inches.

The next example will illustrate the interpolation of the results in Appendix A when the cylinder is not thermally-thick. The interpolation rule for these cylinders is first developed as follows. A heat energy balance on a thin section of cylindrical wall can be written:

$$\rho c \ \Delta r \ \left(\frac{dT}{dt}\right) = qs \qquad (B-5)$$

For the nuclear thermal pulse, the surface heat transfer rate is proportional to the product $A \cdot H_m$. Hence equation (B-5) can be integrated and solved for the surface temperature at the time of peak heating. The result is,

$$T \sim \frac{A \ H_m \ t_m}{\rho c \ \Delta r} \qquad (B-6)$$

and Δr can be replaced by,

$$\Delta r = Ro \ \left(1 - \frac{Ri}{Ro}\right) \qquad (B-7)$$

Equations (B-1), (B-6) and (B-7) can be combined to get a representation of the dimensionless surface temperature i.e.,

$$T^* \sim \left(\frac{\alpha t_m}{Ro^2}\right) \ \left(\frac{1}{1 - Ri/Ro}\right) \qquad (B-8)$$

Although equation (B-8) has been derived for the surface temperature of a thin cylinder, it will be used as the interpolation rule for all of the temperatures of non-thick cylinders. The success in doing this is illustrated by the following example.

Example 3: Interpolation of Non-Thick Cylinder Results

An aluminum alloy cylinder (6061-T6) of outer radius 2.56 inches and inner radius 1.79 inches is exposed to the thermal environment of the nuclear weapon in example 1 ($t_m = 1.0$ seconds, $H_m = 48.7$ cal/cm^2-sec). Find the surface and midplane temperature history where the cylinder angle is 0 degrees.

Solution: (a) Surface temperature

Step 1: Compute Ri/Ro $\quad$ Ri/Ro $= \dfrac{1.79 \ \text{in}}{2.56 \ \text{in}} = 0.7$

Hence an inner radius ratio results for which no set of figures in Appendix A applies.

Step 2: Compute $\alpha t_m/Ro^2$. $\quad \dfrac{\alpha t_m}{Ro^2} = \dfrac{0.637 \ \frac{cm^2}{sec} \ 1.0 \ sec}{\left(2.56 \ in \ 2.54 \ \frac{cm}{in}\right)^2} = 0.015$

Figures 5.1 and 5.2 show that for these values of the basic parameter $\alpha t_m/Ro^2$ and Ri/Ro, the cylinder is not thermally thick except perhaps for very small values of dimensionless time. The temperature history for this problem will be found from Appendix A and the interpolation rule for non-thick cylinders, equation (B-8). The nearest values of

Ri* and $\alpha t_m/Ro^2$ for which values are given are 0.6 and 0.8, and 0.01 and 0.025, respectively. Double interpolation is necessary for this type of problem. The first interpolation will be done in two parts to find the temperature history at a radius ratio of 0.7 and values of $\alpha t_m/Ro^2$ of 0.025 and 0.010. The first part is accomplished by first using Appendix A for a radius ratio of 0.6 and 0.8 while keeping $\alpha t_m/Ro^2$ at .025. Following the first seven steps of example 1 for a radius ratio of 0.6 gives the temperature history below from Figure A-3.1.1.

t*	0.5	1.0	1.4	1.8	2.8	4.0	8.0	12.0	20.0
T*	.0391	.132	.168	.165	.155	.148	.137	.128	.112

Similarly, the dimensionless temperature history for a radius ratio of 0.8, given by Figure 2.1.1 is:

t*	0.5	1.0	1.4	1.8	2.8	4.0	8.0	12.0	20.0
T*	.0391	.135	.179	.190	.215	.232	.242	.234	.211

Now, to get the temperature history for Ri* = 0.7 and $\alpha t_m/Ro^2$ = .025 it is necessary to interpolate the above temperature histories using rule (B-8). Since only Ri* varies, equation (B-8) states that the interpolation is proportional to $1/(1 - Ri^*)$. That is, $1/(1 - Ri^*)$ is equal to 2.5, 3.33 and 5.0 for Ri* equal to 0.6, 0.7 and 0.8 respectively. Thus, the dimensionless temperatures for Ri* = 0.7 are equal to the dimensionless temperatures at Ri* = 0.6 plus (3.33 - 2.5)/(5.0 - 2.5) or 3.33 percent of the increment in the dimensionless temperatures between 0.6 and 0.8. Calculating the dimensionless temperature history by this procedure leads to the following result for Ri* = 0.7 and $\alpha t_m/Ro^2$ = 0.025.

t*	0.5	1.0	1.4	1.8	2.8	4.0	8.0	12.0	20.0
T*	.0391	.133	.172	.173	.175	.176	.172	.163	.145

The above procedure is repeated for radius ratios of 0.6 and 0.8 but this time for $\alpha t_m/Ro^2$ = 0.010. Then, the two resulting temperature histories are interpolated using the above interpolation rule. The resulting temperature history for Ri* = 0.7 and $\alpha t_m/Ro^2$ = .010 found by this procedure is:

t*	0.5	1.0	1.4	1.8	2.8	4.0	8.0	12.0	20.0
T*	.0246	.0824	.104	.102	.0952	.0896	.0816	.0794	.0749

It now remains to complete the double interpolation by interpolating the above results derived for $\alpha t_m/Ro^2$ = .025 and .010 for the problem value of .015. This will be accomplished by using the interpolation rule, equation (B-8), for variation of $\alpha t_m/Ro^2$. That is, the dimensionless temperatures for $\alpha t_m/Ro^2$ = .015 are equal to the dimensionless temperatures at $\alpha t_m/Ro^2$ = .010 plus 33.3 percent

of the increment in dimensionless temperatures between those at 0.010 and 0.025. Calculating the dimensionless temperature history from the preceding two tables and the above interpolation rule leads to the following result for $\alpha t_m/Ro^2 = .015$ and $Ri^* = 0.7$.

t^*	0.5	1.0	1.4	1.8	2.8	4.0	8.0	12.0	20.0
T^*	.0294	.0993	.126	.126	.122	.118	.112	.107	.0982

Once these dimensionless temperatures have been found, it remains only to do steps 8 and 9 of example 1 to find the actual temperature history.

Step 8: Find t_m and $AH_m Ro/k$. $t_m = 1.0$ second (given)

$$\frac{AH_m Ro}{k} = \frac{1.0\,(48.7\ \ cal/cm^2 sec)\,2.56\ in\ 2.54\,\frac{cm}{in}}{0.397\,\frac{cal}{sec\text{-}cm^{\circ}C}} = 767^{\circ}C$$

Step 9: Compute the temperature history for $TI = 20^{\circ}C$

$$T = \left(\frac{AH_m Ro}{k}\right)\ T^* + TI$$

t (second)	0.5	1.0	1.4	1.8	2.8	4.0	8.0	12.0	20.0
$T(^{\circ}C)$	43.4	99.1	121	120	117	114	109	106	98.2

A calculation using the computer program described in reference (4) was made to check the results derived by the interpolation rule used in the above calculation. The corresponding temperature history found by the laborious numerical computation is:

t (second)	0.5	1.0	1.4	1.8	2.8	4.0	8.0	12.0	20.0
$T(^{\circ}C)$	43.9	101	123	120	114	111	110	108	101

Thus, it can be concluded that the interpolation rule, equation (B-8), can be used to accurately find the surface temperatures for cylinders which are not thermally-thick and which have basic dimensionless parameters not given in Appendix A.

Solution: (b) Midplane temperatures

The procedure for computing the midplane temperatures using the interpolation rule, equation (B-8), is identical to that used to find the surface temperatures. These computations will not be repeated but the final result will be given. That is, the temperature history for $TI = 20^{\circ}C$ at the midplane found by an interpolation of the data in Appendix A is the following:

t (second)	0.5	1.0	1.4	1.8	2.8	4.0	8.0	12.0	20.0
$T(^{\circ}C)$		21.4	33.1	50.1	63.0	81.6	94.0	101	101	95.7

Also, the numerical calculation of these same midplane temperatures using the computer program of reference (4) leads to the following result.

t (second)	0.5	1.0	1.4	1.8	2.8	4.0	8.0	12.0	20.0
$T(^{\circ}C)$		21.5	36.2	54.6	69.1	86.4	96.1	105	105	99.7

Thus, it can be concluded that the interpolation rule, equation (B-8), can be used to accurately find the interior temperatures for cylinders which are not thermally-thick.

The results of a final example will be presented to show that it is possible to extrapolate the data of Appendix A. Extrapolation is necessary when basic dimensionless variables, Ri* or $\alpha t_m/Ro^2$, result which fall outside the range of these variables which are covered by Appendix A (see also Table 1). An example will be given to show that the interpolation rule, equation (B-8), can also be used to extrapolate the results of Appendix A.

Example 4: Extrapolation of Non-Thick Cylinder Results

An aluminum alloy cylinder (6061-T6) of outer radius 1.68 inches and inner radius 1.596 inches is exposed to the thermal environment of the nuclear weapon in example 1 (t_m = 1.0 seconds, H_m = 48.7 cal/cm^2 -sec). Find the surface temperature history where the cylinder angle is 0 degrees.

Solution

Step 1: Compute Ri/Ro. $Ri/Ro = \dfrac{1.596 \text{ in}}{1.68 \text{ in}} = 0.95$

An inner radius ratio outside the range of radius ratios given in Appendix A has resulted.

Step 2: Compute $\alpha t_m/Ro^2$. $\dfrac{\alpha t_m}{Ro^2} = \dfrac{0.637 \frac{cm^2}{sec} \cdot 1.0 \text{ sec}}{\left(1.68 \text{ in} \cdot 2.54 \frac{cm}{in}\right)^2} = 0.035$

A value of $\alpha t_m/Ro^2$ has resulted which requires interpolation since it also is not given in Appendix A. Furthermore, the cylinder is not thick for these values of the basic parameters therefore equation (B-8) is the interpolation rule to be used. The procedure for computing the temperature history for this example is identical to that of example 3. First results are extrapolated to the radius ratio of 0.95 and then interpolated for an $\alpha t_m/Ro^2$ of 0.035. The details of doing this will be omitted and only the final result presented. Thus, the temperature history for an initial temperature of 20°C found by this procedure is the following.

t (second)	0.5	1.0	1.4	1.8	2.8	4.0	8.0	12.0	20.0
T (^{o}C)	55.2	202	337	429	548	600	635	609	545

Similarly, the temperature history can be computed using the numerical computer program of reference (4). This leads to the result.

t (second)	0.5	1.0	1.4	1.8	2.8	4.0	8.0	12.0	16.0
T (^{o}C)	60.5	222	356	438	562	611	645	621	557

Thus, it can be seen by comparison that the interpolation rule can also be used to extrapolate the data on Appendix A and a reasonably accurate answer can be expected.
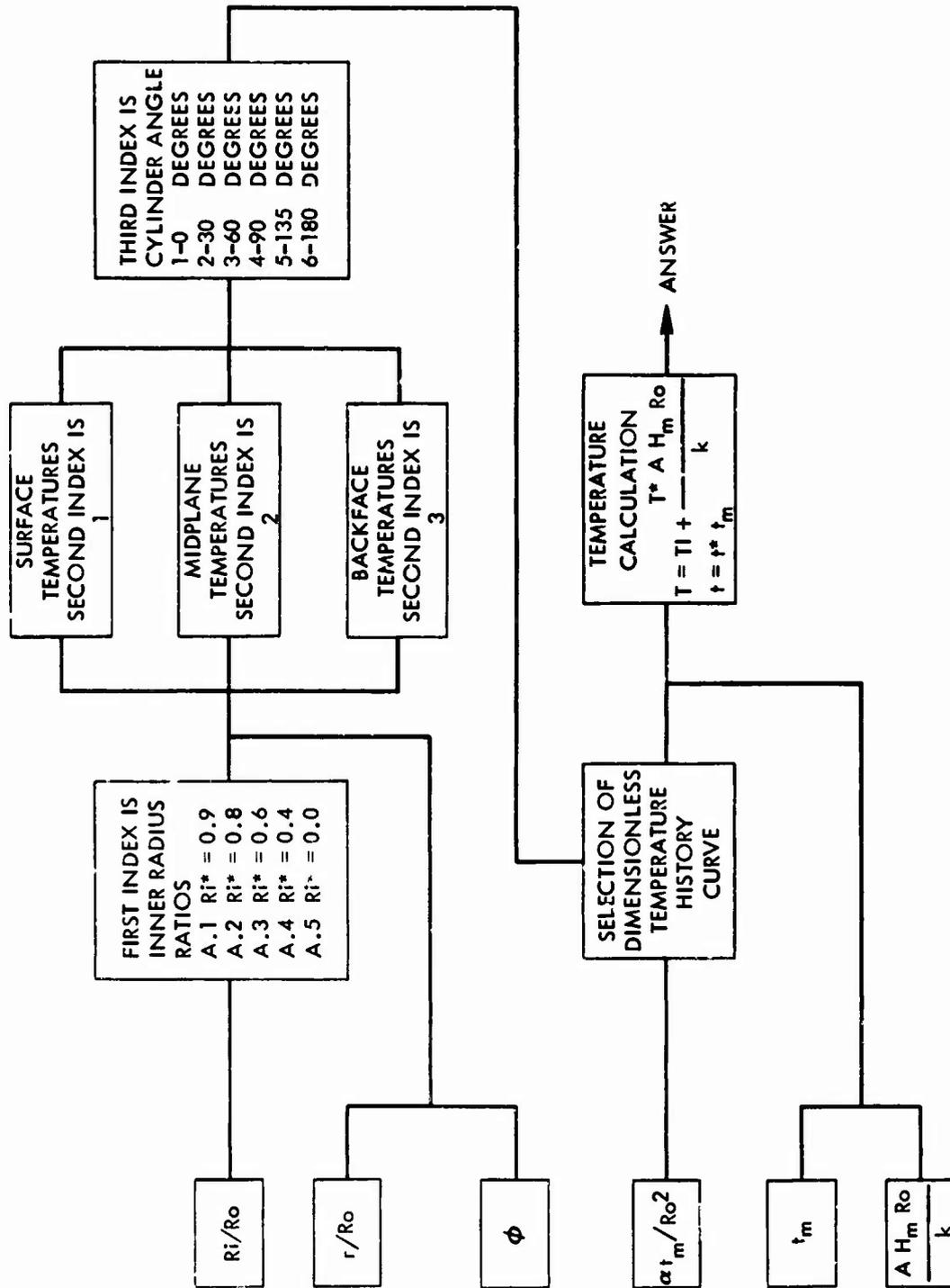
FIG. (B-1.1) SCHEMATIC DIAGRAM ILLUSTRATING THE USE OF THE FIGURES IN APPENDIX A